Pharmacological WDR5 WIN site inhibition as an anti-leukemia target

By

Erin R. Aho

Dissertation
Submitted to the Faculty of the
Graduate School of Vanderbilt University
in partial fulfillment of the requirements
for the degree of

DOCTOR OF PHILOSOPHY
in
Cell and Developmental Biology
May 31, 2019
Nashville, Tennessee

Approved:

Maureen Gannon, Ph.D.

Scott Hiebert, Ph.D.

Ethan Lee, M.D, Ph.D.

Jason MacGurn, Ph.D.

William P. Tansey, Ph.D.

ACKNOWLEDGEMENTS

First and foremost, I would like to thank my mentor, Dr. Bill Tansey, for your exceptional training. Your leadership and example has helped me grow immensely as a scientist. I would not be where I am today without your guidance. I also thank all of the members the Fesik lab who have contributed to the WDR5 inhibitor project over the years. It has been a pleasure to work with each of you, and my thesis work would not have been possible without the compounds you discovered. A special thank you to Ms. Shelly Lorey, for the countless hours you spent screening compounds with me during the early phases of the project and for ensuring that our lab runs smoothly. Thank you to all of the other members of the Tansey lab, past and present, who have helped to train me and support me over the years. Thank you, Jing Wang and Dr. Qui Liu, for your bioinformatics expertise. Your analyses of the RNA-seq and ChIP-seq data sets were essential for the completion of the studies presented in this thesis. Thank you to my Thesis Committee comprised of Dr. Ethan Lee, Dr. Maureen Gannon, Dr. Jason MacGurn, and Dr. Scott Hiebert. I have enjoyed each of our meetings, and I am very lucky to have had such a supportive, encouraging and engaged Thesis Committee. Finally, I thank my loving family for their enduring support and encouragement. You have been there for me every step of the way and for that I am forever grateful.

TABLE OF CONTENTS

Page

LIST OF TABLES

Table Page

LIST OF FIGURES

Figure Page

CHAPTER I

INTRODUCTION

Abstract

The epigenetic regulator WDR5 is a promising therapeutic target in leukemias expressing oncogenic translocations of the *MLL1* histone methyltransferase gene. Despite validation of the WIN site of WDR5 as a pharmacological anti-cancer target, the molecular mechanism through which inhibition of the WIN site kills certain leukemia cell types remains unclear. This lack of clarity stems from an insufficiency in understanding of the genes regulated by WDR5 and the primary effects of WDR5 WIN site inhibitors. In order to better decipher the biological consequences of inhibiting WDR5 in leukemia cells, the Fesik Laboratory discovered novel and potent small molecule inhibitors of the WDR5 WIN site that could be utilized as tool compounds in biological experiments. By utilizing these novel tool compounds, I found that WDR5 regulates the expression of a select set of ribosome protein genes that is conserved across disparate cell types. WDR5 is displaced from chromatin at these genes upon small molecule inhibitor treatment and, ultimately, displacement of WDR5 from chromatin causes reduced expression of WDR5-bound genes, impeded protein translation, induction of nucleolar stress, and p53-dependent apoptosis in MLL-fusion leukemia cells.

Overview

In recent years, a growing number of studies have illuminated roles for epigenetic and chromatin regulators in tumorigenic processes. The advancement in our understanding of how epigenetic regulators contribute to the tumorigenic phenotype of cancer cells has lead to an increased number of therapeutic approaches that target these pathways (Bennett and Licht 2018). Despite the advancements made in epigenetic-targeted anti-cancer therapeutic strategies, the rate a which investigational drugs are approved for clinical use remains low. Therefore, it is necessary to expand the number of highly validated anti-cancer targets to increase the chances that breakthroughs in cancer treatment can be made. In this chapter, I

give an overview of WD Repeat Domain 5 (WDR5), an epigenetic regulator implicated in many cancer types (Cao, Townsend et al. 2014, Kim, Banerjee et al. 2014, Grebien, Vedadi et al. 2015, Zhu, Sammons et al. 2015, Neilsen, Chakraborty et al. 2018, Sun, Guo et al. 2018). I discuss the roles of WDR5 as an epigenetic and chromatin regulator, detail a protein-protein interaction domain on WDR5 that is amenable to small-molecule inhibition, and describe studies that have validated this site as a therapeutic target in cancer. While a handful of WDR5 inhibitors have been described, a lack of understanding of the genes regulated by WDR5 and the primary direct effects of these inhibitors hinders their utility. A more detailed insight into how WDR5 inhibitors function in cancer is needed; which is the purpose of my work. Finally, I present a summary of the studies detailed throughout this thesis utilizing two novel and potent small molecule WDR5 inhibitors which were used as tools to better understand the genes that are regulated by WDR5 and the mechanism by which WDR5 inhibitors kill cancer cells.

The roles of WDR5 as a chromatin and transcriptional regulator

WD Repeat Domain 5 (WDR5) is a WD40 repeat-containing protein that forms a seven bladed β-propeller structure. WDR5 is extraordinarily well-conserved across species, with nearly 90% of the amino acid sequence identity shared among mammalian cells. In fact, human and mouse WDR5 are identical (Guarnaccia and Tansey 2018), thus highlighting the importance WDR5 in conserved biological processes. WDR5 has no enzymatic activity itself, but instead primarily functions as a scaffolding protein for many multi-protein complexes with diverse functions in epigenetic and chromatin regulation (Lu, Tao et al. 2018).

WDR5 is most well known for its role as a core member of the SET/MLL family of histone methyltransferse (HMT) complexes, which catalyze di- and tri-methylation of lysine 4 on histone H3 (H3K4me2 and H3K4me3) (Figure 1-1A). H3K4me2 and H3K4me3 are epigenetic modifications associated with actively transcribed genes. There are six human histone methyltransferase complexes, and each includes one unique catalytic subunit: SET1A, SET1B,

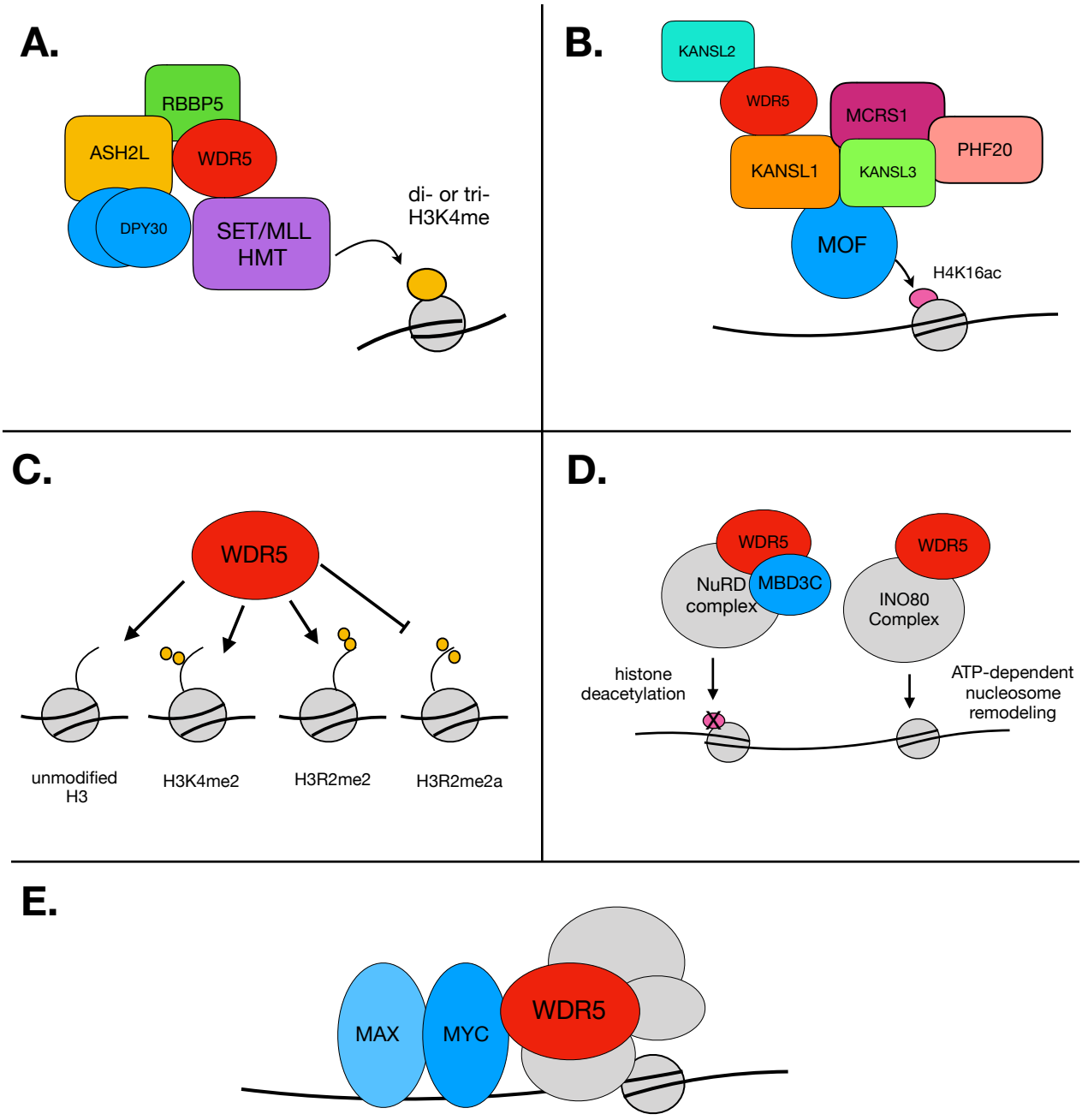

1.1 WDR5 has diverse functions as an epigenetic and transcriptional regulator. (A) WDR5 within the WRAD complex promotes full catalytic activation of SET/MLL family histone methyltransferases. (B) WDR5 is a member of the NSL histone acetyltransferase complex. (C) WDR5 acts as an epigenetic reader of histone H3 tails. (D) WDR5 is a member of the NuRD and INO80 chromatin remodeling complexes. (E) WDR5 facilitates recruitment of the transcription factor MYC to chromatin.

MLL1, MLL2, MLL3 or MLL4. The basal histone HMT activity of each catalytic subunit is low and full activation is mediated by binding of a set of regulatory factors called the WRAD complex. The WRAD complex is composed of WDR5, RBBP5, ASH2L, and DY30. WDR5 is a critical component of the WRAD complex because it acts to bridge interaction between RBBP5 and the SET/MLL HMT (Trievel and Shilatifard 2009). Binding of WDR5 is required for full catalytic activation of MLL1 and SET1A (Alicea-Velazquez, Shinsky et al. 2016). The interaction domain via which WDR5 binds SET/MLL HMTs will be further detailed below.

Although the function of WDR5 as a regulator of SET/MLL complex assembly and activity is the the most well-understood, it has been determined that WDR5 protein levels are roughly 10-fold higher than other WRAD proteins (van Nuland, Smits et al. 2013), suggesting that WDR5 has functions outside of the SET/MLL complexes. Indeed, WDR5 associates with several proteins to form a second distinct epigenetic writer complex called the non-specific lethal (NSL) complex (Figure 1-1B). In addition to WDR5, the NSL complex is comprised of the acetyltransferase MOF, KANSL1, KANSL2, KANSL3, PHF20 and MCRS1. MOF is the catalytic subunit of the NSL complex and mediates histone H4 lysine 16 acetylation (H4K16ac), an epigenetic mark associated with transcriptional activation. The NSL complex controls expression of thousands of of diverse genes (Dias, Van Nguyen et al. 2014). The precise way in which WDR5 contributes to the activity of the NSL complex has not been determined.

In addition to functioning as a scaffold for epigenetic histone methyltransferase and acetyltransferase writer complexes, WDR5 functions as an epigenetic reader by binding to both modified and unmodified histone H3 tails (Wysocka, Swigut et al. 2005) (Figure 1-1C). Although WDR5 can engage unmodified H3, WDR5 had been proposed to function as a reader of the methylation status at histone H3 lysine 4 (H3K4) by preferentially binding di-methylated H3K4 over unmodified H3K4. Additionally, WDR5 “reads” the methylation status of arginine 2 of histone H3 (H3R2) (Migliori, Muller et al. 2012) (Figure 1-1C). H3R2 di-methylation can exists in two forms. Asymmetric di-methylation of histone H3 arginine 2 (H3R2me2a), is a repressive epigenetic mark that occurs when two methyl groups are placed on the same terminal nitrogen atom of an arginine side chain (Guccione, Bassi et al. 2007). In contrast, symmetric di-methylation of histone H3 arginine 2 (H3R2me2) occurs when one methyl group is placed on each of the two terminal nitrogen groups of the arginine side chain, and is enriched at genomic loci that are transcriptionally poised. WDR5 cannot bind H3R2me2a but can engage H3R2me2

and WDR5 binding to chromatin is enriched at sites of H3R2me2 (Migliori, Muller et al. 2012). Thus although the biological purpose of the epigenetic reader function of WDR5 is unclear, the inability of WDR5 to engage repressive H3R2me2a and preferentially bind H3R2me2 at transcriptionally poised loci, or H3K4me2 at active genes underscores the general role of WDR5 as a transcriptional activator.

WDR5 has also been identified as a member of several chromatin remodeling complexes (Figure 1-1D). For example, WDR5 is a member of the Nucleosome Remodeling and Deacetylase (NuRD) complex. Within the NuRD complex, WDR5 directly interacts with the subunit MBD3C. MBD3C is expressed primarily in embryonic stem cells, suggesting that the role of WDR5 in NuRD complex-mediated nucleosome remodeling and deacetylation is stem cell specific (Ee, McCannell et al. 2017). The role of WDR5 in stem cell chromatin remodeling extends beyond the NuRD complex. Additionally, WDR5 interacts with Ino80 within the INO80 complex, a SWI/SNF family chromatin remodeler. Ino80 is the chromatin remodeling ATPase within the INO80 complex. The INO80 complex promotes expression of genes needed to maintain stem cell pluripotency. WDR5 is required for Ino80 promoter occupancy at pluripotency genes, where the complex functions to maintain an open chromatin architecture and recruit Mediator and RNA polymerase II to promote gene transcription (Wang, Du et al. 2014). Several less-characterized interactions between WDR5 and chromatin remodeling complexes have been noted including direct interaction between WDR5 and the chromatin remodeling enzyme CHD8 (Thompson, Tremblay et al. 2008, Yates, Menon et al. 2010), and the ATAC histone acetylation and nucleosome remodeling complex (Wang, Faiola et al. 2008).

In addition to its epigenetic writer and reader functions and roles in chromatin remodeling, WDR5 interacts directly with several sequence specific transcription factors. Our lab recently demonstrated that WDR5 directly binds the oncogenic transcription factor c-MYC (Thomas, Wang et al. 2015) (Figure 1-1E). It was discovered that interaction between WDR5 and c-MYC is needed for c-MYC to associate with chromatin. Loss of c-MYC and WDR5 interaction attenuates the ability of c-MYC to induce pluripotent stem cell formation and drive tumorigenesis in a mouse model. WDR5 interaction is conserved among the MYC family of proteins, as L-MYC (Thomas, Wang et al. 2015) and N-MYC (Sun, Bell et al. 2015) both also directly bind WDR5 in the same fashion as c-MYC (further discussed below). Other identified sequence specific

transcription factors that directly bind WDR5 include OCT4 (Ang, Tsai et al. 2011), Twist1 (Malek, Gajula et al. 2017) and HSF2 (Hayashida 2015).

As the interest in WDR5 biology grows, even more diverse functions are beginning to be illuminated. For instance, WDR5 was identified as a member of the PRC1.6 polycomb repressor complex (Aranda, Mas et al. 2015) and the WHHERE complex, which is required for proper retinoic acid signaling during establishment of embryo symmetry (Vilhais-Neto, Fournier et al. 2017). Little is known about the role of WDR5 within these poorly characterized complexes. Not only does WDR5 have an extensive array of protein binders, but WDR5 was found to interact with a handful of long non-coding RNAs. WDR5 binds the long non-coding RNAs HOTTIP (Yang, Flynn et al. 2014), NeST (Gomez, Wapinski et al. 2013), GClnc1 (Sun, He et al. 2016) and HOXD-AS1 (Gu, Chen et al. 2017). The interactions between WDR5 and long non-coding RNAs has been proposed to facilitate WDR5 recruitment to specific genomic loci (Gomez, Wapinski et al. 2013, Yang, Flynn et al. 2014, Sun, He et al. 2016, Gu, Chen et al. 2017), though more thorough investigation of the mechanism that underlies this idea is needed.

The multitude of identified protein and RNA WDR5 interaction partners underscores the fact that despite its lack of enzymatic activity, WDR5 contributes to many epigenetic, transcriptional, and chromatin remodeling processes. The full repertoire of WDR5 functions are still being uncovered, as many of the studies listed above simply identified WDR5 as a member of a specific complex but did not mechanistically detail how WDR5 contributes to the biological activity or localization of the complex. Increased awareness of how WDR5 functions will aid in determining the utility of WDR5 as an anti-cancer epigenetic target.

The role of WDR5 in cancer

WDR5 has been implicated in many diverse cancer types, making it an attractive chromatin and transcriptional regulator for targeted anti-cancer therapy. WDR5 has been identified as a possible therapeutic target in three cancer types that express specific oncogenic mutations. Arguably the most well-known example is the implication of WDR5 in leukemias expressing oncogenic translocations of the MLL1 histone methyltransferase. When MLL1 is translocated in leukemias, it results in formation of a fusion protein that retains the N-terminus of MLL1 but the C-terminus, including the HMT domain, is replaced by another protein. Over 70 different MLL1-

fusion partners have been identified, but 80–90% of all MLL1 gene translocations are fusions of MLL1 with AF4, AF9, ENL, ELL, AF10 or AF6 (Ballabio and Milne 2012). The mechanism by which the fusion proteins promote leukemogenesis is incompletely understood. Interestingly, MLL-fusion leukemias nearly always retain expression of WT MLL1, suggesting that WT MLL1 contributes to leukemogenesis. It has been proposed that the activity of WT MLL1 and the MLL1-fusion complex cooperate in some way to drive over expression of key genes needed to transform hematopoietic cells (Figure 1-2A) (Ballabio and Milne 2014). Because WDR5 is critical for HMT activity of WT MLL1 (Li, Han et al. 2016), WDR5 has been implicated in promoting leukemogenesis in MLL-fusion cells. shRNA mediated knock-down of WDR5 in mouse bone marrow cells transformed with an MLL-AF9 fusion protein resulted in drastically reduced colony formation (Cao, Townsend et al. 2014), thus supporting the notion that WDR5 contributes to leukemogenesis; however, this is an empirical observation and the mechanism by which WDR5 functions in the context of an MLL-fusion oncoprotein remains unclear.

Second, WDR5 has been connected to acute myeloid leukemias expressing a mutant form of the transcription factor CCAAT/enhancer binding protein α (C/EBPα) called C/EBPα p30. C/EBPα p30 was found to interact directly with WDR5 and co-localize with WDR5, the rest of MLL1 HMT complex and H3K4me3 on chromatin at genes that promote cellular proliferation. H3K4me3 was elevated in the promotor region of C/EBPα p30 bound genes compared to wild type C/EBPα cells. Upon inducible WDR5 knock-down, H3K4me3 was reduced at WDR5 and C/EBPα p30 co-bound genes and an increase in expression of genes related to myeloid differentiation was observed. The same effects were not observed when WDR5 was knocked down in cells expressing WT C/EBPα (Grebien, Vedadi et al. 2015). Together, these findings suggesting that WDR5 may contribute to leukemogenesis in C/EBPα mutant AML by promoting MLL-1 mediate H3K4me3 at genes bound by C/EBPα p30 (Figure 1-2B).

Third, WDR5 has been implicated in cancers expressing p53 gain-of-function missense mutations. It was found that p53 gain-of-function mutations allow p53 to aberrantly bind to and up-regulate several chromatin regulating factors including MLL1. MLL1 was found to be over-expressed in patient derived tumor samples with p53 gain-of-function mutations, but not in p53-null or WT p53 samples. p53 gain-of-function cells also exhibited elevated levels of H3K4me3. Proliferation of p53 gain-of-function cells was reduced after knockdown of MLL1, suggesting that the activity of MLL1, which is WDR5-dependent, is required for p53 gain-of-function cell

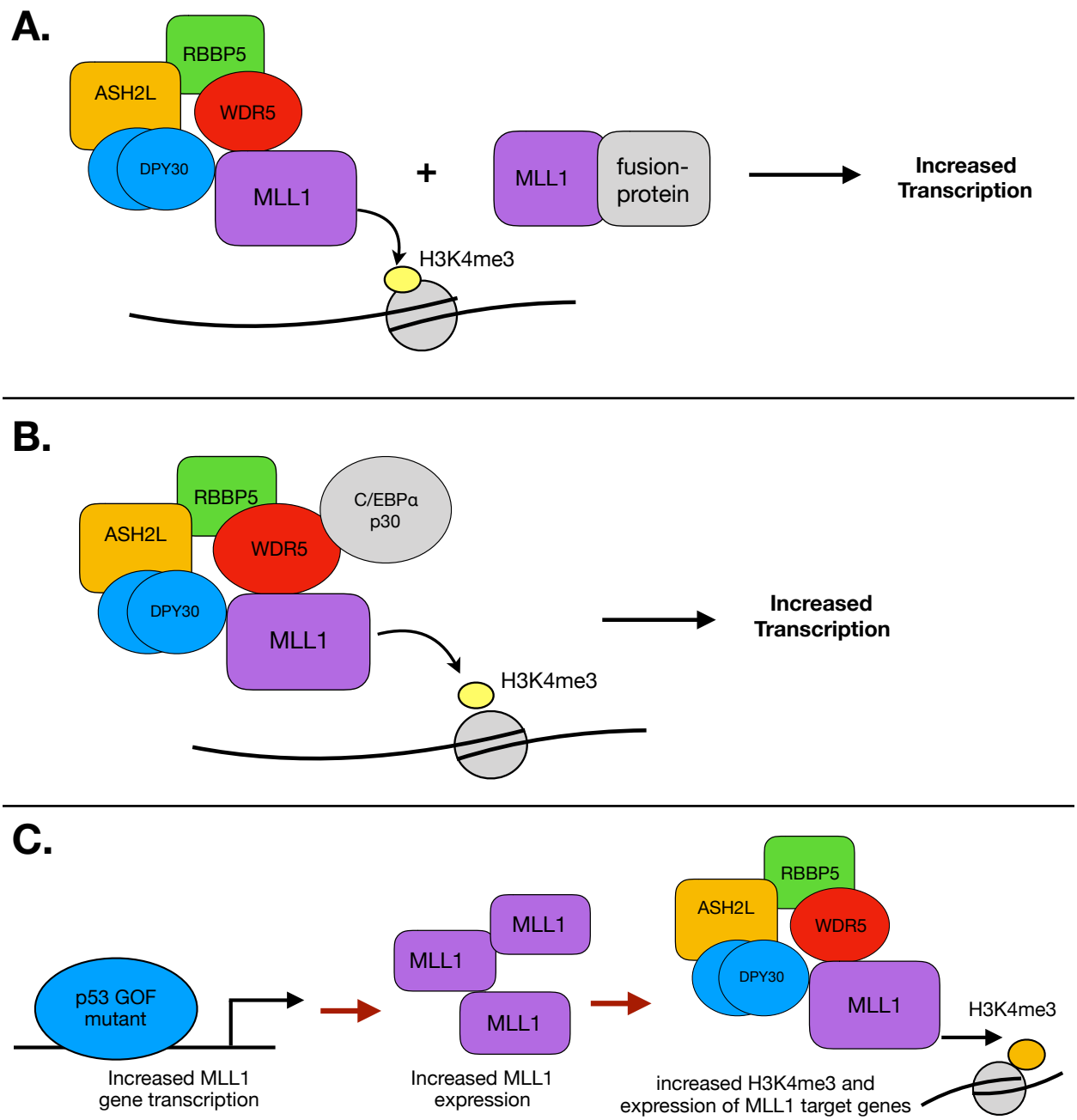

Figure 1-2. Models of how WDR5 contributes to cancers expressing specific oncogenic mutations. (A) WDR5 facilities MLL1-mediated H3K4me3 which cooperates with the activity of oncogenic MLL1-fusion protein complex at genes that drive the leukemic phenotype. (B) WDR5 interacts with mutant C/EBPα p30 and promotes MLL1-mediated H3K4me3 at genes that promote cellular proliferation. (C) p53 gain-of-function mutants increase expressing of chromatin regulatory factors including MLL1. WDR5 facilitates MLL1 HMT activity to promote expression of genes that promote cancer cell proliferation.

proliferation. These findings lead to the idea that WDR5 contributes to this cancer type by promoting MLL1-mediated H3K4me3 (Zhu, Sammons et al. 2015) (Figure 1-2C).

In addition to the roles of WDR5 in cancers with specific oncogenic lesions listed above, WDR5 has also been more generally associated with promoting tumor cell proliferation in several cancer types. Over-expression of WDR5 has been implicated in acute myeloid (AML) and acute lymphoblastic leukemias (ALL) (Ge, Song et al. 2016), as well as colon (Neilsen, Chakraborty et al. 2018), prostate (Kim, Banerjee et al. 2014), bladder (Chen, Xie et al. 2015), and gastric cancers (Sun, Guo et al. 2018). High WDR5 expression tends to be positively correlated with worse prognosis. For example, high WDR5 expression in AML and ALL is associated with high risk leukemia, poor complete remission rates and increased liver, spleen and bone marrow infiltration of leukemia cells (Ge, Song et al. 2016). Evidence also supports the idea that WDR5 is needed to maintain cancer cell growth, as proliferation of WDR5 over-expressed colon cancer lines, but not normal cells, is inhibited by shRNA-mediated depletion of WDR5. WDR5 depletion in colon cancer lines also reduces global levels of H3K4me3. These data indicated that WDR5 may support colon cancer cell growth by promoting H3K4me3 (Neilsen, Chakraborty et al. 2018). Similar results were obtained in AML and ALL cells, as WDR5 knockdown inhibited cell proliferation and induced apoptosis. Again, WDR5 knock-down reduced global H3K4me3, thus also implicating the H3K4me3 regulating function of WDR5 in AML and ALL (Ge, Song et al. 2016). WDR5 has been implicated in breast cancer by interacting with the polycomb protein Cbx8 in a non-canocical fashion in mammary carcinoma-derived tumorspheres to promote tumorigenic expression of Notch signaling genes. WDR5 knock-down reduced tumor-sphere formation, clonogenicity, invasiveness, and expression of specific Notch-network genes. In contrast, over-expression of WDR5 promoted enhanced tumor-sphere formation (Chung, Sun et al. 2016), thus suggesting WDR5 is important for breast cancer cell growth.

In addition to promoting tumor cell growth, WDR5 has been implicated in promoting the epithelial-mesenchymal transition in cancer cells, a critical step in order to drive cancer cell invasion and metastasis (Kalluri and Weinberg 2009). WDR5 has been shown to interact with the histone deacetylase, HDAC3, under hypoxic conditions and this interaction promotes up-regulation of mesenchymal genes that promote metastatic phenotypes in non-small cell lung carcinoma cells (Wu, Tsai et al. 2011). WDR5 is also associated with promoting expression of

genes needed for increased cell migration, invasion and metastasis in breast carcinoma (Chen, Lorton et al. 2017) and prostate cancer (Malek, Gajula et al. 2017).

Finally, WDR5 has been shown to contribute to tumorigenicity through its interaction with MYC, a transcription factor that is dysregulated in the majority of cancers (Thomas, Foshage et al. 2015). Our lab has shown that genetic inhibition of the interaction between WDR5 and c-MYC prevents c-MYC from associating with chromatin, which is necessary for MYC to promote tumorigenesis (Thomas, Wang et al. 2015). WDR5 was subsequently identified as an epigenetic regulator required for pancreatic ductal adenocarcinoma (PDAC) tumor maintenance in a loss of function screen using patient derived xenographs. WDR5 showed high protein expression level in human PDAC xenografts and the interaction between MYC and WDR5 was important for maintaining proper DNA replication and PDAC tumor cell growth (Carugo, Genovese et al. 2016). Others have found that WDR5 interaction with N-MYC is required for N-MYC to drive expression of genes that promote tumorigenesis in neuroblastoma cells (Sun, Bell et al. 2015), thus implicating the WDR5-MYC interaction as another way that WDR5 can promote tumor cell growth. Together, the studies described above demonstrate a broad contribution of WDR5 to cancer and predict that WDR5 inhibition may have efficacy in many different cancer types.

WDR5 as a target of small molecule inhibition

Due to the many associations formed between WDR5 and cancer, targeting WDR5 may have therapeutic benefit in a variety of caner types. In order to inhibit the functions of WDR5 that promote tumor cell growth or maintenance, a site on the WDR5 protein, that when bound by an inhibitor, can block the oncogenic functions of WDR5 must be identified. It is well-established that WDR5 contains two distinct protein-protein interaction domains on opposite sides of the protein (Guarnaccia and Tansey 2018). All of the protein and RNA binders of WDR5 for which the interactions have been mapped were found to engage WDR5 at one of these two sites. Therefore, the two protein-protein interaction domains of WDR5 may be able to be targeted for therapeutic benefit.

The first WDR5 protein-protein interaction domain that will be discussed is called the WDR5-binding motif or WBM. The WBM is formed by a shallow hydrophobic cleft surrounded by positive charges (Thomas, Wang et al. 2015). Figure 1-3 illustrates the location of the WBM site

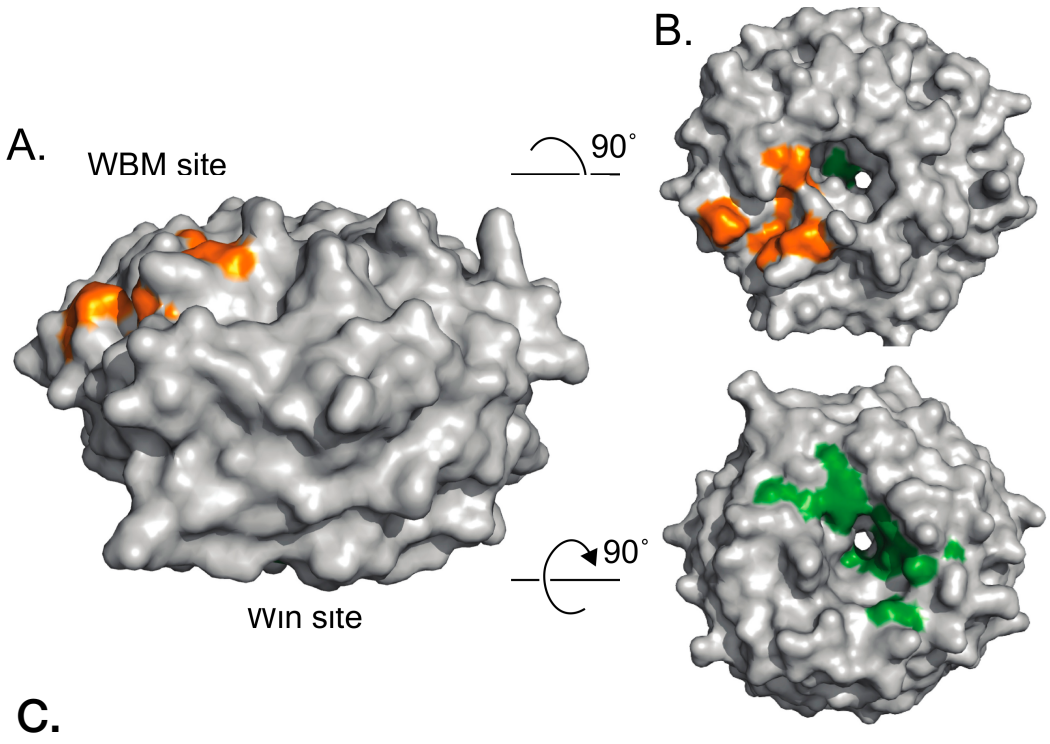

C.

WBM site binders:	
c-MYC	(EEIDVV)
L-MYC	(EEIDVV)
N-MYC	(EEIDVV)
RBBP5	(EEVDVT)
KANSL2	(DDLDVV)

WIN site binders:	
MLL1	(ARA)
MLL2	(ARS)
MLL3	(ARS)
MLL4	(ARA)
SET1A	(ARS)
SET1B	(ARS)
H3	(ART)
KANSL1	(ART)
MBD3C	(ARC)
WDR5	(ARA)

Figure 1-3. The two protein-protein interaction domains of WDR5 and their respective binding partners. This figures was adapted from Guarnaccia and Tansey. *J. Clin. Med.* **2008**, 7, 21; doi:10.3390/jmc7020021. (A) Side view of the WDR5 protein structure with the locations of the WBM and WIN protein-protein interaction domains indicated. (B top) The top view of WDR5 is shown and the residues corresponding to the WBM site are shown in orange. (B bottom) Bottom view of WDR5 with the residues corresponding to the WIN site shown in green. (C) Characterized WDR5 binders of the WBM and WIN site are listed with their respective motifs that engage WDR5 listed in parentheses.

on the surface of WDR5. The protein structure images shown in Figure 1-3 were created by Alissa Guarnaccia and were perviously published (Guarnaccia and Tansey 2018). Residues composing the WBM site include Asn225, Tyr228, Leu240, Phe266, Val268, and Gln289.

Proteins known to bind to the WBM site of WDR5 include c-MYC, L-MYC, N-MYC, RBBP5 and KANSL2. Binding of proteins to the WBM is mutually exclusive so only one WBM binder can engage WDR5 at a time. The characterized WBM binding motif sequence found in the MYC family of proteins is EEIDVV (Thomas, Wang et al. 2015) while the WBM motifs found in RBBP5 and KANSL2 are EEVDVT and DDLDVV, respectively (Guarnaccia and Tansey 2018). Mutation of the L240 residue within the WIN site of WDR5 leads to loss of WDR5 interaction with WBM site binders (Thomas, Wang et al. 2015). This finding has strong therapeutic implications, as loss of MYC binding to WDR5 reduces tumorigenicity (Thomas, Wang et al. 2015). The ability to therapeutically inhibit the oncogenic function MYC, traditionally considered an “undrugable” protein, by blocking the WBM of WDR5 is incredibly exciting; whether such a shallow cleft on WDR5 can be pharmacologically targeted, however, remains to be determined.

The second protein-protein interaction domain in WDR5 is called the WDR5-interacting site or WIN site. The WIN site is located within the central pore created by the seven-bladed propeller structure on the opposite face of WDR5 from the WBM (Figure 1-3). More specifically, the WIN site encompasses residues Ala65, Ser91, Asp107, Phe133, Tyr191, Tyr260, and Phe263 of WDR5. The WIN site of WDR5 functions as an arginine side chain binding pocket (Guarnaccia and Tansey 2018). The consensus sequences that bind the WIN site are called “WDR5 interacting” or WIN motifs and consist of a short Ala-Arg-Ala, Ala-Arg-Ser or Ala-Arg-Thr sequence. The arginine side chain of a WIN motif engages the central pore of the WIN site and makes a critical cationic pi-stacking interaction with the aromatic rings of Phe133 and Phe263. This interaction is critical for WIN site/WIN motif engagement, and mutation of the arginine to alanine in the WIN motif or Phe133 to alanine in the WIN site result in loss of binding (Karatas, Townsend et al. 2010). Proteins known to interact with the WIN site of WDR5 through engagement of a WIN motif at the WIN site include the SET/MLL type catalytic subunits SET1A, SET1B, MLL1, MLL2, MLL3 and MLL4, histone H3 tails, KANSL1 of the NSL complex, MBDC3 of the NuRD complex, and even WDR5 itself (Guarnaccia and Tansey 2018). The short ~30

amino acid unstructured loop at the N-terminus of WDR5 contains an Ala-Arg-Ala WIN motif and was shown to bind an adjacent WDR5 molecule at the WIN site in a crystal structure (Schuetz, Allali-Hassani et al. 2006), although the biological relevance or function of this interaction is unknown. As for the WBM site, binding at the WIN site is mutually exclusive. As stated above, the role of WDR5 in regulating the H3K4me3 activity of MLL1 has been strongly implicated in several cancer cell types and the WIN site of WDR5 is critical for this function. Binding of WDR5 to MLL1 occurs by engagement of a WIN motif in MLL1 with the WIN site of WDR5 (Dharmarajan, Lee et al. 2012). In contrast to the WBM site, the relatively small size of the WIN site and its well defined and stable structure make the WIN site an excellent target for small molecule inhibition.

The WDR5 WIN site as a validated cancer therapeutic target in MLL-leukemia

As stated above, the small and well-defined structure of the WDR5 WIN site and the connection between the WIN site and MLL1-mediated H3K4me3 in several different cancer types, make the WIN site of WDR5 an attractive target for small molecule inhibition. Cancers expressing MLL-fusions, mutant C/EBPα, and p53 gain-of-functions would all be expected to be sensitive to WDR5 WIN site inhibition. The use of inhibitors and monobodies that block the WIN site (described further below) have demonstrated that inhibiting the WIN site of WDR5 selectively blocks proliferation and induces apoptosis and differentiation of leukemia cells expressing an MLL-fusion but not non-fusion leukemias or normal blood cells (Cao, Townsend et al. 2014, Gupta, Xu et al. 2018). Thus, the WIN site of WDR5 has been validated as a pharmacological target in MLL-leukemia.

In the validation studies, sensitivity of MLL-leukemia cells to WDR5 WIN site inhibition was empirically established, but the mechanism through which WDR5 WIN site inhibition functions remains unclear. Although WIN site inhibition has been proposed to function by blocking WDR5/MLL1 interaction, and thus MLL1 HMT activity in MLL-leukemia (Karatas, Townsend et al. 2010, Cao, Townsend et al. 2014, Gupta, Xu et al. 2018), when considering how small molecule inhibitors of the WIN site might function, it is important to remember the diversity of functions that WDR5 has (discussed above). A small molecule inhibitor of the WDR5 WIN site would be expected to prevent interaction between WDR5 and the histone methyltransferases MLL1, MLL2, MLL3, MLL4, SET1A, SET1B, modified and unmodified histone tails, and KANSL1 of the

NSL complex. Additionally, WDR5 and MBDC3 interaction in the NuRD would be inhibited in ES cells. Due to the multitude of interactions that occur at the WIN site, it is imperative to keep in mind that cellular effects could be due to inhibition of any of the known WIN site binders or perhaps even a WIN site binder yet to be identified. Therefore, while the WIN site has been validated as a therapeutic target in MLL-leukemia (Cao, Townsend et al. 2014, Gupta, Xu et al. 2018), moving forward it is imperative to use unbiased experimental approaches when possible to determine the mode by which WIN site inhibitors function. In doing so, it is more likely that we can refine what we know about how WDR5 functions in cancer cells and how WDR5 WIN site inhibition can best be used for therapeutic benefit.

Inhibitors of the WDR5 WIN site

Several WDR5 WIN site inhibitors with a range of WDR5 binding affinities and biochemical properties have been described. One of the earliest small molecule WDR5 WIN site inhibitors, WDR5-0103, was reported in 2013 (Senisterra, Wu et al. 2013). WDR5-0103 has a moderate WDR5 binding affinity with a K_d of 450 nM. *In vitro* MLL1 histone methyltransferase assays were used to assess the ability of the compound inhibit MLL1 HMT activity and thus to displace binders of the WIN site. WDR5-0103 only weakly inhibited the catalytic activity of MLL1 *in vitro* with an IC_{50} of 39 μM. No experiments investigating the effects of WDR5-0103 in cells were shown.

The WDR5 WIN site small molecule inhibitor, OICR-9429, was discovered at the same institution as WDR5-0103. OICR-9429 is more potent than WDR5-0103 and binds to WDR5 with a K_d of 93 ± 28 nM and a co-crystal structure clearly demonstrates that OICR-9429 binds the WIN site of WDR5 (Grebien, Vedadi et al. 2015). OICR-9429 has been studied in the context of acute myeloid leukemia expressing the C/EBPα p30 mutation. OICR-9429 decreases the amount of MLL1 that co-immunoprecipitates with WDR5 in a dose dependent manner, demonstrating that it can displace proteins from the WIN site. Treatment of C/EBPα p30 cells with OIRC-9429 increased expression of myeloid differentiation markers and induced morphological changes indicating differentiation. Additionally, OICR-9429 treatment selectively reduced viability of AML patient leukemia cells with mutations in the C/EBPα N-terminus but had little effect on the viability of AML patient cells with other types of mutations. OICR-9429 was also shown to have anti-proliferative effects in colon cancer cell lines that over-express WDR5

(Neilsen, Chakraborty et al. 2018) and p53 gain-of-function cell lines(Grebien, Vedadi et al. 2015). Interestingly, experiments utilizing OICR-9429 in the context of MLL-fusion leukemia have not been published.

Recently, a high-throughput screen of 592 FDA approved drugs sought to find drugs that inhibit MLL1 activity (Zhang, Zheng et al. 2018). Piribedil was identified as an inhibitor of MLL1 by blocking WDR5/MLL1 interaction. Piribedil was approved for the treatment of Parkinson's disease. Piribedil demonstrated selective growth inhibition for leukemia cell lines expressing MLL-fusions but not a non-MLL fusion cell line. However, the proliferation assay GI_{50}s for the MLL-fusion cell lines were found to be extremely high (65 μM - 92 μM), indicating that Piribedil has only weak biological activity against MLL-fusion leukemias. Nonetheless Piribedil was shown to selectively reduce clonogenicity, induce apoptosis, decrease expression of MLL1 and MLL1-fusion target genes, and decreased global levels of H3K4me3 and H3K4me2 in MLL-fusion cell lines but not non-MLL-fusion cells. While the data reported for Piribedil is certainly intriguing, the concentrations used were extremely high (up to 160 μM), making it difficult to determine if the effects seen are specific for WDR5 WIN site inhibition. In fact, no K_d for the affinity of Piribedil for WDR5 nor direct evidence that Piribedil binds the WIN site, such as a co-crystal structure, were reported. Combined with possible unwanted effects on brain chemistry as a dopamine receptor agonist, the weak activity in leukemia cells make Piribedil unlikely to be a strong clinical candidate for cancer treatment.

Much more convincing validation of the WDR5 WIN site as a therapeutic target in MLL-leukemia has been provided by studies utilizing the cyclic peptidomimetic MM-401 that binds the WIN site of WDR5 with a K_d of ~ 1nM (Cao, Townsend et al. 2014). MM-401 was optimized from the earlier and less potent linear pepitodomemetic MM-101 made by the same group (Karatas, Townsend et al. 2013). Like the the arginine of a WIN motif, an arginine guanidinium moiety of MM-401 inserts into the central pore of the WIN site where it is sandwiched by the aromatic rings of F133 and F263 (Cao, Townsend et al. 2014). MM-401 inhibits MLL1 HMT activity with an IC_{50} of 320 nM *in vitro*, but does not inhibit the catalytic activity of MLL2, MLL3, MLL4 or SET1A. MM-401 selectively reduces proliferation of MLL-AF9 transformed mouse bone marrow cells with a GI_{50} of ~10 µM, but did not inhibit normal bone marrow progenitor cells. MM-401 was also shown to induced dose-dependent apoptosis and G1 arrest, and induce morphological changes indicative of differentiation of MLL-AF9 transformed mouse bone marrow cells. Testing

of MM-401 in human leukemia cell lines showed moderate proliferative inhibition for MLL-fusion cell lines with GI_{50}s ranging from ~12-30 μM. Finally, MM-401 modestly reduced levels of H3K4me3 and me2 at MLL1 targets genes that have been implicated in promoting MLL-leukemogenesis (Cao, Townsend et al. 2014), fueling the assumption that WDR5 WIN site inhibitors function by blocking MLL HMT activity. Recently, a more potent cyclic peptidomimetic, MM-589, was discovered by the same group (Karatas, Li et al. 2017). MM-589 binds WDR5 with an IC_{50} of 0.90 nM and inhibits the MLL1 H3K4 HMT activity *in vitro* with an IC_{50} of 12.7 nM. No mechanistic or cellular investigations have been published to date for MM-589. In sum, the use of MM-401 helped to solidify the WIN site as a therapeutic target in MLL-leukemia.

The data validating WDR5 as a therapeutic target in MLL-fusion cells obtained for MM-401 was subsequently corroborated by the use of the monobody, Mb(S4) (Gupta, Xu et al. 2018). Mb(S4) is a synthetic peptide that binds the WIN site of WDR5 and can be ectopically expressed in cells. Mb(S4) was shown to inhibit WDR5/MLL1 and WDR5/histone H3 peptide interaction in *in vitro* pull-down assays, demonstrating its ability to block the WIN site. Mb(S4) has a binding affinity for WDR5 with a K_d of 5 nM and inhibits MLL1 HMT activity *in vitro*. Induction of Mb(S4) expression in MLL-AF9 transformed mouse bone marrow cells causes a 2-fold reduction in expression of genes associated with MLL-leukemogenesis, induced differentiation and reduced colony formation. *In vivo* proof of principle for targeting the WIN site of WDR5 was provided by inducing expression of Mb(s4) in established MLL-AF9 tumors in mice, resulting in increased leukemia latency and animal survival compared to a mutant version of Mb(S4) that does not bind WDR5. Together, these data validate the WIN site as a therapeutic target, but a lack of detailed mechanic studies makes it unclear how Mb(S4) brings about cell death in MLL-fusion cells. Additionally, Mb(S4) requires ectopic expression in cells to function and so it can not be used a cancer therapeutic.

While the previously published WDR5 WIN site inhibitors have provided information needed to validate the WIN site as a therapeutic target in leukemia cells harboring an oncogenic MLL-fusion, little is known about the direct effects of these inhibitors. Long-time points of three days up to weeks of treatment were used in previous WDR5 inhibitor studies (Cao, Townsend et al. 2014, Gupta, Xu et al. 2018) due to the fact that other epigenetic inhibitors targeting MENIN, DOTL1 and EZH2 take about a week to induce cellular effects (Knutson, Wigle et al. 2012, Daigle, Olhava et al. 2013, Borkin, He et al. 2015). The rational for why these inhibitors take so

long to affect cancer cells is because the existing histone methylation is believed to be stable and thus takes a long time to be removed or diluted by cell division. However, only investigating the effects of WDR5 WIN site inhibitors after several days of treatment makes it hard to separate the direct and indirects effects. Therefore, the development of novel highly potent WDR5 WIN site inhibitors, coupled with an experimental approach that can determine the direct effects of WIN site inhibition has tremendous value. Understanding precisely how WDR5 WIN site inhibitors function and the genes that are regulated by WDR5 is imperative to define how WDR5 WIN site inhibitors can be used as a cancer therapeutic approach.

Summary of Thesis

The WIN site of WDR5 is an established pharmacological target in MLL-fusion leukemias, yet the mechanisms through which targeting this site functions is unclear. The work presented in this thesis utilize two novel WDR5 WIN site inhibitors discovered by the Fesik Laboratory, C3 and C6. C3 and C6, along with their respective regioisomeric negative controls, were used to challenge the assumption that WDR5 WIN site inhibitors function in MLL-leukemia cells by blocking the histone methyltransferase (HMT) activity of MLL1 and to elucidate the repertoire of genes that are regulated by WDR5. C3 and C6 both selectively inhibit the HMT activity of MLL1 but not other MLL family HMTs *in vitro*. We also found that C3 and C6 are able to engage WDR5 in living cells and do so in a manner that correlates with their relative affinities for WDR5. I then empirically determined that sensitivity of leukemia cell lines to WDR5 WIN inhibition correlates with expression of an oncogenic MLL-fusion protein and wild-type p53, suggesting that p53 may be involved in cellular response to WDR5 WIN site inhibition. Time course analyses of sensitive cells treated with our WDR5 WIN site inhibitors allowed me to determine that changes in cell fate, such as cellular proliferation inhibition and apoptotic marker induction, can be seen within the first several days of inhibitor treatment. Thorough evaluation of the early and primary effects of WDR5 WIN site inhibitors was previously lacking and therefore this became a focused of my studies. By utilizing chromatin immunoprecipitation (ChIP) and ChIP-seq, we found that WDR5 is not bound to genes classically associated with MLL-leukemia, as was previously assumed, but instead WDR5 is enriched at a discrete set of ribosomal protein genes (RPGs) that is conserved across disparate cell types. We demonstrate that the primary mechanism of action of WDR5 inhibitors is the rapid and comprehensive displacement of WDR5 from chromatin at WDR5-bound genes. In doing so, we uncovered that the WIN site is required to tether WDR5 to

chromatin. By using PRO-seq, we attained superb temporal resolution in the transcriptional changes that occur in response to WDR5 WIN site inhibition. We determined that WDR5-bound RPGs are the direct transcriptional targets of WDR5 WIN site inhibitors and they are repressed within minutes of compound treatment. Although C3 and C6 both potently and selectively inhibit MLL1 histone methyltransferase activity *in vitro*, I found that the cellular response to WDR5 WIN site inhibition is likely not related to inhibition of MLL1 HMT function, as H3K4me3 is not reduced at WDR5-regulated genes after WDR5 displacement. The use of RNA-seq subsequently allowed elucidation of the long-term secondary effects of WIN site inhibition on mRNA expression. We determined that compound treatment induces genes that regulate the cell cycle and DNA synthesis in sensitive cells and that a significant proportion of the secondary gene expression changes overlap with those seen after p53 induction. Aligned with this observation, I found that p53 protein levels are elevated upon WDR5 WIN site inhibition and that knock-down and knock-out of p53 both rescue sensitivity to compound treatment. Finally, consistent with the decrease in expression of genes encoding protein synthesis machinery, I found that WDR5 WIN site inhibition initiates a translation choke and induces nucleolar stress in sensitive cells. In sum, these data define a conserved set of genes that are regulated by WDR5, the primary and secondary effects of WDR5 WIN site inhibitors, and how the cellular responses of sensitive and insensitive leukemia cell lines are the same and different.

CHAPTER II

MATERIALS AND METHODS

High Through-put Chemical Fragment Screening and Chemical Synthesis

The methods used to perform the initial fragment screening to identify WDR5 WIN site-binding chemical fragments and the chemical synthesis of the compounds reported in this thesis have been extensively described in previous publications (Wang, Jeon et al. 2018, Aho, Wang et al. 2019). Because the medicinal chemistry was performed outside of the Tansey Lab by the chemists in the Fesik laboratory, the methods pertaining to compound synthesis will not be detailed here. Please refer to the aforementioned publications for further details.

Histone Methyltransferase Assays

HMT inhibition activity assays were performed at Reaction Biology Corp. Briefly, each of the purified HMT enzymes (MLL1, MLL2, MLL3, MLL4, SETD1A or SATD1B) were mixed with the purified regulatory subunits WDR5, RBBP5, ASH2L and DPY30 to form active HMT complexes. Complexes were incubated with increasing doses of C3, C6, or the negative control compounds, tritiated SAM (S-adenosyl-L-[methyl-^{3}H]methionine) as the methyl group donor, and the substrate. For MLL1, MLL2, MLL3, and MLL4 complexes an H3 peptide was used as the substrate; For SETD1A and SETD1B complexes core histones were used as the substrate. The amount of tritiated methylation transferred to the substrate was measures and IC_{50}s for the inhibition of HMT activity were calculated.

Proliferation Assays

I completed proliferation assays with the help of Ms. Shelly Lorey. Cell proliferation was assayed using the Promega CellTiter-Glo Luminescent Kit. White, opaque, flat-bottomed 96-well plates were used. 5,000 cells were seeded per well for all cell lines in three-day assays, except 2,000 cells were seeded for MA93, MA93Ras, and MA93 FLT3/ITD to prevent overgrowth. For seven day assays 600 cells were seeded per well. Cells were treated with 0.1% DMSO vehicle only and at least five two-fold dilutions of WDR5 inhibitors with a top concentration of 50 μM. Final DMSO concentration was 0.1% in all compound treatment experiments. Each concentration of

inhibitor was tested in triplicate wells and at least two biological replicates were performed. The total volume of cells with inhibitor was 100 μl per well. 200 μl of sterile PBS was added to all of the empty wells around the edge of the plate to prevent evaporation. Three and seven-day proliferation assay plates were incubated at 37^{o}C for the appropriate amount of time. After incubation, the plates were allowed to reach room temperature before adding 50 μl of CellTiter-Glo reagent per well. Plates were incubated at room temperature, covered from light, for 30 minutes before the luminescence was measured using the CellTiter-Glo protocol on a GloMax plate reader. MTS assay (Promega CellTiter 96 AQ_{ueous} Non-Radioactive Cell Proliferation Assay kit) was used to measure proliferation of RN2 cells. 2,500 cells were seeded into clear, flat-bottomed 96-well plates and treated with inhibitors as stated above. After a 72-hour incubation, 20 μl of MTS solution was added per well and plates were incubated at 37^{o}C for 1.25 hours, then absorbance at 490 nm measured using a Bio-Rad iMark Microplate reader. For both CellTiter-Glo and MTS assays, the raw luminescence values were normalized to the DMSO vehicle only wells and PRISM software was used to generate GI_{50} values. Error bars on proliferation curves represent standard errors of the mean.

Growth and Viability Time Course

MV4:11 cells were plated at a density of 1 x 10^5 cells/ml and treated with 0.1% DMSO only, 2 μM C6 or 2 μM C6nc. After 1, 2, 3, and 6 days, cells were stained with trypan blue and counted using an automated cell counter. Viability and cell density was measured three times for each sample at each time point, then averaged. On day 3, cells were spun down and resuspended in fresh media with fresh compound added. DMSO and C6nc-treated cells were replated to 1 x 10^5 cells/ml to prevent overgrowth. The time course was repeated with three biological replicates and error bars represent the standard error of the mean.

Cellular Thermal Shift Assay (CETSA)

CETSA was completed by our collaborators Dr. Ken Cheng and Dr. Mathew Hall at the National Center for Advancing Translational Sciences (NCATS) as previously described (Jafari, Almqvist et al. 2014). To determine the melting temperature of WDR5, K562 or MV4:11 cells were dispensed into PCR tubes at a density of ~1,000,000 cells/tube in 99 μl of DMEM. One microliter of DMSO was added to each tube and the cell suspension mixed by vortexing. Cells were then subjected to 3 minutes of heat in a 96-well thermal cycler at temperatures of 46, 50, 54, 58, 62, 66, 70, 74, 78, 82, 86, and 90^{o}C. Immediately after heating, cells were snap frozen in

a CoolSafe Chamber (USA Scientific) surrounded by dry ice. To perform the isothermal dose-response of compounds against WDR5, K562 or MV4:11 cells were dispensed into PCR tubes at a density of ~1,000,000 cells/tube in 99 μl of DMEM. One microliter of compound, or DMSO, was added to each tube, mixed by vortexing, and incubated at 37^{o}C for one hour. Cells were then heated at 79 ^{o}C for 3 minutes in a 96-well thermal cycler. Immediately after heating, cells were snap frozen prior to lysate preparation. To prepare cell lysates, frozen cells were subjected to six rapid freeze-and-thaw cycles. After the first thaw, 1 μl of protease inhibitor cocktail (Sigma) was added to the cell lysates. Cell lysates were centrifuged at 4^{o}C and 20,000 × g for 20 minutes. Samples were prepared by transferring 60 μl of supernatant into 20 μl of NuPAGE 4X LDS sample buffer (ThermoFisher) with 5 μl NuPAGE Sample Reducing Agent (10X) (ThermoFisher) and then heated for 15 minutes at 95^{o}C. Note that in this experiment, cells without the 3-minute heating served as 100% stabilization and used for normalization purpose. Protein lysates were separated on a NuPAGE Novex 4-12% Bis-Tris gel (ThermoFisher) and transferred onto PVDF membrane using an iBlot 2 Dry Blotting System (ThermoFisher). Membranes were blocked overnight with 5% nonfat dry milk (BIO-RAD) in PBST–Phosphate Buffered Saline (ThermoFisher) with 0.5 % Tween-20 (Sigma). Membranes were then incubated for 1 hour with 1:1,000 of rabbit monoclonal anti-WDR5 (D9E1I) antibody, washed three times for 15 minutes in PBST, incubated with 1 : 1,000 anti-rabbit HRP linked IgG. After washing three times for 15 minutes in PBST, blots were incubated with SuperSignal West Dura Extended Duration Substrate (ThermoFisher). The chemiluminescence signals were captured by BIO-RAD CHEMDOC Imaging System, quantified by ImageQuant TL (GE Healthcare) and analyzed using Prism (GraphPad). Error bars on proliferation curves represent standard errors of the mean. Two independent biological replicates were performed.

Cell Cycle Analysis

Cell cycle analyses were performed as described (Kim and Sederstrom 2015), with slight modification. MV4:11 cells were treated for 0, 1, 2, 3 or 6 days with 2 μM C6, 2 μM C6nc, or 0.1% DMSO vehicle control. Fresh media and compound was added on day three. At each time point, one million cells were collected per sample and washed once with PBS then resuspended in 500 μl of PBS. Cells were fixed by adding cells drop-wise to 4.5 mL ice cold 70% ethanol while vortexing, then incubated for at least two hours at -20^{o}C. Cells were washed in FACS buffer (PBS with 2% FBS, 1 mM EDTA) then stained with 500 μl PI Staining Solution (PBS with

10 μg/mL propidium iodide, 100 μg/mL RNase, 2 mM $MgCl_2$) for 20 minutes at room temperature, protected from light. Propidium iodide fluorescence was measured using a BD LSR II Flow Cytometer and cell cycle distribution was analyzed using BD FACSDIVA software. At least 10,000 events were recorded per sample. Doublets were excluded prior to analysis of cell cycle distribution. The time course was repeated with three biological replicates and error bars represent the standard error of the mean. Flow Cytometry experiments were performed in the Vanderbilt University Flow Cytometry Shared Resource.

Induction of Apoptosis

MV4:11 cells were treated for 0, 1, 2, 3 or 6 days with 2 μM C6, 2 μM C6nc, or 0.1% DMSO only. Fresh media and compound was added on day 3. As a positive control for apoptosis induction, cells were treated with 2 μM Camptothecin for 4 hours. $5x10^5$ cells were collected per sample and resuspended in 100 μl of 1x Annexin V Binding Buffer (Invitrogen V13246). 0.5 μl of Alexa Flour488-conjugated Annexin V (Thermo A13201) was added per sample, then incubated for 15 minutes. Cells were resuspended in 400 μl fresh 1x Annexin V Binding Buffer + 10 ng of propidium iodide and incubated for 10 minutes. Samples were then kept on ice and Alexa Flour488 and propidium iodide fluorescence was measured using a BD LSR II Flow Cytometer and the percentage of apoptotic cells was analyzed using FlowJo software. At least 10,000 events were recorded per sample. After doublet exclusion, an unstained control sample was used to set the quadrant gating. The time course was repeated with three biological replicates and error bars represent the standard error of the mean. Flow Cytometry experiments were performed in the Vanderbilt University Flow Cytometry Shared Resource.

Induction of PARP1 cleavage

MV4:11 cells were treated for 1, 2, 3 or 6 days with 2 μM C6nc and C6, or 0.1% DMSO only. Four million cells were washed in PBS then lysed for 10 minutes on ice in 200 μl Kischkel buffer (50 mM Tris pH 8.0, 150 mM NaCl, 5 mM EDTA, 1% Triton X100, Protease inhibitor cocktail, 1 μM PMSF). Whole cell extracts were sonicated for 15 seconds then clarified by centrifugation. Laemmli Sample buffer was added and samples were boiled for 10 minutes before running on a 4-20% mini-PROTEAN TGX gel (BioRad) and transferring to PVDF membrane. Membranes were blocked in 5% milk in TBST for 20 minutes then probed with appropriate antibodies.

Chromatin Immunoprecipitation (ChIP)

ChIP assays were performed as described (Thomas, Wang et al. 2015). Cells were treated with inhibitors, as indicated, then washed in PBS and cross-linked with 0.75–1% formaldehyde at room temperature for 10 minutes. The reaction was quenched with 125 mM glycine for 10 minutes at room temperature, after which cells were washed with ice cold PBS. Cells were lysed in Formaldehyde Lysis Buffer (50 mM HEPES pH 7.5, 140 mM NaCl, 1 mM EDTA, 1% Triton, 1% SDS, and Complete Protease Inhibitor cocktail) using 250 μl of buffer per $1x10^7$ cells, on ice, for 10 minutes. Chromatin was sheared by 25-minute sonication (BioRuptor) to yield a mean chromatin size of ~250 bp, and debris cleared by centrifugation. Sheared chromatin was diluted 10-fold in Formaldehyde Lysis Buffer without SDS before immunoprecipitation overnight at 4^{o}C using the appropriate antibody and Protein A agarose. Chromatin from 6 million cells was used per reaction. Immune complexes were washed sequentially with Low Salt Wash buffer (20 mM Tris pH 8.0, 150 mM NaCl, 2 mM EDTA, 1% Triton), High Salt Wash Buffer (20 mM Tris pH 8.0, 500 mM NaCl, 2 mM EDTA, 1% Triton), LiCl Wash buffer (25 mM LiCl, 1 mM EDTA, 1% Triton) and twice with TE (pH 8.0). Protein–DNA complexes were de-crosslinked overnight at 65^{o}C in Elution Buffer (TE, 0.1% SDS, 40 μg Proteinase K). Proteinase K was heat inactivated for 20 minutes 95^{o}C then 150 μl of TE was added. 1 μl of DNA was used in a 15 μl PCR reaction using KAPA SYBR FAST qPCR Master Mix 2X Universal and quantified on an Eppendorf Realplex2 Mastercycler in triplicate. ChIP signals were calculated as percent input. ChIP experiments were completed in biological triplicate with error bars representing the standard error of the mean. ChIP primer sequences are shown in Table 1.

Chromatin Immunoprecipitation–Sequencing (ChIP-seq)

The ChIP-seq assays were completed by Dr. Caleb Howard. MV4:11 cells were grown to 10^6 cells/ml and treated for 4 hours with 0.1% DMSO, 2 μM C6, or 2 μM C6nc. Cells were concentrated to 4 x 10^6 cells/ml in PBS and cross-linked with 1% formaldehyde for 10 minutes at room temperature followed by quenching with 125 mM glycine for 10 minutes. Cells were washed with ice-cold PBS and lysed in 250 μl 1% SDS FA Buffer (50 mM HEPES, pH 7.5; 140 mM NaCl; 1 mM EDTA; 1% Triton X-100; 1% SDS; 1x Roche Protease Inhibitor, EDTA-Free) per 10^7 cells and incubated on ice for 10 minutes. Chromatin was sheared with a Bioruptor (Diagenode, UCD-200) on highest setting, alternating between 30 seconds on/30 seconds off, to achieve an average fragment size of ~250 nucleotides; cellular debris was then cleared through centrifugation for 10 minutes at 16k g at 4^{o}C. Sheared chromatin was diluted ten-fold

Table 1. ChIP and mRNA primer sequences
SNHG15 Ebox ChIP primer (left): CGCCACTGAACCCAATCC
SNHG15 Ebox ChIP primer (right): TCTAGTCATCCACCGCCATC
SNHG15 Gene Body ChIP primer (left): AATTATGTGTCCAGGGTTGC
SNHG15 Gene Body ChIP primer (right): CACCGGCTTCTATATTCCAC
HOXA9 pr#1 ChIP primer (left): ACGAATCTGTTGGTCGTTTC
HOXA9 pr#1 ChIP primer (right): AATCGCATTGTCGCTCTAC
HOXA9 pr#2 ChIP primer (left): TCGTTGGCCACAATTAAAAC
HOXA9 pr#2 ChIP primer (right): TTAATGGTCCGATGTTTTGC
HOXA9 exon 1 ChIP primer (left): CCACGCTTGACACTCACACT
HOXA9 exon 1 ChIP primer (right): CTTCGCTGGGTTGTTTTTCT
HOXA9 intron 1 ChIP primer (left): AGCCCAGCGCGCCTTTTGTA
HOXA9 intron 1 ChIP primer (right): GCAAGAAGTGGAAGGAATCG
HOXA9 intron 2 ChIP primer (left): TTTGAGAGTGGGAGGAAGGA
HOXA9 intron 2 ChIP primer (right): TGCACGCAGTAAAACTTTGG
HOXA9 3’ UTR ChIP primer (left): TTTTTGCACCAGACGAACAG
HOXA9 3’ UTR ChIP primer (right): TCAGCATTCATTTCCTCCAA
MYOD1 exon 1 ChIP primer (left): TCTATGACGACCCGTGTTTC
MYOD1 exon 1 ChIP primer (right): GAGTGCTCTTCGGGTTTCAG
MYOD1 intron 1 ChIP primer (left): ACCCCAGGAAGTGAGGAAGT
MYOD1 intron 1 ChIP primer (right): ACAAGGGGGTCCTCTCTCTC
MYOD1 intron 2 ChIP primer (left): CTCCTCCTTCATGGAGCTGT
MYOD1 intron 2 ChIP primer (right): TTCATCTCCTGCACCACTTC
MYOD1 3’ UTR #1 ChIP primer (left): GAGACCCTCGCAGACCTAAG
MYOD1 3” UTR #1 ChIP primer (right): GGGTTACGGTTACACCTGCT
MYOD1 3’ UTR #2 ChIP primer (left): ATGGTGTGTGGTGCTACAGG
MYOD1 3’ UTR #2 ChIP primer (right): CCACGGCGGTATAAATTAGC
SNHG15 -250 to - 171 ChIP primer (left): CAGGACCCTAAACTCTACGC
SNHG15 -250 to - 171 ChIP primer (right): AGCGTTTGGGGTAGATGAC
SNHG15 + 260 to +357 ChIP primer (left): ACCCCAGTAGGTGGGATG

Table 1. ChIP and mRNA primer sequences (continued)
SNHG15 + 260 to +357 ChIP primer (right): CCCACTCTACAGCCTCTCTT
SNHG15 + 476 to +580 ChIP primer (left): TTCCTCAGGGAAAATTAAACC
SNHG15 + 476 to +580 ChIP primer (right): CCTTGGGAATGAACAGGAG
SNHG15 + 616 to +709 ChIP primer (left): TCTACTTCATGTGCCTGGTC
SNHG15 + 616 to +709 ChIP primer (right): AATACTGCCTTTTCCCCTTC
SNHG15 + 1210 to +1309 ChIP primer (left): AGATCCGTGCCATCTAATGT
SNHG15 + 1210 to +1309 ChIP primer (right): TAGTCATCTGAAATGTGGCTA
RPL35 ChIP primer (left): ACAGGCCTAGGTGGCAGATA
RPL35 ChIP primer (right): ATGGTGAGAGCTGCGGAAT
RPS24 ChIP primer (left): AGTCATCTGCCGCGTATCC
RPS24 ChIP primer (right): GACAGAAACGGCCAGAGAAG
RPL23 ChIP primer (left): TCCTGCCATCTCAACTCTCC
RPL23 ChIP primer (right): GCGCTTTGCTCTCCTTCAG
EIF4G3 ChIP primer (left): CCTTTCACGGCAATATCCTC
EIF4G3 ChIP primer (right): GAAGAAAATCCACCGGCATC
SERBP1 ChIP primer (left): CTTGTTCTCTGCTGCCTTCA
SERBP1 ChIP primer (right): ATCATGCCTGGGCACTTACA
E2F3 ChIP primer (left): CTCCAGAGCCCCGATTATTT
E2F3 ChIP primer (right): AGCCCCCTCTCTCTCTTTTC
RPL35 mRNA primer (left): AACAGCTGGACGACCTGAAG
RPL35 mRNA primer (right): ACTGTGAGAACACGGGCAAT
RPL14 mRNA primer (left): GTCTCCTTTGGACCTCATGC
RPL14 mRNA primer (right): ATGGCCTGTCTCCTCACTTG
RPS24 mRNA primer (left): GACACCGTAACTATCCGCACT
RPS24 mRNA primer (right): TCTTAGGCACTGTCGCCTTC
RPS11 mRNA primer (left): TCCCGCGGTACTACAAGAAC
RPS11 mRNA primer (right): ACCAGTGAAGGGGCATTTC
GAPDH mRNA primer (left): AAGGTGAAGGTCGGAGTCAAC
GAPDH mRNA primer (right): GTTGAGGTCAATGAAGGGGTC
TP53 mRNA primer (left): AATTTGCGTGTGGAGTATTT
TP53 mRNA primer (right): GTACAGTCAGAGCCAACCTC

Table 1. ChIP and mRNA primer sequences (continued)
TP53INP1 mRNA primer (left): CTTCCTCCAACCAAGAACCA
TP53INP1 mRNA primer (right): CTGCTGAGAAACCAGTGCAA

with 0% SDS FA Buffer to achieve a final concentration of 0.1% SDS and IgG or appropriate anti-WDR5 antibody added. Samples were rotated overnight at 4°C. Protein-A agarose beads (Roche, 11 134 515 001) were washed three times with 1% FA Buffer and blocked for 20 minutes on rotator with 10 μg BSA and 100 μl 1% SDS FA Buffer per 15 μl bed volume of Protein-A agarose beads. 100 μl blocked bead slurry was added to each sample and rotated for 4 hours at 4°C. Beads were washed by rotating beads for 5 minutes at room temperature with 1 ml of the following buffers: once with Low Salt Buffer, once with High Salt Buffer; once with LiCl Wash Buffer; and twice with TE. Washed chromatin-bound beads were suspended in 50 μl TE, 5 μl 1% SDS, and 1 μl Proteinase K and incubated overnight at 65°C. The following day, 300 μl TE was added and protein removed by phenol chloroform extraction. DNA was precipitated by adding 36 μl 3 M NaOAc, pH 5.2, 10 μg glycogen, and 1 ml 100% ethanol and centrifugation for 10 minutes at 16k g at 4°C. DNA pellets were washed once with 70% ethanol and air dried. DNA pellets were suspended in 100 μl TE and used for next generation sequencing (NGS) library preparation. Indexed libraries were made using the DNA Ultra II Library Prep Kit for Illumina (New England BioLabs, Inc., E7645). Library quality was assessed using the 2100 Bioanalyzer (Agilent) and libraries were quantitated using KAPA Library Quantification Kits (KAPA Biosystems). Pooled libraries were subject to 50 bp single-end sequencing according to the manufacturer's protocol (Illumina HiSeq 3000). Sequencing was performed by the Vanderbilt Technologies for Advanced Genomics (VANTAGE) Shared Resource. Bcl2fastq2 Conversion Software (Illumina) was used to generate de-multiplexed Fastq files.

Cellular Fractionation

These assays were performed as described (Mendez and Stillman 2000)**.** MV4:11 cells were treated for 4 hours with 36 μM C3 or 0.1% DMSO only. 1 x10^7 cells were collected and washed twice in PBS. Cells were resuspended in 200 μl Buffer A [10 mM HEPES, pH 7.9, 10 mM KCl, 1.5 mM $MgCl_2$, 0.34 M sucrose, 10 % glycerol, 1 mM DTT (added fresh), 1x protease inhibitor cocktail (added fresh)] and incubated on ice for 8 minutes. Samples were centrifuged at 1,300 x g at 4°C for 5 minutes. The supernatant (S1 fraction) and pellet (P1 fraction) were separated and S1 was clarified by high-speed centrifugation at 4°C for 10 minutes. The resulting supernatant (S2 fraction) was collected and the pellet (P2 fraction) was discarded. The P1 fraction was washed once with 500 μl Buffer A and centrifuged 1 minute at 1,300 x g. The P1 fraction was lysed by resuspending in 100 μl Buffer B [3 mM EDTA, 0.2 mM EGTA, protease inhibitor cocktail (added just before use)] and incubating for 30 minutes on ice, followed by

centrifugation at 1,700 x g at 4C for 5 minutes. The resulting supernatant (S3 fraction) was separated from the chromatin-enriched pellet (P3 fraction). P3 was washed once with 500 μl Buffer B and resuspended in 100 μl SDS sample buffer and boiled for 10 minutes. 5% of each fraction was run on an 8% SDS-PAGE gel and protein distribution probed by Western blotting.

Immunofluorescence and Confocal Microscopy

General procedures for immunofluorescence were taken from (Nicolae, Aho et al. 2014). For nucleophosmin (NPM) staining, cells were treated for 72 hours with 4 μM C6, 4 μM C6nc or 0.1% DMSO only. For γ-H2AX staining, cells were treated for 24 hours with 4 μM C6, 4 μM C6nc or 0.1% DMSO only. As a positive control for DNA damage, cells were treated for 1 hour with 2 μM camptothecin. As a positive control for nucleolar stress, cells were treated with 5 nM actinomycin D for 6 hours (Burger et al., 2010). Cells were washed once in PBS, then 100,000 cells/sample were attached to slides via a Cytospin for 3 minutes at 800 rpm. Cells were fixed with 4% paraformaldehyde for 10 minutes at room temperature, followed by extraction with 0.3% Triton X100 for 10 minutes on ice. Slides were blocked with 5% BSA + 0.1% Triton X100 in PBS for 30 minutes at room temperature. Primary antibody was added (1:5,000 Abcam ab11174 for γ-H2AX, and 1:2,000 Sigma B0556 for NPM) in PBS with 3% BSA and incubated overnight at 4°C. After washing in PBS, secondary antibody [1 drop Alexa Fluor488 goat anti-Rabbit ReadyProbes Reagent (Thermo R37116) in 3 mL PBS for γ-H2AX or 1:2,000 Alexa Fluor488 goat anti-mouse IgG (Thermo A11001) in 3% BSA in PBS for NPM] was added and incubated for 1 hour at room temperature. Slides were washed in PBS, then nuclei were counterstained with 20 μM DRAQ5 in PBS for 10 mins at 37°C. Slides were mounted with ProLong Diamond Antifade mountant. Images were collected using a Leica TCS SP5 scanning confocal microscope. Nuclear γ-H2AX staining intensity was quantified for all cells in 5 representative fields of view imaged with the same laser power and gain settings with Fiji software (Schindelin, Arganda-Carreras et al. 2012) and plotted in Prism with error bars representing the standard deviation. The ratio of nuclear to nucleoplasmic NPM staining in individual cells from two biological replicates was quantified using Fiji and plotted in Prism with error bar representing the standard deviation. Prism was used to perform a one-way ANOVA with a post-hoc Dunnett's test in order to compare the mean of each treatment to that of the DMSO-only treated control sample for both the mean nuclear gamma-H2AX signal and ratio of nucleolar to nucleoplasmic NPM staining quantifications. Level of significance was determined using a 95% confidence interval.

Precision nuclear run-on sequencing (PRO-Seq)

PRO-seq was performed by Dr. Pankaj Archaya. 30 million MV4:11 cells were treated with compound C3 and harvested after either 15, 30, or 60 minutes. As a reference control, cells were treated with 0.1% DMSO for 60 minutes. Cells were washed twice with cold PBS, resuspended in 10 ml of cold swelling buffer (10 mM Tris-Cl pH 7.5, 2 mM $MgCl_2$, 3 mM $CaCl_2$, 300 mM Sucrose, protease inhibitors), and incubated on ice for 5 minutes. After incubation, cells were pelleted by centrifugation, resuspended in 2 ml cell lysis buffer (swelling buffer + 10% glycerol + 0.1% Triton X-100) and incubated on ice for 5 minutes. Cells were then Dounce-homogenized 50 times, after which 5 ml of lysis buffer was added and nuclei collected by centrifugation. The nuclei were washed once with 5 ml lysis buffer, followed by one wash with 1 ml freezing buffer (50 mM Tris-Cl pH 8.3, 40% glycerol, 5 mM $MgCl_2$, 0.1 EDTA), resuspended in freezing buffer at density of 2 x 10^7 nuclei/100 µl, and stored at -80^{o}C until nuclear run-on assays could be performed.

Nuclear run-on assays were performed as described (Kwak, Fuda et al. 2013). Briefly, nuclei were thawed on ice and 2 x 10^7/100 µl nuclei added to an equal volume of pre-warmed 2x nuclear run-on reaction mix (10 mM Tris-Cl pH 8.0, 300 mM KCl, 1% Sarkosyl, 5 mM $MgCl_2$, 1 mM DTT, 375 µM ATP, biotin-11-CTP, GTP and UTP, and 0.8 U/µl SuperaseIN). Run-on reactions were performed for three minutes at 30^{o}C, and then terminated by addition of three volumes of TRIzol LS. RNA was extracted and precipitated in isopropanol, followed by a 75% ethanol wash. Extracted RNA was fragmented by base hydrolysis using 0.2 M NaOH on ice for 10 minutes. After incubation, the reaction was neutralized by addition of one volume of 1 M Tris-Cl, pH 6.8. Thirty microliters of Dynabeads® MyOne™ Streptavidin T1 magnetic beads (Invitrogen) were then added to collect biotinylated RNA fragments, and incubated on a nutator for 20 minutes at room temperature according to the manufacturer's instructions. After incubation, beads were sequentially washed with high salt (2M NaCl, 50 mM Tris-Cl pH 7.4, 0.5% Triton X-100), medium salt (300 mM NaCl, 10 mM Tris-Cl pH 7.4, 0.1% Triton X-100), and low salt (5 mM Tris-Cl pH 7.4, 0.1% Triton X-100) wash buffers. RNA was eluted from the beads by two TRIzol extractions followed by isopropanol precipitation and a 75% ethanol wash.

3’ RNA adaptor ligation was carried out in a 10 µl reaction containing 10 pmol of 3’ RNA adaptor, 10 U T4 RNA ligase I (NEB), 10 nmol of ATP, and SuperaseIN, at 20^{o}C for 6 hours. Adaptor-ligated biotinylated RNA was purified by Streptavidin bead binding and RNA extraction as

described above. The 5' ends of RNA fragments were repaired by incubation with Tobacco Acid Pyrophosphatase (TAP, Epicentre), followed by Polynucleotide Kinase (PNK, NEB) treatment according to manufacturer's instructions. RNA was extracted using TRIzol and precipitated with isopropanol followed by a 75% ethanol wash. 5' RNA adaptor ligation was carried out in a 10 µl reaction containing 10 pmol of 5' RNA adaptor, 10 U T4 RNA ligase I, 10 nmol ATP, and SuperaseIN, at 20°C for 6 hours. Adaptor-ligated biotinylated RNA fragments were purified by Streptavidin bead binding and TRIzol extraction as described above, and then reverse-transcribed using 25 pmol RP1 primer (for TRU-seq sequencing). An aliquot of cDNA was serially diluted and used for standard PCR amplification to determine optimal PCR cycle number. The final library amplification was carried out by using 12.5 pmol RPI-index primers (for TRU-seq barcodes, Illumina) and Phusion polymerase (NEB). Libraries were run on PAGE gel and and library fragments between 140 and 300 bp was excised. The libraries were purified and submitted to the Vanderbilt Technologies for Advanced Genomics (VANTAGE) for sequencing on an Illumina HiSeq 2000.

RT-qPCR Quantification of mRNA Expression

Cells were lysed in 500 μl Trizol, after which total RNA was extracted using the Zymo Research Direct-zol RNA MiniPrep kit with on-column DNase digestion. After extraction, 1 μg of RNA was reverse transcribed using MuLV reverse transcriptase (Life Tech N8080018) in 20 μl reaction, then diluted three-fold with nuclease-free water. 1 μl of cDNA was used in a 15 μl qPCR reaction using KAPA SYBR FAST qPCR Master Mix 2X Universal and quantified on an Eppendorf Realplex2 Mastercycler in triplicate. Relative mRNA expression of genes of interest was quantified using the CT method, normalized to signals from GAPDH. mRNA expression studies were completed in triplicate with error bars representing the standard error of the mean. Primer sequences used can be found in Table 1.

RNA-Seq

Cells were treated for 72 hours with 2 μM C6, 2 μM C6nc, 2 μM Nutlin-3, or 0.1% DMSO. Cells were washed in PBS then lysed in 500 μl Trizol. RNA was isolated using the Zymo Research Direct-zol RNA MiniPrep kit with on-column DNAse digestion following the manufacturer's instructions. Library preparation with rRNA depletion and paired-end 150 base pair sequencing on an Illumina HiSeq was performed by GENEWIZ. Prior to sequencing, RNA integrity was assessed by 2100 Bioanalyser (Agilent) and concentration was assayed by Qubit. RNA-Seq for

MV4:11 and K562 cells treated with C6nc, C6 and DMSO was completed with 5 biological replicates. MV4:11 cells treated with Nutlin-3 and DMSO was completed with 3 biological replicates

Quantifying Relative Protein Synthesis Rates

Protein synthesis rates were measured by pulsing cells with O-propargyl-puromycin (OPP) (Signer, Magee et al. 2014). Briefly, MV4:11 cells were treated for 1, 2, 3 or 6 days with 2 μM of C6nc, 2 μM C6 or 0.1% DMSO vehicle control. At each time point, 2 million cells were collected per sample and pulsed with 50 μM OPP for 1 hour at 37^{o}C. For a positive control for inhibition of protein synthesis, 100 μg/ml of cycloheximide was added to DMSO treated cells and incubated at 37^{o}C for 30 minutes prior to addition of OPP. Cells were then washed with ice-cold phosphate-buffered saline (PBS) and fixed in 500 μL of PBS with 1% paraformaldehyde (PFA) for 15 minutes on ice, then washed again in PBS. Cells were permeabilized with 500 μL of PBS + 3% FBS + 0.1% saponin for 5 minutes then washed in PBS + 3% FBS. The Click-it Cell Reaction Buffer Kit (Thermo C10269) was used to conjugate 500 nM Alexa Flour647-Azide (Thermo A10277) to OPP following the manufacturer's instructions. Samples were washed in PBS + 3% FBS, then resuspended in 1 ml PBS. To control for background staining, a sample of DMSO treated cells was subjected to the same staining procedure, but no OPP was added. Relative Alexa647 fluorescence was quantified using a Becton Dickinson (BD) LSR II flow cytometer and analyzed using FlowJo software. At least 10,000 events were recorded per sample. Doublets were excluded prior to analysis. The time course was repeated in biological triplicate with error representing standard error of the mean. Flow Cytometry experiments were performed in the Vanderbilt University Flow Cytometry Shared Resource.

p53 and p21 Induction Western Blots

Cells were treated for 24 hours with C6nc and C6 (2 μM for MV4:11 and 3 μM for Molm13), or 2 μM Nutlin-3, or a 0.1% DMSO only vehicle control. Four million cells were washed in PBS then lysed for 10 minutes on ice in 200 μl Kischkel buffer (50 mM Tris pH 8.0, 150 mM NaCl, 5 mM EDTA, 1% Triton X100, protease inhibitor cocktail, 1 μM PMSF). Whole cell extracts were sonicated for 15 seconds then clarified by centrifugation. Laemmli Sample buffer was added and samples were boiled for 10 minutes before running on a 4-20% mini-PROTEAN TGX gel (BioRad) and transferring to PVDF membrane. Membranes were blocked in 5% milk in TBST for 20 minutes then probed with appropriate antibodies.

Cycloheximide (CHX) Chase

MV4:11 cells were treated for 24 hours with 2 μM C6, 2 μM Nutlin-3 or DMSO only. After 24 hours, two million cells were collected for each treatment as the "time 0" sample. To the remainder of the sample, CHX was added to a final concentration of 50 μg/ml. At time points of 15, 30, 60, 120, and 180 minutes, two million cells for each treatment were collected, snap frozen in liquid nitrogen, and stored at -80^{o}C until processing. Cell pellets were lysed in 200 μl of Kischkel buffer (50 mM Tris pH 8.0, 150 mM NaCl, 5 mM EDTA, 1% Triton X100, protease inhibitor cocktail, 1 mM PMSF), extracts sonicated and then cleared by centrifugation. Laemmli Sample buffer was added and samples were boiled for 10 mins before running on a 4-20% mini-PROTEAN TGX gel (BioRad) and transferring to PVDF membrane. Membranes were blocked in 5% milk in TBST for 20 minutes then probed with appropriate antibodies.

Polysome fractionation

The polysome fractionation assay was performed by Dr. April Weissmiller. Polysome enrichment experiments were performed as previously described (Yang, Halaby et al. 2006). Briefly, 15 x 10^6 MV4:11 cells were plated with either 5 μM C6 or DMSO control for 24 hours and then lysed in polysomal buffer (10 mM MOPS, pH 7.2, 250 mM NaCl 2.5 mM MgOAc, 0.5% NP-40, 200 ug/ml heparin; containing 50 μg/ml cyclohexamide, 1 mM PMSF, 20 units of Superase Inhibitor, protease inhibitor cocktail) for 10 minutes on ice. Debris was cleared by centrifugation. A portion of the supernatant representing the total RNA served as the total RNA fraction sample. Polysomes in the supernatant were recovered by centrifugation (100,000 x *g*) for 1 hour. Pelleted polysomes were resuspended in polysomal buffer and all supernatant remaining served as the monosomal fraction. RNA from total, polysomal, and monosomal fractions were extracted using Trizol-LS followed by purification and DNAse treatment using Direct-zol RNA miniPrep (*Zymol*). All extracted RNA was subjected to reverse transcription using MuLV reverse transcriptase as described below. Differences in mRNA levels between fractions were quantified using an Eppendorf Realplex2 Mastercycler using the Ct method. mRNA primer sequences can be found in Table 1. For each fraction, mRNAs of interest were normalized to GAPDH and then the percent of the total RNA for monosomal or polysomal fractions was calculated. These final values representing the percent monosomal or polysomal mRNA were then made relative to DMSO treatment.

Lentiviral Production and Transductions

pLKO-p53-shRNA-941 and pLKO-p53-shRNA-427 plasmids were a gift from Todd Waldman [Addgene plasmid # 25637 and # 25636 respectively; (Kim, Lee et al. 2007). Scrambled shRNA pLKO.1 plasmid was a gift from David Sabatini [Addgene plasmid # 1864; (Sarbassov, Guertin et al. 2005). pLKO.3G was a gift from Christophe Benoist & Diane Mathis (Addgene plasmid # 14748). Plasmids used are listed in Table 2. To allow for GFP+ cell sorting instead of puromycin selection of transduced cells, shRNA sequences from pLKO-p53-shRNA-941, pLKO-p53-shRNA-427, and scrambled shRNA pLKO.1 were cloned into the pLKO.3G vector using *Spe*I and *Nde*I restriction enzymes (NEB). to create plasmids pLKO.3G-p53-shRNA-941, pLKO.3G-p53-shRNA-427, and pLKO.3G-shRNA-scrambled plasmids, respectively. These plasmids were transfected into HEK293T cells along with the pCMV-Pax2 and pMD2 packaging vectors using the calcium phosphate method. pCMV-Pax2 was a gift from Jonathan Epstein (Addgene plasmid # 36052) and pMD2.G was a gift from Didier Trono (Addgene plasmid # 12259). Virus-containing media was harvested 24 and 48 hours post-transfection and filtered through a 0.45 μm filter. For viral transduction, one million MV4:11 cells were resuspended in 2 mL RMPI-1640 + 10% FBS + 1% penicillin/streptomycin. 8 μg/ml polybrene and 1 ml of filtered virus was added to the cells and incubated for 20 minutes. Cells were centrifuged at 800 x g for 30 minutes then gently resuspended and plated in a 6-well plate. Cells were incubated overnight at 37^{o}C. The transduction procedure was repeated two more times. GFP+ cells were sorted using a BD FACSAria III with a 100 µm nozzle. Cell sorting was performed in the Vanderbilt University Flow Cytometry Shared Resource. shRNA mediated knock-down of p53 in sorted GFP+ cells was validated via western blot.

Generation of p53-null MV4:11 and Molm13 cell lines

Lentiviral production and transduction was completed as stated for shRNA knock-down experiments, above. plentiCRISPRv2, a gift from Feng Zhang (Addgene plasmid # 52961), was modified to express a gRNA against p53 (GAGCGCTGCTCAGATAGCGA; pLentiCRISPRv2–TP53) or EGFP (GAGCTGGACGGCGACGTAAA; pLentiCRISPRv2–EGFP). Plasmids used are listed in Table 2. Two days after transduction, cells were selected with 2 µg/ml of puromycin for eight days. After selection with puromycin, the resistant cell populations were cloned by single cell sorting into a 96-well plate using a BD FACSAria III. Clones were validated for p53 knockout by western blot and Tracking of Indels by Decomposition (TIDE) sequencing analysis

Table 2. Plasmids	
Recombinant DNA	**Source**
pCL10A1	Novus Biologicals
pLKO-p53-shRNA-941	Kim et al., 2007 (Addgene plasmid #25637)
pLKO-p53-shRNA-427	Kim et al., 2007 (Addgene plasmid #25636)
Scramble shRNA pLKO.1	Sarbassov et al., 2005 (Addgene plasmid #1864)
pLentiCRISPRv2	Addgene plasmid #14748
pLentiCRISPRv2–TP53 gRNA #4	Genscript
pLentiCRISPRv2–EGFP	This study
pLKO.3G	Addgene plasmid #14748
pLKO.3G-p53-shRNA-941	This study
pLKO.3G-p53-shRNA-427	This study
pLKO.3G-shRNA-scramble	This study
pMD2 (VSV-G Env)	Provided by A. Reynolds
pCMV-PAX2 (GAG and POL)	Provided by A. Reynolds

(Brinkman, Chen et al. 2014). Proliferation assays and p53 induction blots were done as for the p53 shRNA knockdown.

QUANTIFICATION AND STATISTICAL ANALYSIS:

ChIP-Seq Data Analysis

The ChIP-seq data analysis was performed by Jing Wang under the mentorship of Dr. Qi Liu. ChIP-Seq reads were aligned to the human genome using Bowtie2 (Langmead, Trapnell et al. 2009). Peaks in each sample were called using MACS2 with q-value of 0.01 (Feng, Liu et al. 2012). Peaks were annotated using the Homer command annotatePeaks (http://homer.ucsd.edu/homer/). Consensus peaks in each condition were identified using DiffBind [Stark, R. & Brown, G.D. DiffBind: differential binding analysis of ChIP-seq peak data (Bioconductor, 2011)]; peaks occurring at least two replicates in each condition were included. Peaks identified in at least one condition were combined into a final peak set to identify differential peaks across conditions. Read counts were normalized to the total mapped reads, and differential peaks were determined by DESeq2 (Love, Huber et al. 2014), which calculated the $\log_2$ fold changes, Wald test p-values, and adjusted p-values (False Discovery Rate, FDR) by the Benjamini-Hochberg procedure. Significantly changed peaks were assessed with FDR<0.05.

PRO-Seq Analyses

The PRO-seq analysis was performed by Dr. Pankaj Acharya. Low quality reads were trimmed from raw reads using Trimmomatic-0.32 (Bolger, Lohse et al. 2014). Reverse complements were generated using “fastx_reverse_complement” from FASTX-Toolkit. Reverse-complemented reads were aligned to the human genome hg19 using Bowtie2 [version 2.2.4; (Langmead and Salzberg 2012). Reads mapped to rRNA loci and reads with mapping quality of less than 10 were removed. The reads were normalized by the RLE implemented in the DESeq2 (Love, Huber et al. 2014). NRSA (http://bioinfo.vanderbilt.edu/NRSA/), a tool to provide a comprehensive analysis on nascent transcriptional profiles for known genes and novel enhancers, was used to estimate RNA polymerase abundance in proximal-promoter and gene body regions of genes, to calculate pausing index and pausing index alterations, and to detect enhancers and quantify eRNA changes. Briefly, the promoter-proximal region is defined by examining each 50 bp window with a 5 bp sliding step along the coding strand spanning ±500

bp from known TSSs. The 50 bp region with the largest number of reads is considered as the promoter-proximal region and its read density is calculated (Core, Waterfall et al. 2008). The gene body is defined as the region from +1 kb downstream of a TSS to its transcription termination site (TTS). Pausing index for each gene is calculated as the ratio of promoter-proximal density over gene body density. Significance of pausing is evaluated by Fisher's exact test (Core et al., 2008). NRSA first calls novel transcripts using HOMER, and then identifies intergenic, bidirectional transcripts as eRNA pairs (Hah, Danko et al. 2011, Hah, Murakami et al. 2013). NRSA detects enhancers by integrating those eRNA pairs. Enhancers are considered to be novel if their centers do not fall in any enhancer region based on the FANTOM5 database (Lizio, Harshbarger et al. 2015). DESeq2 (Love, Huber et al. 2014) was implemented to detect significant transcriptional changes for promoter-proximal, gene body regions, and enhancers, accounting for the batch effect. Transcriptional changes were assessed with a FDR<0.05 and a fold change ≥ 1.5 were considered significant.

RNA-Seq Data Analysis

The RNA-seq data analysis was performed by Jing Wang under the mentorship of Dr. Qi Liu. RNA-Seq reads were aligned to the human reference genome hg19 using STAR (Dobin, Davis et al. 2013) and quantified by featureCounts (Liao, Smyth et al. 2014). Read counts were normalized by the Relative Log Expression (RLE) method. Differential analysis were performed by DESeq2 (Love, Huber et al. 2014), which determined the $\log_2$ fold changes, Wald test p-values, and adjusted p-value (FDR) by the Benjamini-Hochberg procedure. The significantly changed genes were assessed with a FDR<0.05.

CHAPTER III

DISCOVERY AND OPTIMIZATION OF PICOMOLAR WDR5 WIN SITE INHIBITORS

Introduction

Recent advances in our knowledge of epigenetic processes that contribute to cancer has spurred interest in the concept that epigenetic regulators can be targeted to treat malignancy. Currently there are dozens of small molecule epigenetic inhibitors in clinical trials, but due to the high failure rate of new investigational drugs, it is important to develop inhibitors of additional epigenetic targets to increase the chance of improving cancer treatment. Over the last several years, the WIN site of WDR5 was been validated as a therapeutic target in leukemias expressing an oncogenic MLL1-fusion protein. Several inhibitors of the WDR5 WIN site, including the peptidomimetic MM-401 and the monobody Mb(S4), have been shown to have utility in an MLL-leukemia context by blocking proliferation and colony forming potential of MLL-fusion cells (Cao, Townsend et al. 2014, Gupta, Xu et al. 2018). Although WIN site inhibitors have been proposed to act in MLL-fusion cells by modulating MLL1-mediated H3K4 methylation, the mechanism through which these inhibitors functions has not been elucidated. Furthermore, MM-401 does not show high cellular potency and does not have drug-like properties. Expressing Mb(S4) in MLL-AF9 cells significantly inhibits leukemia progression in a mouse model, validating WDR5 as anti-leukemia target in vivo, but the gene encoding Mb(S4) must be expressed in cancer cells to function, thus limiting its potential as a therapeutic. If WDR5 WIN site inhibition is to be pursued further as a cancer therapeutic strategy, a detailed examination of the mechanism of action of WDR5 WIN site inhibitors and the development of highly potent small molecule inhibitors are needed.

We reasoned that by discovering novel and potent WIN site inhibitors with picomolar affinity, we could use the inhibitors as tool compounds to better detailed the molecular mechanism of action of WDR5 inhibitors, thus defining the utility of inhibiting WDR5 in MLL-leukemia and possibly other cancer types as well. The most informative approach to understanding the utility of WIN site inhibition in an MLL-leukemia context would be to discover small molecules that bind the

WIN site with an affinity much higher than that of most protein-protein interactions (i.e., in the picomolar range), and would thus be expected to disrupt the majority of WDR5 WIN site binders, known or unknown. In this chapter, I provide an overview of the high-throughput screening approach used by the Fesik lab to identify novel chemical fragments that bind the WIN site of WDR5. I then describe the structure-based medicinal chemistry method used to expand the initial fragment hits into the potent tool compounds C3 and C6, which were chosen as my first- and second-generation tool compounds to perform the molecule mode of action studies that comprise this thesis.

Results

Identification of first generation WDR5 WIN site-binding small molecules

To identify small molecules that bind the WIN site of WDR5, the Fesik laboratory conducted a fragment-based high-throughput screen of a library of chemical fragments. The details on how they performed the fragment-based screen have been published (Wang, Jeon et al. 2018). Briefly, the Fesik Lab utilized heteronuclear multiple quantum coherence (HMQC), a type of multidimensional nuclear magnetic resonance (NMR), to identify chemical fragments that bind the WIN site of WDR5. This technique uses the ^{1}H and ^{15}N spectra of an ^{15}N-labeled protein of interest to identify shifts in the peaks of the protein's spectra upon ligand binding. Control spectra were first generated for ^{15}N-labeled WDR5 in complex with an MLL1 WIN motif-containing peptide to identify shifts in the WDR5 spectra that occur when the WIN site is occupied. Then a chemical fragment library that contained roughly 13,800 different fragments was screened by incubating mixtures of 12 fragments at a time with the ^{15}N-labeled WDR5. The fragments that caused peak shifts similar to the MLL1 peptide were flagged as hits for WDR5 WIN site binding.

Follow-up validation screening of individual compounds from the hit mixtures identified 47 fragment hits. One of these fragment hits was Compound 1, C1, which binds WDR5 with a K_d of 66 μM (Figure 3-1A). The Fesik Lab solved the X-ray crystal structure of C1 when complexed with WDR5 (Figure 3-1B). Several smaller structural sub-pockets (S_1, S_2, S_3, S_4, S_5, S_6, and S_7)

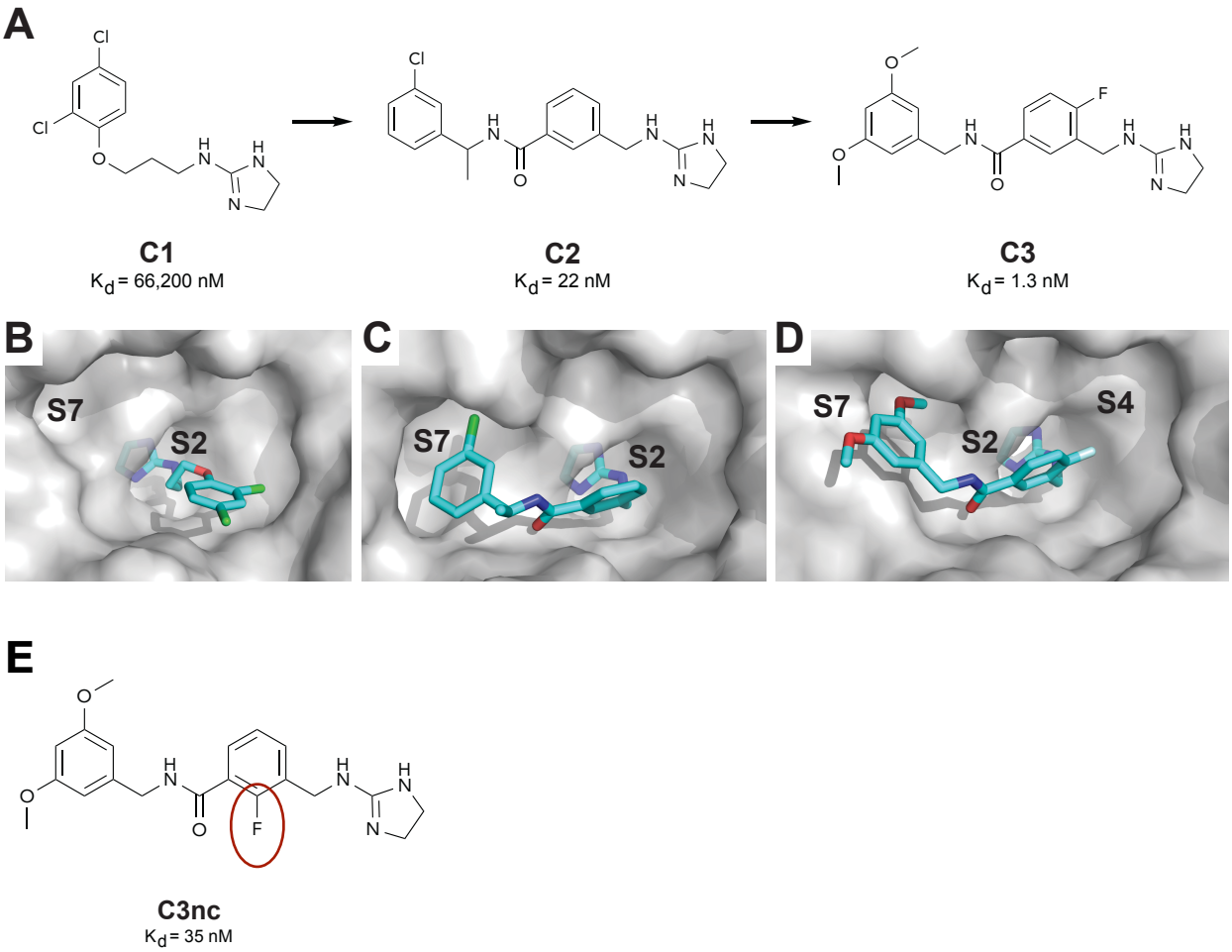

Figure 3-1. Discovery of first generation small molecule WIN site inhibitors. (A) Elaboration of fragment hit C1 into our first generation chemical probe C3. X-ray co-crystal structures of WDR5 bound to (B) the fragment hit C1, (C) C2, and (D) C3. (E) Structure of the negative control compound for C3, C3nc.

within the WIN site of WDR5 have previously been defined (Wang, Jeon et al. 2018), with the S_2 pocket being located deep within the central pore of WDR5. The S_2 pocket binds the MLL1 arginine-3765 guanidine side chain, and this interaction has been shown to greatly contribute to the total binding affinity to WDR5 (Patel, Vought et al. 2008). The Fesik Lab found that the cyclic guanidine group of C1 binds deep into the S_2 pocket of WDR5, making a cation pi-stacking interaction with phenylalanines-133 and -263, mimicking the interaction made by arginine-3765 of MLL1. To improve the affinity of C1, structure-based design was used to expand the compound outwards to access additional nearby WIN site sub-pockets. Expanding C1 out to the S_7 sub-pocket with a benzyl amide yielded compound C2 (Figure 3-1A) with about a 3,000-fold improvement in affinity. In the X-ray structure of WDR5 bound to C2 (Figure 3-1C) the benzyl group in the S_7 pocket was found to form a hydrogen-bonding interaction with the carbonyl oxygen with the backbone NH of cystine-261 in WDR5. Further optimization of C2 led to C3 (Figure 3-1A), with a K_d of 1.3 nM. Compound C3 provides improved binding by modifying the substituents on the benzylic ring to better occupy the S_7 sub-pocket, and by inclusion of a fluorine atom on the phenyl core that points towards the S_4 sub-pocket (Figure 3-1D).

I selected C3 as my first-generation chemical probe to explore the cellular consequences of WDR5 WIN site blockade. C3 was selected for several reasons. C3 is a novel WDR5 WIN site inhibitor, as it is structurally distinct from all of the previously published WDR5 WIN site inhibitors (Cao, Townsend et al. 2014, Grebien, Vedadi et al. 2015, Karatas, Li et al. 2017, Gupta, Xu et al. 2018, Zhang, Zheng et al. 2018). C3 was also one of our most potent binders of WDR5 at the time that I began my mode of action studies. The effects of our tool compounds on cellular proliferation of a panel of leukemia cell lines will be throughly detailed in Chapter IV, but I will briefly describe here how proliferation data was used to facilitate tool compound selection. Due to the precedent in the literature (Cao, Townsend et al. 2014), we reasoned that a WDR5 WIN site inhibitor should inhibit the proliferation of MV4:11 (MLL-leukemia). We also reasoned that MV4:11 cells should be 3-5 fold more sensitive to WDR5 WIN site inhibition than K562 (non-MLL-Leukemia) cells. We also expected that a potent small-molecule inhibitor should have an MV4:11 proliferation assay GI_{50} less than ~10 μM. C3 was one of the first compounds to meet these criteria.

In order to be more confident that the effects of C3 I discovered in my molecular mode of action studies were due to on-target activity, we wanted to generate an inactive negative control

compound that was as similar to C3 as possible but did not inhibit the WIN site of WDR5. The Fesik Lab designed and synthesized a negative control compound for C3 called C3nc (Figure 3-1E). C3nc is identical in structure to C3 with the exception of the placement of the fluorine atom circled in red in Figure 3-1E. The positioning of this fluorine atom in C3nc reduces the binding affinity to WDR5 by about 30-fold compared to C3 by creating steric hindrance with the protein.

Identification of second-generation WDR5 WIN site-binding small molecules

C3 was a promising first-generation tool compound, however over time the Fesik Lab continued to optimize their structure-based drug design to make tool compounds with even better potency. To obtain a tool compound more potent that C3, the Fesik Lab started with a different fragment hit, Compound 4, abbreviated C4 (Figure 3-2A). Like C1, C4 binds deep into the S_2 pocket of WDR5 and makes a pi-stacking interaction with phenylalanines-133 and -263 (Figure 3-2B). A strategy similar to that used for our first-generation tool compounds was again employed to optimize this initial hit fragment. Although C4 bind the S_2 pocket, it does not bind to any of the other nearby sub-pockets within the WDR5 WIN site. By extending the compound outward to reach the S_7 sub-pocket Compound 5 (C5) was created (Figure 3-2C), which has a 220-fold improvement in binding affinity. A further improvement in affinity was achieved with Compound 6 (C6) by additionally occupying the S_4 sub-pocket (Figure 3-2D). C6 has a K_d of ~100 pM and an X-ray crystal structure of C6 in complex with WDR5 can be seen in Figure 3-3. Key interactions between C6 and WDR5 include a hydrogen bond of the carbonyl oxygen to cystine-261 and pi-stacking of the imidazole-imine with F133 and F263 in the S_2 sub-pocket.

Once the more potent compound C6 became available, I selected C6 as my second-generation chemical probe for molecular mode of action studies. Again, C6 exhibited selective proliferative inhibition for MV4:11(MLL-leukemia) cells over K562 (non-MLL-Leukemia) cells and had improved cellular potency than C3 (Table 4). Cellular proliferation studies for C6 will be detailed further in Chapter IV. As with C3, the Fesik Lab created a negative control compound for C6, called C6nc (Figure 3-2E) that is as similar in structure to C6 as possible but has a binding affinity for the WIN site above the limit of detection. C6nc only differs from C6 in the attachment point of the S_2-binding imidazole-imine group circled in red in Figure 3-2E. Repositioning the attachment of this chemical group lead to a greater than 1,000-fold reduction in binding affinity.

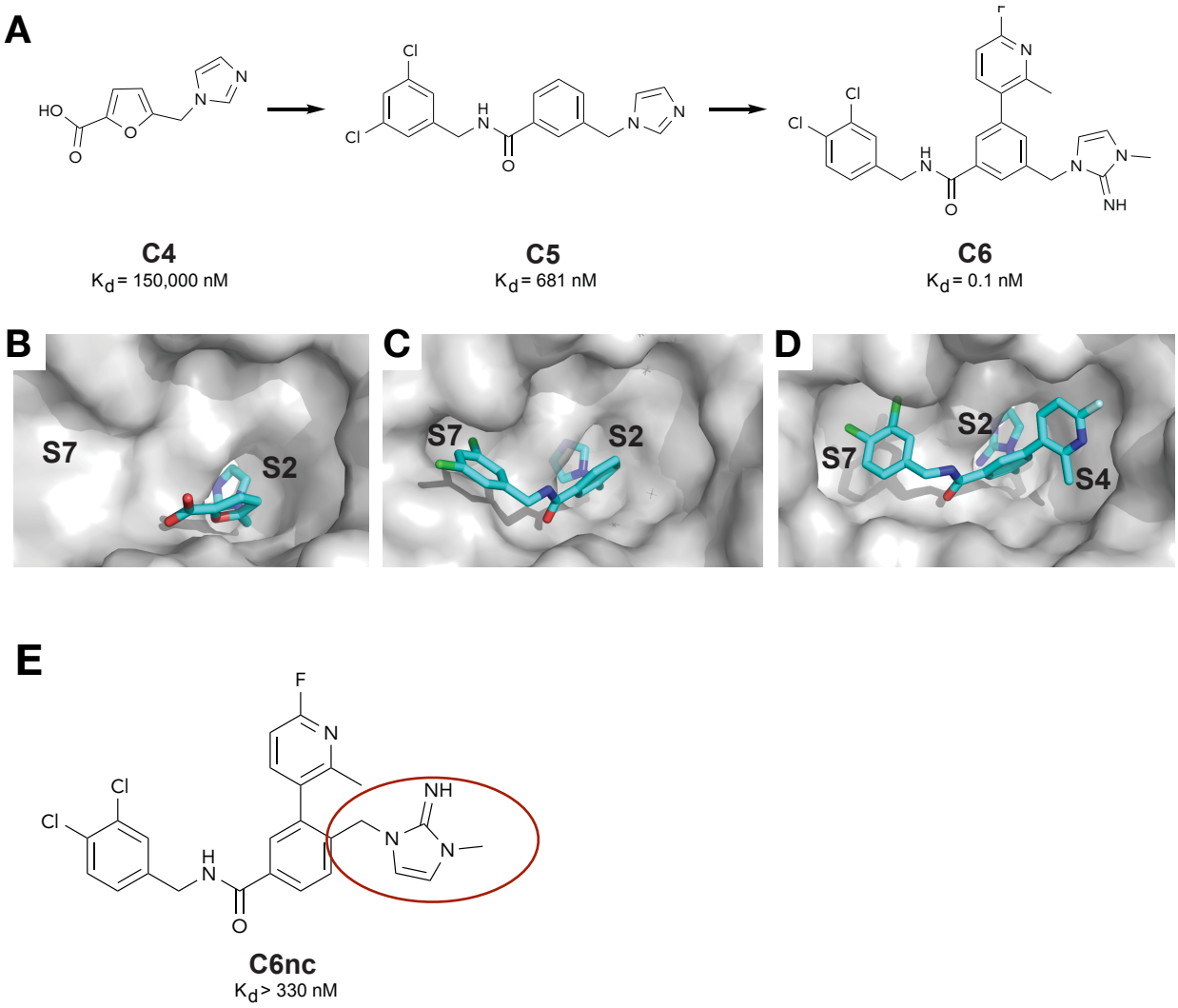

Figure 3-2. Discovery of second generation small molecule WDR5 WIN site inhibitors. (A) Elaboration of fragment hit C4 into our second generation chemical probe C6. X-ray co-crystal structures of WDR5 bound to (B) the fragment hit C4, (C) C5, and (D) C6. (E) Structure of the negative control compound for C6, C6nc.

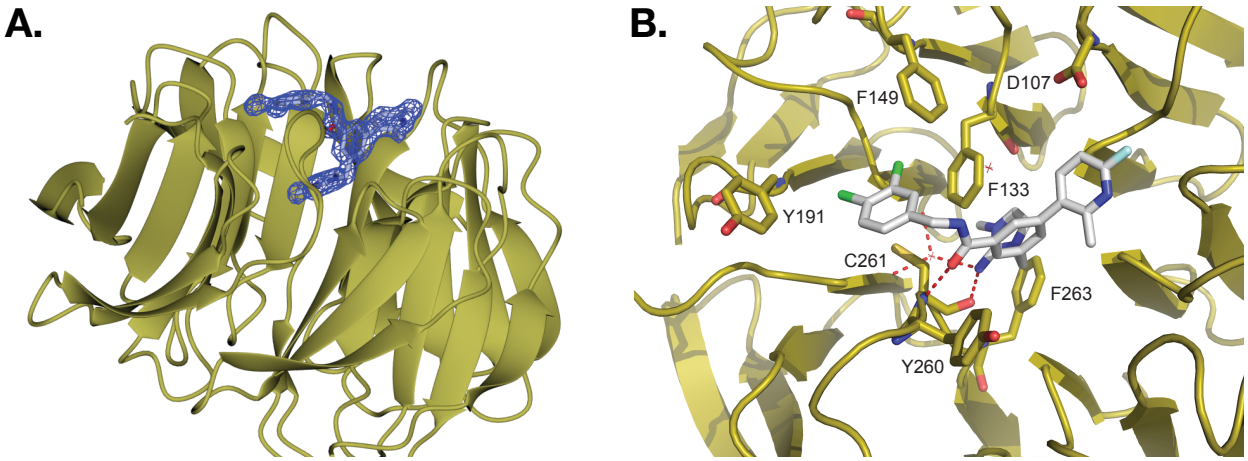

Figure 3-3. X-ray co-crystal structure of C6 bound to the WIN site of WDR5. The WDR5 protein is displayed as gold ribbons; C6 is displayed as colored sticks with the electron density map contoured in blue in A. (B) A zoomed-view of the WIN site with C6 bound; key residues are labeled and shown as sticks. Interactions of C6 with the protein include a hydrogen bond of the carbonyl oxygen to C261 and pi-stacking of the imidazole-imine with F133 and F263 in the S_2 sub-pocket.

Effect of WDR5 WIN site inhibition on MLL complex histone methyltrasnferase activity in vitro

WDR5 is known to be a member of all six human MLL/SET type histone methyltransferase (HMT) complexes which include MLL1, MLL2, MLL3 MLL4, SETD1A and SETD1B. However, it has been shown that engagement of the WDR5 WIN site with a WIN peptide in the histone methyltransferase is only required for the HMT activity of the MLL1 complex (Li, Han et al. 2016)**.** Therefore, I hypothesized that compounds that inhibit the WDR5 WIN site will inhibit the HMT activity of MLL1 but not the other five MLL/SET type HMTs. In order to test this, *in vitro* HMT inhibition assays were performed by Reaction Biology Corp. In these assays, each of the purified HMT enzymes were mixed with the purified regulatory subunits WDR5, RBBP5, ASH2L and DPY30 to form active HMT complexes. These complexes were incubated with increasing doses of C3, C6, or the negative control compounds, tritiated SAM (S-adenosyl-L-[methyl-^{3}H]methionine) as the methyl group donor, and the substrate. For MLL1, MLL2, MLL3, and MLL4 complexes an H3 peptide was used as the substrate; For SETD1A and SETD1B complexes core histones were used as the substrate. The amount of tritiated methylation transferred to the substrate was measures and IC_{50}s for the inhibition of HMT activity were calculated (Table 3).

As expected, C3 and C6 inhibited the HMT activity of the MLL1 complex. The degree to which C3 and C6 inhibited MLL1 was consistent with their relative affinities for the WDR5 WIN site, with C6 showing roughly a 10-fold greater HMT inhibition as well as a 10-fold stronger binding affinity. C3nc and C6nc did not show measurable inhibition of any HMT complexes, as expected. We further tested C6 for inhibition of the other five MLL/SET complexes. We found that robust inhibition of HMT activity was specific for the MLL1 complex, with no measurable inhibition of MLL3, SETD1A or SETD1B observed. Inhibition of MLL2 and MLL4 was measurable but these IC_{50}s were 500- and 250-fold higher, respectively, than the MLL1 complex, indicating that strong HMT inhibition after C6 treatment is MLL1 specific. Together these assays demonstrate that C3 and C6 are able to bind to and inhibit the WIN site of WDR5.

Table 3. Inhibition of in vitro HMT activity by WDR5 win site inhibitors

Compound	MLL1 HMT IC_{50} (nM)	MLL2 HMT IC_{50} (nM)	MLL3 HMT IC_{50} (nM)	MLL4 HMT IC_{50} (nM)	SETD1A HMT IC_{50} (nM)	SETD1B HMT IC_{50} (nM)
C3	175.5 ± 113.6	-	-	-	-	-
C3nc	> 3,000	-	-	-	-	-
C6	19.9 ± 9.6	9,700	>20,000	5,100	>20,000	>20,000
C6nc	> 3000	-	-	-	-	-

HMT data is n = 2 except for C3 with MLL1 (n=18) and C6 with MLL1 (n=6). MLL1, MLL2, MLL3, and MLL4 HMT assays used an H3 peptide as substrate; SETD1A and SETD1B assays used core histones as substrate. "-" = not measured

Discussion

The WDR5 WIN site has been validated as a therapeutic target in MLL-leukemia, but new potent small molecules that inhibit this site are needed to better investigate the mechanism of action of WDR5 WIN site inhibition and to drive the development of a WDR5 targeted therapeutic strategy forward. Several inhibitors of the WDR5 WIN site have been described, including the monobody Mb(S4) (Gupta, Xu et al. 2018), the moderately potent (K_d ~100 nM) small molecule OICR-9429 (Grebien, Vedadi et al. 2015), the higher affinity (K_d ~1 nM) peptidomimetic MM-401 (Karatas, Townsend et al. 2013, Cao, Townsend et al. 2014) and piribedil, an FDA approved dopamine agonist used to treatment Parkinson's disease (Zhang, Zheng et al. 2018). However, all of these inhibitors have drawbacks. For instance, the Mb(S4) monobody is a synthetic peptide that binds WDR5 but it requires ectopic expression in cell to function. While Mb(S4) has been beneficial to validate WDR5 as an anti-MLL-leukemia target, genetic engineering to express the monobody in all of a patient's cancer cells is not a feasible therapeutic approach at this time. The peptidomimetic MM-401 has therapeutic disadvantages as well. Peptidomimetics are often plagued by poor membrane permeability, metabolic instability, and low oral bioavailability (Qvit, Rubin et al. 2017), making it uncertain if MM-401 is a strong therapeutic candidate. OICR-9429 is a small molecule inhibitor of the WIN site, but it has not previously been published in the context of MLL-leukemia, and as shown in chapter IV, OICR-9429 has weak cellular efficacy in the MLL-leukemia cell lines that I tested (GI_{50} of ~ 30 μM). The FDA approved drug piribedil has been shown to reduce growth and differentiation of MLL-fusion cells, but again does so only very weakly, as the concentrations tested ranged from 20 - 160 μM (Zhang, Zheng et al. 2018).

The compounds C3 and C6 presented here represent a new and exciting pair of potent small molecule WDR5 inhibitors. C3 has a binding affinity similar to the peptidomimetic MM-401 (both close to 1 nM), without the metabolic stability concerns that plague peptidomimetics. With a WDR5 binding affinity of 100 pM, C6 binds to the WIN site much tighter than any of the previously published inhibitors to date. The chemical groups of C3 and C6 that bind into the S_2 pocket of WDR5, the pocket that contributes the most to WIN site ligand binding (Patel, Vought et al. 2008), are different from each other as well as the published inhibitors. This means that C3 and C6 belong to two distinct novel chemical series of small molecule WDR5 WIN site inhibitors. The HMT inhibition assays presented above demonstrate our compounds inhibit the activity of a

pre-formed MLL1 complex. While this does not necessarily mean that our inhibitors kill cancer cells by mitigating MLL1-mediated H3K4me3, it is a significant finding because it demonstrates that our inhibitors are able to disrupt large protein complexes to bind to the WIN site of WDR5.

The mode of action experiments presented throughout this thesis will utilize C3 and C6 to investigate the molecular mode of action of WDR5 WIN site inhibition. The experiments are not necessarily presented in chronological order of when they were completed. Therefore, any experiment shown with only C3 was completed before C6 was developed and the more potent compound C6 was always preferentially used once it became available. Utilizing a more potent compound allowed me to reduce the concentration of compound used while retaining the same level of biological activity, thus helping to mitigate possible off-target effects induced by treatment with high levels of a weaker compound. Also by using both C3 and C6 in some of the same assays I could determine whether the activity of the compounds correlated with their binding affinity to WDR5. The fact the C3 and C6 are from two distinct chemical series is also beneficial because by finding that they have the same biological effects, I could be confident that the biological effects stem from WDR5 WIN site inhibition and not off target effects.

While C3 and C6 are improved over the previously published WDR5 inhibitors, unfortunately neither C3 nor C6 posses the pharmacokinetic properties required for *in vivo* efficacy experiment in mouse models. For instance, the rate of compound clearance from the blood stream is too rapid to maintain sufficient levels in the circulation over time. Continued optimization of our inhibitors has developed compounds with about a 1,000-fold improvement in potency, more balanced pharmacokinetic properties and increased oral bioavailability. These compounds will be utilized in the near future to complete maximum tolerable dose studies and *in vivo* MLL-leukemia cell xenograph experiments to assess the efficacy of our compounds in live animals. Despite the inability to use C3 and C6 for *in vivo* studies, these early yet potent WDR5 inhibitors are excellent tool compounds for investigating the biological consequences of WDR5 WIN site blockade in cell lines, which is the focus of this thesis.

CHAPTER IV

WDR5 INHIBITION BLOCKS GROWTH AND INDUCES APOPTOSIS OF MLLr-LEUKEMIA CELLS

Introduction

In the introduction to this thesis, I detailed the evidence that led to the proposal of WDR5 WIN site inhibition as a therapy for MLLr cancers. For example, the peptidomimetic MM-401 and the monobody Mb(S4) targeting the WDR5 WIN site have previously been shown to selectively inhibit proliferation of MLL-fusion cells without inhibiting normal bone marrow cells nor non-MLLr leukemia cells (Karatas, Townsend et al. 2013, Zhou, Liu et al. 2013, Gupta, Xu et al. 2018). It was shown that peptidomimetic treatment of, or monody expression in, MLL-fusion cells results in apoptosis, differentiation and cell cycle arrest. Additionally, shRNA-mediated knock-down of WDR5 greatly reduces the transformation capacity of mouse bone marrow cells transduced with the MLL-AF9 fusion protein (Cao, Townsend et al. 2014). Together, these data have contributed to the validation of WDR5 as an anti-leukemia target in MLLr cells. Based upon the precedent in the literature, I hypothesized that our WDR5 WIN site inhibitors C3 and C6 will selectively inhibit proliferation of leukemia cell lines harboring an MLL-fusion. To determine the effect of WDR5 WIN site inhibition on leukemia cell growth, I performed proliferation assays in a panel of both human and murine leukemia cell lines with a variety of genetic mutations. Once I determined the cell lines in which cellular proliferation was blocked, I exacted the mode by which the number of cells was reduced (e.g. cytostasis, differentiation, apoptosis induction, necrosis) in order to further characterize how our WIN site inhibitors elicit their anti-proliferative effects.

In summary, I first demonstrate that sensitivity of cells to the WDR5 WIN site inhibitors C3 and C6 correlates with the WDR5 binding affinity of C3 and C6, with cells being more sensitive to the stronger WDR5 binder C6 than C3. Sensitivity to C3 and C6 also correlates with expression of an MLL-fusion and wild-type p53. Additionally, C3 and C6 are shown to engage WDR5 within intact cells. Lastly, a collection of differentiation, cell cycle and apoptosis studies utilizing C6 indicate that changes in cell fate are induced rapidly, within the first several days of C6

treatment and persist for at least 6 days. In sum, these data shed novel light onto what confers cellular sensitivity to WDR5 WIN site inhibition, and provide a comprehensive and quantitative profile of the cell fate of sensitive cells over time in response to WDR5 WIN site inhibitor treatment.

Results

Effect of WDR5 WIN site inhibition on leukemia cell line proliferation

The WDR5 WIN site peptidomimetic MM-401 and the WIN site-binding monody Mb(S4) have previously been shown to selectively inhibit the proliferation of cell lines and primary murine bone marrow cells expressing MLL-fusion proteins (Cao, Townsend et al. 2014, Gupta, Xu et al. 2018). Due to this precedent in the literature, I asked if C3 and C6, which are structurally distinct from MM-401, are selective for cell lines expressing an MLL-fusion protein in a proliferation assay. To test this concept, I selected a panel of leukemia cell lines that included a variety of both MLL-fusion and non-fusion cell lines in order to empirically determine if sensitivity correlates with MLL-fusion expression (Table 4). I was also interested in determining if sensitivity to C3 and C6 correlates with expression of an oncogenic driver other than an MLL-fusion, such as mutant RAS or JAK, or with p53 status. Therefore, the panel of human leukemia cell lines I selected also included some cell lines with these non-MLL-fusion oncogenes and a variety of p53 statuses.

The CellTiter-Glo assay was implemented to measure proliferation because it is a simple and rapid method for quantifying viable cell number. The assay is also high-throughput and allows for rapid screening of several compounds and cell lines in a 96-well plate format. The procedure only involves adding a single reagent (CellTiter-Glo Reagent) directly to cells cultured in a 96-well plate. CellTiter-Glo reagent lyses cells and supplies luciferin, luciferase and other proprietary reagents necessary to measure the ATP present in the well using a bioluminescent reaction. The intensity of the luminescent signal produced is proportional to the amount of ATP present, and the amount of ATP is directly proportional to the number of metabolically active cells present in the culture (Riss, Moravec et al. 2004). I performed proliferation assays, with the

Table 4. Cellular sensitivity to WIN site inhibitors and their matching negative controls

Cell Line	C6 GI_{50} (μM)	C6nc GI_{50} (μM)	C3 GI_{50} (μM)	C3nc GI_{50} (μM)	p53 status	Notable mutations
MV4:11	3.20 +/- 0.213	42.0 +/- 9.02	6.67 +/- 0.519	> 50	WT	MLL–AF4, FLT3/ITD
Molm13	6.43 +/- 0.683	> 50	10.3 +/- 1.03	> 50	WT	MLL–AF9, FLT3/ITD
HL60	14.8 +/- 1.10	> 50	> 50	> 50	null	NRAS (Q61L)
K562	25.4 +/- 2.07	31.7 +/- 2.45	> 50	> 50	null (Q136fs)	
THP-1	> 50	> 50	> 50	> 50	null (C174fs)	MLL–AF9, NRAS (G12D)
HEL	> 50	> 50	> 50	> 50	M133K	JAK2 V617F
NOMO-1	> 50	> 50	> 50	> 50	null (C242fs)	MLL–AF9
SET-2	> 50	> 50	> 50	> 50	R248W	JAK2 V617F
MONO-Mac-6	31.7 +/- 2.32	> 50	ND	ND	R273H	MLL-AF9
GDM-1	> 50	> 50	ND	ND	WT	
MA93	5.04 +/- 0.431	30.3 +/- 5.94	22.1 +/- 3.60	> 50	p53+	MLL–AF9
MA93 FLT3/ITD	2.47 +/- 0.137	26.2 +/- 4.75	21.2 +/- 2.11	> 50	p53+	MLL–AF9, FLT3/ITD
MA93 RAS	20.75 +/- 2.625	> 50	> 50	> 50	p53+	MLL-AF9, NRAS (G12D)
RN2	11.2 +/- 1.48	> 50	8.65 +/- 0.989	> 50	p53+	MLL-AF9, NRAS (G12D)

The indicated cell lines were treated with at least a five-point serial dilution set of compounds for three days, and cell numbers were determined by either MTS assay (RN2) or CellTiter-Glo (all other lines). Cell numbers for each dose were normalized to those from DMSO-treated samples, and used to calculate mean GI_{50} values, which are shown +/- standard error of the mean (SEM). “> 50" means that the top concentration used (50 μM) did not reduce cell number below 50% of DMSO treated cells. "ND" means not determined. The p53 status of each cell line is shown; MA93, MA93 FLT3/ITD, MA93 RAS, and RN2 cells are positive for expression of p53 protein (p53+) as determined by western blot, but whether p53 is mutant in these cells is unknown. Mutation information was collected from ATCC, DMSZ, or the Broad Institute Cancer Cell Line Encyclopedia.

help of Ms. Shelly Lorey, by treating the panel of leukemia cell lines with increasing doses of C3 and C6 and their negative controls C3nc and C6nc for three days. Proliferation of compound-treated samples was normalized to DMSO-treated control samples. The concentration at which proliferation was inhibited by 50% compared to DMSO-treated cells (GI_{50}) for each cell line and WDR5 WIN site inhibitor are listed in Table 4. An arbitrary cutoff of a GI_{50} of around 10 μM or less was set to determine the sensitive cell lines, and I reasoned that insensitive cell lines should show at least a 3-fold increase in GI_{50} compared to the sensitive cell lines based on the existing literature (Cao, Townsend et al. 2014).

After compiling the proliferation data, first I asked if C3 and C6 are selective for cell lines expressing an MLL-fusion protein. Across the board the negative control compounds C3nc and C6nc had little to no effect on cellular proliferation in any of the cell lines tested. Among all of the human leukemia cell line tested, I found that the tighter WIN site binder C6 exhibits stronger proliferative inhibition than C3, as expected. I found that the MLL-AF4 and MLL-AF9 expressing cell lines MV4:11 and Molm13, respectively, were both sensitive to C3 (MV4:11 GI_{50} = 6.7 μM, Molm13 GI_{50} = 10.3 μM) and C6 (MV4:11 GI_{50} = 3.2 μM, Molm13 GI_{50} = 6.4 μM). However HL60, K562, THP-1, HEL, NOMO-1, SET-2, MONO-Mac-6 and GDM-1 cells were all insensitive to both C3 and C6, and in most cases the GI_{50}s were greater than the highest concentration tested (50 μM). This was surprising considering that THP-1, NOMO-1 and MONO-Mac-6 all express an MLL-AF9 fusion, which has been strongly implicated in conferring sensitivity to WDR5 WIN site inhibition (Biswas, Milne et al. 2011, Marschalek 2011, Ballabio and Milne 2014). The leukemia cell line proliferation data indicated that expression of an MLL-fusion is not sufficient to confer sensitivity to C3 or C6.

The unexpected finding that an MLL-fusion is not sufficient to confer sensitivity lead me to ask whether sensitivity to C3 and C6 correlated better with expression of the non-MLL oncogenic drivers JAK and NRAS. All of the human cell lines tested that express JAK or $NRAS^{G12D}$ activating mutations were found to be insensitive to C3 and C6. However, I did find that a robust response to C3 and C6 in MLL-fusion cells appears to correlate with p53 status, as MLLr cell lines with wild-type p53, such as MV4:11 and Molm13, were more sensitive than MLLr lines with mutant p53 such as THP-1, NOMO-1 and MONO-Mac-6. GDM-1 expresses wild-type p53, but does not express an MLL-fusion protein and is also insensitive to C3 or C6. Together, these observations suggest that JAK and RAS mutations are not sufficient to confer sensitivity and

that p53 may be involved in the cellular response to WIN site inhibition in leukemia cell lines harboring an MLL-fusion.

When comparing the human leukemia cell lines, I also noted that the two most sensitive cell lines MV4:11 and Molm13 both express an Internal Tandem Duplication of the receptor tyrosine kinase FLT3 (FLT3/ITD). FLT3/ITD and $NRAS^{G12D}$ are two of the most common co-occurring mutations with MLL-fusions in leukemias (Marschalek 2011). Therefore, I was interested in further interrogating, in a more genetically controlled model, whether expression of either of these two mutations play a role in conferring sensitivity. To address this question, I performed the same proliferation assay described above on human CD34-positive cord blood cells transformed by expression of an MLL-AF9 fusion protein (MA93), either alone or in conjunction with FLT3/ITD (MA93 FLT3/ITD) or $NRAS^{G12D}$ (MA93 RAS) (Table 4). These cells were graciously gifted to me by Dr. Chris Vakoc of Cold Spring Harbor and were previously validated as an efficient model of MLL-AF9 mediated MLL-leukemia in mouse transplantation experiments (Wei, Wunderlich et al. 2008). These isogenic cell lines allowed for direct comparison of different oncogenic mutation combinations by eliminating confounding factors that may have been present due to background genetic variation in the non-isogenic human leukemia cell lines described above.

Again, I found that the three isogenic cord blood cell lines were all insensitive to the negative controls C3nc and C6nc and were more sensitive to the tighter WDR5 binder C6 than C3. MA93 FLT3/ITD cells were the most sensitive to C6 with a GI_{50} of ~2 μM followed closely by MA93 with a GI_{50} of ~5 μM. These C6 GI_{50}s were similar to those seen for C6 treated MV4:11 and Molm13 cells. However, unlike MV4:11 and Molm13, the MA93 and MA93 FLT3/ITD cells were not sensitive to C3. One possible explanation for this is that perhaps the biological threshold needed to inhibit proliferation in CD34+ cord blood cells is higher than MV4:11 and Molm13 cells and the activity of C3 is not potent enough to reach this threshold, but the tighter WDR5 binder C6 is potent enough to induce sensitivity. The roughly two-fold lower GI_{50} of the MA93 FLT3/ITD compared to MA93 suggests that FLT3/ITD in addition to MLL-AF9 might confer a slight increase in sensitivity over MLL-AF9 alone, but FLT3/ITD is not required for sensitivity. The MA93 RAS cell line was the most resistant to WDR5 WIN site inhibition of the three isogenic lines with a C6 GI_{50} of ~21 μM and a C3 GI_{50} > 50 μM. Together, these findings suggest FLT3/

ITD is not required for sensitivity and that the $NRAS^{G12D}$ mutation may actually hinder sensitivity to WDR5 WIN site inhibition in MLL-fusion cells.

Third, I tested the murine cell line RN2, which was isolated from the spleen of terminally ill recipient mice after implantation of MLL-AF9 + $NRAS^{G12D}$ transformed hematopoietic stem cells (Table 4). These cells were a gift from Dr. Chris Vakoc of Cod Spring Harbor and have been previously used to model MLL-leukemia both *in vitro* and *in vivo* (Zuber, Shi et al. 2011, Mazurek, Park et al. 2014). This method for production of primary murine MLL-AF9 leukemia cells has been extensively used to study both the basic biology of MLL-leukemogenesis and drug discovery, and therefore I was interested in investigating how C3 and C6 function in this model.

MTS assay was used to quantify proliferation of RN2 cells, as this cell line was engineered to express luciferase for *in vivo* whole animal imaging, which is incompatible with the luciferase-based CellTiter-Glo assay. The MTS assay is performed by adding the MTS compound [3-(4,5-dimethylthiazol-2-yl)-5-(3-carboxymethoxyphenyl)-2-(4-sulfophenyl)-2H-tetrazolium, inner salt] to cells in a 96-well plate. NAD(P)H-dependent dehydrogenase enzymes present in metabolically active cells reduce the MTS compound to generate a colored formazan dye. The formazan dye is then quantified by measuring the absorbance at 490 - 500 nm (Riss, Moravec et al. 2004). Cell number is proportional to the absorbance, and the absorbance of compound treated cells was normalized to DMSO treated controls. RN2 cells were not inhibited by either negative control compound. RN2 cells were sensitive to C3 and C6, but were the only cell line tested to show a higher GI_{50} for C3 (GI_{50} = ~ 9 μM) compared to C6 (GI_{50} = ~ 11 μM). The MTS assay has a much smaller dynamic range than the CellTiter-Glo assay. For example, by performing a cell titer I have found that CellTiter-Glo readings ranging from 0 to ~70,000,000 RLUs are still in the dynamic range and the DMSO treated wells after a three-day proliferation assay are typically about 30,000,000- 40,000,000 RLUs, meaning that the dynamic range is very large for this assay. In contrast, the MTS absorbance assay readings for the the same three-day proliferation assay typically only range from ~ 0.1 for back ground absorbance to ~ 1.0 in DMSO treated wells, meaning that the dynamic range is very small. Since the difference in GI_{50} between C6 and C3 for the sensitive cell lines Molm13 and MV4:11 is less than two-fold in the CellTiter-Glo assay, it is possible that the smaller dynamic range of the MTS assay makes

it is harder to differentiate the GI_{50} of C3 and C6 and may explain the discrepancy in GI_{50} compared to the relative Kd's of C6 and C3.

For more in depth mechanism of action studies, I selected two representative cell lines, MV4:11 (MLL-AF4) and K562 (no fusion) as sensitive and non-sensitive cell lines, respectively. CellTiter-Glo proliferation assay curves for MV4:11 and K562 cells treated with C3, C6 and the negative control compounds can be found in Figure 4-1. The dose range used for the assays in this figure was not broad enough to capture the full range of cellular effects from 100% to 0% for each curve. The maximum dose used was limited by the need for the DMSO concentration to not exceed 0.1%. The lowest concentrations used was able to detect MV4:11 cell killing for both C3 and C6, as proliferation less than ~20% on the Y axis represents a cell number less than the number of cells plated at the beginning of the experiment, as determined by performing a cell titer (data not shown).

I next chose to focus on our most potent tool compound, C6, to determine how WDR5 WIN site inhibition affects MV4:11 cells growing in culture. Because the CellTiter-Glo assay measures ATP levels as a proxy for live cell number, it can not definitively determine whether the absolute number of cells is decreased or if there is just diminished ATP production. I investigated whether the absolute number of cells is decreased after WDR5 WIN site inhibition by counting the number of live cells per mL in MV4:11 cultures treated with C6 or C6nc over time (Figure 4-2). Cells were treated for a total of six days, with fresh compound and media added on day 3. In order to prevent the cultures from over growing, on day 3 the DMSO and C6nc treated cells were replated to 1.0 x 10^5 cell/mL ("replate" in Figure 4-2). The time-course analysis revealed that a statically significant ($p = 0.008$) inhibition of proliferation begins within two days of treatment with C6 and persists throughout the rest of the 6 day time course. No changes in growth were observed for cells treated with C6nc. Importantly, this experiment demonstrated that the absolute number of cells in the culture does in fact decrease with C6 treatment over time.

Finally, I asked if OICR-9429 (Grebien, Vedadi et al. 2015), a chemically distinct WIN site inhibitor with a less potent WDR5 binding affinity (OICR-9429 K_d = 30 nM compared to 1.3 nM for C3 and 0.1 nM for C6) (Bolshan, Getlik et al. 2013), also reduces the proliferation of MV4:11 cells in a three day proliferation assay. OICR-9429 has been shown to inhibit proliferation of

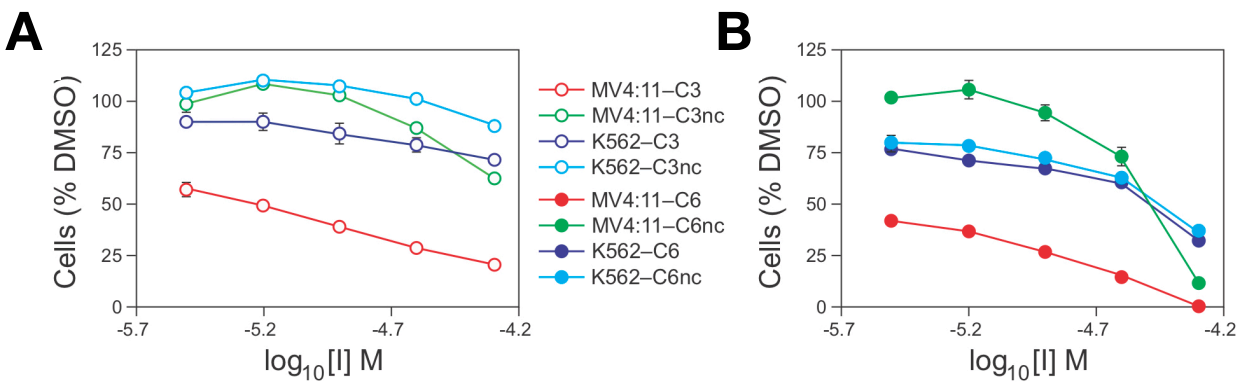

Figure 4-1. WDR5 WIN site inhibitors block proliferation of MLLr-Leukemia cells. (A) Dose-response curves for compound C3 and its negative control, C3nc. Results from three-day proliferation assays are shown, normalized to DMSO-treated samples. (B) As in (A), but for compounds C6 and C6nc. n = 3, error bars represent standard error of the mean (SEM).

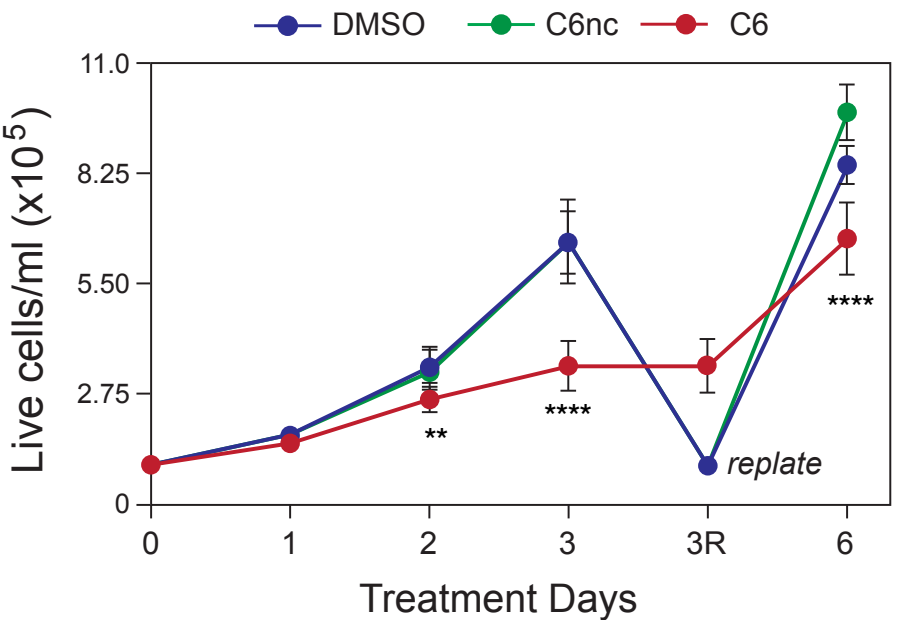

Figure 4-2. WDR5 WIN site inhibition reduces MV4:11 growth rate over time. MV4:11 cells were treated with DMSO, or 2 μM C6 or C6nc. Live cells/mL quantified at the indicated time points. To prevent culture overgrowth, the DMSO and C6nc treated samples were replated at day three (3R) to the original starting density and treatment continued. n = 3, error bars represent standard deviations of the mean. p-values were determined compared to DMSO by two-tailed Student's t-test. ** indicates p = > 0.01, **** indicates p = > 0.0001.

CEBPA-mutant AML cells, but there are no published studies in an MLLr context to date. OICR-9429 was less potent than C3 and C6, having a three day GI_{50} of 31 +/- 1.8 μM (Figure 4-3), consistent with its weaker binding affinity to WDR5.

WDR5 WIN site inhibitor target engagement in leukemia cell lines

In oder to be confident that our WDR5 WIN site inhibitors have the ability to reach their intended target *in vivo*, it is necessary to provide evidence that the compounds engage WDR5 within intact cells. Cellular thermal shift assay (CETSA) can be used to quantify engagement of our inhibitors with WDR5 within both sensitive (MV4:11) and insensitive (K562) cells. This assay functions on the principal that a protein is more thermally stable when a ligand, such as a small molecule inhibitor, is bound to it (Jafari, Almqvist et al. 2014). CETSA involves treating cells with the compound of interest, then heating the cells to the temperature at which the target protein would normally denature (70ºC for WDR5). Then cells are lysed and cell debris and aggregates are separated from the soluble protein fraction by centrifugation. Unbound proteins denature and precipitate after heating, but ligand-bound proteins remain in solution and can be analyzed by Western blot. CETSA was performed by our collaborators Ken Cheng and Dr. Matt Hall at the National Center for Advancing Translation Sciences (NCATS). Cells were treated with C3, C6, the negative control compounds or DMSO for one hour. Because CETSA was performed at 70 ºC, much higher than normal physiological temperature, direct relationships between the CETSA EC_{50}s and the proliferation GI_{50}s or the K_ds can not be drawn, however correlative observations can be made.

It was found that the EC_{50}s of WDR5 engagement for C3 in MV4:11 and K562 cells are 2.5 μM and 2.9 μM, respectively, and for C6 are 60 nM and 100 nM respectively (Figure 4-4). These data indicate that target engagement correlates with the compounds' binding affinity to WDR5, with the tighter binder having a lower CETSA EC_{50}. The differences in how each compound interacts with WDR5 between MV4:11 and K562 cells does not correlate with the effect of the compounds in the proliferation assay. For instance, the CESTA EC_{50}s of K562 and MV4:11 cells treated with C3 are quite similar, yet the proliferation GI_{50} of K562 (> 50 μM) is much higher than MV4:11 cells (6.7 μM). The same pattern is seen with C6. Despite the modest ~1.7-fold increase in the CESTA EC_{50} in K562 cells treated with C6 as compared to MV4:11, the proliferation GI_{50} of K562 (25.4 μM) is roughly 8-fold higher than MV4:11 cells (3.2 μM). Therefore, the differential cellular response to these compounds seen in the proliferation assay can not be explained by

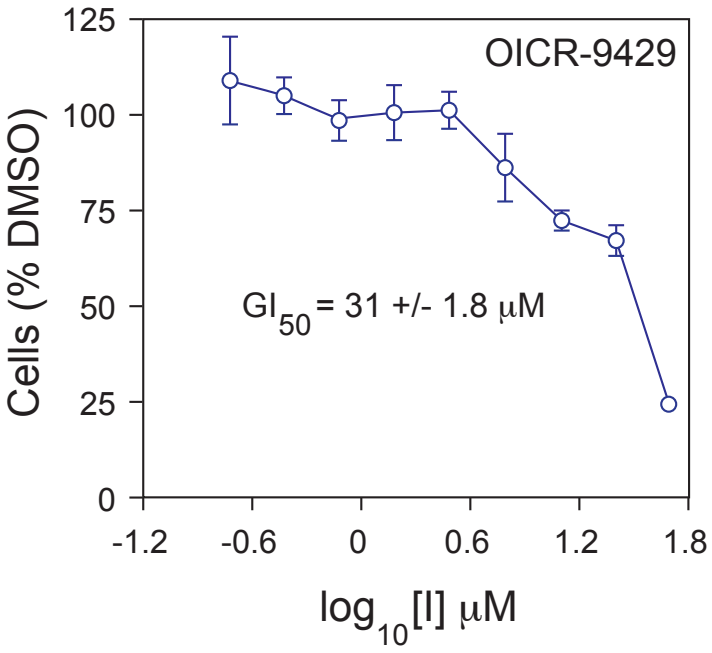

Figure 4-3. OICR-9429 inhibits the proliferation of MV4:11 cells. Three day proliferation assay dose-response curve for MV4:11 cells treated with compound OICR-9429. n = 3, error bars represent standard error of the mean (SEM). The GI_{50} is shown +/- the SEM.

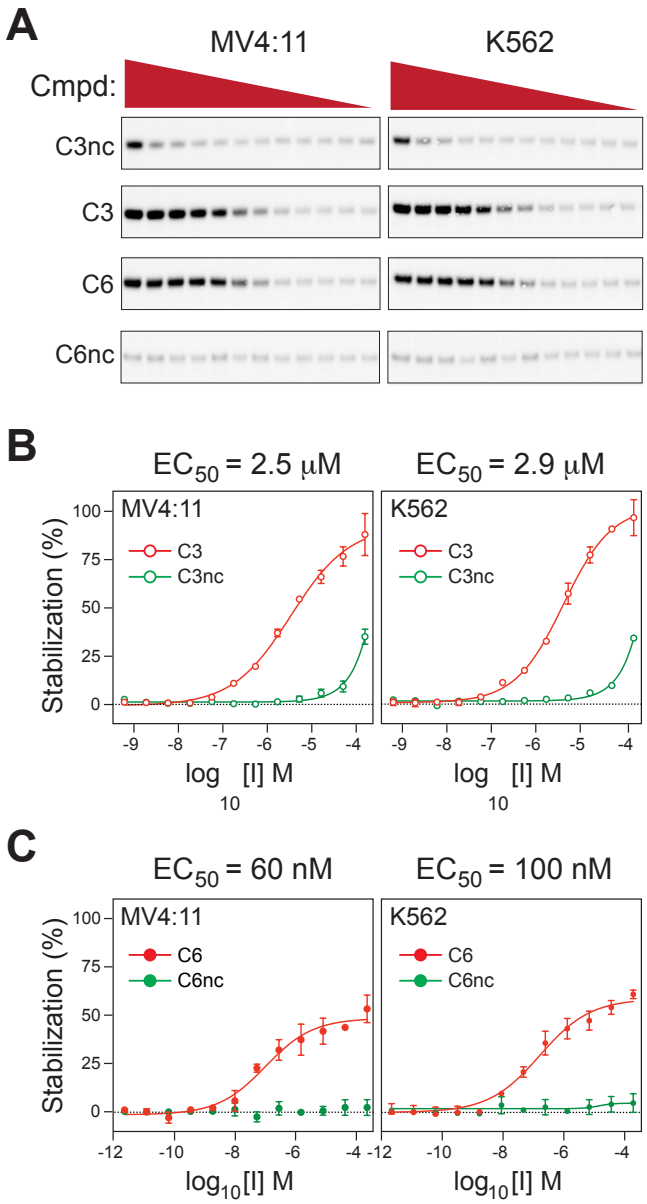

Figure 4-4. WIN site inhibitors engage WDR5 equivalently in MV4:11 and K562 cells. (A) Western blots of WDR5 reaction products from a representative CETSA assay. "Cmpd" refers to the concentration of each compound used, with the triangles indicating compound titrations. In each case, the top concentration used was 100 μM. Because of differing potencies, the dilution series were different for C3/C3nc (serial three-fold dilutions) versus C6/C6nc (serial five-fold dilutions). For each pair of active/inactive compounds, concentrations in MV4:11 and K562 cells were identical. Compound treatment was for one hour at 37°C. (B) Quantification of CETSA data for C3 or C3nc in MV4:11 (left) and K562 (right) cells. Stabilization is defined as the percentage of soluble WDR5 at each dose point, relative to the total pool of non-denatured WDR5 protein. EC_{50} values for C3 in each cell type are shown above the graph. Measurable EC_{50} values for C3nc in either cell type could not be obtained. (C) As in (B) but for C6 and C6nc. Measurable EC_{50} values for C6nc in either cell type could not be obtained.

differences in the ability of the inhibitor to engage WDR5. Instead, it is much more likely that the differences in sensitivity between MV4:11 and K562 cells is due to a biological difference in the way these cells respond to WDR5 WIN site inhibition.

Effect of WDR5 WIN site inhibition on cellular differentiation

After establishing that C3 and C6 inhibit the proliferation of MV4:11 and Molm13 cells (Table 4), I sought to further characterize the fate of these cells upon WDR5 WIN site inhibition. One possible cause for reduced cell number seen in the CellTiter-Glo proliferation assay could be cellular differentiation. I employed Wright-Giemsa staining, a simple yet effective technique to assay for differentiation by visualizing changes in hematopoietic cell morphology. The Wright-Giemsa stain is composed of a combination of the basic dyes methylene blue, azure A and azure B, and the acidic dye eosin. This mixture of dyes differentially stains various cellular components either pink, purple or blue, allowing for the distinction between the various hematological cell types (Dunning and Safo 2011). Immature myeloid blasts appear as cells about 15-20 μm in diameter, with a high nuclear to cytoplasmic ratio. The nucleus is purplish blue in color, surrounded by lighter blue cytoplasm without the presence of granules. As myeloid blasts differentiate into neutrophils, eosinophils, basophils or macrophages distinct morphological changes can be seen with Wright-Giemsa staining (Linden, Ward et al. 2012). Hallmarks of differentiation include a transitioning of the nuclear shape from round to oval, then horse shoe-shaped, and finally segmentation into multiple lobes. Also, the nuclear to cytoplasmic ratio is decreased, the cytoplasm becomes much paler in color, and distinct pigmented cytoplasmic granules develop.

The WDR5 WIN site peptidomimetic MM-401 has previously been shown to selectivity induce morphological changes consistent with myeloid lineage differentiation, such as smaller multi-lobed nuclei and a lightening of the cytoplasm in Wright-Giemsa stained MV4:11 cells (Cao, Townsend et al. 2014). However, these changes were not seen in K562 cells. I hypothesized that MV4:11 and Molm13 cells would show signs of differentiation after WDR5 WIN site inhibitor treatment, but K562 cells would not. I chose to focus on only the most potent of our tool compounds, C6. Two sensitive cell lines, MV4:11 and Molm13. MV4:11 cells were treated for 3 days with DMSO or 2 μM C6 or C6nc and Molm13 cells were treated with DMSO or 3 μM C6 or C6nc. Three day treatment at 2 μM or 3 μM was selected because at these concentrations and time point MV4:11 and Molm13 cell proliferation is reduced by roughly 50%, leaving a sufficient

number of intact cells needed to perform the staining. As a negative control K562 cells were also treated with 2 μM C6 or C6nc, or DMSO, as the proliferation of this cell line is not hindered by 2 μM of C6, and therefore, was not expected to differentiate.

The Wright-Giemsa staining indicated that all three cell types exhibit a blast like phenotype after DMSO treatment, with a high nuclear to cytoplasmic ratio, purple nuclei and bluish cytoplasm (Figure 4-5). No nuclear morphological changes were induced by C6 or C6nc compared to DMSO in any cell type after 3 days of treatment, nor was the presence of distinct granules in a very pale colored cytoplasm observed. The appearance of unstained “vacuole”-like structures was observed in some MV4:11 and Molm13 cells with C6 treatment. The presence of vacuoles in mature macrophages has been described (Liao, Humphrey et al. 2011), however, this characteristic occurs after changes in nuclear shape and cytoplasmic granules become evident. Therefore, I concluded that the C6 induced “vacuoles” were unlikely to be evidence of macrophage differentiation, though the identity of these structures remains unknown. Together these data do not provide convincing evidence of differentiation in any of the three cell types tested after C6 treatment. The possibility of differentiation can not be entirely ruled out. Further quantitative assessment of specific genetic markers of differentiation by flow cytometry or RT-qPCR would strengthen this claim.

Effect of WDR5 WIN site inhibition on the cell cycle

Next, I aimed to quantitatively assess how the distribution of the different phases of the cell cycle in MV4:11 cells is affected by WDR5 WIN site inhibition. Flow cytometric analysis of cells stained with propidium iodide (PI) is one of the simplest and most commonly used methods for measuring cell cycle distribution (Schafer 1998, Darzynkiewicz, Bedner et al. 2001). The fluorescent DNA dye PI stains cells in proportion to the amount of DNA present, therefore the cell’s fluorescence is proportional to its DNA content. DNA content within a cell changes throughout the cell cycle. Cells in the quiescent non-dividing state (G_0) and the first gap phase (G_1) are diploid. During S phase, the DNA is replicated to generate two identical copies of each chromosome, and therefore the DNA content increases in proportion to the progression through S phase. Once the cell enters the second gap phase (G_2), and later the mitotic phase (M) the cell now is tetraploid and has twice the DNA content as G_0 and G_1 cells. Apoptotic cells can also be readily identified because apoptosis induced DNA fragmentation causing cells to have fractional DNA content less than that of G_1 cells, also termed sub-G_1 DNA content. The

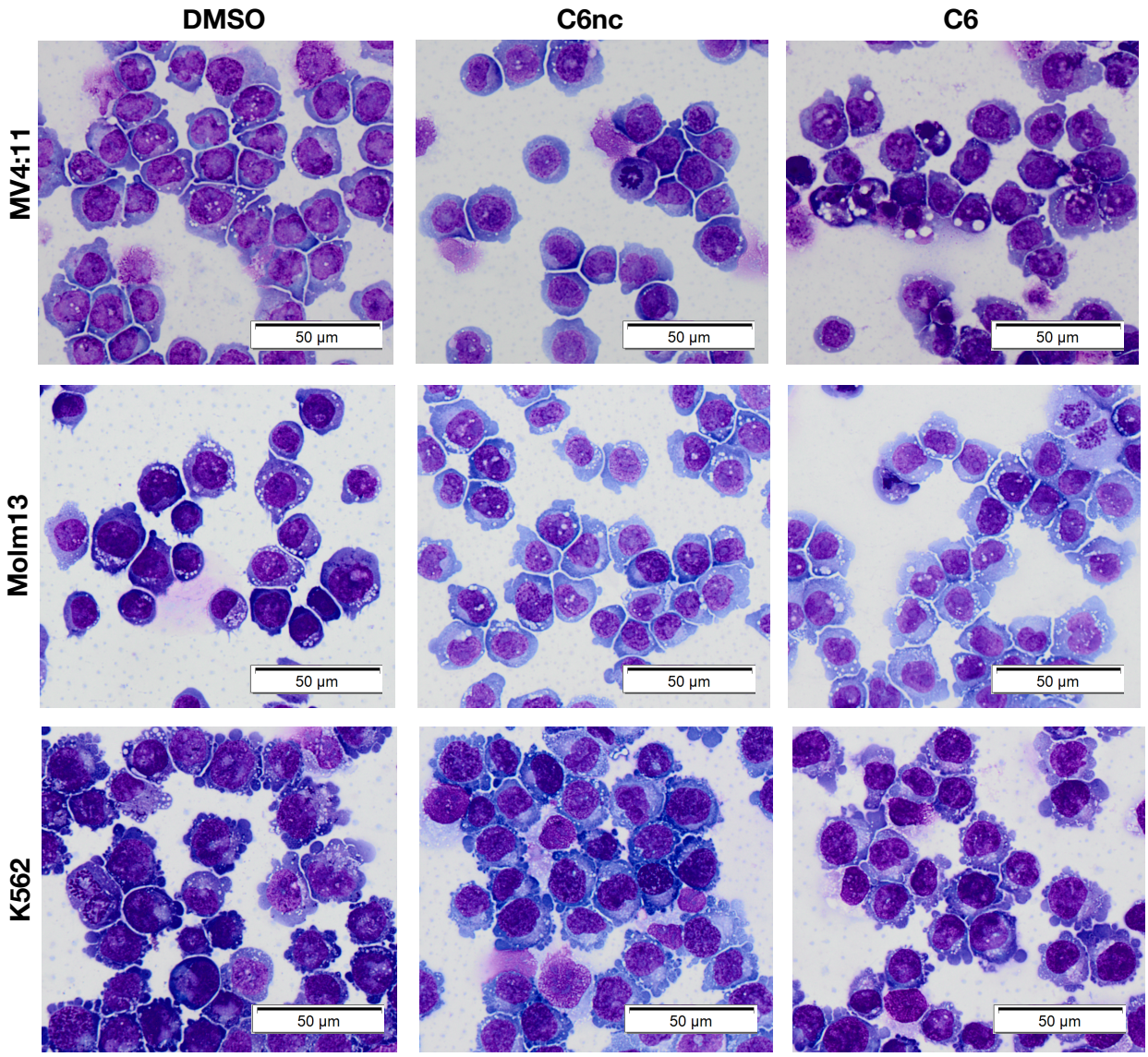

Figure 4-5. C6 does not induce differentiation after 3 days of treatment. Wright-Giemsa stains of MV4:11 (sensitive), Molm13 (sensitive) and K562 (insensitive) cells after three days of treatment with with 0.1% DMSO, or 2 μM C6 or C6nc for MV4:11 and K562 cells and 3 C6 or C6nc for Molm13 cells. Representative pictures shown. The staining was repeated with 3 biological replicates.

proportion of cells in the G_0/G_1, S, or G_2/M phases can be easily distinguished by plotting a histogram of PI fluorescence for the cell population .

I utilized PI staining and flow cytometry to determine how our most potent WDR5 WIN site inhibitor, C6, affects cell cycle distribution. MV4:11 cells were treated with DMSO, or 2 μM C6 or C6nc for 0, 1, 2 , 3 or 6 days, with fresh media and compound added on day 3 to prevent overgrowth of the culture. The cells were fixed, permeabilized and stained with PI. Then the mean percentage of cells in each cell cycle phase was determined and presented as bar graphs (Figure 4-6). p-values for C6nc or C6 compared to DMSO for each cell cycle phase at each time point can be found in Table 5. When comparing DMSO and C6nc treatment at each time point, only the sub-G_1 category for 1 day of treatment reached statical significance ($p = .043$). All other phases at all time points failed to show a significant difference between DMSO and C6nc treatment. Therefore, as expected, C6nc has no considerable effects on cell cycle distribution compared to DMSO.

C6 treated cells exhibited no alterations in cell cycle distribution at the one day time point compared to DMSO, but statically significant differences did begin to appear on day 2 (Figure 4-6, Table 5). On day 2, an increase in sub-G_1 and G_1 cells, and a decrease in S and G_2/M cells was observed. This suggests a slowing of cell growth and an induction of cell death (Darzynkiewicz, Bedner et al. 2001). On day 3 the number of cells with sub-G_1 content was further increased. No difference in G_1 cells was observed on this day compared to DMSO, but the number of S and G_2/M cells were significantly lower. By day 6, the number of sub-G_1 cells had increased to nearly 60% of the population and a drastic decrease in G_1 cells had occurred since day 3. Together, these data demonstrate a progressive and dramatic decrease in C6-treated MV4:11 proliferation and an increase in programmed cell death induction over time.

Effect of WDR5 WIN site inhibition on apoptosis induction

To further investigate the effect of WDR5 WIN site inhibition on cell viability over time, I again chose to focus on the effects elicited by our most potent inhibitor C6. I treated MV4:11 cells for 0, 1, 2, 3 or 6 days with DMSO, 2 μM C6 or C6nc and then performed a trypan blue exclusion assay (Figure 4-7A). Tyrpan blue is a stain that is excluded from live cells, which have intact plasma membranes, but stains dead cells which do not have intact membranes. The number of cells that exclude the blue stain represents the number of viable cells (Strober 2001). I found

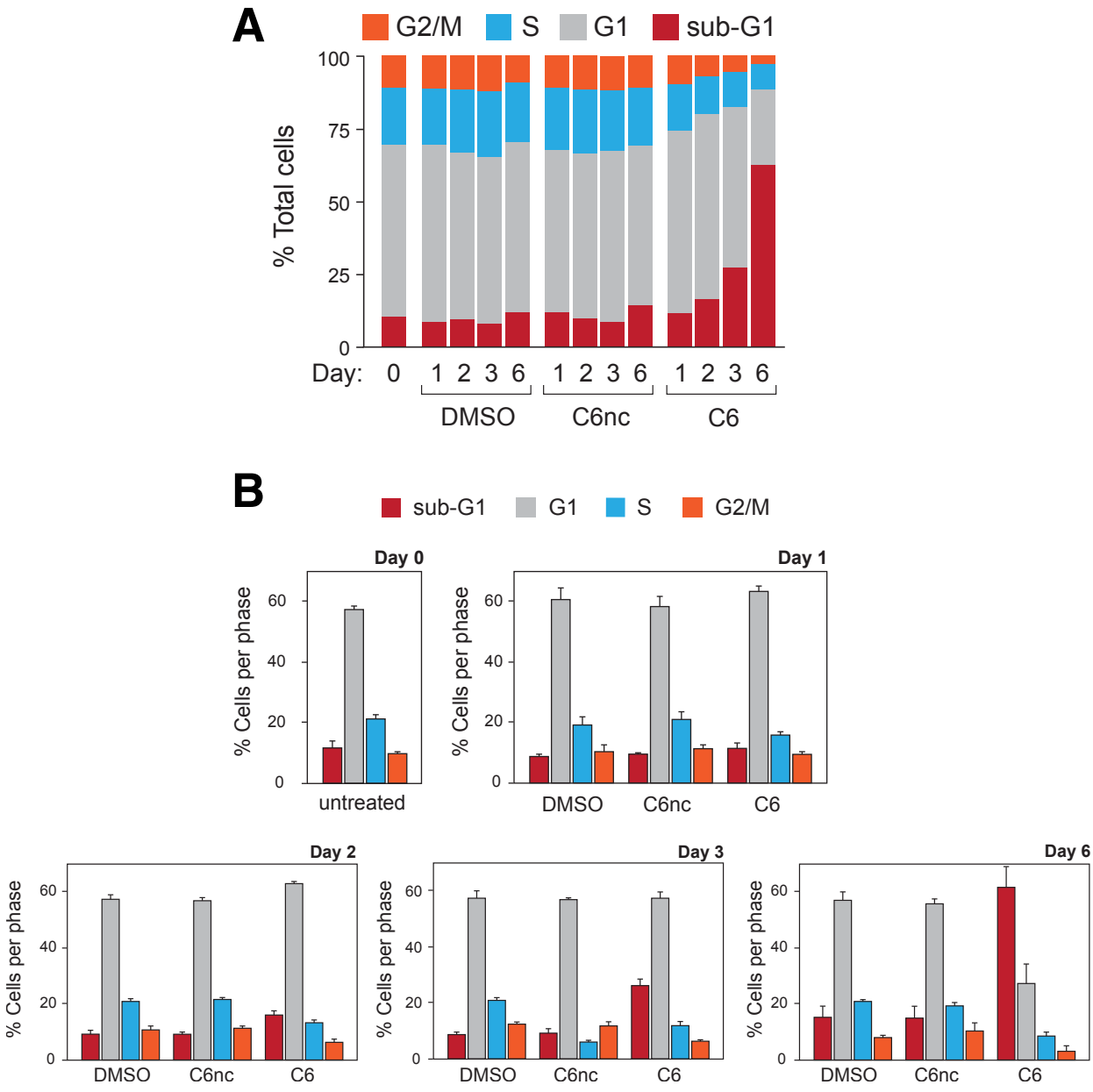

Figure 4-6 WDR5 WIN site inhibition increases the percentage of cell with sub-G1 DNA content over time. (A) Stacked bar graph showing the distribution of cell cycle phases as determined by flow cytometry, in MV4:11 cells treated with DMSO, or 2 μM C6nc or C6 for the indicated times. (B) The same data as in (A) presented as unstacked bar graphs with error bars representing the standard error of the mean. n = 3.

Table 5. p-values for MV4:11 cell cycle distribution over time after C6nc and C6

	C6nc p-value	C6 p-value
DAY 1		
sub-G1	0.043	0.23
G1	0.62	0.57
S	0.78	0.072
G2/M	0.77	0.70
DAY 2		
sub G1	0.98	**0.0087**
G1	0.67	**0.0047**
S	0.89	**0.0015**
G2/M	0.61	**0.016**
DAY 3		
sub-G1	0.68	**0.0021**
G1	0.59	0.92
S	0.14	**0.0014**
G2/M	0.82	**0.0019**
DAY 6		
sub-G1	0.98	**0.0069**
G1	0.88	**0.015**
S	0.38	**0.0005**
G2/M	0.40	**0.016**

p-values for three biological replicates of the cell cycle distribution time course were calculated using a two-tailed Student's t-test comparing C6nc to DMSO or C6 to DMSO. p-values less than 0.05 were considered significant and are shown in bold.

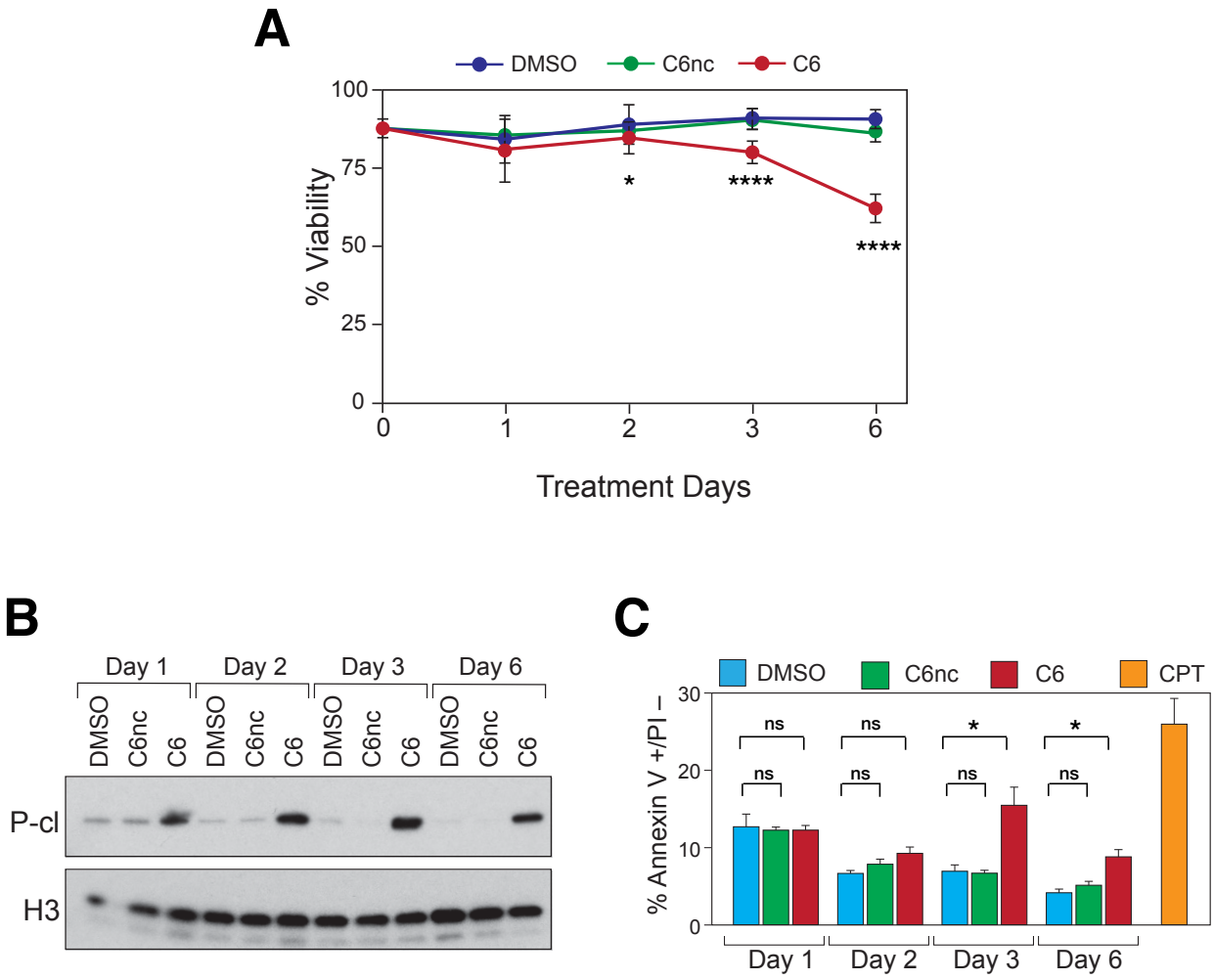

Figure 4-7. WDR5 WIN site inhibitors induce apoptosis. (A) MV4:11 cells were treated with DMSO, or 2 μM C6 or C6nc, samples collected at the indicated time points, and live cells quantified via trypan blue exclusion. To prevent culture overgrowth, the DMSO and C6nc treated samples were replated at day three to the original starting density and treatment continued. n = 3, error bars represent standard deviation of the mean. (B) Western blot for cleaved PARP-1 (P-cl) or histone H3 in lysates from MV4:11 cells treated with DMSO, 2 μM C6nc or 2 μM C6 for the indicated times. This experiment was repeated in biological duplicate. (C) Bar graph showing the percentage of Annexin V positive and propidium iodide (PI) negative cells in MV4:11 cells treated with DMSO , or 2 μM C6nc or C6 for the indicated days. Camptothecin (CPT) was used as a positive control for induction of apoptosis. n = 3, error bars represent standard error of the mean. For (A) and (C), p-values were determined compared to DMSO by two-tailed Student's t-test. "ns" means "not significant" ($p = > 0.05$), * indicates $p = < 0.05$, **** indicates $p = < 0.0001$.

that the viability of cells treated with C6 was not significantly different than DMSO treated cells ($p = 0.34$) after one day of treatment. The viability began to significantly and progressively decrease from 84% on day 2 ($p = 0.02$) to 64% on day 6 ($p = > 0.0001$). The cell viability of C6nc treated cells was not significantly different than DMSO treated cells at any time point.

Because a decrease in cell viability by trypan blue exclusion could be due to either apoptosis or necrosis, I probed for more direct hallmarks of apoptosis. Caspases are a family of cysteine proteases that function as the primary mediators of apoptosis (Oliver, de la Rubia et al. 1998). Upon induction of apoptosis, caspases become activated and proteolytically cleave specific protein substrates, which then contribute to the molecular and morphological changes that occur during apoptosis. One such substrate of caspases 3 and 7 is PARP-1, a DNA repair enzyme that is inactivated upon cleavage. The appearance of cleaved PARP-1 serves as a relatively early marker for caspase-mediated apoptosis and can be detected via Western blot. I treated MV4:11 cells overtime with 2 μM C6 or C6nc, then probed whole cell lysates with an antibody specific for a fragment of PARP-1 that is generated after cleavage by activated caspases 3 and/or 7 (Figure 4-7B). I found that C6 induces caspase-mediated cleavage of PARP-1 relative to DMSO. Notably, I could detect cleaved PARP-1 within 24 hours following treatment, indicating that C6 begins to influence cellular processes soon after exposure.

I further assayed for direct hallmarks of apoptosis induction by staining for the presence of phosphatidylserine on the surface of treated cells. In viable cells, phosphatidylserine is localized to the inner leaflet of the cell membrane. Upon induction of apoptosis, phosphatidylserine is translocated to the outer leaflet, where it can be detected by binding of the recombinant protein annexin V conjugated to a fluorophore. By staining with annexin V and propidium iodide (PI), a non-cell permeable DNA stain, I could easily quantify viable cells (annexin V -/PI -), apoptotic cells (annexin V +/PI -) and necrotic or very late apoptotic cells (annexin V +/PI +) via flow cytometry (Darzynkiewicz, Bedner et al. 2001). As a positive control for apoptosis, MV4:11 cells were treated with 2 μM of the DNA damaging agent camptothecin (CPT). I found that the proportion of apoptotic cells after C6nc treatment was not significantly different than DMSO treated cells at any time point. The number of apoptotic cells after C6 treatment trended toward an increase starting on day 2 and was significantly increased on day 3 ($p = .006$) and day 6 ($p = .006$) (Figure 4-7C). This was later than the other markers of apoptosis assayed above. The annexin V+/PI- state of the cells is transient and will shift to annexin V+/PI+ overtime as the cell

dies (Darzynkiewicz, Bedner et al. 2001). It is possible that the annexin V+/PI- state is more temporally dynamic than the other apoptotic markers measured, and therefore a smaller proportion of the cells were identified as apoptotic during the snap shot in time when annexin V staining was completed.

The cells within the population were not synchronized in the cell fate experiments described above. Therefore, individual cells within the population could undergo events at different times, thus spreading the proliferative arrest and/or cell death of the cells within the population out over time. However, by considering all of the cell fate data described above, a consistent timeline of the effects of C6 on MV4:11 cells becomes apparent. These experiments demonstrate that C6 effects MV4:11 cells fairly quickly, with a sensitive marker of early apoptosis (PARP-1 cleavage) being detected within 24 hours, before a reduction in total cell number is observed. Most of the cell fate assays show significant changes on day 2. The growth of the cell population is inhibited (live cell count/mL and cell cycle analysis) and the presence of dead (trypan blue exclusion) or dying cells (PARP-1 cleavage, sub-G1 cells, annexin V+/PI- cells) in the culture is increased. The number of dead or dying cells continues to drastically increase over time from 2 to 6 days.

Because I found that induction of apoptosis and proliferative inhibition increased over the 6-day time course, I was interested in determining if the cellular efficacy of our compounds would increase if the proliferation assay was extended to 7 days. I hypothesized that the GI_{50}s for MV4:11 cells treated with C3 and C6 would decrease in concentration when treated for 7 days compared of 3 days. To test my hypothesis, I repeated the CellTiter-Glo proliferation assay for MV4:11 cells treated for 7 days (Figure 4-8). Indeed, the GI_{50} of C3 treated cells decreased from 6.7 μM after 3 days to 930 +/- 70 nM after 7 days, and the GI_{50} of C6 treated cells decreased from 3.2 μM after 3 days to 257 +/- 62 nM after 7 days. These data indicate that while evidence of WDR5 WIN site inhibitor treatment affecting cellular processes can be seen within the first 24 hours of treatment, the magnitude of cellular inhibition increases over time. Overall the data presented in this subsection greatly improve our understanding of how a population of sensitive cells responds to inhibitor treatment over time.

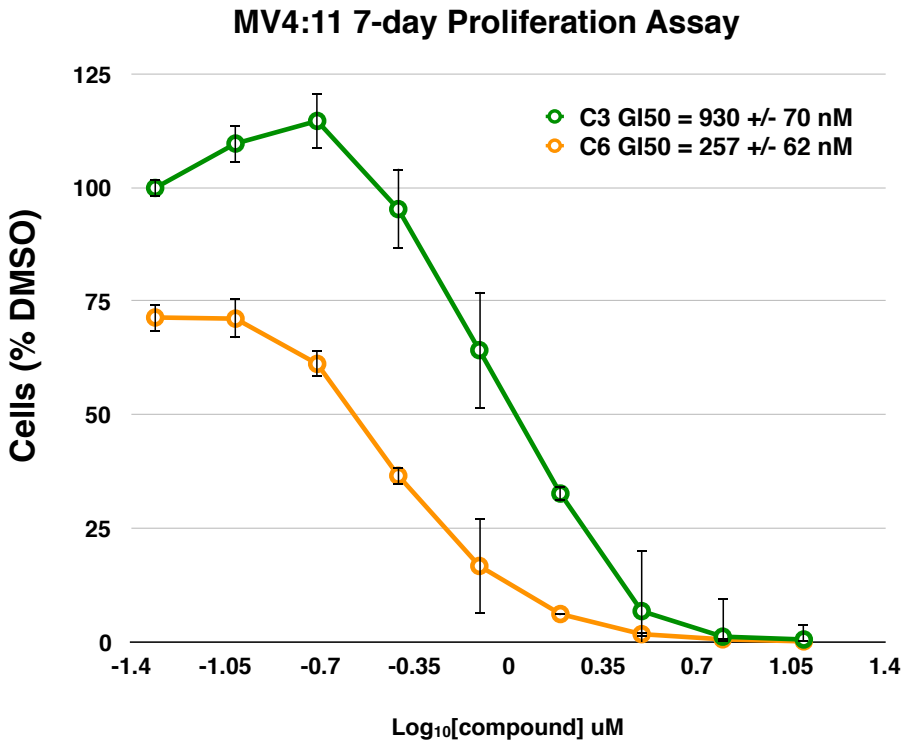

Figure 4-8. Inhibition of MV4:11 proliferation after 7 days of C3 or C6 treatment. Dose-response curves for compounds C3 and C6 after 7-day treatment of MV4:11 cells. Error bars represent standard error of the mean (SEM). GI_{50}s +/- the SEM are shown.

Discussion

The WIN site of WDR5 has been validated as a therapeutic target in leukemia cell lines expressing an oncogenic MLL-fusion protein (Cao, Townsend et al. 2014, Karatas, Li et al. 2017, Gupta, Xu et al. 2018), yet the mode by which WIN site inhibitors function requires more rigorous investigation. WDR5 WIN site inhibition has also been stated to selectively kill MLLr leukemia cell lines but not WT MLL1 cell lines, yet the effects of peptidomimetic MM-401 and the monobody Mb(S4) have only been reported for a small number of MLLr cell lines. The small molecule WDR5 inhibitor OICR-9429 has not been published in the context of MLL-Leukemia to date. Therefore, it is important to expand the number and variety of leukemia cell lines tested to determine if the selectivity of WIN site inhibition for MLLr cell lines withstands further testing. In order to understand how WDR5 WIN site inhibitors function, and thus to understand if WIN site blockade is a valuable cancer therapeutic strategy, it is also important to understand how sensitive cells respond to inhibitor treatment over time.

In this chapter, I first investigate the effects of our WDR5 WIN site inhibitors C3 and C6 on a panel of leukemia cell lines to identify sensitive cell lines and determine if sensitivity correlates with MLL-fusion expression. I report that while some cell lines that express an MLL-fusion such as MV4:11 and Molm13 are sensitive to C3 and C6, others such as NOMO-1, MONO-Mac-6 and THP-1 are very resistant. Therefore, expression of an MLL-fusion alone is not sufficient to confer sensitivity to WDR5 WIN site inhibition. This was very surprising given the model of MLL-leukemogenesis that provided the initial rationale in the field for targeting the WDR5 WIN site (Ballabio and Milne 2014, Cao, Townsend et al. 2014). This model predicts that any leukemia cell expressing an MLL-fusion will be sensitive to WDR5 WIN site inhibition. The MLL-fusion complex cooperates with wild-type MLL1 HMT activity at key oncogenic loci such as *HOXA9* and *MEIS1* to drive leukemogenesis. By blocking interaction of WDR5 and the WIN peptide of MLL1, the wild type complex could be thwarted and MLL-leukemogenesis would be selectively ameliorated. While WDR5 has been validated as an anti-MLL-leukemia target (Cao, Townsend et al. 2014, Gupta, Xu et al. 2018), the observation that an MLL-fusion alone is not sufficient to confer sensitivity indicates that our understanding of how WDR5 contributes to MLL-leukemogenesis is incomplete. The detailed evaluation of the mechanism of our inhibitors presented throughout this thesis, therefore helps to uncover novel basic biology of how WDR5 functions in the context of MLL-leukemia.

Several observations presented here support the idea that the selective proliferative inhibition observed is due to on-target activity of our compounds. First, the proliferation demonstrate a structure activity relationship (SAR) of C3 and C6, meaning that as the *in vitro* binding affinity (potency) of the WDR5 inhibitor increases, so does the cellular growth inhibition (efficacy). The difference between the magnitude of potency and efficacy for C3 and C6 is considerable, with K_ds being in the low nanomolar to picomolar range and GI_{50}s being in the micromolar range. A shift between potency and efficacy is a common phenomenon in drug discovery because the compound potency (K_d) is measured *in vitro* under well-defined and static conditions with purified proteins; However, the efficacy assays performed in cells are dynamic and are influenced by more elaborate pharmacokinetic parameters. These parameters include, but are not limited to, compound molecular weight, membrane permeability, rate of diffusion, lipophilicity, solubility, metabolization, compound efflux and target protein concentration. In addition, cells may utilize biological mediators not present in *in vitro* potency assays to respond to and actively mitigate the action of a compound. The compound likely also has to compete with other proteins for binding to the target protein in cells, which does not occur with the purified proteins used in *in vitro* assays (Waldman 2002). The shift in potency and efficacy is consistent between C3, C6 and OICR-9429 which are all from distinct chemical series. Additionally, the CETSA target engagement EC_{50}s for C3 and C6 (2.5 μM and 60 nM, respectively) in MV4:11 cells correlate with their respective WDR5 binding affinities (1.3 nM and 0.1 nM) and also correlate with the GI_{50}s of sensitive cell lines in the proliferation assays (Table 4). C3 and C6 also both selectively inhibit the HMT activity of MLL1 *in vitro* but not other SET-type complexes that do not require WDR5 WIN site engagement (chapter III). Together, these structure/activity relationships provide evidence that our WDR5 WIN site inhibitors have on-target activity and that the induction of apoptosis observed is due to WDR5 inhibition. This idea is further strengthened by the observation that the negative control compounds C3nc and C6nc have little to no activity in cells despite only minute rearrangements in structure relative their active counterparts.

In this chapter, I also empirically determine that the sensitivity of the leukemia cell lines tested correlates best with expression of wild type p53 and an MLL-fusion. This was unexpected, as expression of wild type p53 has not been previously reported as being a contributing factor to WDR5 inhibition sensitivity; although, most MLL-fusion cells retain wild type p53 because the

fusion protein can stimulate repression of p53 transcriptional activity (Wiederschain, Kawai et al. 2005). All of the published MLL-fusion cells lines that were tested for sensitivity to MM-401 express wild type p53 (Cao, Townsend et al. 2014), and thus the correlation between p53 and sensitivity may have simply been missed due to the choice of cell lines used. My observation that sensitive correlates with p53 expression in MLL-fusion cells suggests that p53 is involved in the cellular response to WIN site inhibition.

The hypothesis that p53 is involved in the cellular response to WIN site inhibition fits well with the observation that C6 induces markers of programed cell death such as increased sub-G1 DNA content, cascade-dependent PARP-1 cleavage and Annexin V staining. MM-401 has also been shown to increase G_1 cells and decreased G_2/M and S cells on day 2 (sub-G_1 cells were not quantified) and induce apoptosis in MLL-fusion cells (Cao, Townsend et al. 2014). p53 is known to function as a master regulator of the cell cycle and apoptotic pathways (Brady and Attardi 2010). Direct and stringent genetic approaches used to test the assumption that p53 is involved in the response to WDR5 WIN site inhibition will be presented in chapter VIII. It is also imperative to note that the proliferation data shown in this chapter simply correlate C3 and C6 sensitivity with expression of an MLL-fusion in conjunction with wild type p53. Further direct assessment of whether expression of an MLL-fusion in a wild type p53 background can confer sensitivity is needed and will be addressed in more detail in the Future Directions sub-section of chapter IX.

In contrast, to the findings presented here, MM-401 and Mb(S4), have been shown to induce morphological changes in MLL-fusion cells that are consistent with myeloid differentiation (Cao, Townsend et al. 2014, Gupta, Xu et al. 2018). However, Mb(S4) has a relatively weak Kd of 5 nM for WDR5 binding and the concentration of the “dose” of Mb(S4) present in cells was not quantitatively determined (Gupta, Xu et al. 2018). No morphological changes consistent with differentiation were observed with C6 after 3 days. It should also be noted that in the published studies utilizing MM-401 and Mb(S4), WDR5 was inhibited for much longer than 3 days. Cells were treated with MM-401 for 7 days and cells expressed Mb(S4) for roughly three weeks before being stained. The rational for doing so was related studies targeting other epigenetic regulators (Bernt, Zhu et al. 2011, Knutson, Wigle et al. 2012, Borkin, He et al. 2015) which theorize that epigenetic marks are stable and thus time is required to allow for removal or dilution of the existing marks before cellular inhibition occurs. The lack of differentiation

observed with C6 is not believed to be due to off-target effects of C6 as the structure activity relationships discussed above support on-target activity. Sufficient numbers of cells do not remain after 3 days of 2 uM C6 treatment to complete the staining as was done for MM-401 or Mb(S4). In the future the longer-term effects of inhibiting WDR5 could be tested by treating with a lower dose of C6. From the experiments presented in this chapter, I am not able to fully determine whether C6 functions differently from MM-401, Mb(S4) or OICR-9429, or if they function via the same mechanism, but C6 is more potent. Therefore, in subsequent chapters, I utilize OICR-9429 treatment side-by-side with C6 to address whether the effects observed are specific for C6 or if there is a conserved mechanism of action utilized by other known WDR5 inhibitors.

The time course experiments presented indicated that changes in cell fate can begin to be seen early after WDR5 WIN site inhibition, within about 2 days. This early response to WDR5 inhibitor treatment contrasts with studies utilizing small molecule inhibitors targeting DOTL1 (Bernt, Zhu et al. 2011), Menin (Borkin, He et al. 2015) and EZH2 (Knutson, Wigle et al. 2012), which all take 5-10 days to observe significant cellular effects. As stated above, the rational for why these inhibitors take so long to affect cancer cells is because the existing histone methylation is believed to be stable and thus takes a long time to be removed or diluted by cell division. If this is true, the fact that WDR5 WIN site inhibitors function quickly suggests that inhibiting WDR5 may not kill cells by inhibiting MLL1-mediated histone methylation. To date a thorough detailing of the rapid response of MLLr cells to WDR5 WIN site inhibition that occurs on the order of hours, not days, after treatment has not been published by others. I believe that the long-time points used in other studies fail to focus on the primary mechanism of action that precede apoptosis induction. A better understanding of this early response to WDR5 inhibition in sensitive cells and how that may differ from insensitive cells is critical to fully understand the biological consequences of WDR5 WIN site inhibition. Together, the results presented in this chapter lead me to focus further on the early and direct consequences of WDR5 WIN site inhibition. Understanding the biological changes at short time points is necessary to fully elucidate the mechanism through which our WDR5 WIN site inhibitors function and understand the full extent of their utility in combatting cancer

CHAPTER V

WDR5 BINDING IS ENRICHED AT A DISCRETE SUBSET OF RIBOSOMAL PROTEIN GENES

Introduction

The major objective of this thesis is to utilize novel and potent small molecule inhibitors to discover the biological consequences of inhibiting the WDR5 WIN site in MLL-leukemia cells. It is reasonable to propose that the mechanism through which WDR5 WIN site inhibitors impede the growth of MLL-fusion cells is connected to the role of WDR5 as a chromatin and transcriptional regulator (Guarnaccia and Tansey 2018). Therefore, I hypothesized that the primary mechanism of action of our WDR5 WIN site inhibitors would occur at genomic sites where a robust WDR5 signal can be detected by techniques such as chromatin immunoprecipitation (ChIP). However, the full repertoire of genes that are bound by WDR5 has not been described to date, making it hard to predict what the full impact of WDR5 inhibition on transcriptional regulation may be. Therefore, in order to best address my hypothesis that WDR5 inhibitors function at WDR5-bound loci, I needed to first determine the genomic loci with enrichment of WDR5 in unperturbed leukemia cells. I predicted that the set of WDR5-bound genes would include genes classically associated with MLL-leukemogenesis, such as *HOXA9* (Thorsteinsdottir, Kroon et al. 2001). Furthermore, it was unknown whether the genes that are bound by WDR5 in cell lines that are sensitive (MV4:11) and insensitive (K562) to WDR5 inhibition are the same or different. I initially hypothesized that the WDR5-bound genes in MV4:11 cells, which express an MLL-fusion, would include genes classically associated with MLL-leukemogenesis, but K562 cells which, do not express a fusion, would not. This prediction could explain why the two cell lines have different cellular responses to WDR5 WIN site inhibition.

To address my hypotheses, I began by using ChIP in a biased fashion to assess WDR5 enrichment at *HOXA9,* a gene tightly linked to MLL-leukemogenesis. WDR5 has also been implicated in driving the over-expression of *HOXA9* in MLL-fusion cells (Milne, Kim et al. 2010, Wu and Shu 2011, Lu, Tao et al. 2018). Next, the genome-wide binding of WDR5 was

determined in an unbiased fashion by Dr. Caleb Howard using ChIP coupled to next generation sequencing (ChIP-seq) in both MV4:11 and K562 cells. The genes bound by WDR5 in the two cell types were then compared. Finally, Gene Ontology (GO) analysis was implemented to determine if the genes bound by WDR5 in either cell type cluster into any particular biological function or pathway.

In sum, the data presented in this chapter determine that robust ChIP signal of WDR5 was not found at any classically MLL-leukemia associated genes, such as *HOXA9*. Additionally, enrichment of WDR5 on chromatin appears to be functionally distinct from the role of WDR5 as a component of the H3K4me3 machinery. Finally, we define a discrete and conserved set of ribosomal protein genes that are bound by WDR5 across disparate cell types, thus suggesting that WDR5 is a major regulator of ribosome protein gene transcription, and forecasting that WIN site inhibitors may function by inhibiting ribosome protein gene production.

Results

Probing localization of WDR5 on chromatin at the HOXA9 locus

HOXA9 is a developmental transcription factor primarily expressed in immature blood cells and is normally down-regulated as hematopoietic cells differentiate (Krivtsov and Armstrong, 2007). Over-expression of HOXA9 is sufficient to transform mouse bone marrow stem cells and persistent elevated expression of HOXA9 is a hallmark of MLL-leukemias. The mechanism though which over-expression of HOXA9 is maintained has not been fully elucidated, however studies have implicated WDR5 as a critical factor in this process. For instance, it has been shown that MLL1-null mouse embryonic fibroblasts (MEFs) have no H3K4me3 at the *Hoxa9* locus as detected by ChIP and that expression of HOXA9 is very low (Milne, Kim et al. 2010). However, upon ectopic expression of the *MLL1* gene, MLL1 and H3K4me3 can both be detected at the *HOXA9* locus and HOXA9 expression rises. It was also shown in MLL1-null MEFs that ectopically expressed MLL-AF9 fusion protein cannot be detected by ChIP at the *HOXA9* promoter unless WT MLL1 is also expressed. The authors proposed that WT MLL1-mediates H3K4me producing an “open” chromatin structure that allows the MLL-fusion protein to bind and up-regulate *HOXA9*. Since interaction of WT MLL1 with the WIN site of WDR5 is required for the HMT activity of MLL1 *in vitro* (Xu, Li et al. 2016), the presence of both WT MLL1

and H3K4me3 at *HOXA9* has been used to infer that WDR5 is also present at this gene. This idea has been perpetuated in reviews of MLL1/WDR5 complex function in MLL-leukemogenesis (Wu and Shu 2011, Lu, Tao et al. 2018).

Because WDR5 has been inferred to be involved in MLL1-mediated catalysis of H3K4me at the *HOXA9* locus, but this was not definitively shown, I first asked if binding of WDR5 could be detected at *HOXA9*. Chromatin immunoprecipitation was used to detect WDR5 binding to chromatin in MV4:11 cells, an MLL-fusion cell line shown to be sensitive to WDR5 inhibitor treatment in chapter IV. Chromatin immunoprecipitation is a method used to investigate the interaction between a specific protein and genomic DNA region. Cells are harvested and formaldehyde, a reversible protein-DNA cross-linking agent, is added to stabilize protein-DNA interactions. The cross-linked chromatin is fragmented using sonication followed by immunoprecipitation of the protein of interest with an antibody. The protein-DNA cross-links are then reversed and the precipitated DNA fragments are purified. Finally, quantitative polymerase chain reaction (qPCR) is used to detect the amount of precipitated DNA from a specific locus of interest (Carey, Peterson et al. 2009).

I first identified a reproducible and robust positive control locus for WDR5 binding by investigating WDR5 binding a the *SNHG15 Ebox* locus. Small nucleolar RNA host gene 15 (*SNHG15*) encodes a long non-coding RNA (Dong, Meng et al. 2018). This locus was identified as a robust site of WDR5 binding in a previously published WDR5 ChIP-seq data set in HEK293 cells from our lab (Thomas, Wang et al. 2015). As a negative control, the *SNHG15 gene body* (GB) primer set from the aforementioned publication was used, as this site is not bound by WDR5. In addition to performing the ChIP with an antibody against WDR5, I included samples immunoprecipitated with a normal rabbit IgG antibody to control for background binding in the pull-down. I confirmed that the *SNHG15 Ebox* locus is also a robust and reproducible WDR5 binding site in MV4:11 cells and that the gene body is devoid of detectable WDR5 above background (Figure 5-1A).

After establishing good negative and positive control loci for WDR5 binding to chromatin in MV4:11 cells, I used the same ChIP DNA fragments to assess the presence of WDR5 at the

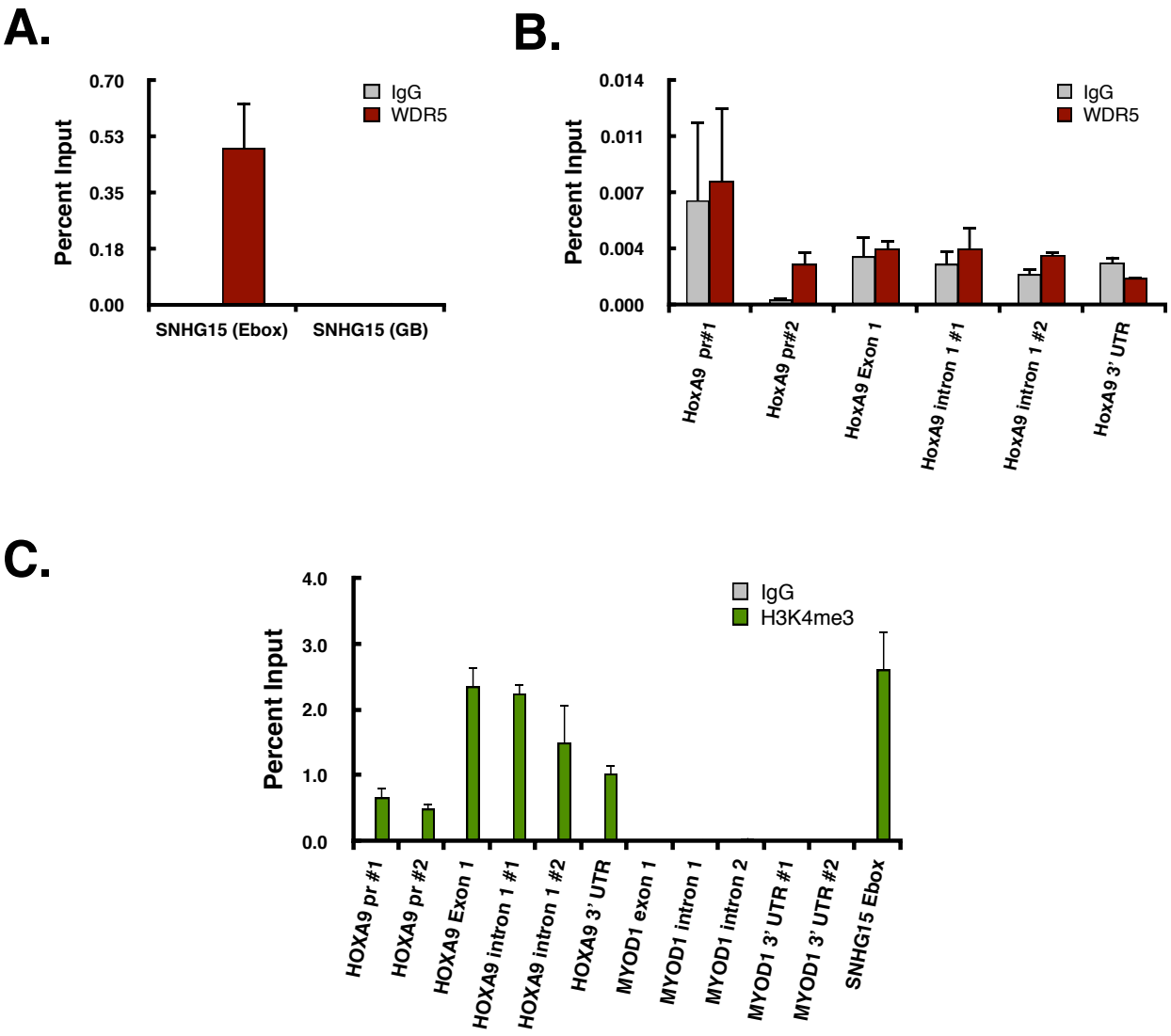

Figure 5-1. WDR5 fails to be detected on chromatin at the *HOXA9* locus. (A) Chromatin immuno-precipitation (ChIP) of WDR5 and IgG control at positive SNHG15 (Ebox) and negative SNHG15 (GB) control loci for WDR5 binding. (B) ChIP of WDR5 and IgG control at six loci spanning along *HOXA9* from the promoter (pr) to the 3' UTR. (C) ChIP of H3K4me3 and IgG control at six loci spanning along *HOXA9* from the promoter (pr) to the 3' UTR, five loci spanning from the first intron to the 3' UTR of *MYOD1*, and *SNGH15* Ebox. All error bars represent the standard error of the mean (SEM), and each experiment was completed in biological triplicate (n = 3).

HOXA9 locus. I designed a set of six primer pairs for loci spread out along the gene. WDR5 binding was not detectable above the IgG antibody background with any of the *HOXA9* primer sets (Figure 5-1B). It should be noted that the Y-axis maximum of Figure 5-1A is 50-fold higher than that of Figure 5-1B. Because the same ChIP samples were used to detect WDR5 at the positive control locus *SNHG15 Ebox* (Figure 5-1A), the absence of ChIP signal seen at the *HOXA9* locus (Figure 5-1B) was not due to a failure to immunoprecipitate WDR5 during the ChIP procedure.

Despite the lack of robust WDR5 ChIP signal at the *HOXA9* locus, I did find that this locus is enriched in H3K4me3 (Figure 5-1C). This was expected as *HOXA9* is expressed in MV4:11 cells and in general, high levels of H3K4me3 can be detected in the promoter region of active genes (Barski, Cuddapah et al. 2007). MYOD1, a myocyte specific gene (Brennan, Edmondson et al. 1990), was used as a negative control for the H3K4me3 ChIP, as this gene is silenced in MV4:11 cells and therefore is devoid of H3K4me3 (Figure 5-1C). Importantly, the lack of robust WDR5 ChIP signal at *HOXA9* demonstrates that detectable enrichment of WDR5 on chromatin is not required for H3K4me3 to be present. Perhaps WDR5 within an HMT complex binds too transiently with chromatin to be efficiently cross-linked and pulled-down by the ChIP protocol used. Or perhaps the histones could be epigenetically modified prior to insertion into chromatin so WDR5 does not need to be enriched on chromatin for H3K4me3 to be placed. Alternatively, perhaps the epitope recognized by the monoclonal Cell Signaling antibody used can not be accessed when WDR5 is incorporated into certain multi-protein complexes (see below). My findings suggest that at sites of robust WDR5 ChIP signal, WDR5 is likely important for a function unrelated to HMT complexes. This concept will be expanded further in the discussion of this chapter and revisited in subsequent chapters of this thesis.

Genome-wide localization of WDR5 on chromatin

After failing to detect WDR5 binding at the *HOXA9* locus despite the presence of H3K4me3, we wanted to determine all of the genomic loci at which robust WDR5 binding can be detected by ChIP. I hypothesized that the primary mechanism of action of WDR5 WIN site inhibitors is to act at sites in the genome that have robust levels of WDR5 binding as determined by ChIP-seq. ChIP-seq combines traditional ChIP with next generation sequencing to identify all of the DNA fragments that are immunoprecipitated. ChIP-Seq for WDR5 was performed by Dr. Caleb Howard in our laboratory to determine the loci where enrichment of WDR5 could be detected in

the sensitive cell line, MV4:11. Analysis of the ChIP-seq data set was performed by Jing Wang of the Vanderbilt Department of Biostatistics under the mentorship of Dr. Qi Liu of the Vanderbilt Center for Quantitative Sciences.

The WDR5 ChIP-seq in MV4:11 cells was initially performed using a rabbit monoclonal anti-WDR5 antibody called D9E1I that was purchased from Cell Signaling. As a control for background binding, ChIP-seq was also performed with a normal rabbit IgG antibody. The Cell Signaling D9E1I antibody detected 158 WDR5 binding peaks in MV4:11 cells (Figure 5-2). We were initially surprised by the relatively small number of WDR5 peaks detected by D9E1I. Monoclonal antibodies, such as D9E1I, detect a single epitope in the protein of interest. We wondered whether the low peak number could be due to inaccessibility or "masking" of the epitope detected by DE91I at some loci when WDR5 is engaged in specific protein-protein interactions. The epitope in WDR5 detected by the DE91I antibody is not known. Caleb subsequently repeated the WDR5 ChIP-seq experiment in MV4:11 cells using a different polyclonal WDR5 antibody called 429A that was purchased from Bethyl. The Bethyl antibody is a rabbit polyclonal antibody that recognizes epitopes mapped to a region between residues 1 and 50 of human WDR5. Polyclonal antibodies are a mixture of antibodies from different B cells that recognize multiple epitopes on the same antigen. By using a mixture of antibodies that detect different epitopes, it is less likely that WDR5 will fail to be detected in ChIP-seq due to epitope "masking". The Bethyl antibody detected 149 WDR5 binding peaks in MV4:11 cells (Figure 5-2). There was a high degree of overlap between the WDR5 peaks found with the two antibodies, with 67% of the Cell Signaling peaks also detected by the Bethyl antibody. The high degree overlap in the WDR5 binding peaks and the fact that both antibodies detected a fairly small number of peaks led us to believe that epitope "masking" was unlikely to explain the relatively low number of WDR5 peaks found with the Cell Signaling antibody. Ultimately, I chose to focus my studies on ChIP-seq data obtained with the Cell Signaling WDR5 antibody because subsequent testing of the Bethyl antibody by Dr. Lance Thomas in our laboratory showed that the Bethyl antibody recognizes some non-WDR5 species (personal communication).

We were next interested in determining where in the gene WDR5 is bound relative to the transcriptional start site (TSS). When analyzing all of the WDR5 peaks detected with the Cell Signaling antibody in MV4:11 cells, Jing Wang found that WDR5 binds mostly within 5 kilobases upstream and downstream of the TSS (Figure 5-3). Identifying that WDR5 tends to bind

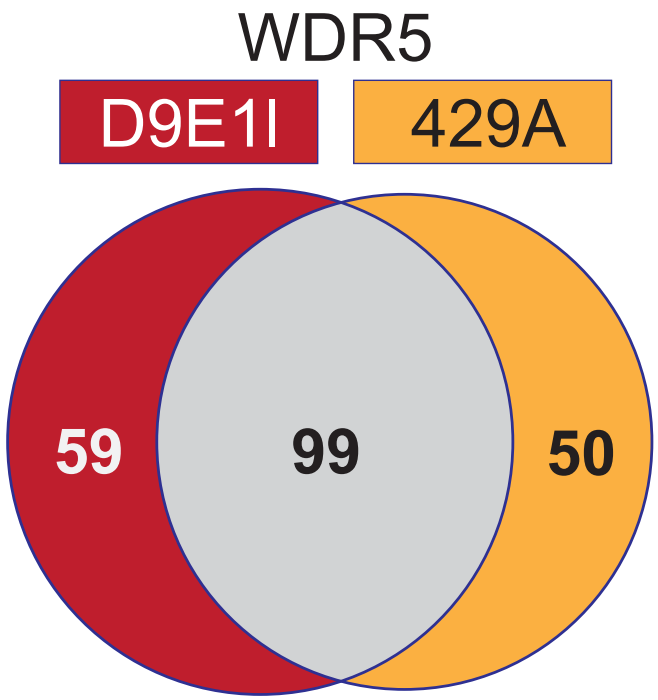

Figure 5-2. Overlap of WDR5 binding peaks in MV4:11 cells detected with two different WDR5 antibodies. Venn diagram showing the overlap in MV4:11 WDR5 binding peaks as determined by ChIP-seq using the D9E1I rabbit monoclonal antibody from Cell Signaling and the 429A rabbit polyclonal antibody from Bethyl.

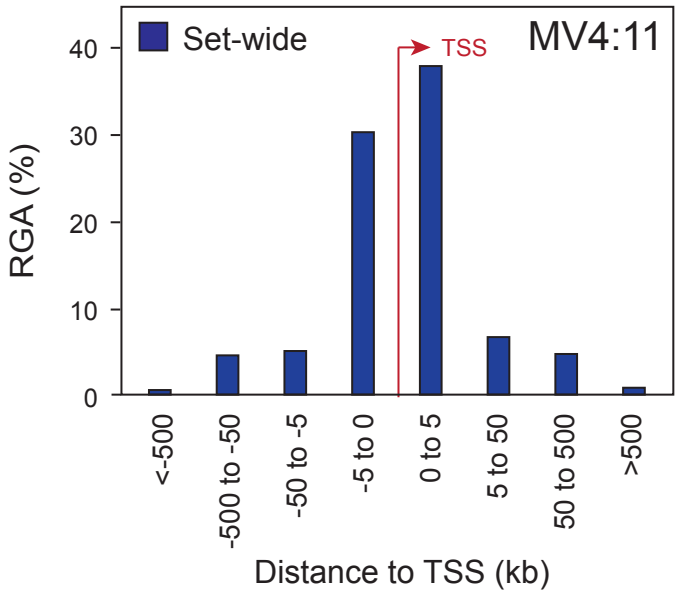

Figure 5-3. WDR5 binding on chromatin in MV4:11 cells is primarily TSS proximal. Distribution of WDR5 binding sites in MV4:11 cells binned according to distance from the annotated TSS. RGA refers to region-gene association. Set-wide indicates that all of the WDR5 peaks found in MV4:11 cells were included in this analysis.

relatively close to the TSS also helped us to confidently make gene assignments to WDR5 peaks. Consistent with my ChIP data presented in Figure 5-1B, the WDR5 ChIP-Seq did not detect binding of WDR5 to *HOXA9* nor any other classic MLL-leukemia connected genes. Figure 5-4 compares representative Interactive Genomics Viewer screen grabs from the MV4:11 WDR5 and IgG control ChIP-seq experiments. The Y-axis scales for IgG and WDR5 are the same for all genes shown. There is no WDR5 peak observed at the *HOXA9*, *HOXA10*, or *MEIS1* loci, three genes implicated in MLL1-fusion protein mediated leukemogenesis (Guenther, Lawton et al. 2008, Bernt, Zhu et al. 2011). In contrast, the screen grabs for two representative genes found to be bound by WDR5, *RPL35* and *RPS24,* show strong promoter proximal WDR5 binding peaks. Importantly, the ChIP-seq insured that a WDR5 peak was not simply missed in the *HOXA9* ChIP-qPCR experiment (Figure 5-1B) due to the peak being located outside of the genomic regions amplified by my six primers sets. I concluded that WDR5 is not enriched at MLL-leukemia associated genes, and therefore, inhibition of the WDR5 WIN site is unlikely to function by directly inhibiting MLL-leukemia associated genes. The effect of WDR5 WIN site inhibition on gene expression will be the subject of chapter VI.

I was next interested in seeing if the genes assigned to the WDR5 peaks in MV4:11 cells had a common functionality or were involved in a certain biological pathway. By determining a common type of gene bound by WDR5, it could be possible to infer which biological pathways WDR5 regulates. This could allow me to better understand how WDR5 WIN site inhibitors elicit their anti-proliferative effects. Gene Ontology (GO) analysis was used to determine if the genes bound by WDR5 in MV4:11 cells have a common functionality. GO terms are groups of genes based on their molecular function, cellular component or biological process. GO analysis determined which GO terms appeared more frequently than would be expected by chance when examining the set of GO terms assigned to the genes that are bound by WDR5 (Dessimoz and Škunca 2017). The top eight most significant GO terms for WDR5-bound genes in MV4:11 cells are shown in Figure 5-5. All eight GO terms were found to be connected to the ribosome. Upon closer inspection, it was found that 41 out of the 158 WDR5-bound genes were ribosomal protein genes (RPGs). We also observed WDR5 binding to genes encoding a subset of translation initiation factors including EIF3B, EIF3D, EIF4G1, EIF4G3, and EIF4A2 and 46 out of the 158 WDR5 bound genes were found to be functionally connected to protein translation. I concluded that genes connected to protein translation and the ribosome were likely to be directly regulated by WDR5 in sensitive cells.

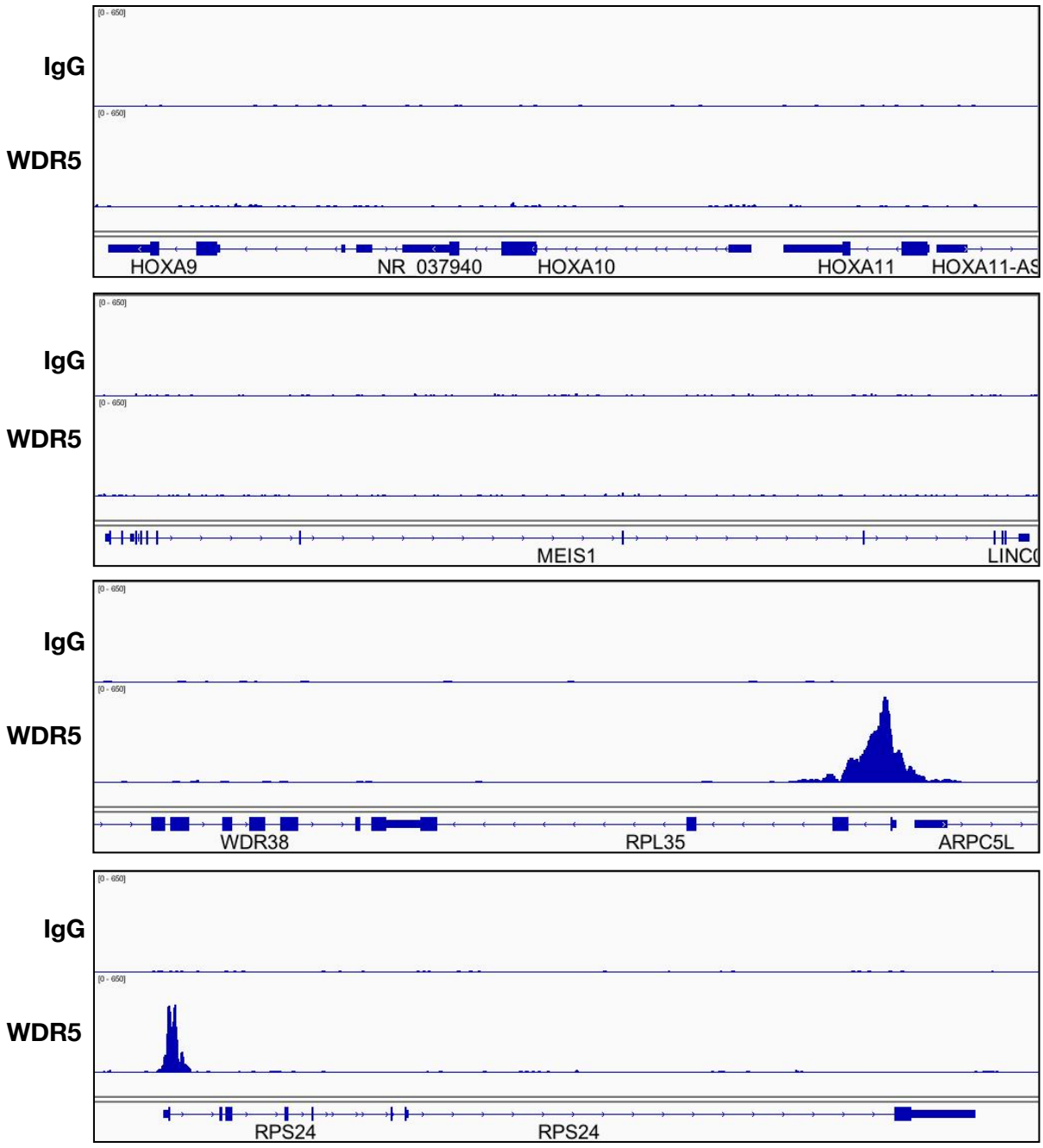

Figure 5-4. **WDR5 is robustly bound to ribosomal protein genes but not MLL-leukemia associated genes in MV4:11 cells.** Integrative Genomics Viewer screen grabs from one representative ChIP-seq replicate showing IgG control or WDR5 peaks in MV4:11 cells at the *HOXA9/HOXA10/HOXA11*, *MEIS1*, *RPL35*, and *RPS24* loci. The Cell signaling WDR5 antibody was used. The Y-axis scale is the same for all loci and for IgG control and WDR5.

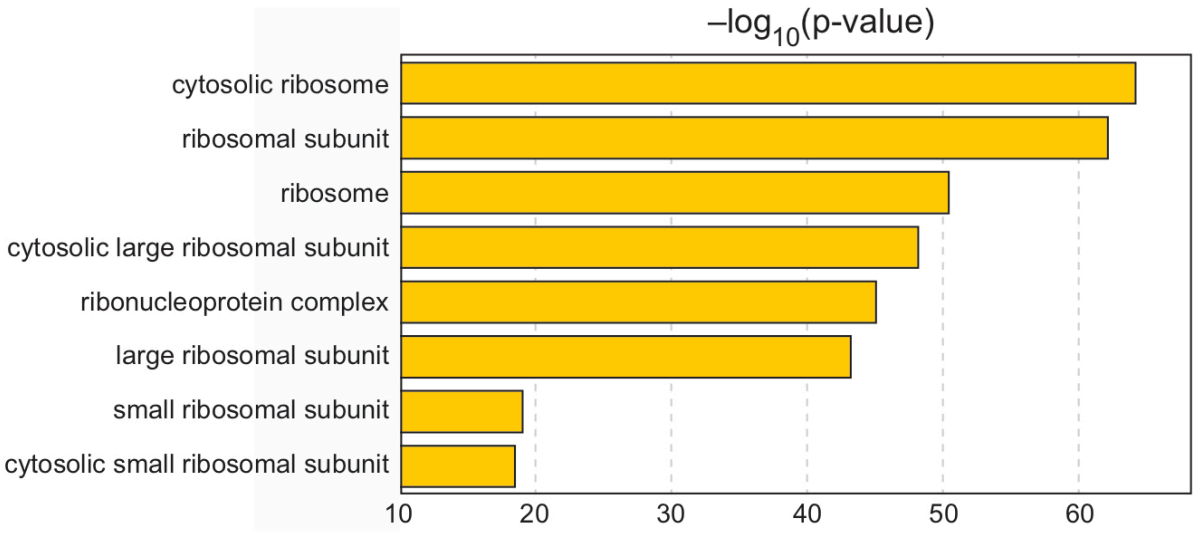

Figure 5-5. WDR5 binding is enriched at ribosomal protein genes in MV4:11 cells. Top eight gene ontology (GO) enrichment categories for genes bound by WDR5 in DMSO-treated MV4:11.

I also wanted to understand whether the genomic localization of robust WDR5 ChIP signal is the same or different in sensitive and insensitive cell lines. I hypothesized that the localization of WDR5 is different in sensitive and insensitive cells, and therefore, may explain why these cells have different responses to WDR5 WIN site inhibition. To assess whether the localization of WDR5 is the same or different in sensitive and insensitive cells, Caleb performed WDR5 or IgG control ChIP-seq in the insensitive cell line, K562. The WDR5 peaks found in K562 cells were then compared to those found in MV4:11 cells (Figure 5-6). 525 binding sites were detected with the Cell Signaling antibody in K562 cells, and there was a high degree of overlap between peaks found in K562 cells with those found in MV4:11 cells. Of all the MV4:11 WDR5 binding sites, roughly 72% (or 133 out of 158) were also found in K562 cells and only 25 genes were only bound in MV4:11 cells. We determined where in the gene WDR5 is bound in K562 cells relative to the transcriptional start site (TSS) as was done for MV4:11 cells. Again, Jing Wang found that WDR5 binds mostly within 5 kilobases upstream and downstream of the TSS (Figure 5-7). This indicated that the location of WDR5 binding within the genes is the same in sensitive and insensitive cells, and overall the sets of genes bound by WDR5 in MV4:11 and K562 cells are much more alike than different.

As for MV4:11 cells, we were interested in determining if the genes bound by WDR5 in K562 cells were enriched in a common functionality or biological pathway. GO analysis was again used to determine which GO terms, if any, appeared more frequently in the K562 WDR5-bound gene list than would be expected by chance. All of the top eight significant GO terms found for WDR5 bound genes in K562 cells were the same as that for MV4:11 cells (Figure 5-8). As for MV4:11 cells, the WDR5-bound genes in K562 cells were shown to have a highly significant enrichment in GO terms connected to the ribosome. This was not surprising due to the high degree of overlap in the sets of genes bound by WDR5 in MV4:11 and K562 cells. 46 WDR5-bound genes in K562 cells were found to be RPGs. Again binding of WDR5 was found at the translation initiation factors including EIF3B, EIF3D, EIF4G1, EIF4G3, and EIF4A2. The ChIP-seq data suggests that genes connected to the ribosome and protein synthesis are likely an important cohort of genes regulated by WDR5 in both MV4:11 and K562 cells. Therefore, we determined where WDR5 is bound relative to the transcriptional start site in just the ribosomal protein genes (Figure 5-9). We found high conservation of WDR5 binding within 0 to 5 kilobases downstream at the ribosomal protein genes in both cell types.

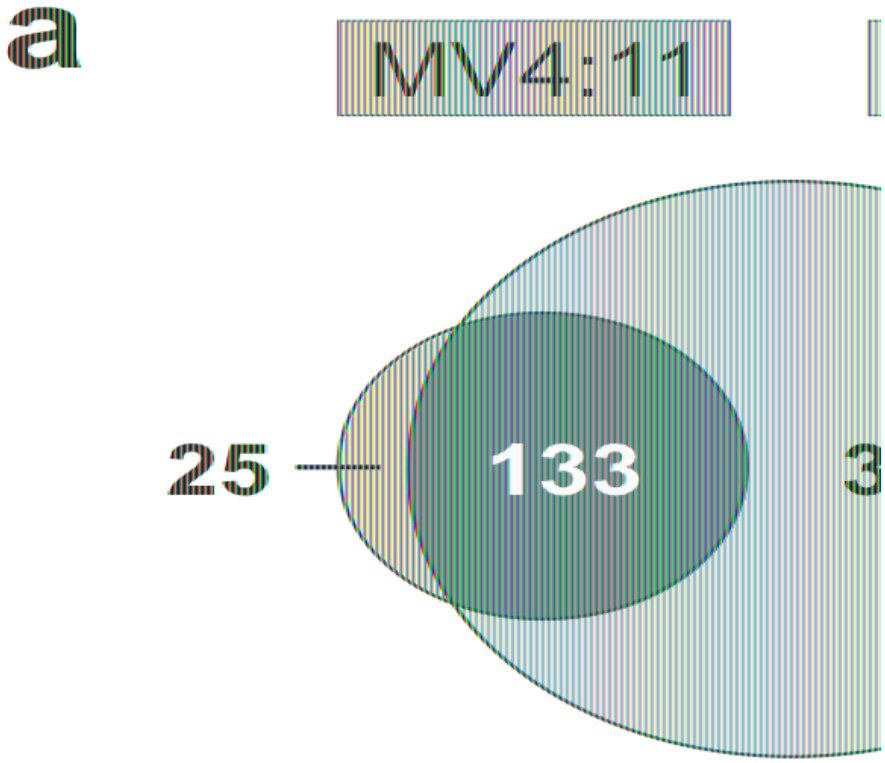

Figure 5-6. Overlap of WDR5 binding peaks in MV4:11 and K562 cells. Venn diagram showing the overlap of binding sites for WDR5 mapped by ChIP-Seq in MV4:11 and K562 cells.

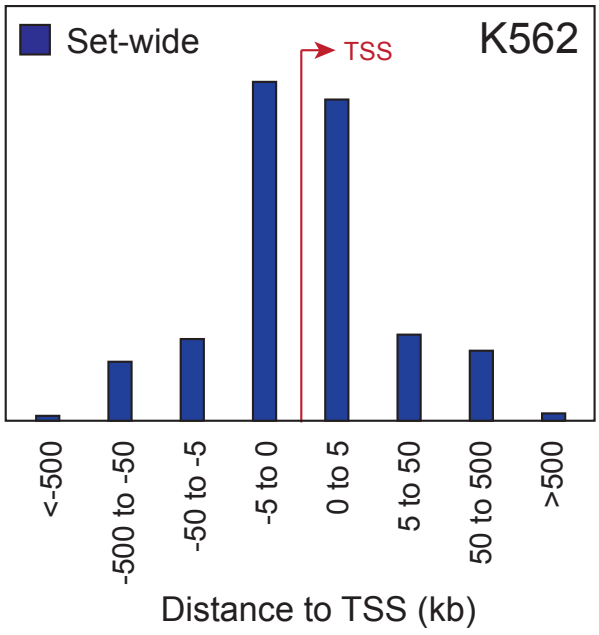

Figure 5-7. WDR5 binding on chromatin in K562 cells is primarily TSS proximal. Distribution of WDR5 binding sites in K562 cells binned according to distance from the annotated TSS. RGA refers to region-gene association. Set-wide indicates that all of the WDR5 peaks found in K562 cells were included in this analysis.

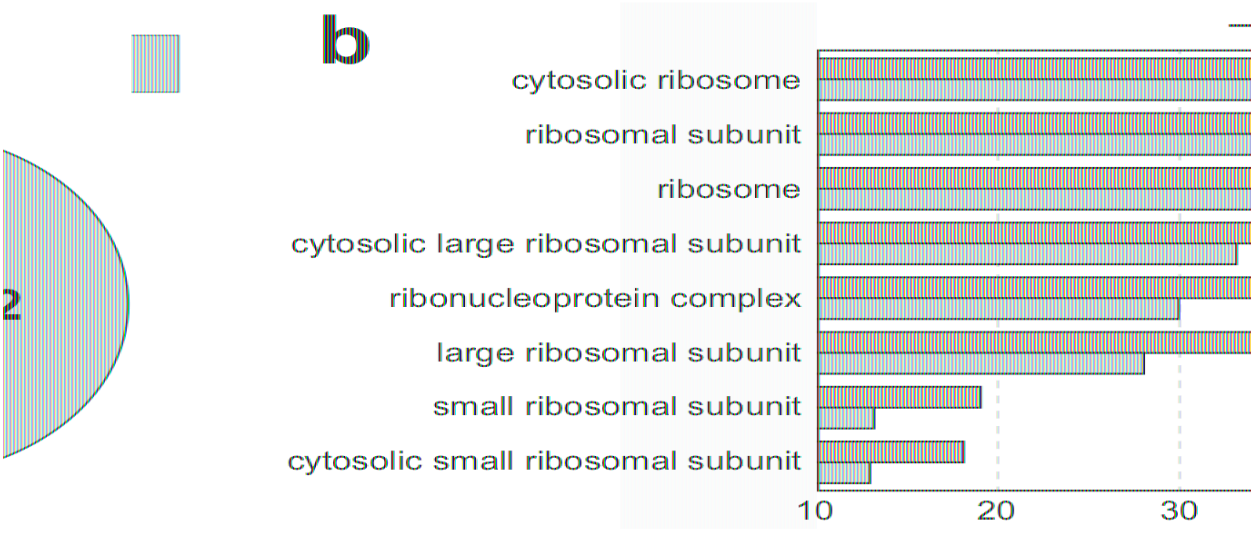

Figure 5-8. WDR5 binding is enriched at ribosomal protein genes in both MV4:11 and K562 cells. Top eight gene ontology (GO) enrichment categories for genes bound by WDR5 in DMSO-treated MV4:11 (yellow) or K562 (blue) cells.

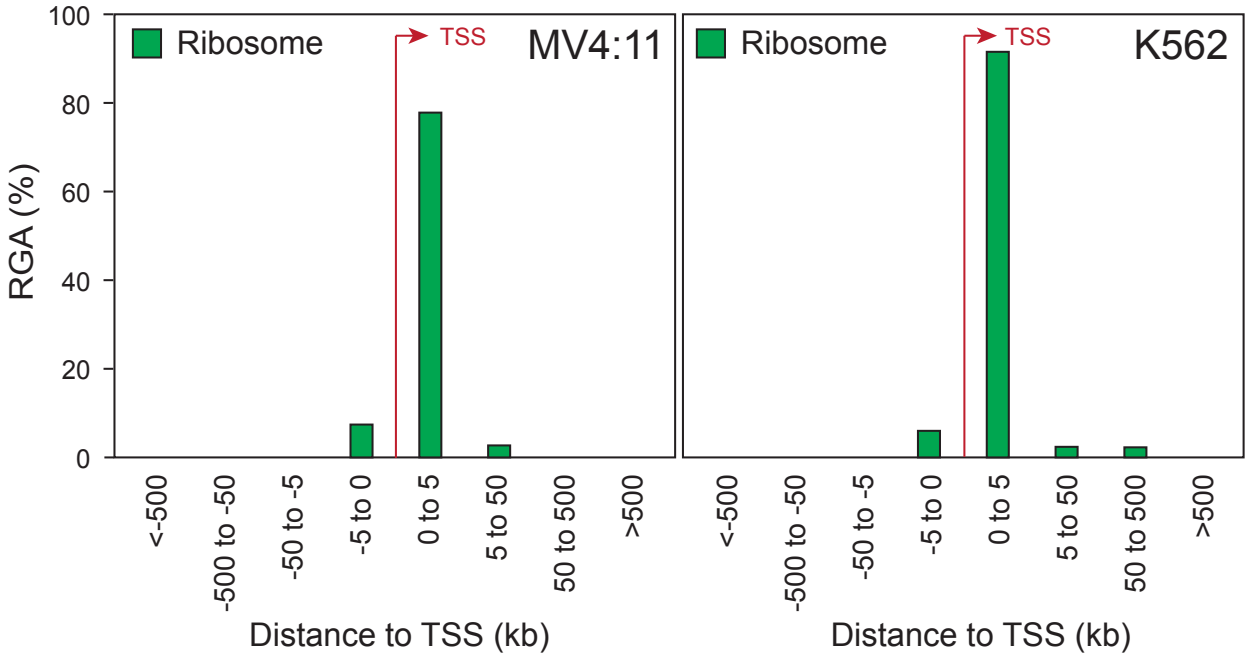

Figure 5-9. WDR5 binding on chromatin at ribosomal genes in MV4:11 and K562 cells is primarily TSS proximal. Distribution of WDR5 binding sites in MV4:11 and K562 cells binned according to distance from the annotated TSS. RGA refers to region-gene association. "Ribosome" indicates that only the WDR5 peaks found at ribosomal protein genes were included in this analysis.

The GO analysis of the WDR5 ChIP-seq data sets determined that WDR5-bound genes are enriched for RPGs in both MV4:11 and K562 cells. To better visualize whether the RPGs bound by WDR5 in MV4:11 and K562 cells are the same set of RPGS, we constructed Figure 5-10. Figure 5-10, also termed the “ribosomogram”, lists all of the RPGs of the large and small ribosomal protein subunits, with an orange box indicating that WDR5 was bound to that gene in the WDR5 ChIP-seq. WDR5 was found to be bound at a specific subset of RPGs, corresponding to ~40% of the small, and ~70% of the large subunit RPGs in both MV4:11 and K562 cells. To investigate whether this pattern of WDR5 localization at RPGs is unique to MV4:11 and K562 cells, published WDR5 ChIP-Seq data sets from the LnCap metastatic prostate cancer cell line (Kim, Banerjee et al. 2014) and the BGC823 gastric adenocarcinoma cell line (Sun, He et al. 2016) were analyzed. The analysis revealed a strikingly similar distribution of WDR5 binding across RPGs in these disparate cell types. The enrichment of WDR5 at a select subset of RPGs suggests that these are a major class of genes regulated by WDR5 and the conservation of WDR5 binding at a discrete set of RPGs across cell types suggests a conservation of WDR5 function at these genes. This observation also suggests that regardless of cell type, RPGs may represent a major class of genes effected by WDR5 WIN site inhibitors.

Discussion

The therapeutic utility of inhibiting WDR5 at the WIN site in the context of MLL-leukemia has been well established (Cao, Townsend et al. 2014, Gupta, Xu et al. 2018, Zhang, Zheng et al. 2018), but exactly how WIN site blockade functions in MLL-fusion cells is unclear. I reasoned that the primary mechanism of action of our WDR5 inhibitors would be connected to the functions of WDR5 as a chromatin and transcriptional regulator (Guarnaccia and Tansey 2018). Therefore, in this chapter we use ChIP and ChIP-seq to determine the full repertoire of robust WDR5 enrichment on chromatin in an MLL-leukemia context. I posited that these loci would likely be the primary transcriptional targets of WDR5 inhibition. We also compare the sets of WDR5-bound genes in leukemia cell lines that are both sensitive (MV4:11) and insensitive (K562) to WDR5 WIN site inhibition. By understanding the full repertoire of WDR5-bound/regulated genes in both sensitive and insensitive cells, I was able to better understand which

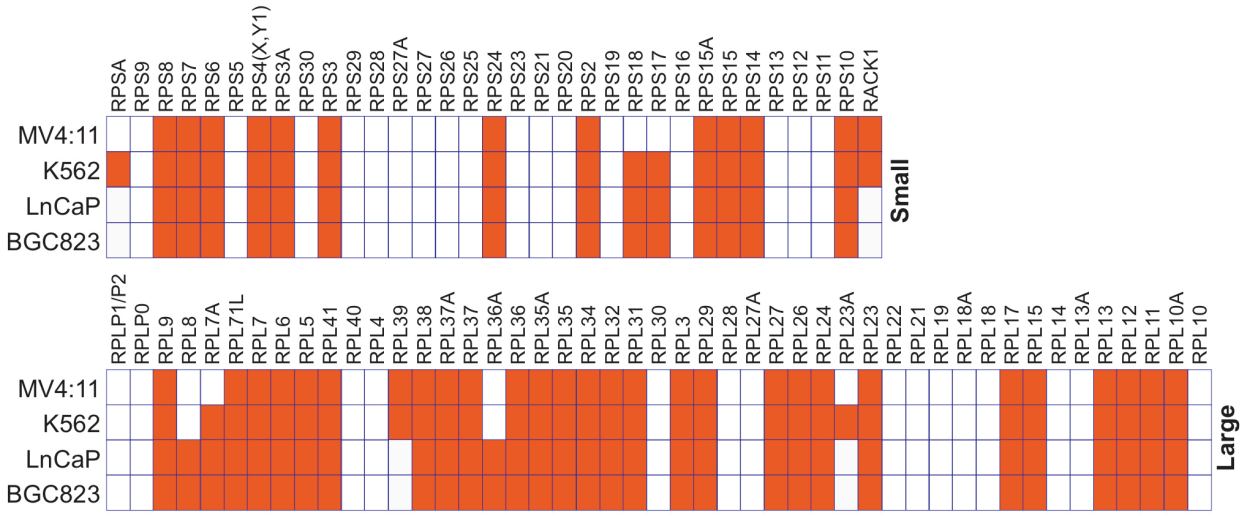

Figure 5-10. WDR5 binding to a select set of ribosomal protein genes is conserved across cell types. Small (top) and large (bottom) ribosome protein genes (RPG) are listed; an orange-filled box indicates that WDR5 is bound to that RPG in the indicated cell types. MV4:11 and K562 cell data were completed for this study. Data from LnCaP and BGC823 cells are from GSE55279 (WDR5 ChIP-Seq, EtOH-treatment) and GSE63763 (WDR5 NC_ChIPSeq), respectively.

genes are regulated by WDR5 and make testable predictions about how our WDR5 WIN site inhibitors may function.

A previous study sought to utilize ChIP-seq to assay genome-wide binding of WDR5, WT MLL1, MLL-AF9 and H3K4me in primary murine bone marrow cells transformed with the MLL-AF9 fusion protein (Xu, Li et al. 2016). They found that only 40% of the WDR5 peaks overlapped with WT MLL1 peaks. In contrast, H3K4me2 was found at nearly all MLL1 peaks and nearly all WDR5 peaks, as well as many other genes that were not bound by either MLL1 or WDR5. Taken together, these data indicate that while WDR5 is needed for MLL1-mediated H3K4me *in vitro* (Xu, Li et al. 2016), and H3K4me is a common feature of both WDR5 peaks and MLL1 peaks, it should not be assumed that the presence of MLL1 will coincide with WDR5 binding. The authors also found that both WT MLL1 and MLL-AF9 can be detected by ChIP-seq at the *HOXA9* locus in MLL-AF9 leukemia cells. The presence of WT MLL1 and H3K4me at *HOXA9* was used to infer that WDR5 would also be present, but localization of WDR5 at *HOXA9* was not explicitly detailed, raising the question as to whether *HOXA9* is a bona fide WDR5 regulated gene.

Here, we found by that WDR5 is bound to a relatively small cohort of genes and this cohort did not contain any classic MLL-leukemia associated genes such as *HOXA9* (Thorsteinsdottir, Kroon et al. 2001), despite the presence of H3K4me3 at *HOXA9*. Furthermore, despite WDR5 being a member of all six human MLL/SET histone methyltransferase complexes, stable association of WDR5 to chromatin was only found at 158 genes in MV4:11 cells. Roughly ~15,000 genes are transcriptionally active in MV4:11 cells, as determined by the RNA-seq experiment detailed in chapter VII. All of the actively transcribed genes are expected to be enriched in H3K4me3 (Barski, Cuddapah et al. 2007), yet stable association of WDR5 with chromatin was only detected at a tiny fraction of all actively transcribed genes. Therefore, these data indicate that at sites of robust WDR5 ChIP signal, WDR5 is likely to be functioning in a manner distinct from its role as a regulator of H3K4me3. This point will be revisited and underscored throughout subsequent chapters of this thesis as more data supporting this claim are presented. For example, I later use our WDR5 WIN site inhibitors to interrogate what happens to both WDR5 and H3K4me3 on chromatin (chapter VI) and gene expression of WDR5-bound genes after WIN site-blockade (chapter VII), both of which support the idea that sites of robust WDR5 ChIP signal on chromatin can be separated from its HMT functions.

The gene ontology analysis presented in this chapter helped to shed light on what kind of genes WDR5 regulates at site of robust ChIP signal. We found that WDR5 binding was enriched at a specific set of ribosomal protein genes (RPGs). The link between WDR5 and RPGs has not previously been reported; However, The Cancer Dependency Map initiative (Tsherniak, Vazquez et al. 2017), which correlated results from ~500 genome-wide loss of function screens, reported that six of the top 10 correlated dependency profiles for WDR5 are RPGs. This finding supports the notion that WDR5 is meaningfully connected to ribosome homeostasis. Discovering the connection between WDR5 and RPGs in an MLL-fusions context is also significant because it has recently been shown that an important part of the transcriptional repertoire of MLL-fusion oncoproteins includes increased transcription of genes connected to ribosomal and nucleolar processes (Garcia-Cuellar, Buttner et al. 2016). Therefore, inhibiting WDR5-regulated RPGs in an MLL-fusion context which has aberrant ribosomal and nucleolar processes may not be tolerated, and thus could result in selective cellular inhibition of MLL-fusion cells. This idea needs further testing, and a stringent experiment which directly addresses whether expression of an MLL-fusion can confer sensitivity to WDR5 inhibitors will be discussed in the Future Directions sub-section of chapter IX.

The observation that the set of RPGs to which WDR5 can be robustly detected by ChIP is conserved across disparate cell types, suggests that the function of WDR5 at these genes is also conserved across cell types. However, why only a defined subset of RPGs is regulated by WDR5 and how WDR5-mediated regulation of these genes contributes to cellular activities and ribosome function in normal and cancerous cells remains unknown. It is possible that the specific RPGs that are regulated by WDR5 have some common function or property that requires them to be transcriptionally regulated in unison. One such property may be a specific DNA sequence motif that is common to the set of WDR5-bound ribosomal protein genes. Audra Foshage in our laboratory has been interested in addressing whether a common sequence motif exists at WDR5-bound RPGs. To date she has not identified a specific motif that is required for WDR5 enrichment at RPGs, but further study is needed. WDR5 is not able to directly bind to DNA, so WDR5 must rely on its association with other protein factors to engage chromatin. Perhaps the set of RPGs bound by WDR5 is bound by a common critical co-factor that recruits WDR5 to these loci. Another possibility is that a specific epigenetic landscape “flags” loci for WDR5 recruitment. To date, the biological reasoning behind the binding of WDR5 to some, but

not all, RPGs has not been discovered, though this question is an active topic of investigation by other members of the Tansey lab.

The information gleaned from the WDR5 ChIP and ChIP-seq experiments described above lead me to formulate several new hypotheses about the molecular mode of action of our WDR5 WIN site inhibitors. First, I hypothesized that the primary mechanism of action of WDR5 WIN site inhibition is connected to the role of WDR5 at genes where WDR5 can be robustly detected on chromatin by ChIP, which are primarily RPGs. Due to the high conservation of WDR5 binding at RPGs across cell types, I propose that the primary mode of action of our WDR5 inhibitors is the same regardless of cell type, and therefore sensitivity to WIN site inhibition is conferred by something downstream of the primary effects of the inhibitors. Lastly, I hypothesize that WDR5 inhibition will not reduce H3K4me3 levels at genes where WDR5 is enriched on chromatin, as I now believe that WDR5 likely functions independently from HMT activity at these loci. I will investigate these questions and others in the next several chapters of this thesis.

CHAPTER VI

DISPLACEMENT OF WDR5 FROM CHROMATIN BY WIN SITE INHIBITION

Introduction

In the previous chapter, I detail the genomic loci to which WDR5 is enriched on chromatin in cell lines that are both sensitive and insensitive to our WDR5 WIN site inhibitors. By elucidating the repertoire of genes bound by WDR5, I was able to better understand the types of genes that may be regulated by WDR5. I found that WDR5 is not enriched at genes associated with MLL-leukemogenesis such as *HOXA9*, *HOXA10,* and *MIES1* (Guenther, Lawton et al. 2008, Bernt, Zhu et al. 2011), but rather at genes involved in protein synthesis including a discrete set of ribosomal protein genes (RPGs). Furthermore, the set of WDR5-bound ribosomal protein genes is conserved in two other disparate cancer cell types, suggesting that RPGs are an important and conserved set of genes regulated by WDR5. Based upon these findings, I proposed that the mechanism through which WDR5 WIN site inhibitors function is likely connected to the role of WDR5 as a chromatin or transcriptional regulator (Guarnaccia and Tansey 2018) at the conserved set of RPGs. I also proposed that the primary mode of action of our WDR5 WIN site inhibitors is the same regardless of cell type, due to the high conservation of WDR5 enrichment at RPGs across cell different cell types. Finally, I hypothesized that WDR5 inhibition will not reduce H3K4me3 levels at genes where WDR5 is enriched on chromatin, as I now believe WDR5 likely functions independently from HMT activity at these loci.

Published studies describing the effects of the small molecule WDR5 WIN site inhibitor OICR-9429 (Grebien, Vedadi et al. 2015, Neilsen, Chakraborty et al. 2018) and the monobody Mb(S4) (Gupta, Xu et al. 2018) have not investigated whether the repertoire of WDR5-bound genes is altered when the WIN site is inhibited. In order to best understand why some leukemia cell lines are sensitive and some are insensitive, it is important to detail the effects of WDR5 WIN inhibitors in both contexts not just sensitive MLL-fusion cells. By comparing and contrasting the effects of WDR5 WIN site inhibition in sensitive and insensitive cells I hope to uncover the

biology that underlies sensitivity determination, which may have important implications for which types of cancer cells can be effectively killed by WDR5 inhibitors.

In this chapter, I first use WDR5 ChIP to investigate the effects of WDR5 WIN site inhibitor treatment on WDR5 binding to chromatin at select conserved protein synthesis genes found to be enriched in WDR5 binding by ChIP-seq (chapter V). The investigation is then expanded by using WDR5 ChIP-seq to address how WDR5 binding to chromatin is affected across the whole genome after WDR5 inhibitor treatment. We then corroborate the findings from the WDR5 ChIP and ChIP-seq experiments using a paralleled genetic approach to disrupt the WDR5 WIN site. Finally, I test whether WDR5 inhibitor treatment affects the level of H3K4me3 at WDR5-bound genes. In sum, we found that both chemical and genetic inhibition of the WDR5 WIN site results in the rapid and comprehensive displacement of WDR5 from chromatin at WDR5-bound genes. H3K4me3 levels were not affected by WDR5 inhibitor treatment at the select WDR5-bound genes tested. The data presented in this chapter demonstrate that the WIN site is required to tether WDR5 to chromatin, and WDR5 WIN site inhibition does not block H3K4me3 of genes with robust WDR5 enrichment on chromatin.

Results

Effect of WDR5 WIN site inhibition on WDR5 binding to chromatin at protein synthesis genes

In chapter V, the full repertoire of WDR5 binding sites in both sensitive (MV4:11) and insensitive (K562) cells was determined. We detected robust WDR5 binding to a discrete set of genes connected to protein synthesis in MV4:11 and K562 cells as well as other disparate cancer cell types. Therefore, this discrete set of protein synthesis genes likely represent an important and conserved cohort of genes that are regulated by WDR5. I reasoned that WDR5-bound genes, including the conserved set of RPGs, would be the primary targets of WDR5 WIN site inhibition. Because the role of WDR5 at all of the sites found to be enriched in WDR5 by ChIP-seq was unclear, I felt that simplest and most straight forward approach would be to investigate whether WDR5 WIN site inhibition effects enrichment of WDR5 on chromatin.

I began by treating MV4:11 cells for three days with 36 μM C3 or C3nc or DMSO only. This experiment was completed before the more potent inhibitor C6 was available. I treated the cells for three days with 36 μM C3 because at this time point and concentration profound inhibition of

cellular growth was observed. Chromatin immunoprecipitation (ChIP) followed by quantitative polymerase chain reaction (qPCR) was used to detect WDR5 binding to chromatin as described in chapter V. The Cell Signaling antibody was used for all WDR5 ChIP experiments in this chapter. Pull-down with a rabbit IgG antibody was used as a control for background binding in the pulldown. WDR5 binding after compound treatment was assessed at five loci, *SNHG15 E-box, RPL23, RPL35, RPS24,* and *EIF4G3* (Figure 6-1A), which were found to be robustly bound by WDR5 via ChIP-seq (chapter V). I used the *SNHG15* gene body locus as a negative control for WDR5 binding (Thomas, Wang et al. 2015 and chapter V). I found that three day C3 treatment reduced WDR5 ChIP signal by more than 90% at all five of the loci tested. C3nc treatment showed no significant effect on WDR5 binding at the five loci tested. The *SNHG15* gene body did not show a statistically significant decrease in WDR5 binding after C3 treatment compared although the difference in Y-axis scale of the *SNHG15* gene body and E-box graphs should be noted. The percent input detected at the gene body was 10-fold less than that detected at the *SNHG15* E-box after C3 treatment, indicating only extremely low levels of WDR5 ChIP signal can be detected at the gene body locus.

The WDR5 ChIP experiment at the *SNHG15 E-box, RPL23, RPL35, RPS24,* and *EIF4G3* loci supported my hypothesis that WDR5 WIN site inhibitor treatment will reduced WDR5 binding to chromatin. However, a possible alternative explanation could be that C3 treatment reduced WDR5 protein expression and therefore less WDR5 is available in the cell to bind chromatin. To address this possibility, I treated MV4:11 cells for three days with 36 μM C3 or C3nc or DMSO only and then collected whole cell lysates. I ran the lysates on an SDS-PAGE gel and performed a Western blot for WDR5 or histone H3 as a loading control (Figure 6-1B). The Western blot indicated that WDR5 protein levels are not diminished in C3 treated cells. Therefore, the reduced binding of WDR5 to the five loci tested by ChIP was not due to a decrease in WDR5 expression. From this experiment, I concluded that WDR5 WIN site inhibitor treatment blocks WDR5 binding to chromatin.

While MV4:11 cell growth is strongly inhibited by three day treatment with 36 μM of C3, K562 cell growth is not. This raised the question of whether C3 treatment blocks WDR5 binding to

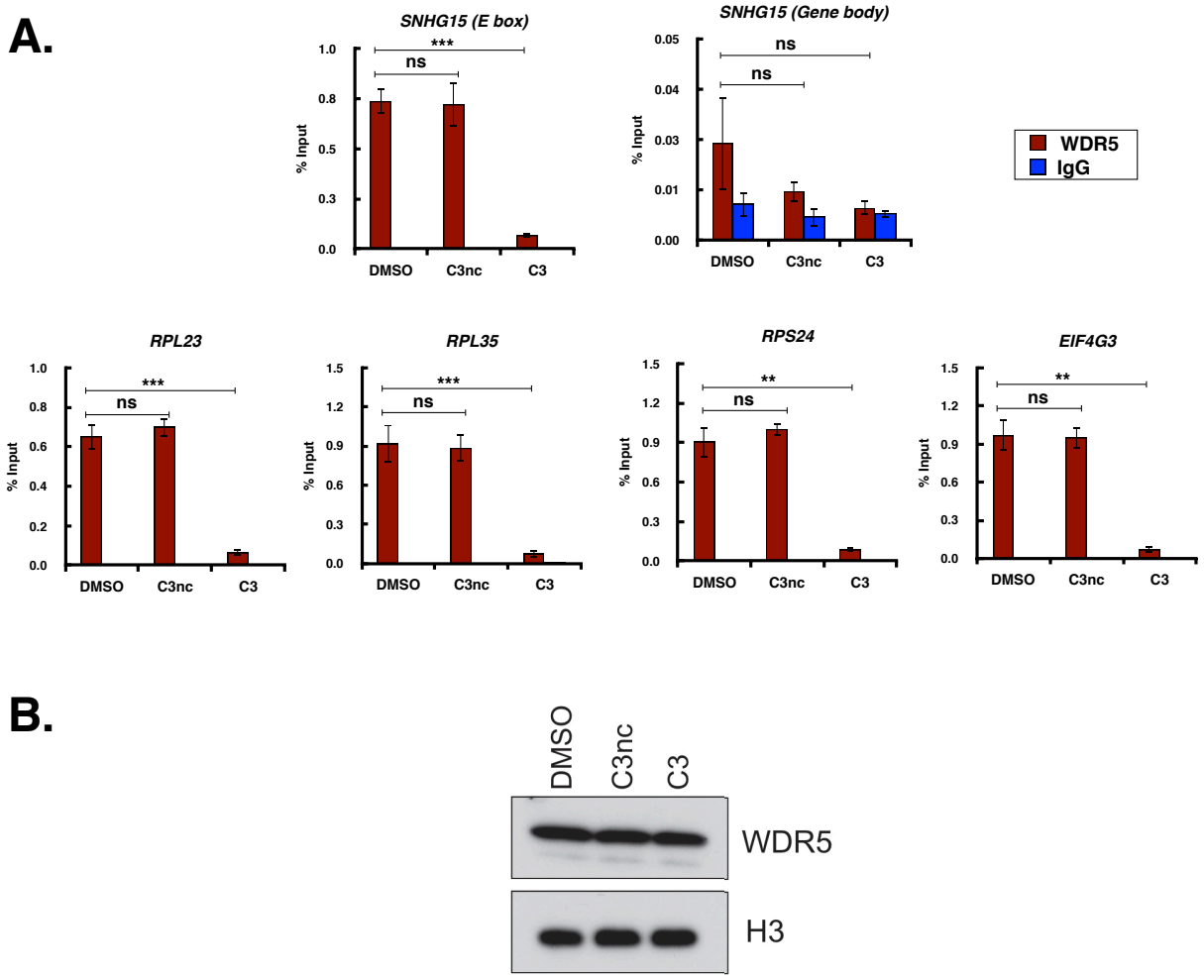

Figure 6-1. Displacement of WDR5 from chromatin in MV4:11 cells after three-day C3 treatment. (A) ChIP for WDR5 or IgG control in MV4:11 cells at five WDR5-bound genes after three days of treatment with 36 μM C3, C3nc or 0.1% DMSO only. n=3 and error bars represent standard error of the mean (SEM). p-values for WDR5 percent input for C3 or C3nc compared to DMSO were determined by two-tailed Student's t-test. "ns" means not significant, ** means $p < 0.01$, *** means $p < 0.0001$. (B) Western blot probing for WDR5 or H3 loading control after three days of treatment with 36 μM C3, C3nc or 0.1% DMSO only.

chromatin in K562 cells. Due to the high degree of conservation of WDR5 target genes found by ChIP-seq across cell types suggesting conserved function of WDR5 at these genes (chapter V), I expected that WDR5 would be displaced from chromatin after inhibitor treatment regardless of cell type. To test this prediction I treated K562 cells for three days with 36 μM C3, C3nc or DMSO only (Figure 6-2). Indeed, I again found that WDR5 binding to all five loci tested (*SNHG15 Ebox, RPL23, RPL35, RPS24,* and *EIF4G3*) was reduced by roughly 10-fold after C3 treatment in K562 cells. Again, no significant decrease in WDR5 binding was observed with C3nc treatment.

My preliminary WDR5 ChIP experiments in MV4:11 and K562 cells showed a reduction in WDR5 ChIP signal at WDR5-bound genes after C3 treatment, but I wondered whether the WDR5 binding is reduced in intensity or whether the peak may have just shifted location in the gene and therefore failed to be detected by my qPCR primer sets used in Figures 6-1 and 6-2. The qPCR primer sets only measure relatively small DNA amplicons (~120 base pairs). To determine if the WDR5 peak shifts location along WDR5-bound genes after inhibitor treatment, I utilized a set of seven primer pairs that assay different locations along *SNHG15, a* representative WDR5-bound gene (Figure 6-3). Consistent with Figure 6-1A, I found that three day 36 μM C3 treatment of MV4:11 cells strongly reduced WDR5 binding at the *SNHG15* E-box locus. I did not see an increase at any of the other loci tested. The negative control compound C3nc did not reduce WDR5 binding at any of the loci tested. From this experiment I concluded that C3 treatment displaces WDR5 from chromatin at the five WDR5-bound genes tested in Figure 6-1 and 6-2 without shifting the location of the WDR5 binding peak.

Initially a three day C3 treatment was chosen to assess whether WDR5 inhibition affects WDR5 binding to chromatin because I knew from the proliferation studies in chapter IV that C3 reduced cell growth after three days. However as more experiments were completed, I gained reason to believe that MV4:11 cells respond to WDR5 inhibitor treatment much earlier than three days. For example, in chapter IV I observed PARP1 cleavage in as little as 24 hours of treatment indicating that apoptotic signaling occurs much sooner that three days. Furthermore, we obtained evidence that transcriptional changes can be observed within the first few hours of inhibitor treatment. The effects of WDR5 inhibition on gene transcription will be detailed in chapter VII. I posited that WDR5 displacement from chromatin is likely the primary mechanism of our WDR5 inhibitors, so I expected that WDR5 displacement from chromatin would happen

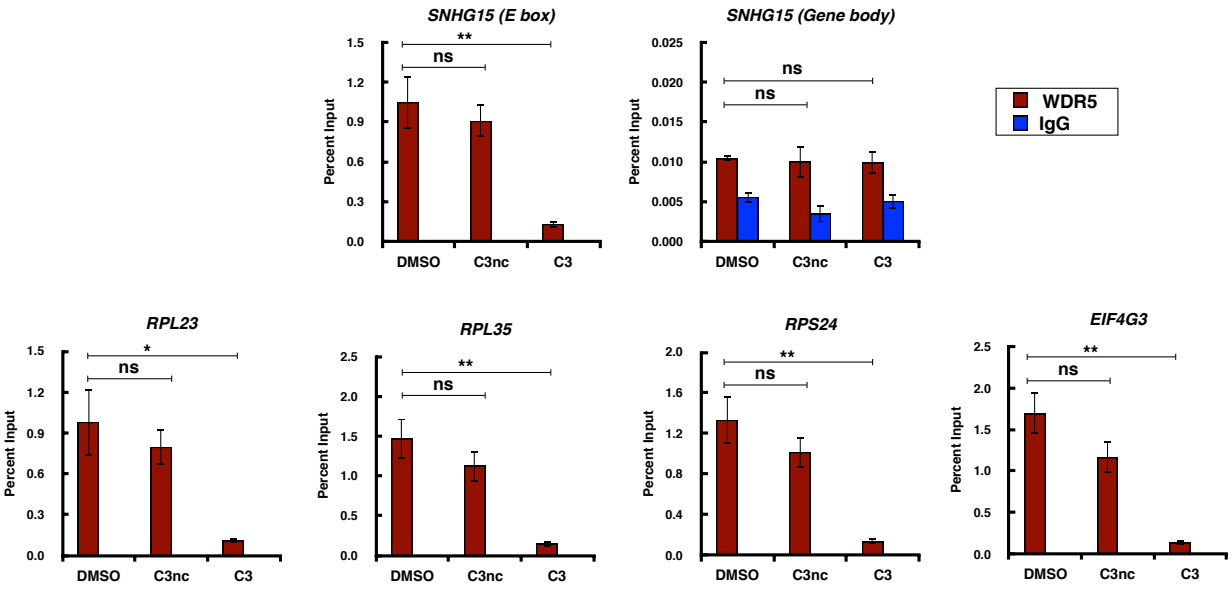

Figure 6-2. Displacement of WDR5 from chromatin in K562 cells after three-day C3 treatment. ChIP for WDR5 or IgG control in K562 cells at five WDR5-bound genes after three days of treatment with 36 μM C3, C3nc or 0.1% DMSO only. n=3 and error bars represent standard error of the mean (SEM). p-values for WDR5 percent input for C3 or C3nc compared to DMSO were determined by two-tailed Student's t-test. "ns" means not significant, * means $p < 0.05$, ** means $p < 0.01$.

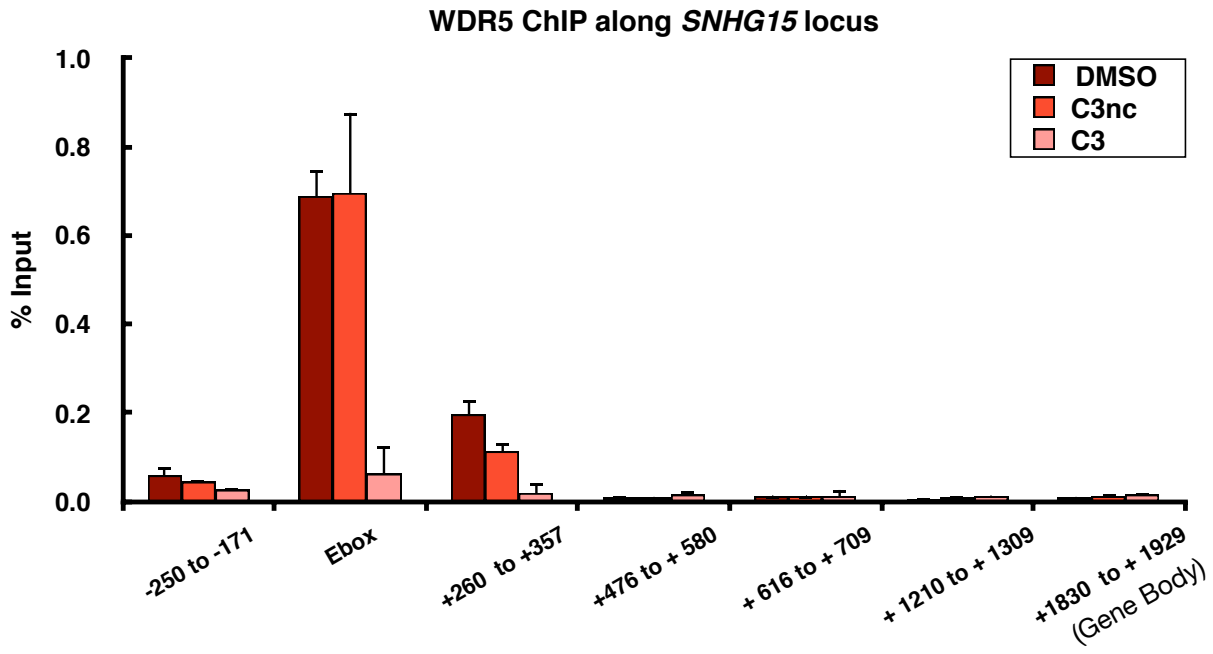

Figure 6-3. WDR5 binding is reduced across the entire *SNHG15* locus after WDR5 WIN site inhibition. ChIP for WDR5 in MV4:11 cells after three days of treatment with 36 μM C3, C3nc or 0.1% DMSO using seven primer sets along the *SNHG15* gene. X-axis lists the 5' and 3' boundaries of the amplicon measured relative to the transcriptional start site (TSS) of *SNHG15*. n=3 and error bars represent standard error of the mean (SEM).

rapidly and precede any transcriptional or cell fate changes. Therefore, I next tested for displacement of WDR5 from chromatin in MV4:11 cells after only four hours of treatment with 36 μM C3 (Figure 6-4). Again I found about a 90% reduction in WDR5 ChIP signal after C3 treatment at all five of the loci tested. No decrease in WDR5 binding was seen for C3nc treatment. This experiment demonstrated that WDR5 displacement from the five genes tested occurs rapidly in response to inhibitor treatment and precedes changes in cellular growth and viability.

Once the more potent compound, C6, became available I wanted to assess the ability of C6 to displace WDR5 from *SNHG15 E-box, RPL35,* and *RPS24*. I performed WDR5 ChIP-qPCR in MV4:11 cells treated for only four hours with 4 μM of C6. At the time that this experiment was completed, C6nc had not yet been discovered so 0.1% DMSO vehicle only treatment served as the negative control (Figure 6-5). Using DMSO treatment as the negative control was not ideal, but subsequent experiments described below using C6nc corroborate the conclusions drawn from this preliminary C6 ChIP experiment. Not surprisingly, C6 was also able to reduced WDR5 binding by roughly 10-fold at all three of the WDR5-bound genes tested.

Together, the experiments presented in this sub-section have several important implications. The WDR5 ChIP experiments after compound treatment strongly suggest that the primary mechanism of action of our WDR5 WIN site inhibitors is the displacement of WDR5 from chromatin. Since WDR5 displacement was observed in K562 cells at concentrations that do not effect K562 growth, it implies that the primary mechanism of WDR5 inhibition is the same in sensitive and insensitive cells and some characteristic downstream of WDR5 displacement confers sensitivity. These data also strongly suggests that the WIN site is required for the stable association of WDR5 with chromatin. Experiments that directly test if the WIN site is required for chromatin binding will be presented below.

Effect of WDR5 WIN site inhibition on genome-wide WDR5 binding to chromatin

The ChIP-qPCR experiments detailed above demonstrate that WDR5 inhibition reduces WDR5 binding to chromatin, however only five WDR5-bound genes were tested. It was unclear whether this result could be generalized to all WDR5-bound genes in both sensitive and insensitive cell lines. I also had not yet tested our most potent compound C6 in K562 cells or

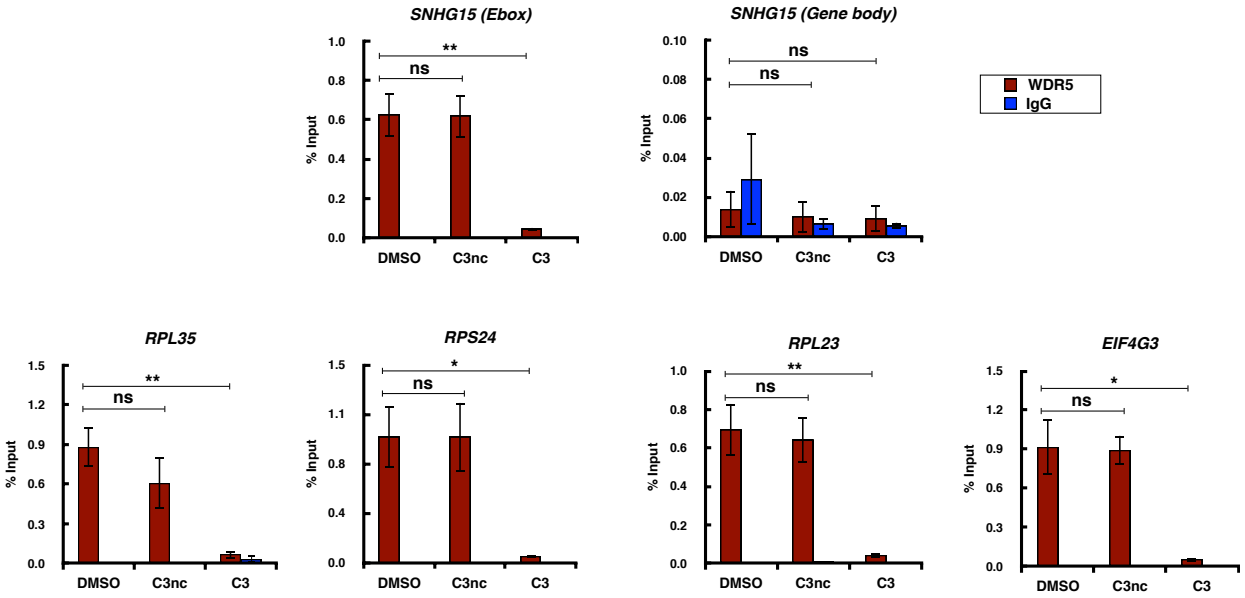

Figure 6-4. Displacement of WDR5 from chromatin in MV4:11 cells after four-hour C3 treatment. ChIP for WDR5 or IgG control in MV4:11 cells at five WDR5-bound genes after four hours of treatment with 36 μM C3, C3nc or 0.1% DMSO only. n=3 and error bars represent standard error of the mean (SEM). p-values for WDR5 percent input for C3 or C3nc compared to DMSO were determined by two-tailed Student's t-test. "ns" means not significant, * means $p < 0.05$, ** means $p < 0.01$.

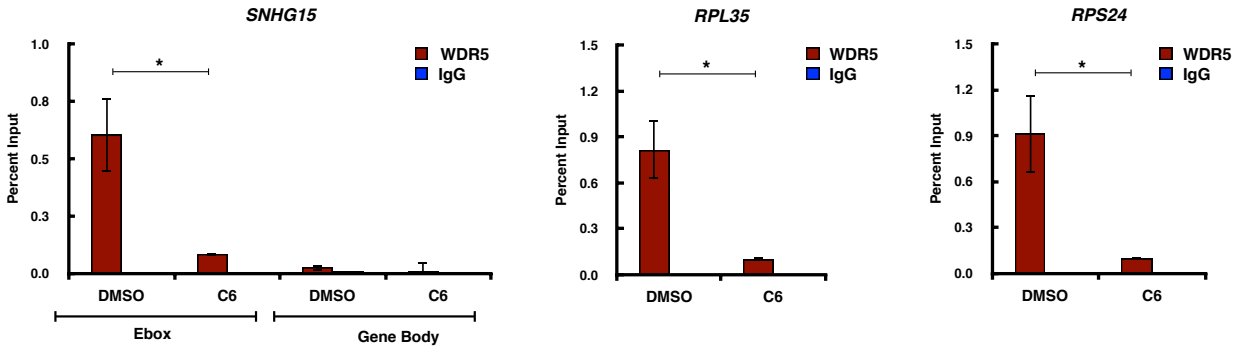

Figure 6-5. Displacement of WDR5 from chromatin in MV4:11 cells after four-hour C6 treatment. ChIP for WDR5 or IgG control in MV4:11 cells at three WDR5-bound genes after four hours of treatment with 4 μM C6 or 0.1% DMSO only. n=3 and error bars represent standard error of the mean (SEM). p-values for WDR5 percent input for C6 compared to DMSO were determined by two-tailed Student's t-test. * means $p < 0.05$.

utilized 6Cnc as a negative control. After completing the WDR5 ChIP-qPCR experiments described above, I hypothesized that the WIN site of WDR5 is required for its stable association with chromatin and therefore displacement of WDR5 from chromatin after WIN site inhibition is a general phenomenon that would be seen at all WDR5-bound genes. To test these predictions, Dr. Caleb Howard treated MV4:11 cells with 2 μM C6, C6nc or 0.1% DMSO for four hours. He then performed ChIP followed by next generation sequencing (ChIP-seq) as described in chapter V. The ChIP-seq data was then analyzed by Jing Wang under the mentorship of Dr. Qi Liu.

A scatterplot was generated for the normalized average read counts of each detected WDR5 binding peak in MV4:11 after C6, C6nc and DMSO treatment (Figure 6-6 left panel). In the scatterplots, the WDR5 peaks are ranked along the X-axis by the most intense DMSO-treated peak to the least intense DMSO-treated peak from left to right. The scatterplots in Figure 6-6 have more WDR5 peaks than the Venn diagram of WDR5 peaks shown in Figure 5-6 because Figure 6-6 shows all WDR5 peaks found in a least one ChIP-seq replicate where as Figure 5-6 shows all WDR5 peaks found in at least two ChIP-seq replicates for each cell line. The scatter plots demonstrate that across the board C6 treatment significantly decreased the intensity of all WDR5 peaks in MV4:11 cells compared to DMSO treatment. In contrast, C6nc treatment had little to no effect on WDR5 peak intensity. There were no cases where the WDR5 peaks increased in intensity or the emergence of new WDR5 peaks after C6 treatment. Based on these data, I concluded that WIN site inhibition results in the rapid and comprehensive loss of interaction of WDR5 with chromatin in MV4:11 cells.

The WDR5 ChIP experiments at the select RPGs tested after C3 treatment, lead me to believe that the same comprehensive loss of WDR5 from chromatin would be seen in K562 cells after C6 treatment. Dr. Howard repeated the WDR5 ChIP-seq, this time treating K562 cells for four hours with 2 μM C6, C6nc or 0.1% DMSO. Scatterplots for the normalized average read counts of each detected WDR5 were created for K562 cells as stated above for MV4:11 cells (Figure 6-6 right panel). Indeed, C6 treatment reduced the intensity of WDR5 peaks at all WDR5-bound genes in K562 cells. Again, no new WDR5 peaks emerged and no WDR5 peaks increased in intensity. I concluded that the rapid and genome-wide displacement of WDR5 from chromatin

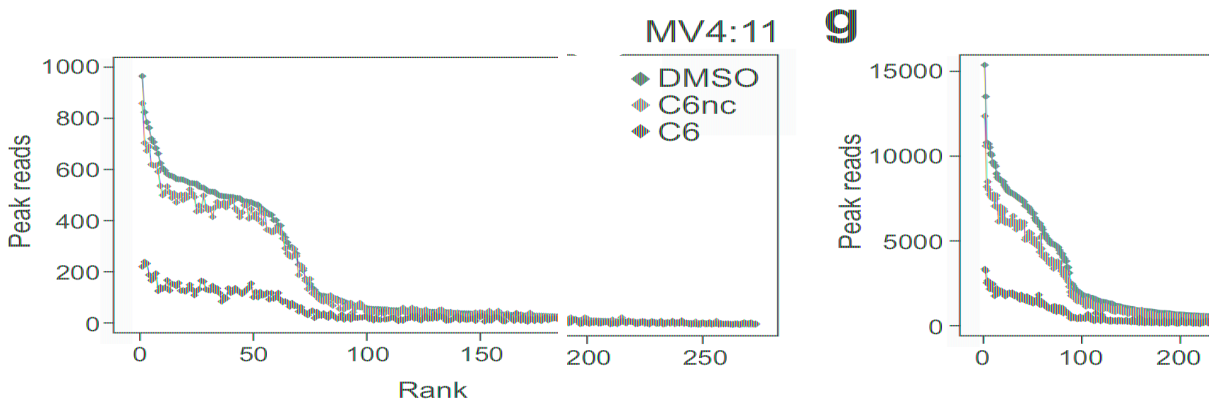

Figure 6-6. WDR5 is displaced from chromatin genome-wide in sensitive and insensitive cells after WDR5 WIN site inhibition. Scatterplot of normalized average read counts for WDR5 binding peaks in DMSO-, C6nc- and C6-treated MV4:11 (left) or K562 (right) cells. Peaks are ranked based on read counts in DMSO-treated cells. n = 3.

occurs in both MV4:11 and K562 cells, despite the differences in how these cell lines respond to WIN inhibitors in growth assays. Therefore, the primary direct effect of the WDR5 WIN site inhibitors is the same in different cell types and the characteristic(s) in these cell lines that determine sensitivity lie down-stream of the primary mechanism of action. Experiments that further investigate the biological events that occur downstream of WDR5 displacement from chromatin will be presented in subsequent chapters of this thesis.

Effect of WDR5 WIN site mutation on WDR5 binding to chromatin

The WDR5 ChIP and ChIP-seq experiments presented above utilizing chemical inhibition of the WDR5 WIN site suggest that the WIN site is required to stably tether WDR5 to chromatin. Next, we interrogated whether displacement of WDR5 from chromatin should be expected when the WIN site is perturbed by using a genetic approach. The aromatic ring of phenylalanines 133 and 263 in WDR5 make a critical pi-pi stacking interaction that greatly contributes to the overall binding affinity of WDR5 with the MLL1 WIN peptide (Patel, Vought et al. 2008), as well as C3 and C6 (chapter III). Phenylalanines 133 and 263 sandwich the arginine side chain of the MLL1 WIN peptide and the S_2-binding chemical groups of C3 and C6. Mutation of phenylalanine 133 to alanine (F133A mutation) removes one of the aromatic rings required to stabilize the pi-pi stacking interaction and has been shown to abolish binding of WDR5 to WIN motifs (Patel, Vought et al. 2008). Therefore, the F133A mutation can be used as a genetic tool to interrogate the consequences of inhibiting the WDR5 WIN site.

To test whether the WDR5 F133A mutation can recapitulate the effects of C3 and C6 on WDR5 binding to chromatin, Dr. Howard utilized HEK293 cell lines made by Dr. Lance Thomas in our lab that stably expressed either FLAG-tagged wild-type (WT) WDR5, FLAG-tagged F133A mutant WDR5 or empty vector control. HEK293 cells were utilized because they can be more easily genetically manipulated by transfection than leukemia suspension cells. By over-expressing the different FLAG-tagged WDR5 constructs in HEK293 cells that express endogenous WT WDR5 we could prevent any deleterious effects that may be caused by expression of the F133A mutant WDR5 alone. The FLAG-tag allowed us to specifically track binding of the transfected WDR5 species to chromatin by using ChIP with a FLAG-specific antibody.

Dr. Howard performed FLAG ChIP-qPCR at a selection of six genes, *E2F3, EIF4G3, RPL23, RPL35, RPS24* and *SERBP1.* All six of these loci were found to be bound by endogenous WDR5 in the unperturbed MV4:11 and K562 cell WDR5 ChIP-seq presented in chapter V. Robust binding to chromatin was observed for FLAG-WT WDR5 at all six loci tested (Figure 6-7A). In contrast, binding to chromatin above the empty vector control was not detected for the FLAG-tagged F133A mutant WDR5. Importantly, all of the FLAG-tagged forms of WDR5 were expressed equally (Figure 6-7B "input"), eliminating the possibility that the FLAG-F133A mutant failed to to be detected by ChIP due to low levels of expression.

In addition to the WIN site, WDR5 contains another protein-protein interaction domain called the WBM located on the opposite side of WDR5 (Odho, Southall et al. 2010, Thomas, Wang et al. 2015). The WBM binds several proteins in a mutually exclusive manner including the MLL regulatory subunit RBBP5, the transcription factor MYC, and the MOF1 acetyltransferase subunit KANSL2 (Guarnaccia and Tansey 2018). As a control, we wanted to be sure that the F1335A mutation did not disrupt binding of proteins to the WBM, which would complicate the interpretation of the ChIP result seen in Figure 6-7A. To test if the F133A mutation affects interactions occurring at the WBM, Dr. Howard performed a co-immunoprecipitation (co-IP). Dr. Howard pulled-down the FLAG-tagged WDR5 constructs from HEK293 whole cell lysates and then probed for co-immuno-precipitating RBBP5 (Figure 6-7B). The L240K mutation of WDR5 resides within the WBM and has been shown to block RBBP5 binding (Thomas, Wang et al. 2015). The L240K mutation was used as a positive control for disruption of the WBM. We confirmed that the F133A mutant retains RBBP5 binding, demonstrating that the F133A mutation specifically disrupts the WIN site of WDR5, but not protein-protein interactions occurring at the WBM site. Together, the paralleled chemical and genetic approaches used define the WIN site of WDR5 as a mode by which WDR5 establishes and maintains association with chromatin.

Effect of WDR5 WIN site inhibition on WDR5 localization

After determining that both pharmacological and genetic inhibition of the WDR5 WIN site both cause displacement of WDR5 from chromatin, I sought to determine if the localization of WDR5 is affected by WIN site inhibition. I hypothesized that WDR5 would be displaced from chromatin after C6 treatment, but would stay in the primarily in the nucleus. To test this hypothesis I first treated MV4:11 cells for four hours with DMSO or 36 μM of C3, the

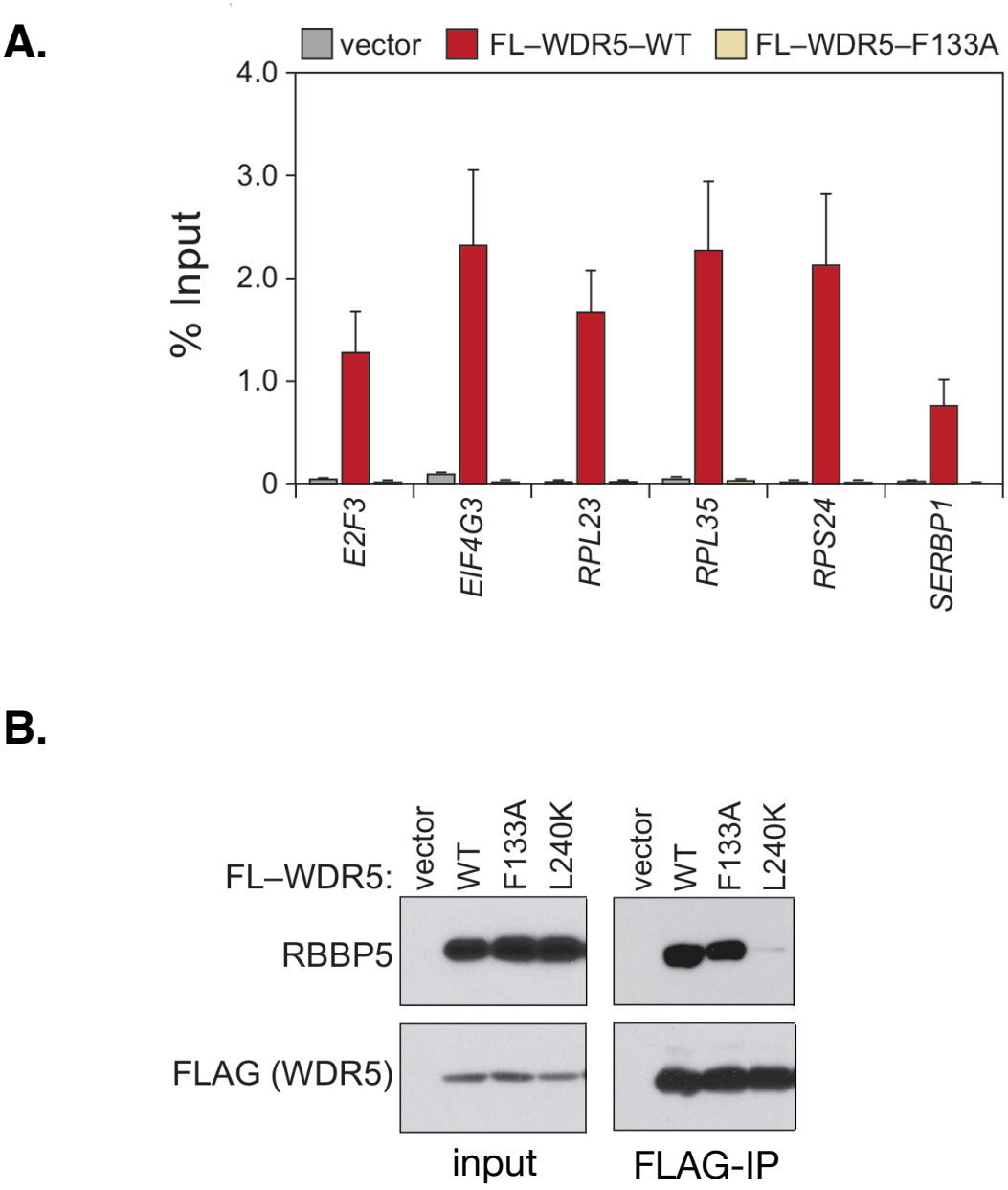

Figure 6-7. WDR5 WIN site mutation displaces WDR5 from chromatin. (A). FLAG ChIP in HEK293 cells stably expressing FLAG-tagged wild-type WDR5, FLAG-tagged F133A mutant WDR5 or empty vector control. n = 3 and errors bars represent standard error of the mean (SEM). (B) Co-immunoprecipitation (coIP) analysis of FLAG (FL)-tagged WT WDR5, or WDR5 point mutants. FLAG-tagged proteins were recovered from HEK293 cells stably expressing the indicated WDR5 mutants, and probed for WDR5 or co-precipitating RBBP5. The F133A WDR5 mutant disrupts the WIN site, but retains RBBP5 binding. The L240K mutant disrupts the RBBP5 binding site.

same time and concentration used for the WDR5 ChIP in Figure 6-1A illustrating displacement of WDR5 from chromatin. C3 was used because C6 had not yet been developed at the time this experiment was completed. After treating the cells I performed a biochemical cellular fractionation assay as previously described (Mendez and Stillman 2000). Briefly, the cellular fractionation assay utilizes various buffers and centrifugation steps to separate cells into a soluble cytosolic (S2) fraction, soluble nuclear (S3) fraction, and insoluble chromatin enriched pellet (P3). By running equal proportions of each fraction on an SDS-PAGE gel and then probing the resulting Western blot with an anti-WDR5 antibody, I was able to detect how the relative enrichment of WDR5 in these three cellular fractions changes after C3 treatment (Figure 6-8). H3 was used a control for the insoluble chromatin enriched pellet (P3).

I found that upon C3 treatment, there was more WDR5 found in the soluble cytosolic (S2) and soluble nuclear (S3) fractions, with a commensurate decrease in the insoluble chromatin enriched pellet (P3) compared to DMSO-treated cells. The cellular fractionation assay indicated that, in general, less WDR5 is bound to chromatin after C3 treatment. This finding is consistent with the ChIP-seq scatter plots shown in Figure 6-6 in which the intensity of WDR5 peaks were decreased at all WDR5-bound loci indicating that displacement of WDR5 from chromatin when the WIN site is block is a genome-wide phenomenon. Again, the cellular fractionation assay supports the notion that the WIN site is required to tether WDR5 to chromatin.

Effect of WDR5 WIN site inhibition on WDR5-bound gene H3K4me3

In chapter V I found that robust WDR5 ChIP signal is enrichment at genes that are connected to protein synthesis, including a discrete and conserved set of ribosomal protein genes. How WDR5 functions to regulate this conserved set of RPGs has not been elucidated. In chapter III I demonstrate that our WDR5 WIN site inhibitors C3 and C6 selectively inhibit MLL1-mediated HMT activity *in vitro.* Therefore, I next asked whether WDR5 WIN site inhibition reduces H3K4me3 at genes that are enriched in WDR5 binding to chromatin.

To assess whether WDR5 WIN site inhibition reduces H3K4me3 at conserved protein synthesis genes with WDR5 enrichment, I treated MV4:11 cells with 36 μM C3, C3nc or DMSO only for four hours and then performed ChIP with a H3K4me3 specific antibody. I used C3 because C6 had not yet been discovered at the time this experiment was completed. In Figure 6-1, I demonstrate that WDR5 is displaced from *SNHG15 E-box, RPL23, RPL35, RPS24,* and

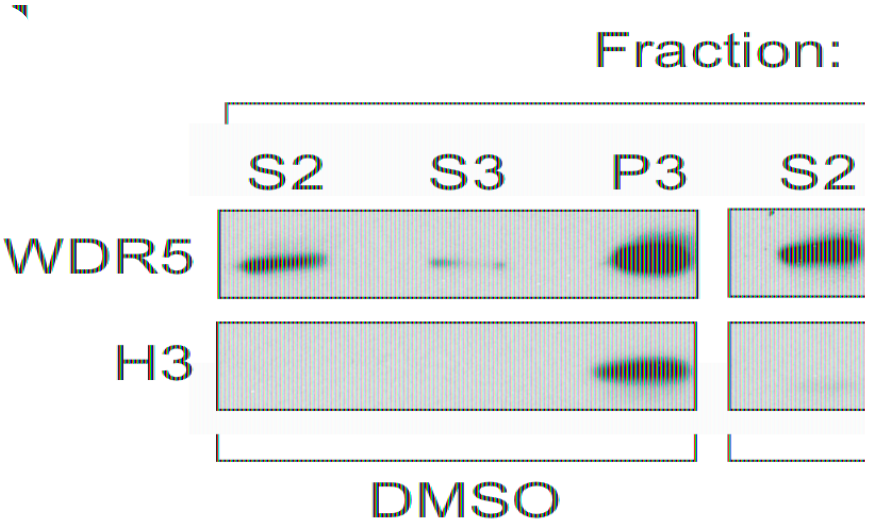

Figure 6-8. Localization of WRD5 after WIN site inhibition. Western blot, showing WDR5 distribution in the soluble (S2), soluble nuclear (S3), or insoluble chromatin enriched pellet (P3) fractions of MV4:11 cells treated for four hours with DMSO or 36 μM of C3. Histone H3 is a control for the specificity of the insoluble chromatin fraction.

EIF4G3 upon WDR5 inhibitor treatment. I quantified H3K4me4 enrichment by qPCR at the same five genes after C3 treatment (Figure 6-9). I found that there was no statistically significant difference in H3K4me3 at any of the five WDR5-bound genes tested after C3 or C3nc treatment compared to DMSO treatment despite loss of WDR5 enrichment at these genes. I only tested five WDR5-bound protein synthesis genes, so I can not claim that H3K4me3 is retained at all WDR5-bound genes after C3 treatment. H3K4me3 ChIP-seq would be needed to assess the genome-wide localization of H3K4me3 after WDR5 WIN site inhibition. However, because the set of RPGs bound by WDR5 is highly conserved across disparate cancer cell types, it suggests that the function of WDR5 at this set of genes is also conserved. The experiment shown in this subsection clearly demonstrates that WDR5 is not required to be robustly bound to chromatin for H3K4me3 to occur and WDR5 likely regulates the conserved set of RPGs by some non-HMT related function.

Discussion

In order to understand the therapeutic utility of inhibiting WDR5 at the WIN site in combatting cancer, it is important to elucidate the full repertoire of WDR5 regulated genes and to understand how blocking the WIN site affects these genes. I hypothesized that the primary mechanism through which our WDR5 inhibitors function would be connected to the functions of WDR5 as a chromatin and transcriptional regulator (Guarnaccia and Tansey 2018) at genes connected to protein synthesis showing robust enrichment of WDR5 on chromatin. In this chapter we use ChIP and ChIP-seq to demonstrate that the primary mechanism of action of C3 and C6 is the rapid, comprehensive and persistent eviction of WDR5 from chromatin. Additionally, our paralleled chemical and genetic approaches using C3 and C6 and the F133A mutation, respectively, allowed us to define a mode by which WDR5 engages chromatin. Finally, the use of H3K4me3 ChIP determined that while our WDR5 inhibitors displace WDR5 from chromatin, H3K4me3 is not reduced in the same time frame. This finding indicated that robust WDR5 enrichment is not required for H3K4me3 of WDR5 target genes and that our compounds likely function by inhibiting some non-HMT associated function of WDR5.

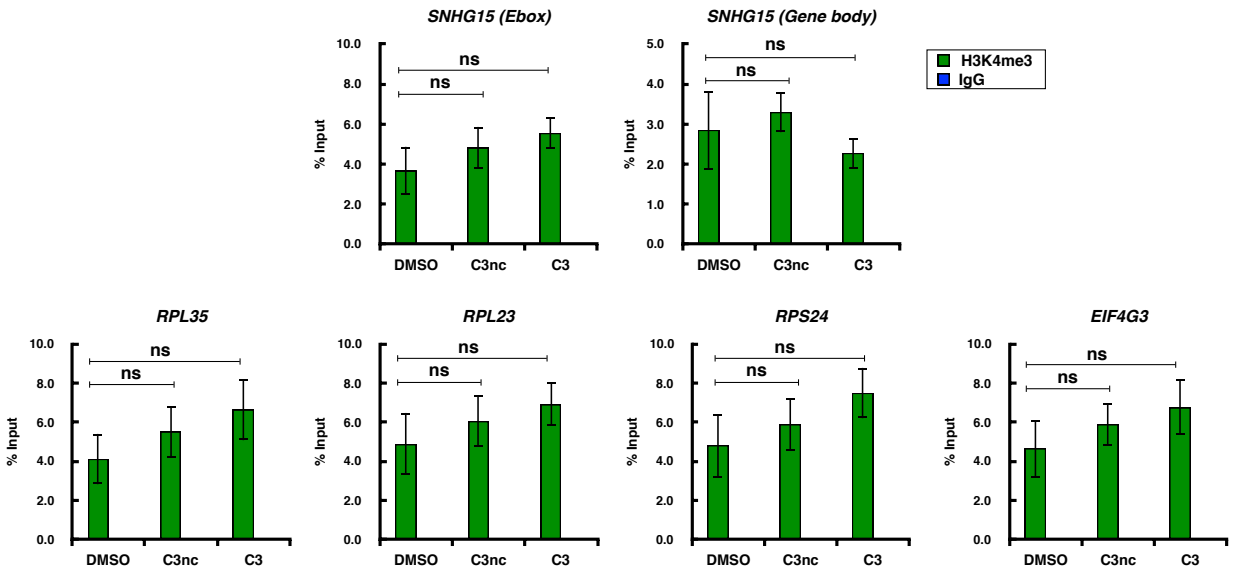

Figure 6-9. H3K4me3 at WDR5-bound genes is not changed after WDR5 WIN site inhibition. ChIP for H3K4me3 or IgG control in MV4:11 cells at five WDR5-bound genes after four hours of treatment with 36 μM C3, C3nc or 0.1% DMSO only. n=3 and error bars represent standard error of the mean (SEM). p-values for H3K4me3 percent input for C3 or C3nc compared to DMSO were determined by two-tailed Student's t-test. "ns" means not significant.

The chemical and genetic approaches used to perturb the WDR5 WIN site presented above support the idea that WDR5 is linked to chromatin through the WIN site. Although the WIN site of WDR5 binds at least a half-dozen interaction partners (Guarnaccia and Tansey, 2018), none of these partners have been proposed to specifically recruit WDR5 to its target genes. WDR5 contains no known direct DNA-binding domains, therefore the interaction of WDR5 with chromatin is likely mediated by the WDR5 WIN site engaging a WIN motif in a chromatin-associate protein and this interaction is likely blocked when treating with a WIN site inhibitor. The WIN-motif containing protein may be one of the characterized WIN site binders, but as there are thousands of proteins encoded in the human genome that carry the core WIN motif (A-R-A/S/T), it is likely that the factor(s) responsible for tethering WDR5 to chromatin is yet to be identified. Alternatively, perhaps the inhibitors block WDR5 engagement with chromatin by allowing WDR5 to gain binding to a protein that blocks chromatin association or the compounds could block signaling events required to locate WDR5 to chromatin. A better grasp of the repertoire of WIN site binders that occur at WDR5-bound genes and the proteins bound to WDR5 after compound treatment is needed to fully understand the mechanism and utility of small molecule WIN site inhibitors. This topic will be revisited in the Future Directions sub-section of chapter IX.

It is also critical to determine which genes are directly impacted by WIN site blockade in order to define the primary mechanism of action of WIN site inhibitors. WDR5 ChIP-seq has previously been performed in murine MLL-AF9 cells treated with the peptidomimietic MM-401 (Xu, Li et al. 2016). It was found that MM-401 treatment caused a decrease in intensity of roughly one third of all WDR5 peaks detected in unperturbed cells. However, the authors chose to focus further analyses on only the WDR5 depleted peaks that were co-bound by MLL1, as it was assumed that the inhibitor mainly functions by blocking WDR5/MLL1 interaction. In doing so, nearly one third of the WDR5 depletion peaks after MM-401 treatment were disregarded. It is well known that several other proteins besides MLL1 bind the WIN site of WDR5 (Guarnaccia and Tansey 2018). It cannot be ruled out that WIN site inhibition elicits its anti-proliferative effects by inhibiting interaction with one or more non-MLL1 proteins. By disregarding the effects of WIN site inhibition at WDR5 peaks that were not bound by MLL1, Xu et al. likely failed to grasp the full picture of how MM-401 effects WDR5 regulated genes.

The experiments using C3 and C6 in this chapter analyzed all sites of WDR5 enrichment identified by ChIP-seq and strongly implicate a specific subset of RPGs as targets of WIN site

inhibition. Due to the recurring and highly consistent binding of WDR5 to a select subset of RPGs in different cell types and the finding that WDR5 is displaced from these genes after inhibitor treatment, I conclude that these RPGs are likely a predominant biological target of WDR5 and thus of WDR5 inhibitors. The data presented here also determine that the primary mechanism of WDR5 inhibitors, i.e. WDR5 displacement, is the same in sensitive and insensitive cell lines. The insensitive cell line, K562, is a chronic myeloid leukemia (CML) cell line in which the brc-abl gene fusion is the oncogenic driver. K562 cells have been shown to be sensitive to the BCR-ABL tyrosine kinase inhibitors nilotinib and imatinib (Jorgensen, Allan et al. 2007), though studies have identified sub-populations that are resistant to imatinib (Hekmatshoar, Ozkan et al. 2018) and to multiple chemotherapeutic drugs such as etoposide (Sugawara, Iwahashi et al. 1991) and daunorubicin (Yanovich, Hall et al. 1989). K562 cells are also more resistant to BDR4 inhibition than other BCR-ABL expressing CML lines (Stewart, Horne et al. 2013). By determining that WDR5 displacement from chromatin occurs in K562 cells that are generally more resistant to drug treatment we are able to conclude that the primary mechanism of WDR5 inhibitors occurs regardless of cell sensitivity and indicates that the characteristic that determines sensitivity lies down-stream of the primary mode of action. We do not yet know how K562 cells evade sensitivity to WDR5 WIN site inhibition but, we can conclude that the mechanism of resistance in K562 is not due to lack of displacement of WDR5 from chromatin or lack of WDR5/compound engagement as demonstrated by the CETSA data presented in chapter IV. Experiments presented in the next few chapters will further described the similarities and difference of how sensitive and insensitive cell lines respond to WDR5 inhibition.

There are a couple of important therapeutic implications of the experiments presented in this chapter. First, overexpression of WDR5 has been reported in numerous malignancies including colon cancer (Neilsen, Chakraborty et al. 2018), hepatocellular carcinoma (Cui, Li et al. 2018), squamous cell carcinoma (Wu, Diao et al. 2018), and gastric cancer (Sun, Guo et al. 2018). WDR5 has also been proposed to promote chemoresistance in bladder cancer (Chen, Xie et al. 2015). Therefore, by displacing WDR5 from chromatin, our inhibitors may be able to attenuate the oncogenic function of WDR5 overexpression in these cancers. Second, although H3K4me3 was not affected by our WIN site inhibitors at the genes tested, our WIN site compounds are potent inhibitors of MLL1-driven HMT activity (chapter III). The MLL1 HMT IC_{50} value for C6 is ~20 nM compared to 320 nM for MM-401 (Cao, Townsend et al. 2014) and C6 has a 250-fold

window of selectivity for MLL1 over other MLL/SET complexes. Inhibition of MLL1-mediated H3K4 methylation has been shown to be a viable strategy for killing cancer cells expressing mutant forms of C/EBPα (Grebien, Vedadi et al. 2015) and p53 (Zhu, Sammons et al. 2015). In these cancers, therefore, as well as others that are MLL1-dependent (Vedadi, Blazer et al. 2017), the ability of our inhibitors to target the HMT activity of MLL1 complexes may be exploited for therapeutic gain.

Together, the data presented in this chapter forecast that WDR5 WIN site inhibitors may function by reducing expression of genes that encode protein subunits of the ribosome and that these changes in RPG transcription are ultimately responsible for killing sensitive leukemia cell lines. In the next chapter, I will test these predictions by characterizing both the rapid primary and secondary gene expression changes after WDR5 inhibition. I will then integrate the gene expression data with the WDR5 ChIP-seq data from this chapter to provide a more detailed understanding of how WDR5 WIN site blockade effects WDR5-bound genes.

CHAPTER VII

WDR5-BOUND GENES ARE REPRESSED BY WIN SITE INHIBITION

Introduction

In order to understand the full utility of WDR5 WIN site inhibition as a therapeutic strategy for cancer, it is critically important to understand which genes are regulated by WDR5, how these genes are affected by WIN site blockade, and how the primary effects of WIN site inhibition leads to growth inhibition and apoptosis induction. To date, this sort of detailed characterization of the mode of action of WDR5 WIN site inhibitors such as OICR-9429, MM-401 and the monobody Mb(S4) has not been done in a manner that would allow for the discrimination of the direct and indirect effects. For instance, gene expression and phenotypic data in these earlier studies was collected days to weeks after inhibitor treatment began (Cao, Townsend et al. 2014, Grebien, Vedadi et al. 2015, Gupta, Xu et al. 2018). Thus, it is not possible to determine which observed effects of the inhibitors were direct or indirect. Shorter time-points must be assessed to be able to identify the direct effects. In previous chapters, we began to methodically dissect the mode of action of WDR5 WIN site inhibition using our potent WDR5 inhibitors C3 and C6. By ChIP-seq, we found that WDR5 is enriched on chromatin at a conserved set of ribosomal protein genes (RPGs) and that WDR5 is displaced from chromatin after WDR5 WIN site inhibition. However we had not yet elucidated how WDR5 WIN site inhibition, and thus displacement from chromatin, affects gene expression. Determining the primary transcriptional targets of WDR5 WIN site inhibitors and the longer-term secondary or compensatory effects on gene expression will provide much needed deeper insight into how WDR5 inhibitors function.

I hypothesized that the primary transcriptional targets of our WDR5 WIN site inhibitors would be RPGs where a robust WDR5 signal can be detected by ChIP (chapter V) since WDR5 was displaced from these loci after inhibitor treatment and WDR5-bound RPGs are conserved across cell types (chapter VI). In order to best address my hypothesis, I needed to separate rapid, early and direct transcriptional changes from the later secondary or compensatory effects on gene expression after inhibitor treatment. I predicted that the primary effects would occur

rapidly before any changes in cell viability or proliferation are observed and would be the same regardless of the cell type treated. In contrast, I predicted that longer WDR5 WIN site inhibitor treatment would allow me to capture the secondary effects on gene expression in addition to the primary the effects. I predicted that the secondary effects would differ between sensitive and insensitive cells and the gene expression changes in sensitive cells would be functionally connected to apoptosis induction or inhibition of cell growth, consistent with the changes in cell fate observed in chapter IV.

To address my hypotheses, we began by using Precision nuclear Run-On and next generation sequencing (PRO-seq) to identify transcriptional changes with very high temporal resolution, thus capturing only the primary effects of our inhibitors. Next, the longer-term steady-state mRNA expression changes were determined in both MV4:11 and K562 cells. Gene Ontology (GO) analysis was implemented to determine if the genes induced and repressed in either cell type after WDR5 WIN site inhibition cluster into any particular biological function or pathway to better characterize the biological consequences of inhibiting the WIN site of WDR5. We then integrated the rapid primary and later secondary gene expression changes with the ChIP-seq WDR5 binding data of chapter V to determine how the gene expression changes relate to the genes bound by WDR5.

In sum, the data presented in this chapter determine the rapid primary transcriptional changes and the long-term steady-state mRNA expression changes that occur in response to WDR5 WIN site inhibition in both sensitive and insensitive leukemia cell lines. We found that in both cell types tested the primary transcriptional targets of our inhibitors are highly enriched in RPGs, indicating that the primary mode of action of our inhibitors is the same in both sensitive and insensitive cells and is connected to WDR5-mediated regulation of RPG expression. In contrast, the long-term steady-state mRNA expression changes that occur in sensitive and insensitive cells are distinct, indicating that while the primary mode of action is the same, sensitive and insensitive cell respond very differently to the initial decrease in RPG expression. By integrating the gene expression data presented in this chapter with the WDR5 ChIP-seq data presented in chapters V and VI, we found that the primary transcriptional targets of WDR5 WIN site inhibitors are a conserved set of WDR5-bound RPGs at which WDR5 enrichment is depleted upon inhibitor treatment. Finally using the structurally distinct WDR5 WIN site inhibitor OICR-9429, I

found that decreased expression of WDR5-bound RPGs is a common response to WDR5 WIN site inhibitors.

Results

Rapid primary effects of WDR5 WIN site inhibition on gene transcription

The direct transcriptional targets of WDR5 WIN site inhibitors have not yet been determined. Defining which genes are directly affected by WDR5 WIN site blockade is critical for understanding precisely how these inhibitor functions. Without detailing how these inhibitors function, it is hard to know their full utility in treating cancer. I hypothesized that the conserved WDR5-bound RPGs (chapter V) would be the primary transcriptional targets of WDR5 WIN site inhibition, as we demonstrated in chapter VI that WDR5 is displaced from these genes upon inhibitor treatment. I also reasoned that because WDR5 was found to be displaced from chromatin in as little as 4 hours after inhibitor treatment (chapter VI), the primary transcriptional changes would occur rapidly in response to WIN site inhibition and should precede changes in cell growth, viability, and apoptotic marker induction. Superb temporal resolution of gene expression changes would be needed to separate the direct effects from the secondary effects, and thus to determine the primary transcriptional targets of the compounds. Therefore, I collaborated with Dr. Pankaj Acharya in the laboratory of Dr. Scott Hiebert to determine the rapid transcriptional changes that occur in MV4:11 cells after WDR5 inhibitor treatment. Dr. Acharya is an expert in Precision nuclear Run-On coupled with next generation sequencing (PRO-Seq), a genomic technique that would provide the high temporal resolution in transcriptional changes needed to determine the direct targets of WDR5 WIN site blockade.

PRO-seq is a global nuclear run-on assay that tracks the genome-wide distribution of transcriptionally-engaged RNA polymerase at base-pair resolution (Kwak, Fuda et al. 2013, Mahat, Kwak et al. 2016). Nuclei of cells are first isolated and nucleotides are washed away to halt transcription but RNA polymerase remains enzymatically active and bound to DNA. Nuclei are isolated by resuspending cells in cold swelling buffer and incubating on ice for 5 minutes. After incubation, cells are pelleted by centrifugation, resuspended in cell lysis buffer and incubated on ice for 5 minutes. Cells are then Dounce-homogenized 50 times and the nuclei collected by centrifugation. Next, a run-on reaction is completed by adding biotin-11-CTP, ATP, GTP and UTP. The biotinylated-CTP terminates transcription when incorporated into the

nascent mRNA transcript by RNA polymerase and labels all of the nascent RNA fragments with biotin. Sarkosyl is also included in the nuclear run-on reaction buffer to prevent transcription initiation by RNA polymerase complexes that were not already transcriptionally engaged. The biotinylated RNA fragments are then extracted using TRIzol LS and isopropanol precipitation. Purified biotinylated RNA fragments are by pull-down on streptavidin-conjugated beads. Adaptor sequences are ligated to the ends of the affinity purified RNA fragments before reverse transcribing and PCR amplifying to create a pool of cDNA fragments that can be identified by next generation sequencing.

To utilize PRO-seq to identify rapid primary changes in gene transcription after WDR5 inhibition, Dr. Acharya treated MV4:11 cells with 36 μM of C3 for 15, 30, or 60 minutes or DMSO only for 60 minutes. 36 μM of C3 was used to ensure that a high level of WDR5 inhibition was reached. Our more potent compound, C6, was not yet discovered at this time. Because we anticipated that WDR5 inhibition would cause transcriptional inhibition due to WDR5 displacement, we asked which genes demonstrated a significant change in gene body associated polymerase after C3 treatment compared to DMSO. The transcriptional changes identified at genes with decreased gene body associated polymerase by PRO-seq were highly statistically significant (p_{adj}=0.0007 to 10^{-28}) yet modest in magnitude, with a 1.5- to 2-fold decrease in transcription compared to DMSO treated cells (Figure 7-1A). We found that there were no instances where C3 promoted an increase in gene body transcription. Across the time-points, we identified a set of 47 transcription units, corresponding to 45 loci, where C3 caused a significant decrease in gene body transcription. The majority (~70% or 32 out of 45 genes) of these genes encode ribosome protein genes. Additionally, most of the transcriptional changes were captured within 15-minute of C3 treatment, indicating that C3 acts quickly to influence transcriptional processes. Since I hypothesized that the primary transcriptional changes identified by PRO-seq would occur at WDR5-bound genes, we integrated the list of 45 genes repressed in the PRO-seq with the list of genes bound by WDR5 in MV4:11 cells in the ChIP-seq (chapter V). We found that 87% (39 out of 45) of the PRO-seq repressed genes were bound by WDR5 in the ChIP-seq. The WDR5-bound genes identified as repressed in the PRO-seq are indicated by a red box to the right of the gene in Figure 7-1A.

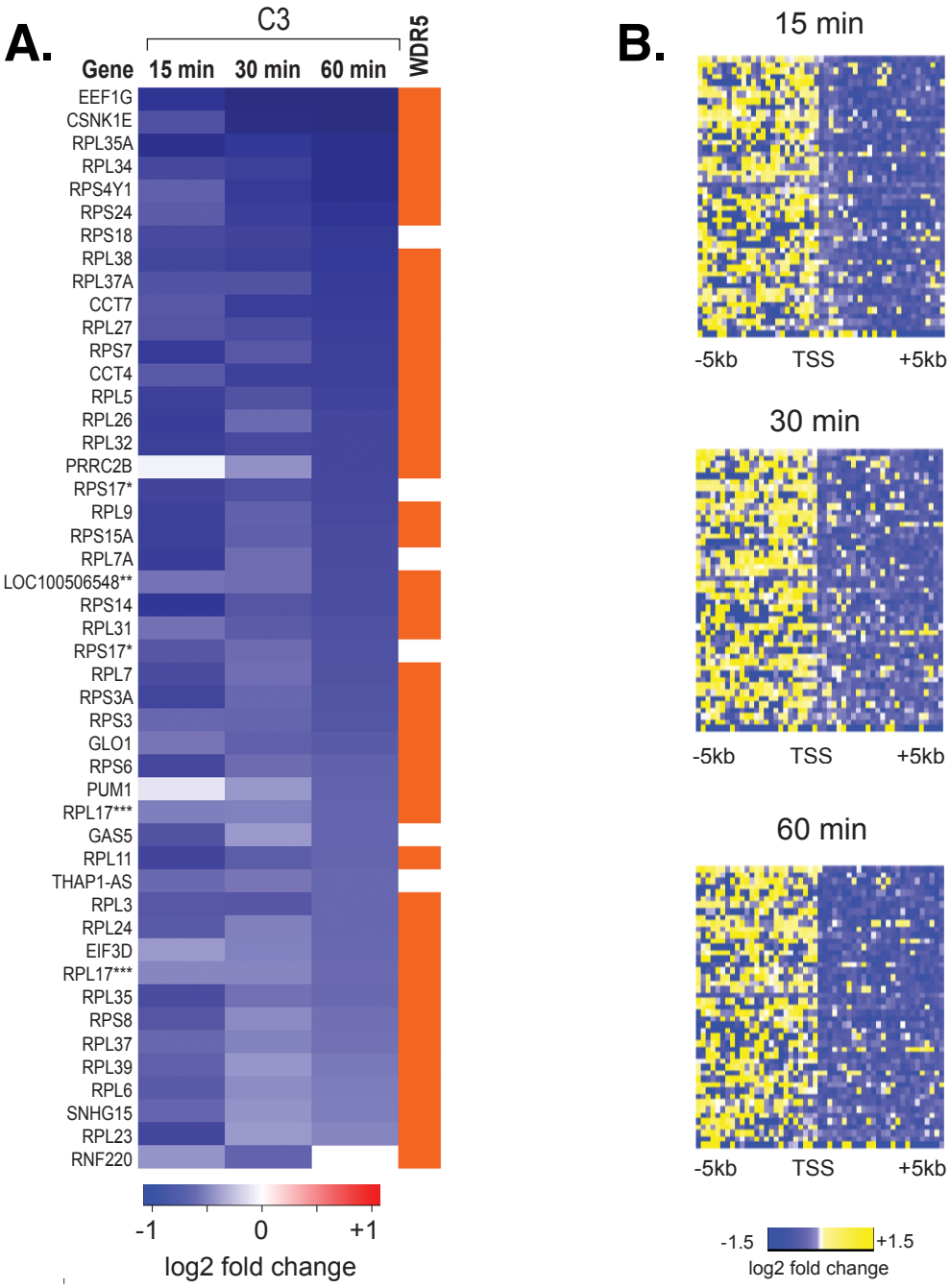

Figure 7-1. Transcription of WDR5-bound genes is rapidly repressed by WIN site inhibition. (A) Heatmap listing genes with significant changes in gene body-associated polymerases in MV4:11 cells treated with 36 μM compound C3, as determined by PRO-Seq. An orange box indicates that WDR5 is bound to the locus. RPS17 (*) and RPL17(***) are listed twice, because two distinct RefSeq IDs were called for those loci. LOC100506548 (**) is read-through transcription from RPL37. (B) Heatmaps displaying log_2-transformed fold change of PRO-Seq read counts in 200 bp bins +/- 5 kb around the TSS of loci showing gene body changes after C3 treatment.

The distribution of active RNA polymerase after 15, 30 and 60 minute C3 treatment can be more directly visualized in the heatmaps displayed in Figure 7-1B. Each row of the heatmaps represent an individual gene found to be decreased in transcription after C3 treatment. Each box depicts the log_2-transformed fold change of PRO-Seq read counts in 200 bp bins +/- 5 kb around the transcriptional start site (TSS) after C3 treatment. Yellow boxes indicate an increase in RNA polymerase enrichment and blue boxes indicate a decrease in RNA polymerase enrichment. It is readily apparent that at the 45 significantly transcriptionally changed genes, C3 treatment increased RNA polymerase enrichment upstream of the TSS and decreased RNA polymerase enrichment downstream of the TSS. The enrichment of polymerase up to -5 kb from the TSS was unexpected and unusual considering that promoter proximal polymerase pausing typically occurs about 20 - 60 nucleotides down stream of the TSS (Adelman and Lis 2012). The reasons for the accumulation of polymerase up stream of the TSS after C3 treatment have not been identified. Perhaps the polymerase upstream of the TSS is due to an increase in divergent transcription, a common feature of transcriptionally active genes in mammalian cells, however the divergent RNA PolII peaks are typically centered only ~ 250 bp upstream of the TSS (Seila, Calabrese et al. 2008). Further investigation into the chromatin modifications or architecture at these genes after C3 treatment may help to provide explanation for the increase in upstream but decrease in downstream RNA polymerase. Together, the heatmaps again highlight the fact that transcriptional repression of these genes occurs very rapidly, within only 15 minutes of compound treatment. Together, Figure 7-1 demonstrates that the direct transcriptional targets of WDR5 WIN site inhibition are highly enriched in WDR5-bound RPGs.

Long-term effects of WDR5 WIN site inhibition on gene transcription

Utilizing PRO-seq to determine the rapid transcriptional effects of C3 was important because we identified that the direct transcriptional targets of WDR5 WIN site inhibition are primarily a set of WDR5-bound ribosomal protein genes. In addition to identifying the direct targets of our inhibitors, it is also critical to understand how WDR5 WIN site inhibition effects gene expression at longer time points when changes in cellular growth, viability and apoptotic markers can be observed. I next reasoned that by extending the inhibitor treatment to three days, I could capture both the primary as well as additional secondary gene expression changes. Determining the secondary gene expression changes that occur after WDR5 WIN site inhibitor treatment would help me to further interrupt the long-term biological consequences of WDR5 WIN site inhibition in sensitive cells and insensitive leukemia cells.

I began by using whole transcriptome sequencing (RNA-seq) to identify changes in MV4:11 steady-state mRNA levels after WIN site inhibition. RNA-seq allows for the identification and quantification of mRNA species expressed in a population of cells. To determine the long-term effects of WDR5 inhibitor treatment on gene expression, I treated MV4:11 cells with 2 μM of our most potent compound C6, C6nc or DMSO only for three days. 2 μM of C6 was used because this concentration is close to the MV4:11 three-day proliferation assay GI_{50} and therefore would allow me to robustly inhibit WDR5 but still retain sufficient numbers of live cells after three days to extract high quality total RNA. C6 was used instead of C3 for the RNA-seq because C6 is more potent and I could use a much lower concentration but still potently inhibit WDR5. The high concentrations of C3 used for the PRO-seq were probably not problematic since the treatment time for the PRO-seq was so short, but we wanted to avoid possible off-targets effects of treating cells with 36 μM C3 long-term. I also wanted to use C6 for the RNA-seq because it served as an orthologous challenge and if C3 and C6 are both on target, the RPGs repressed after short-term C3 treatment in PRO-seq should also be repressed after long-term C6 treatment in the RNA-seq. After the three-day treatment, I extracted and purified total RNA from the treated cells using TRIzol Reagent and a Zymo Research RNA mini-prep kit. To remove any contaminating genomic DNA, I performed an on-column DNAse digestion when using the mini-prep kit. I then submitted total RNA samples for ribosomal RNA depletion, library preparation and next generation sequencing at Genewiz. The RNA-seq experiment was repeated with five biological replicates. The raw RNA-seq data obtained from Genewiz was analyzed by Jing Wang under the mentorship of Dr. Qi Liu. Jing determined all of the genes that were significantly up- or down-regulated after C6 or C6nc treatment compared to DMSO using a False Discovery Rate (FDR) cutoff of less than 0.05.

Figure 7-2A provides an overview of the number of genes that were significantly up- and down-regulated in MV4:11 cells after C6nc and C6 treatment compared to DMSO. In general, the magnitude of the RNA expression changes were modest, with most changes being two-fold or less compared to DMSO treated cells. C6nc induced no significant changes in gene expression compared to DMSO-treated cells, as expected from its lack of biological activity seen in other assays. Compound C6, in contrast, resulted in a number of significant gene expression changes compared to DMSO. Seventy two genes were found to be significantly up-regulated and 462

A.

	MV4:11	
	Up	**Down**
C6nc vs DMSO	0	0
C6 vs DMSO	72	462

B.

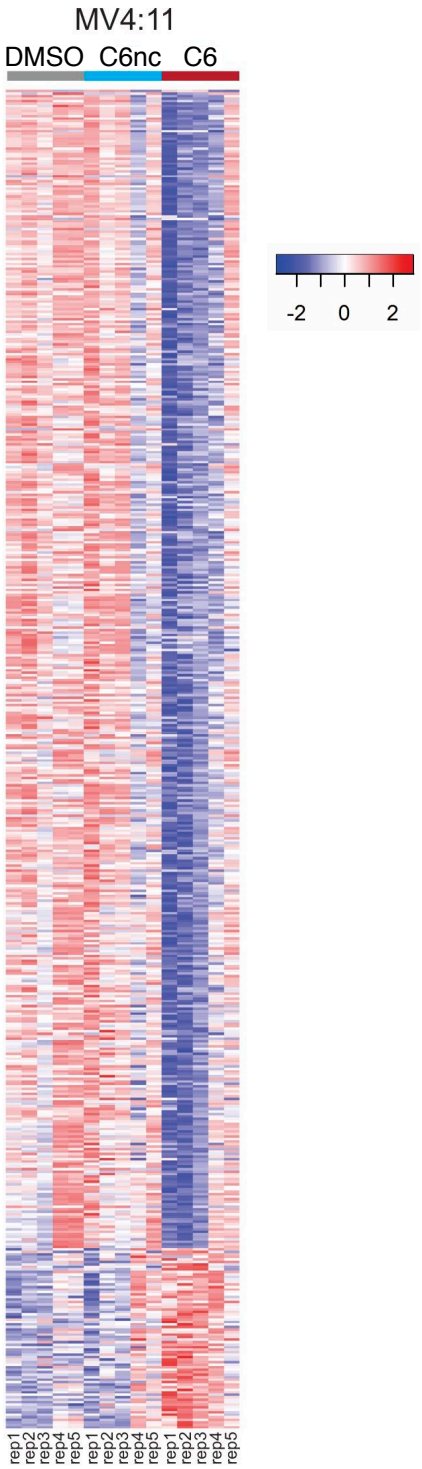

Figure 7-2. Summary of gene expression changes in MV4:11 cells after WDR5 WIN site inhibition. (A) Number of genes significantly up- or down-regulated after C6 or C6nc treatment versus DMSO (FDR < 0.05). (B) Heatmaps displaying z-transformed gene expression for significantly changed genes in C6 versus DMSO (FDR < 0.05) for all five replicates (rep1–rep5) of RNA-Seq, examining the impact of three days of DMSO, or 2 μM C6nc, or C6 treatment of MV4:11 cells.

genes were significantly down-regulated in MV4:11 cells upon C6 treatment. Heatmaps were generated for all of the significantly changed genes (FDR < 0.05) in C6 treated cells compared to DMSO treatment for all five replicates of the RNA-Seq and then hierarchical clustering was done (Figure 7-2B). The RNA-seq experiment was first completed with only three biological replicates. The heat maps for the first three replicates demonstrated inconsistency in the pattern of gene expression changes seen in the C6nc and C6 treatments. Therefore, two more biological replicates were subsequently completed and added to the analysis to help mitigate the variability within treatments. Despite the inconsistency in some of the C6 and C6nc treated replicates, it is clear that in general the pattern of gene expression seen after DMSO and C6nc treatment are very similar, but the pattern of gene expression after C6 treatment is distinct from vehicle or negative control treated samples.

To further dissect the gene expression changes caused by C6 treatment, we first focused on the 72 genes that were induced in MV4:11 cells. We performed Gene Ontology (GO) analysis to determine if the set of genes induced by C6 in MV4:11 cells is more enriched in genes involved in a particular biological function or pathway than would be expected by chance (Figure 7-3A). The top five significantly enriched GO terms found for genes induced by C6 in MV4:11 cells included categories connected to MAP kinase signaling cascades, protein phosphorylation, transcriptional regulation, response to cycloheximide and PI3 kinase signaling. The number of C6 induced genes that fell into each GO term is shown within the bar for each GO term in Figure 7-3A. Although enrichment of these categories was statistically significant, relatively few induced genes (only 2-7 genes) fell into each category and the disparate nature of the enriched categories in MV4:11 cells failed to provide a strong and meaningful biological connection.

Next, we focused on the 462 gene repressed by three-day treatment of MV4:11 cells with C6. GO analysis of genes repressed by C6 in MV4:11 cells identified two main clusters of significantly enriched GO terms (Figure 7- 3B). Cluster 1 includes 3 GO terms connected to protein translation and 1 GO term connected to mRNA transcription and nonsense-mediated decay. The number of C6 repressed genes that fell into each GO term category for cluster 1 ranged from 39 to 48 genes, and 38 genes that fell into Cluster 1 categories were RPGs, indicating that PRGs accounted for most of the genes that fell into each Cluster 1 GO term. Other genes that fell into Cluster 1 GO terms were found to be some nuclear encoded mitochondrial RPGs and translation initiation factors. Because RPGs were also found to be

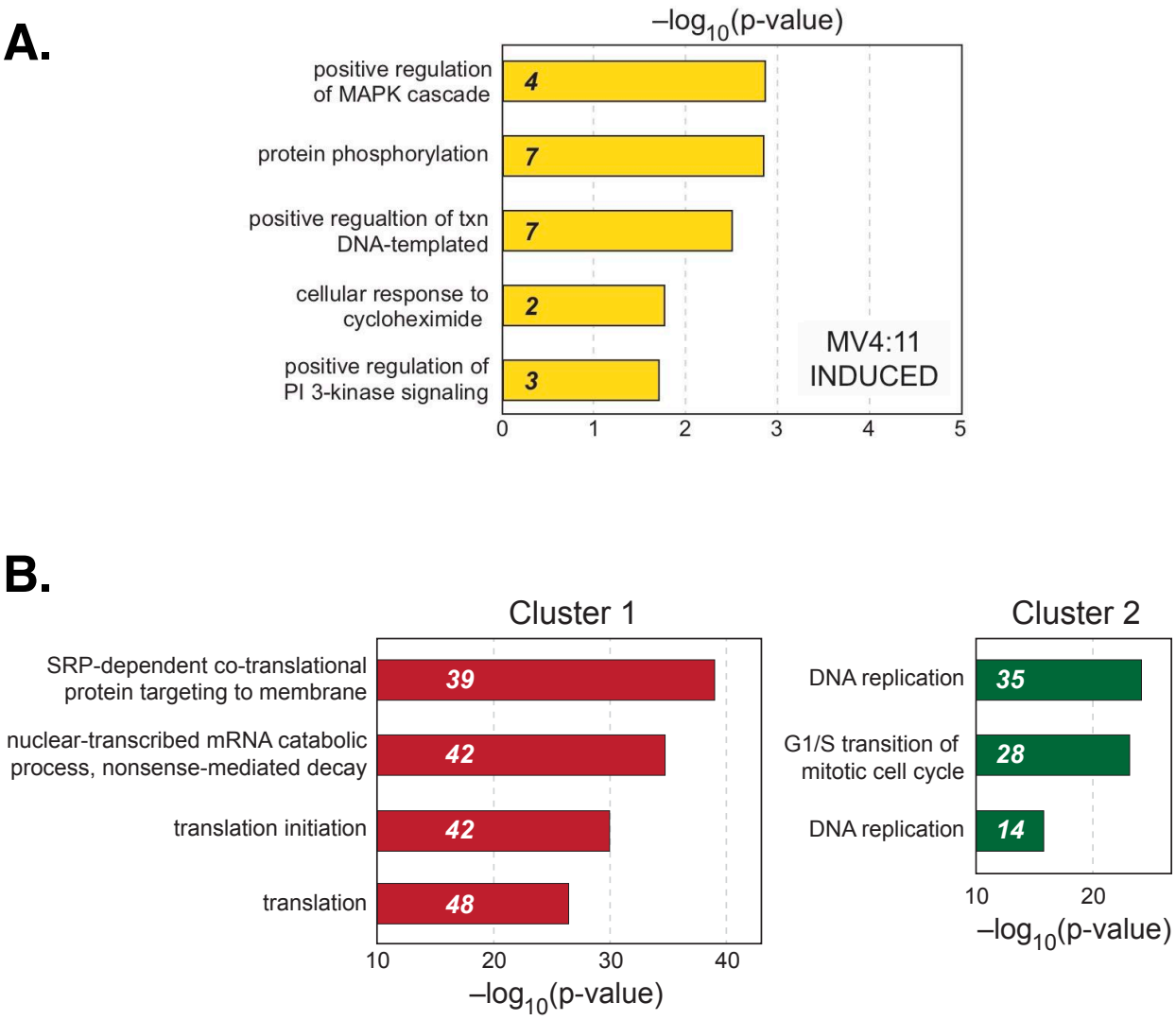

Figure 7-3. GO analysis of genes induced and repressed by C6 in MV4:11 cells. (A) Top five Gene Ontology (GO) enrichment categories for genes significantly induced by three-day 2 μM C6 treatment in MV4:11 cells, as determined by RNA-seq. Numbers in italics represent the number of induced genes in each category. (B) GO enrichment clusters for genes significantly repressed by three-day C6 2 μM treatment of MV4:11 cells, as determined by RNA-seq. Numbers in italics represent the number of repressed genes in each category.

highly enriched in the direct transcriptional targets of C3 identified by PRO-seq, I proposed that the RNA-seq repressed genes from cluster 1 represent the primary transcriptional effects of WDR5 WIN site inhibition in MV4:11 cells. A more direct comparison of the RPGs repressed in the PRO-seq and repressed in the RNA-seq will be detailed late in this chapter.

The other main cluster, Cluster 2, of enriched GO terms found for C6-repressed genes included three GO terms connected to DNA replication, and the cell cycle (Figure 7-3B). Repressed genes that fell into Cluster 2 GO terms included cyclins and cyclin-dependent kinases, as well as DNA replication factors such as PCNA and components of the MCM complex. Because GO terms connected to cell cycle regulation of DNA synthesis were not observed in the PRO-seq, I concluded that C6-repressed genes that fell into Cluster 2 were likely to represent the longer-term secondary effects of WDR5 WIN site inhibition in MV4:11 cells. Repression of cell cycle genes is consistent with the decreased cellular proliferation of MV4:11 cells seen after three days of C6 treatment in the proliferation assays (chapter IV).

I was next interested in comparing the gene expression changes upon C6 treatment in a sensitive leukemia cell line versus an insensitive leukemia cell line. Identifying the similarities and differences in gene expression changes in sensitive and insensitive cells is important because it may help to elucidate why different cell types have different cell fates after WDR5 WIN site inhibition. I hypothesized that the direct transcriptional changes identified above would be common among the sensitive cell line MV4:11 and the insensitive cell line K562, but the secondary effects would be different. Because the primary transcriptional targets were determined to be mostly WDR5-bound RPGs in MV4:11 cells, I posited that C6 would also inhibit WDR5-bound RPGs in K562 cells. Non-ribosomal repressed genes in the MV4:11 cells were connected to the cell cycle and DNA synthesis, which is consistent with the reduced growth of MV4:11 cells after C6 treatment (chapter IV). However, K562 cell growth is not inhibited by 2 μM C6. Therefore, I did not expect C6 to induce gene expression changes of cell cycle/DNA synthesis genes as was found for MV4:11 cells.

To determine the long-term changes in steady-state mRNA expression in K562 cells after C6 treatment, I treated K562 cells for three days with 2 μM C6 or C6nc, or DMSO. I then harvested total RNA as described above for MV4:11 cells and submitted samples for RNA-seq to Genewiz. The RNA-seq data was again analyzed by Dr. Jing Wang in the same manner used for MV4:11

cells. As expected, C6nc had almost no effect on gene expression in K562 cells compared to DMSO, with only one gene being significantly induced and no genes significantly repressed (Figure 7-4A). C6 did induce significant gene expression changes in K562 cells compared to DMSO. In summary, 65 genes were found to be induced by three-day 2 μM C6 treatment and 187 genes were significantly repressed in K562 cells. Heatmaps were generated for all of the significantly changed genes (FDR < 0.05) found in C6, C6nc or DMSO treated K562 cells for all five replicates of the RNA-Seq (Figure 7-4B) as for MV4:11 cells. Once again, it is clearly evident that the pattern of gene expression seen after DMSO and C6nc treatment are very similar to each other. In contrast, the pattern of gene expression after C6 treatment is distinct from the patterns of expression seen with DMSO or C6nc treatment.

To identify if the genes induced by C6 in K562 cells are involved in a particular biological function, GO analysis was performed for the 65 genes that were significantly induced by three-day C6 treatment (Figure 7-5A). All of the top five significantly enriched GO terms found for C6-induced genes in K562 cells were categories connected to oxygen transport and hemoglobin production. The number of C6-induced genes that fell into each enriched GO category is shown in the bar for each GO term in Figure 7-5A. While these five GO terms were significantly enriched, relatively few C6-induced genes (only 3-5 genes) fell into each category, indicated that these GO categories may not represent a majority of the response to C6 in K562 cells. None the less, it has been reported that hemoglobin expression can be observed in some clones derived from the K562 cell line (Testa, Vainchenker et al. 1982). Furthermore, K562 cells can be stimulated to undergo erythroid differentiation and produce gamma-globin mRNA and in culture (Lampronti, Bianchi et al. 2003). Perhaps the induction of a few genes connected to hemoglobin production hints at erythroid differentiation in K562 cells upon C6 treatment. Overall, a strong indication of erythroid differentiation was not identified in the RNA-seq or Wright-Giemsa staining in chapter IV, but it possible that a longer treatment or higher dosage of WDR5 inhibitor may be needed to observed such an effect. Further experimentation would be needed to definitely confirm or rule out differentiation of K562 cells after C6 inhibitor treatment.

I next performed a GO analysis on the 187 genes that were significantly down-regulated by three-day C6 treatment of K562 cells (Figure 7-5B). The top five GO terms for C6-repressed genes in K562 cells indicated a highly significant enrichment of GO terms connected to protein translation. 37 ribosomal protein genes were found to be repressed by C6 treatment in K562

A.

	K562	
	Up	**Down**
C6nc vs DMSO	1	0
C6 vs DMSO	65	187

B.

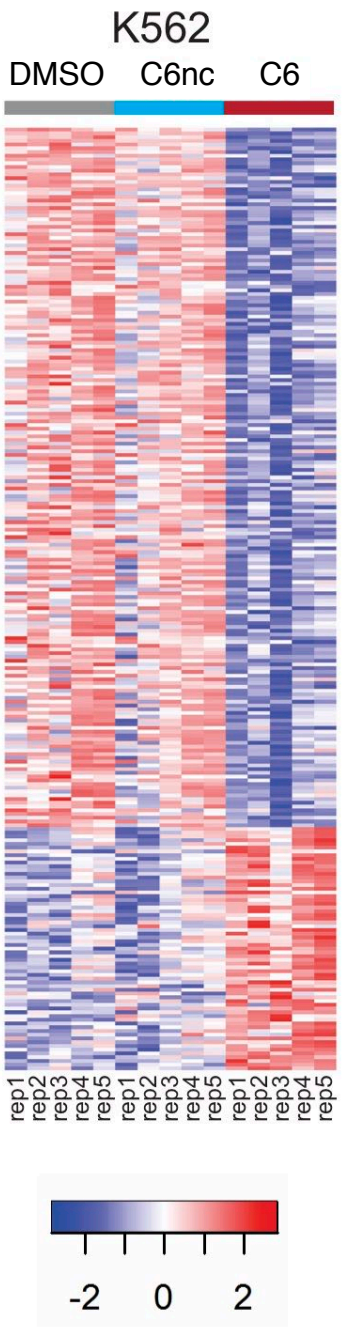

Figure 7-4. Summary of gene expression changes in K562 cells after WDR5 WIN site inhibition. (A) Number of genes significantly up- or down-regulated after C6 or C6nc treatment versus DMSO (FDR < 0.05). (B) Heatmaps displaying z-transformed gene expression for significantly changed genes in C6 versus DMSO (FDR < 0.05) for all five replicates (rep1–rep5) of RNA-Seq, examining the impact of three days of DMSO, or 2 μM C6 or C6nc treatment of K562 cells.

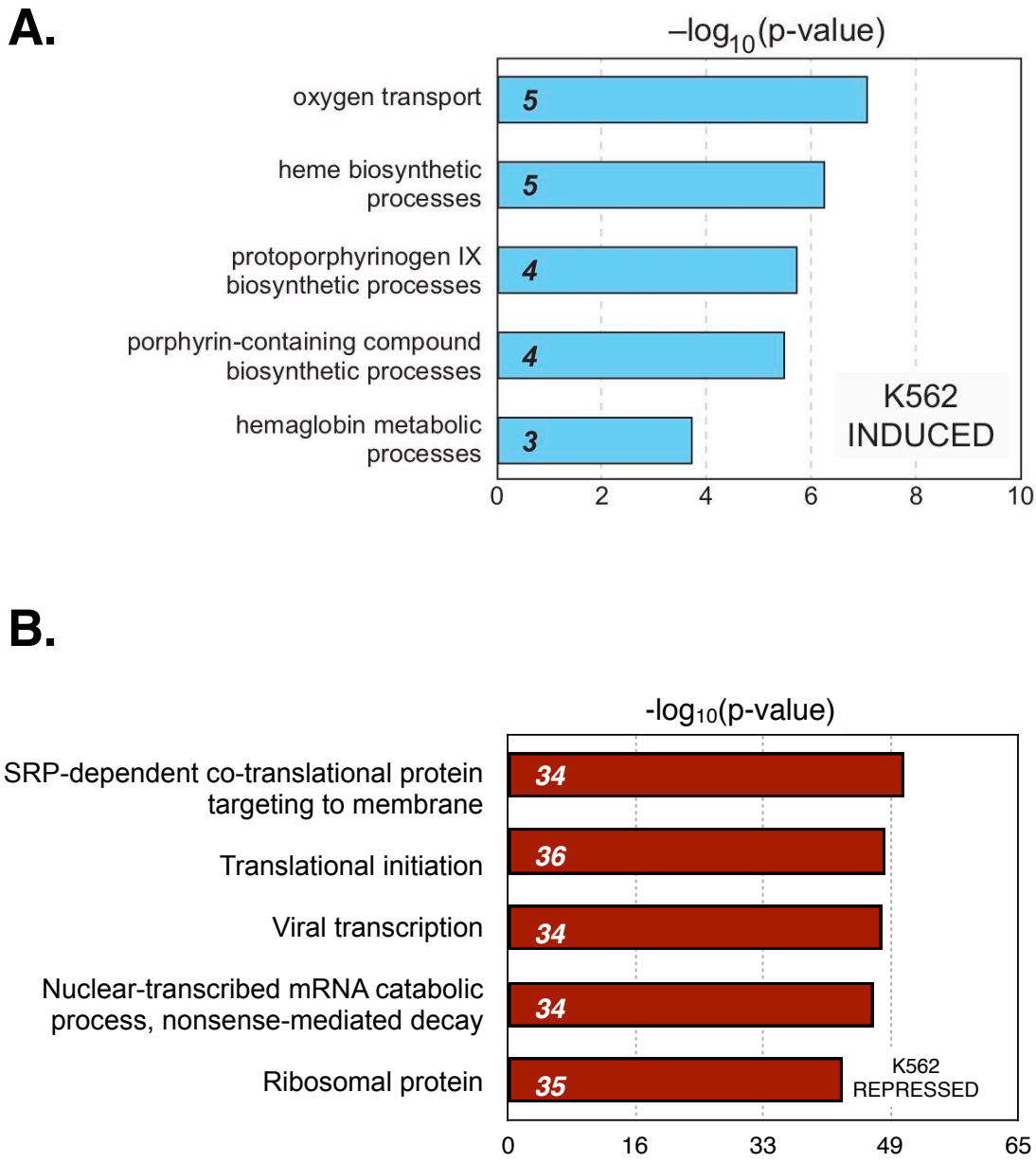

Figure 7-5. GO analysis of genes induced and repressed by C6 in K562 cells. (A) Top five GO enrichment categories for genes significantly induced by C6 treatment of K562 cells. (B) As in (A), but for significantly repressed gene in K562 cells. For both (A) and (B) the numbers in italics within the bars represent the number of C6-induced or -repressed genes in each category.

cells. Together, these data indicated that RPGs represent the major class of genes that are repressed in K562 cells after C6 treatment.

In the paragraphs above, I describe the genes that are significantly up- and down-regulated in the RNA-seq and the enriched GO terms that are associated with these genes in both sensitive and insensitive leukemia cells. Next, we sought to identify how the sets of differentially expressed genes after C6 treatment are the same or different in MV4:11 and K562 cells. In doing so, I could make conclusions about the mechanism of action of C3 and C6 and identify differences in the down-stream biological responses of the two cell types. We began by investigating the overlap between the sets of genes induced by C6 as determined by RNA-seq in MV4:11 and K562 cells (Figure 7-6A). Despite up-regulating a similar number of genes in MV4:11 and K562 cells (72 genes for MV4:11 and 65 genes for K562), we found that the up-regulated genes have almost no overlap. Only one gene was induced by C6 in both MV4:11 and K562 cells (Figure 7-6A). The overall lack of overlap in the genes induced by C6 after three-day treatment suggests that MV4:11 and K562 cells differ in their secondary responses to WDR5 WIN site inhibition.

Next we compared the genes that are repressed by three-day C6 treatment in K562 and MV4:11 cells (Figure 7-6B). I hypothesized that the genes that are repressed in both cell types would be enriched in RPGs and represent the direct transcriptional targets of WDR5 WIN site inhibition. The genes repressed by C6 showed both common and distinct genes in MV4:11 and K562 cells. 390 genes were only repressed in MV4:11 cells. 115 genes were only repressed in K562 cells. 72 genes were repressed in both cell types, accounting for ~ 16% of all MV4:11 repressed genes and ~ 39% of all K562 repressed genes. To further dissect the types of genes that were repressed by WDR5 WIN site inhibition in both cell types, GO enrichment analysis was completed for the 72 common repressed genes. Not surprisingly, it was found that the 72 common repressed genes are highly enriched in GO terms connected to the ribosome (Figure 7-6C), again supporting the idea that RPGs represent an important group of genes regulated by WDR5 in both MV4:11 and K562 cells.

Furthermore, I hypothesized that the common RPGs genes repressed in the RNA-seq would be WDR5-bound genes since WDR5 is displaced from chromatin after C6 treatment. We compared the list of genes that were repressed after three day treatment in both MV4:11 and K562 cells as

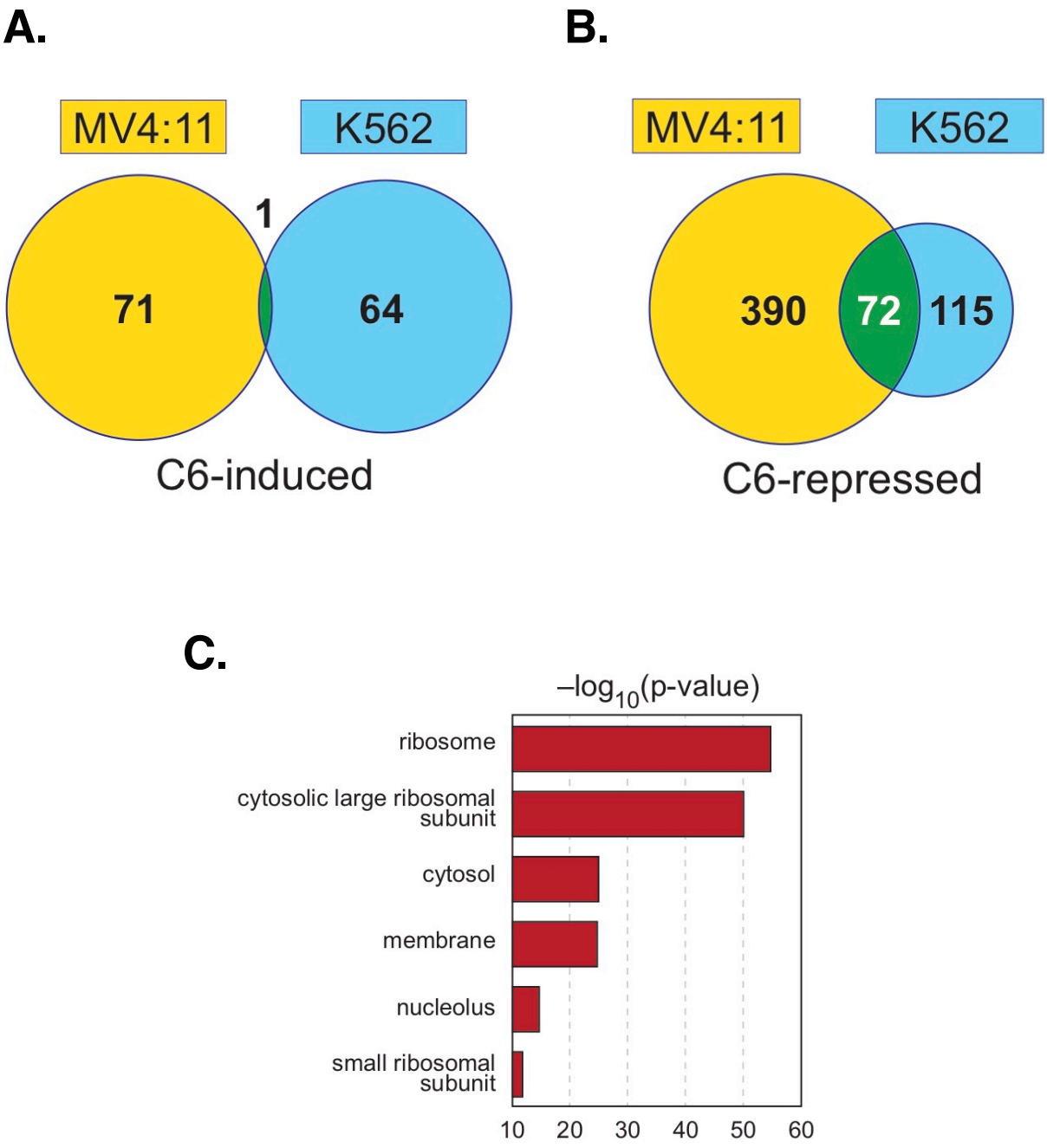

Figure 7-6. Comparison of genes repressed by C6 in MV4:11 and K562 cells. (A) Overlap of genes induced (FDR < 0.05) by three-day C6 treatment in either MV4:11 or K562 cells, as determined by RNA-Seq. (B) As in (A) but for significantly repressed genes. (C) Top six gene ontology (GO) enrichment categories for the 72 genes repressed in both MV4:11 and K562 cells after three-day C6 treatment.

determined by RNA-seq and the list of genes bound by WDR5 in both cell types as determine by ChIP-seq (Figure 7-5A). We found that the majority of all common repressed genes (~ 60 % or 41 out of 72 genes) were also bound by WDR5. To further test my assumption, Gene Set Enrichment Analysis (GSEA) was used. GSEA generates an enrichment score to determine if there is enrichment of a pre-defined unranked gene list (the query list) within a ranked gene list of interest (the reference list). In this case, the query list was the set of genes at which WDR5 was displaced by C6 in the MV4:11 WDR5 ChIP-seq and the reference list was the genes significantly changed by C6 in the MV4:11 RNA-seq ranked from least repressed to most repressed. GSEA analysis moves down the ranked reference gene list in order and asks whether each gene is found in the query list. If the reference gene is in the query list, a black line vertical line is placed above that gene in the ranked list and the enrichment score deviates farther from zero. Indeed, GSEA determined that there was a strong tendency of WDR5-bound genes to be repressed by three days of C6 treatment in MV4:11 cells (Figure 7-7B). I hypothesized that the same phenomenon would be seen for K562 cells. We repeated the GSEA, this time using the list of genes at which WDR5 was displaced from chromatin by C6 in the K562 WDR5 ChIP-seq as the query list and the ranked list of genes significantly changed by C6 in the K562 RNA-seq (Figure 7-7C). Again, we found that genes with WDR5 displacement tended to be repressed by inhibitor treatment in K562 cells. Together Figure 7-7 demonstrates that WDR5-bound genes are broadly repressed by WDR5 WIN site blockade in both cell types.

To better visualize the effects of WDR5 WIN site blockade on RPGs discovered by ChIP-seq, PRO-seq and RNA-seq all at the same time, we created Figure 7-8. This ribosomogram illustrates all of the small and large ribosomal protein genes with an orange box indicating that WDR5 is (i) bound to that RPG in the indicated cell type (ChIP), (ii) if transcription of that gene is rapidly reduced by C6 treatment (PRO-seq), and (iii) if the corresponding transcript levels are reduced by long-term C6 treatment (RNA-seq). We observed a strikingly consistent pattern of RPGs bound by WDR5, repressed in the PRO-Seq, and repressed in the RNA-Seq experiments. Therefore, I concluded that WDR5-bound genes are broadly repressed by WIN site inhibition, and that many of the affected loci belong to a specific and conserved set of RPGs.

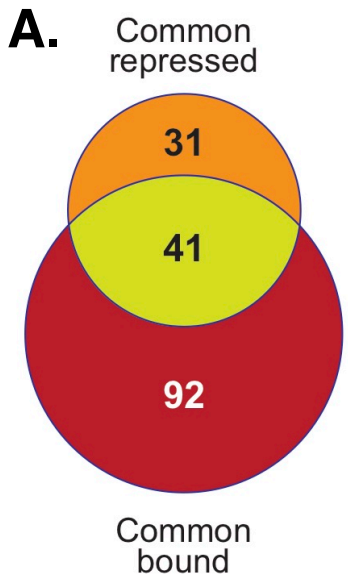

B.

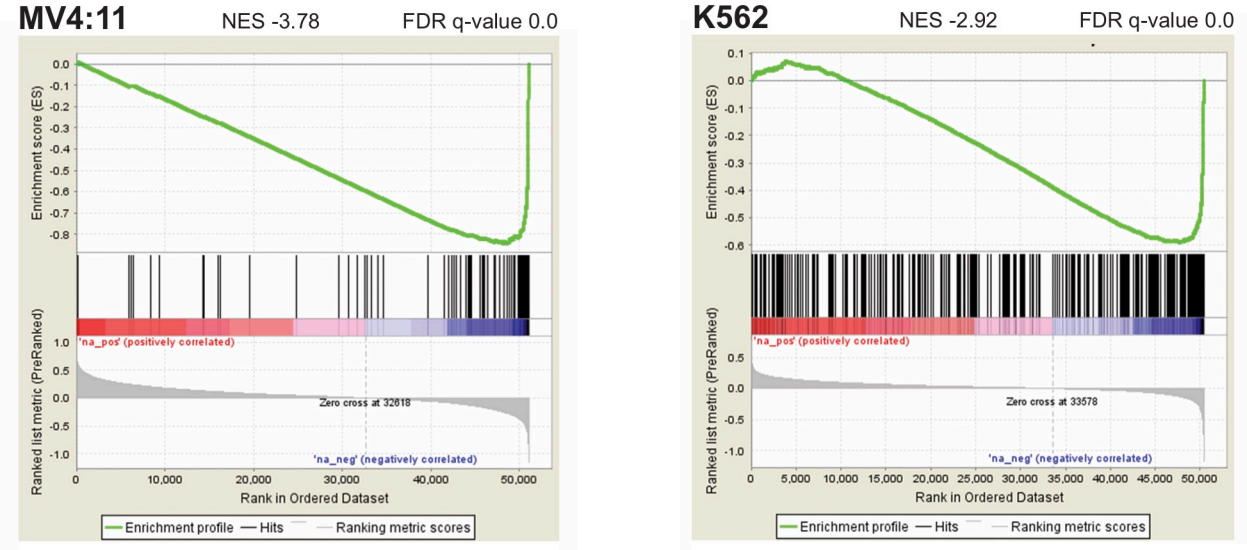

Figure 7-7. WDR5 WIN site inhibition represses transcripts from WDR5-bound genes. (A) Overlap of genes bound by WDR5 in both MV4:11 and K562 cells (Common bound) with genes repressed by C6 treatment in both cell types (Common repressed), as determined by RNA-Seq. (B) Gene set enrichment analysis (GSEA) showing the distribution of genes where WDR5 was displaced from chromatin by C6 against the ranked list of genes that are repressed by C6 in MV4:11 cells as determined by RNA-sesq. (C) As in (B), but for K562 cells.

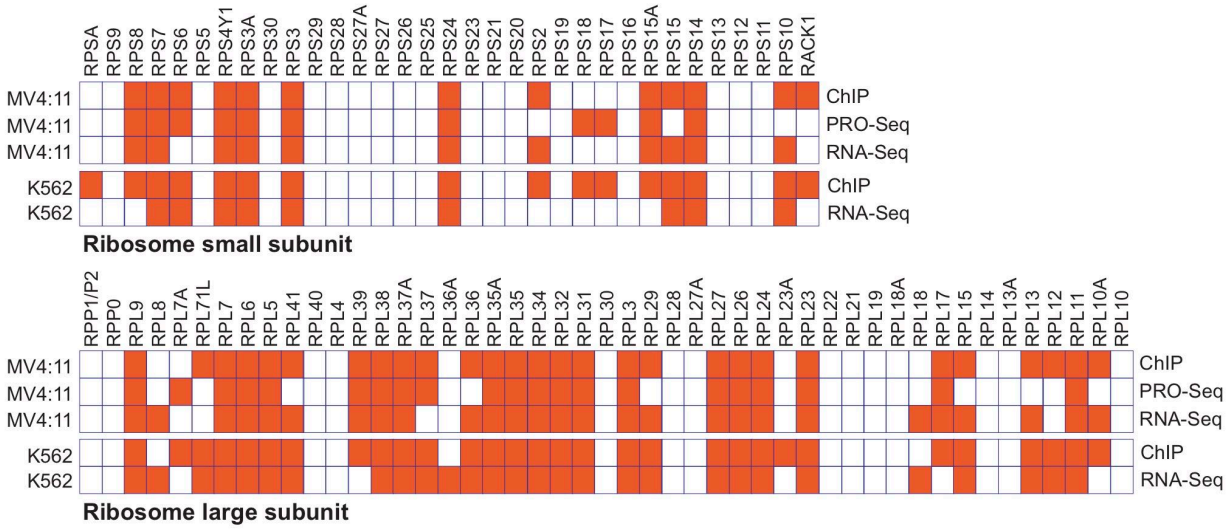

Figure 7-8. WDR5 WIN site inhibition represses transcripts from a discrete set of ribosomal protein genes. All of the small (top) and large (bottom) ribosomal protein genes are listed. An orange box indicates if (i) WDR5 is bound to each RPG in the indicated cell type (ChIP), (ii) transcription of that gene is rapidly reduced by C6 treatment (PRO-seq), and (iii) corresponding transcript levels are reduced long-term by C6 treatment (RNA-seq).

Last, I was interested in determining whether the repression of WDR5-bound RPGs is a mechanism specific to our WDR5 WIN site inhibitors C3 and C6, or if other structurally distinct inhibitors elicit the same effect. The effect of the small molecule WDR5 inhibitor OICR-9429 (Grebien, Vedadi et al. 2015) on RPG expression has not previously been investigated. I hypothesized that the WDR5 inhibitor OICR-9429 would also reduce steady state mRNA levels of WDR5-bound RPGs by roughly 2-fold in MV4:11 cells. To test this prediction, I treated MV4:11 cells for three days with DMSO, 4 μM C6, 4 μM OICR-9429, or 50 μM OICR-9429. I treated MV4:11 cells with concentrations close to 2xGI_{50} of compound (4 μM C6 and 50 μM OICR-9429) to observe the effects of mRNA levels when WDR5 is robustly inhibited. In doing so, I could compare C6 and OICR-9429 when treating with roughly equal cellular potency. Additionally, I treated cells with 4 μM OICR-9429 to test the effects of C6 compared to OICR-9429 when treating at equal micomolar concentration, but not cellular potency. I hypothesized that OICR-9429 would reduce steady-state mRNA levels of WDR5-bound RPGs by roughly 2-fold in MV4:11 only when treating with equal cellular potency as C6 but not equal micromolar concentration, as growth of MV4:11 cells is not inhibited by 4 μM OICR-9429.

After three days, I extracted and purified total RNA from treated MV4:11 cells using a Zymo Research RNA mini-prep kit with an on-column DNAse digestion to remove any contaminating genomic DNA. I then reverse transcribed the RNA to generate cDNA and performed RT-qPCR to quantify relative expression of four RPGs, *RPL35, RPS24, RPS11* and *RPL14*. *RPL35* and *RPS24* were found to be bound by WDR5, and *RPS11* and *RPL14* were not bound by WDR5 in the ChIP-seq experiment presented in chapter V. I quantified expression of the RPGs relative to the “house keeping” gene *GAPDH* using the delta/delta CT method (Schmittgen and Livak 2008). The expression of *GAPDH* was not found to be altered after C6 treatment in the RNA-seq experiment and therefore serves as a good internal control gene. The relative expression of the four RPGs after each compound treatment was then normalized to DMSO treated samples.

I found that expression of *RPL35* and *RPS24*, the two RPGs bound by WDR5, were significantly reduced by about 40% when MV4:11 cells were treated with 4 μM C6 and 50 μM OICR-9429 (Figure 7-9). I did not observe a statistically significant reduction in *RPL35* and *RPS24* expression when treated with 4 μM OICR-9429. Expression of *RPS11* nor *RPL14*, the two RPGs that are not bound by WDR5, were statistically significantly increased in some cases but no treatment conditions caused a decrease in the expression of these genes. Together, this data

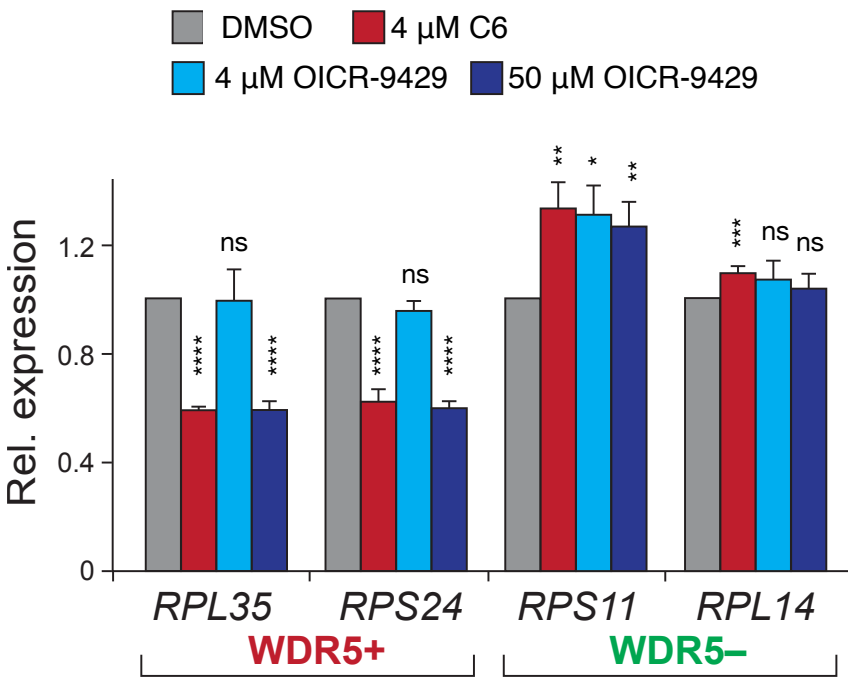

Figure 7-9. OICR-9429 represses WDR5-bound ribosomal protein genes. MV4:11 cells were treated for three days with DMSO, 4 μM C6, 4 μM OICR-9429, or 50 μM OICR-9429, RNA harvested, and the levels of expression of four RPGs were determined by RT-qPCR. DMSO-treated samples are set to 1.0 in each case. *RPL35* and *RPS24* are RPGs that are bound by WDR5 (WDR5+) and *RPS11* and *RPL14* are not bound by WDR5 (WDR5–) as determined by ChIP-Seq. n = 3 independent biological replicates. Error bars represent standard error of the mean (SEM). "ns" means not statistical difference ($p > 0.05$), "****" means $p < 0.0001$, "***" means $p < 0.001$, "**" means $p < 0.01$, "*" means $p < 0.05$. p-values were determined for compound treatment compared to DMSO for each gene by two-tailed Student's t-test.

indicated that expression of RPGs bound by WDR5 is reduced when MV4:11 cells are treated with equal cellular potency of C6 and OICR-9429, but not equal micromolar concentration. The fact that the effect correlates with the affinity of the compound with WDR5 and the GI_{50}s in the proliferation assay strongly indicates that the effect is due to inhibition of WDR5. It also indicates that the mechanism of reducing WDR5-bound RPG expression is not specific to C3 and C6, but instead is a common mode of action used by other WDR5 WIN site inhibitors.

Discussion

Defining both the primary and secondary gene expression changes that occur after inhibitor treatment is critical to decode the mechanism of action of WDR5 WIN site blockade. Previous studies using the monobody Mb(S4) (Gupta, Xu et al. 2018) and the small molecule WDR5 WIN site inhibitor OICR-9429 (Grebien, Vedadi et al. 2015, Zhu, Sammons et al. 2015, Neilsen, Chakraborty et al. 2018) have not identified the full repertoire of gene expression changes that occur after WDR5 WIN site inhibition. RNA-seq has been performed after four-day treatment with the peptidomemtic MM-401 in MLL-AF9 transformed murine bone marrow cells (Xu, Li et al. 2016). However, as stated in previous chapters, the authors of this publication maintain a MLL1-centric approach, as it was assumed that the inhibitor mainly functions by blocking WDR5/MLL1 interaction. To this end, the authors focused only on the significant changes in expression after MM-401 treatment for genes that were bound by MLL1 or by both MLL1 and MLL-AF9. In doing so, the analysis was biased and a full understanding of how MM-401 effects genes expression could not be gleaned. Additionally, the low temporal resolution of RNA-seq after a four-day treatment made it impossible to separate the primary transcriptional targets from the secondary or compensatory effects, and without a parallel RNA-seq data set in a non-MLL-fusion cell line, the differences and similarities in how sensitive and insensitive cells respond to WDR5 WIN site inhibition could not be elucidated.

The use of PRO-seq and RNA-seq presented here coupled with the WDR5 ChIP-seq data presented in chapters V and VI allowed us to identify the full repertoire of both the primary transcriptional targets and later secondary gene expression changes that occur in both sensitive and insensitive leukemia cells after WDR5 inhibition. We did not see changes in expression of any genes classically connected to MLL-leukemogenesis and we did not detect WDR5 enrichment on chromatin at these genes (chapter V), making it unlikely that WIN site inhibitors

function by interfering with MLL1 complexes as was assumed by other investigators. Furthermore, although both C3 and C6 are potent and selective inhibitors of MLL1 HMT activity, I have presented evidence that suggests that the mechanism through which C3 and C6 kill MV4:11 cells is independent of changes in H3K4 methylation. For example, despite displacement of WDR5 from chromatin at *RPL35* and *RPS24*, and decreased expression of these genes, H3K4me3 was not reduced at these genes after WDR5 WIN site inhibition (chapter VI). This finding indicates that WDR5 enrichment on chromatin is not required for H3K4me3 and that WDR5 is likely required for some non-MLL1 associated function at WDR5-bound PRGs.

Instead of inhibition of HMT activity, the primary mechanism of action of C3 and C6 appears to be eviction of WDR5 from chromatin and an immediate and sustained decrease in the expression of WDR5-bound genes. Our PRO-seq and RNA-seq experiments using both C3 and C6 in MV4:11 and K562 cells clearly point to a specific subset of RPGs as direct targets of WIN site inhibition. The extensive overlap between RPGs identified as targets of C3 in the MV4:11 PRO-Seq and those identified as targets of C6 in the MV4:11and K562 RNA-seq reveals a highly consistent mode of action of these two compounds. The consistency in their mode of action is solidified by the fact that both C3 and C6 displace WDR5 from chromatin (chapter VI), and that a distinct WIN site inhibitor, OICR-9429, shows the same selectivity in RPG mRNA inhibition. Additionally, Dr. Lance Thomas in our lab has determined that OICR-9429 also causes WDR5 to be displaced from chromatin at RPGs. Coupled with the recurring and highly consistent binding of WDR5 to the same select subset of RPGs in different cell types, I conclude that these RPGs are the predominant biological targets of WDR5 and thus of WDR5 inhibitors. Our studies illuminate an intimate connection between WDR5 and ribosome biogenesis, and show that WIN site inhibitors have a unique and unexpected mechanism of killing MLL-fusion cancer cells.

However, what is still unclear is what function WDR5 performs at the conserved WDR5-bound RPGs and how this function is impacted by WIN site blockade to ultimately repress expression of these genes. WDR5 has been shown to bind both modified and unmodified histone H3 tails (Schuetz, Allali-Hassani et al. 2006). Perhaps WDR5 binds to specific epigenetic modifications at these genes and then due to its roles as a scaffolding protein (Guarnaccia and Tansey 2018), WDR5 may help to nucleate the assembly of a protein complex needed to promote transcription. Alternatively, it is possible that instead of functioning as an epigenetic reader, the

WIN site binds to a protein already present at the RPGs and then recruits other factors needed to promote transcription. The possible complex that binds WDR5 and promotes transcription may be one of the half dozen chromatin and epigenetic regulating complexes already discovered to bind WDR5, or may be entirely novel WDR5 binders yet to be discovered. WDR5 WIN site inhibition may therefore reduce expression of RPGs by blocking the epigenetic reader or complex assembly functions of WDR5. Recently, our lab discovered that the transcription factor MYC binds the WBM site of WDR5 (Thomas, Wang et al. 2015) and MYC and WDR5 co-localize to chromatin at conserved PRGs in many cell types (personal communications). The interaction between MYC and WDR5 may be important for driving expression of RPGs and by displacing WDR5 at the WIN site, it may be possible to remove MYC from these genes as well and thus block MYC-mediated transcriptional regulation. Elucidating specifically what WDR5 does at RPGs is beyond the scope of this thesis but potential future approaches that could help to determine the role of WDR5 at RPGs will be presented in the future directions subsection of chapter IX.

We have found that the primary effects of WDR5 WIN site inhibition occur in both MV4:11 and K562 cells, yet only MV4:11 cells are killed by WDR5 WIN site inhibition indicating that some yet to be determined biological characteristic(s) that lies down-stream of WDR5 displacement is able to determine whether a cell line is sensitive to WDR5 WIN site inhibition. More information is needed to understand what the biological consequences are of reducing the expression of about half of all RPGs by ~50% in order to make stronger connections between the primary effects and the subsequent secondary induction of proliferative arrest and apoptosis. In doing so, we may able to better understand why some cells are sensitive and some are not and better predict what type of cancer cells could be targeted with WDR5 inhibitors. In chapter IV I empirically determined that MLL-fusion leukemia cell lines expressing wild type p53 were sensitive to our inhibitors C3 and C6 while p53-deficient cell lines were not. Therefore, I hypothesized that p53 is important for the response to WDR5 WIN site inhibitors in sensitive cell lines. In the next chapter, I will detail experiments performed in an effort to better connect the primary and secondary effects of our compounds and investigate the role of p53 in the response to WDR5 WIN site inhibition in sensitive cells.

CHAPTER VIII

WDR5 WIN SITE INHIBITION INDUCES p53-DEPENDENT CELL KILLING AND NUCLEOLAR STRESS

Introduction

In previous chapters I argued that the primary mechanism of WDR5 WIN site inhibitors is the rapid and comprehensive displacement of WDR5 from chromatin at a conserved set of genes connected to protein synthesis, which in turn causes a decrease in expression of these genes. I also described that while the primary effects of WDR5 WIN site inhibitors can be detected within minutes of compound treatment, the secondary effects of inhibited cellular proliferation and cell death occur on the order of days after inhibitor treatment. In order to better understand the biological consequences of inhibiting WDR5, we needed to further elucidate the biological events that occur after the primary effects of compound treatment that bring about the secondary induction of cellular inhibition. Therefore, the main focus of experiments presented in this chapter is to better connect the rapid primary effects of WDR5 WIN site inhibitor treatment with the long-term inhibition of cell growth and induction of apoptosis in sensitive cell lines.

The strong biological connection between WDR5 and RPG expression described in previous chapters strongly suggested that WDR5 WIN site inhibition would disrupt ribosome biogenesis. Therefore, we used a variety of molecular and biochemical techniques to investigate whether the cellular consequences that occur after the primary effects of WDR5 WIN site inhibition are consistent with perturbation of ribosome biogenesis, such as decreased protein synthesis and induction of nucleolar stress. Because I had found that sensitivity of MLL-fusion leukemia cell lines correlated with expression of wild type p53, as shown in chapter IV, I also hypothesized that p53 would be involved in the cellular response to WDR5 WIN site inhibition. That hypothesis is tested in this chapter.

In summary, we found that p53 protein levels are up-regulated in sensitive cell lines, leading to induction of a p53-mediated transcriptional program. p53 induction also occurred in cells treated

with the structurally distinct WDR5 WIN site inhibitor OICR-9429, indicating that p53 induction is a common mode of action of WIN site blockade. I found that C6 resulted in decreased protein synthesis and induction of a nucleolar stress response in sensitive leukemia cells, consistent with a perturbation in ribosome biogenesis. Finally, I found that p53 knock-down and knockout both rescue sensitively to WDR5 WIN site inhibition, indicating that p53 significantly contributes to the response in sensitive cells. Together, the data presented here detail a novel mode by which WDR5 WIN site inhibitors function.

Results

Effects of WDR5 WIN site inhibition on protein synthesis

In the previous chapters of this thesis, I report that the primary mode of action of WDR5 WIN site inhibitors is displacement of WDR5 from chromatin at WDR5-bound genes. WDR5-bound genes were found to be strongly enriched in a discrete set of ribosomal protein genes accounting for ~40% of the small and ~70% of the large ribosomal subunit proteins. In addition, we found that WDR5 is enriched at genes encoding several translational initiation factors including EIF3B, EIF3D, EIF4G1, EIF4G3, and EIF4A2. Displacement of WDR5 from chromatin upon inhibitor treatment was accompanied by a rapid decrease in transcription of WDR5-bound genes that was sustained for at least three days. To date, the biological consequences of reducing about half of all RPGs by 2-fold have not been investigated, making it unclear how cells will respond to such a broad assault on the biogenesis of protein synthesis machinery. I hypothesized that by impeding the expression of a vast number of genes needed for ribosome biogenesis and translational initiation, over time WDR5 WIN site inhibitor treatment would impede the translational capacity of sensitive cells, thus leading to inhibited cell growth and apoptosis.

The relative protein translational capacity of cells can be easily and quickly quantified by fluorescently labeling all of the proteins made in the cell within a given amount of time and then measuring the relative fluorescence of the cells by flow cytometry (Signer, Magee et al. 2014). For this purpose, I used the compound O-propargyl-puromycin (OP-Puro or OPP) to label all of the nascent polypeptides produced during a one hour OP-Puro pulse and then the cells were fixed. OP-Puro is an analog of the protein synthesis inhibitor puromycin. Like puromycin, OP-Puro is taken up by cells in culture and binds in the ribosome acceptor site by mimicking the 3'

end of an aminoacylated tRNA. OP-Puro is incorporated into the nascent polypeptide causing premature translational termination and release of the OP-Puro labeled peptide from the ribosome. Unlike puromycin, OP-Puro contains an alkyne “handle” that can be used to attach a fluorophore with an azide “handle” by copper-catalyzed click chemistry. After labeling the OP-Puro-peptides with the fluorophore, the relative fluorescence, and therefore the relative rate of protein synthesis, can be quantified in individual cells within the population by flow cytometry.

I used the OP-Puro labeling method described above to quantify the relative rates of protein translation in MV4:11 cells treated for 1, 2, 3 or 6 days with 2 μM C6, C6nc or DMSO (Figure 8-1). I displayed the OP-Puro incorporation both as histograms of Alexa647 fluorescence from one representative replicate (Figure 8-1A) and as bar graphs showing the mean OP-Puro fluorescence of the cell population for all three biological replicates (Figure 8-1B). As a positive control for inhibition of translation, the translational inhibitor cycloheximide (CHX) was added to a sample of DMSO treated cells 30 minutes prior to the addition of OP-Puro. As a control for background Alexa647 staining, no OP-Puro was added to a sample of DMSO treated cells. I found that as early as one day after treatment, a right shift in the OP-Puro incorporation curve was observed for C6 treatment, towards that observed in the presence of cycloheximide. A significant change in OP-Puro incorporation was observed on day two of C6 treatment. The impact of C6 on the protein synthesis capacity of MV4:11 cells increased across the time-course, and at six days roughly half of the cells in the C6-treated population incorporated OP-Puro at levels similar to that of cells treated with cycloheximide. The OP-Puro incorporation of C6nc treated cells was not reduced at the 1, 2 or 3 day time points. A statically significant decrease in OP-Puro incorporation was seen at the 6 day time point for C6nc compared to DMSO, though this decrease was modest compared to that observed for C6. Thus, WIN site inhibition leads to an early and progressive decrease in the protein synthesis capacity of MV4:11 cells. Importantly, the decrease in protein production precedes proliferative inhibition, indicating that reduced protein production is not due to reduced cell growth.

Effects of WDR5 WIN site inhibition on p53 expression

By screening a panel of leukemia cell lines with various mutations, as reported in chapter IV, I empirically determined that sensitivity to C3 and C6 correlates with expression of an MLL-fusion protein in combination with wild type p53. This observation led me to speculate that p53 could be involved in the response of sensitive cell lines to WDR5 WIN site inhibition. We also found

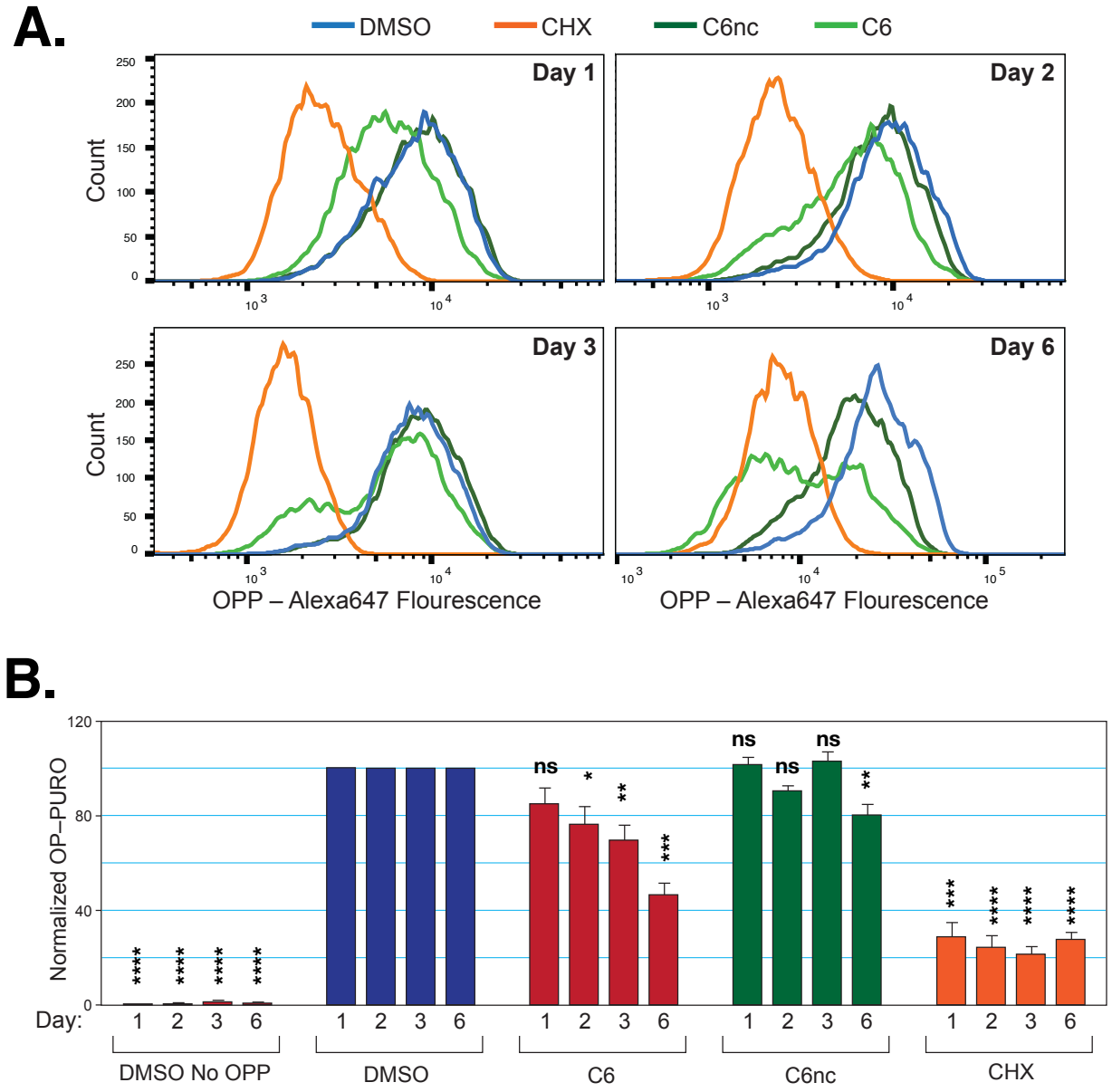

Figure 8-1. WDR5 WIN site inhibition reduces protein translational capacity over time. (A) Representative flow cytometry histograms showing Alexa647-labeled OPP incorporation into nascent polypeptides of MV4:11 cells treated with DMSO, or 2 μM C6nc, or C6 for the indicated time points. As a control for inhibition of translation, cycloheximide (CHX) was added to cells 30 minutes prior to addition of OPP. (B) Bar graph depicting relative mean Alexa647 labeled-OPP incorporation into nascent polypeptides of MV4:11 cells treated with DMSO, or 2 μM C6nc or C6, for 1, 2, 3, or 6 days. No OPP was added to a sample of DMSO treated cells to control for background Alexa647 staining. Mean Alexa647 fluorescence measurements were normalized to DMSO treated samples at each time point. n = 3. "ns" no significant difference ($p > 0.05$). "****" means $p < 0.0001$), "***" means $p < 0.001$, "**" means $p < 0.01$, "*" means $p < 0.05$. p-values were determined by two-tailed Student's t-test for each treatment compared to DMSO at each time point.

that C3 and C6 reduce expression of WDR5 bound RPGs. Disruptions to ribosome biogenesis have been shown to lead to induction of p53, cell cycle arrest and apoptosis in a process known as nucleolar stress, which will be described further below (Russo and Russo 2017). Therefore, I hypothesized that p53 would be induced in sensitive leukemia cell lines after WDR5 WIN site inhibitor treatment.

I tested for induction of p53 protein levels in sensitive cells by treating MV4:11 cells with DMSO, or 2 μM (roughly the $GI_{50)}$ of C6 or C6nc for 24 hours. I chose a 24 hours time point because I knew that an increase in the apoptotic marker cleaved PARP-1 (chapter IV), decreased ribosome transcription (chapter VII), and decreased protein synthesis (Figure 8-1) could all be observed after 24 hours of treatment. Additionally, I was interested in testing for induction of p53 at 24 hours because this time point precedes gross phenotypic changes. I then harvested whole cell lysates and ran samples of the lysates on an SDS-PAGE gel. Finally, I probed the resulting Western blot with antibodies specific for p53 and histone H3 as a loading control (Figure 8-2A). I found that p53 protein levels were modestly increased after 24 hour C6 treatment compared to DMSO. C6nc did not show a significant increase in p53 levels compared to DMSO. I also probed the MV4:11 lysates with an antibody specific for p21, a canonical p53 target gene (Sullivan, Galbraith et al. 2018), to assess whether the p53 protein induction was functional. I found that p21 protein levels were also increased in MV4:11 cells after 24 hour C6 treatment but not C6nc treatment compared to DMSO (Figure 8-2A). The induction of p21 supports the idea that the induction of p53 protein after C6 treatment increases p53 activity. I next wanted to see if p53 and p21 induction after C6 treatment are specific for MV4:11 cells or if this effect can also be seen when a different sensitive cell line, Molm13, is treated with C6. I treated Molm13 cells for 24 hours with roughly the GI_{50} (3 μM) of C6, C6nc or DMSO. I found that indeed p53 and p21 protein levels were also modestly and reproducible induced in Molm13 cells after 24 hour treatment with C6 but not C6nc compared to DMSO (Figure 8-2B). Figures 8-2A and B suggest that p53 and p21 induction is a common response to WDR5 WIN site inhibition in sensitive cells. p53 and p21 induction was not tested in the insensitive cell line K562 because p53 is not expressed in these cells.

I next wondered if p53 and p21 induction is a common mode of action shared with other WDR5 WIN site inhibitors or if this effect is specific to C6. I hypothesized that the small molecule WDR5 WIN site inhibitor OICR-9429 (Grebien, Vedadi et al. 2015) would also induce p53 and

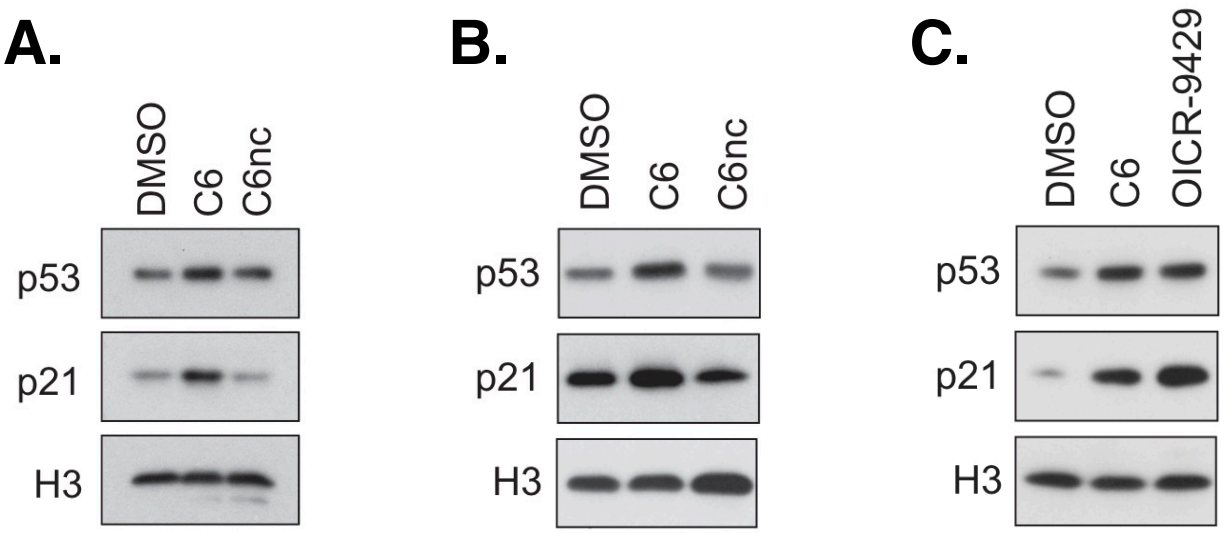

Figure 8-2. WDR5 WIN site inhibition induces p53 and p21 protein levels. (A) Western blot showing the effects of DMSO, or 2 μM C6 or C6nc on p53 and p21 protein levels in MV4:11 cells after 24 hours of treatment. (B) Western blot showing the effects of DMSO, or 3 μM C6 or C6nc on p53 and p21 protein levels in Molm13 cells after 24 hours treatment. (C) Western blot showing the effects of DMSO, 2 μM C6, or 30 μM OICR-9429 in MV4:11 cells after 24 hours of treatment.

p21 protein levels, since I reported in chapter VII that OICR-9429 also reduces expression of WDR5-bound RPGs. To test my hypothesis, I treated MV4:11 cells with DMSO, 2 μM C6, or 30 μM OICR-9429 for 24 hours (Figure 8-2C). The concentrations of compound that I chose were both roughly the three-day proliferation assay GI_{50} of C6 and OIC-9429 to ensure that the compounds were used at equal cellular potency. I found that OICR-9429 also induced a modest but reproducible increase in p53 and p21 protein levels compared to DMSO and the magnitude of induction was comparable to that of C6. I concluded that induction of p53 and p21 protein expression is a common response to WDR5 WIN inhibitors in sensitive cells.

Comparison of gene expression changes induced by WDR5 WIN site inhibition and HDM2 antagonism

We next wanted to further investigate whether the induction of p53 seen after WDR5 WIN site inhibition was functional and led to a p53-mediated cellular response. Because p53 is a transcriptional activator (Sullivan, Galbraith et al. 2018), we reasoned that if the p53 induction is functional, we should see an increase in expression of known p53 direct target genes upon C6 treatment of sensitive cells. To test this hypothesis, we performed a Gene Set Enrichment Analysis (GSEA) using the ranked list of genes differentially expressed in MV4:11 cells after three-day 2 μM C6 treatment as the reference list and a pre-defined list of p53 and p63 target genes (Perez, Ott et al. 2007) defined in the Molecular Signatures Database as the query list (Figure 8-3). The GSEA revealed that p53 and p63 target genes were significantly enriched among the induced genes in MV4:11 cells after three-day C6 treatment. This analysis supports the idea that the p53 induction is functional.

We also tested whether the p53 induction after C6 treatment is functional in another manner by investigating whether part of the transcriptional response to WIN site inhibition can be recapitulated by the small molecule inhibitor Nutlin-3. Nutlin-3 is a small molecule inhibitor of the p53–HDM2 interaction (Vassilev, Vu et al. 2004). HDM2 is the E3 ubiquitin ligase responsible for

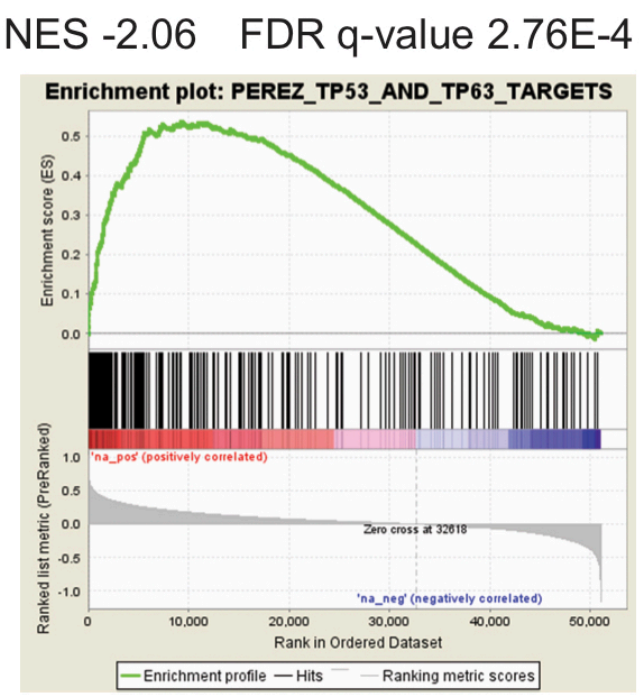

Figure 8-3. The differentially expressed genes after C6 treatment of MV4:11 cells are enriched in p53 and p63 target genes. GSEA of RNA-Seq from MV4:11 cells treated for three days with 2 μM C6 identified significant enrichment in p53 and p63 target genes, as defined in the Molecular Signatures Database.

promoting the proteosome-dependent degradation of p53 under normal conditions. When Nutlin-3 binds to HMD2, HDM2 can not bind to p53 to facilitate its ubiquitination so p53 levels increase. I first confirmed that treatment of MV4:11 cells with 2 μM Nutlin-3 for 24 hours results in increased p53 and p21 protein levels (Figure 8-4A). Next, I used RNA-seq to determine how the steady-state mRNA changes that occur in MV4:11 cells after Nutlin-3 treatment compare to the RNA-seq data obtained for C6 treated cells (chapter VII). I treated MV4:11 cells for three days with 2 μM Nutlin-3 or DMSO. Next, total RNA was extracted and purified using TRIzol reagent and a Zymo Research RNA mini prep kit with on column DNAse digestion to remove any contaminating genomic DNA. Total RNA samples were submitted to Genewiz for ribosomal RNA depletion, library preparation and next generation sequencing. The Nutlin-3 RNA-seq experiment was repeated with three biological replicates. The raw RNA-seq data was analyzed by Jing Wang under the mentorship of Dr. Qi Liu. Jing Wang used a cut-off of FDR < 0.05 to determine the significantly differentially expressed genes in MV4:11 cells after Nutlin-3 treatment compared to DMSO.

In total, 6,123 genes were significantly differentially expressed in MV4:11 cells after Nutlin-3 treatment compared to DMSO (Figure 8-4B). 1,362 genes were up-regulated and 4,761 genes were down-regulated. In general, Nutlin-3 induced a broader array of transcriptional changes than we observed for C6, but Nutlin-3 also induced p53 more potently than C6 under these conditions (Figure 8-4A). C6 treatment resulted in a total of 534 differentially expressed genes in MV4:11 cells compared to DMSO, as determined by RNA-seq (chapter VII). We first compared the 1,362 genes induced by Nutlin-3 and the 72 genes induced by C6 (Figure 8-4C). We found 42 common genes that were induced after both compound treatments, which accounted for ~60% of all of the genes induced by C6. This finding indicates that a significant portion of the genes induced by WDR5 WIN site inhibition can also be seen after p53 induction by HDM2 antagonism.

We next compared the 4,761 genes repressed by Nutlin-3 and the 462 genes repressed by C6 (Figure 8-4D). We found 384 common genes repressed by Nutlin-3 and C6. These 384 genes accounted for ~80% of all of the genes repressed by C6. Interestingly, these common genes did not include the WDR5-bound RPGs. The significant overlap between genes repressed by C6 with those repressed by Nutlin-3 again indicate that a significant portion of the secondary transcriptional changes that occur after C6 inhibition can be attributed to p53 induction.

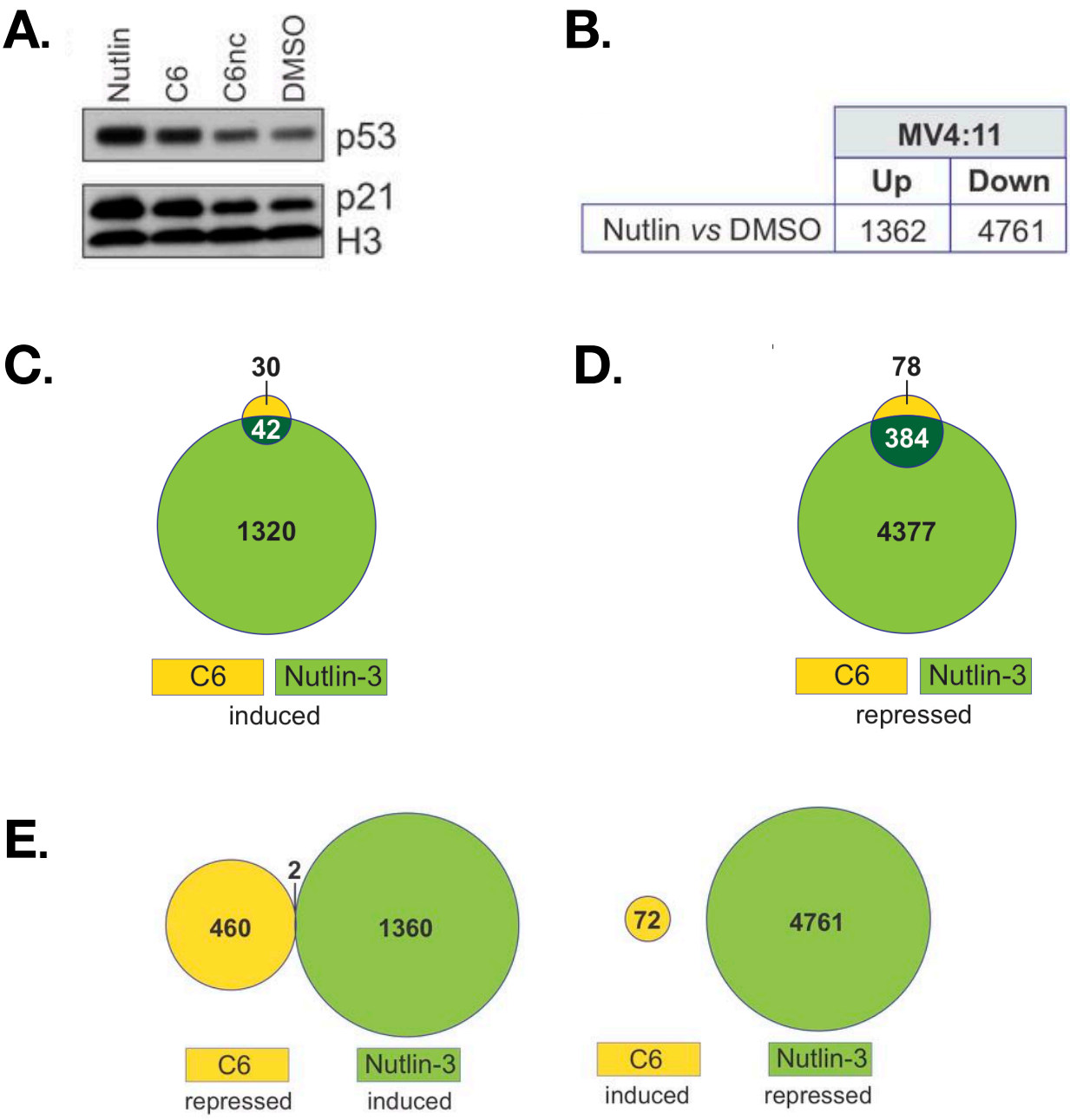

Figure 8-4. WDR5 WIN site inhibition induces transcriptional changes similar to that of an HDM2 antagonist. (A) Western blot for p53 and p21 induction in MV4:11 cells treated for 24 hours with 2 μM Nutlin-3, C6, C6nc or DMSO only. (B) Summary of the genes significantly up- and down-regulated (FDR < 0.05) in MV4:11 cells after three-day 2 μM Nutlin-3 treatment compared to DMSO, as determined by RNA-seq. (C) Overlap of genes induced by three-day 2 μM C6 (n = 5) or 2 μM Nutlin-3 (n = 3) treatment, as determined by RNA-Seq. (D) As for (C) but for repressed genes. (E) Overlap of genes induced by three-day 2 μM Nutlin-3 treatment with genes repressed by 2 μM C6 (left), and overlap of genes induced by three-day 2 μM C6 treatment with genes repressed by 2 μM Nutlin-3 (right), as determined by RNA-Seq.

Furthermore, we investigated whether the differentially expressed genes showed any anti-correlation between C6 and Nutlin-3 (Figure 8-4E). We found that there was little to no anti-correlation seen between the two treatments, with only two genes repressed by C6 but induced by Nutlin-3, and no overlap between the genes induced by C6 and repressed by Nutlin-3.

In sum, the data presented in this section demonstrate that the p53 induction upon WDR5 WIN site inhibitor treatment in sensitive cell lines is functional. The ability of an HDM2 antagonist to phenocopy a majority of the gene expression changes elicited by WIN site inhibition is consistent with the idea that induction of p53 is responsible for a significant portion of the transcriptional changes caused by C6.

The effect of WDR5 WIN site inhibition on DNA damage induction

In the subsections above, I hypothesize that WDR5 WIN site inhibition results in inhibited ribosomal biogenesis leading to p53 induction. While inhibition of ribosomal biogenesis is one stimulus known to promote p53 protein expression and signaling (Golomb, Volarevic et al. 2014, James, Wang et al. 2014), an alternative explanation for the induction of p53 seen in MV4:11 and Molm13 cells upon C6 treatment could be that C6 induces DNA damage. DNA damage is known to induce p53 protein levels and signaling leading to up-regulation of p21, cell cycle arrest and apoptosis (Lakin and Jackson 1999). We did not have reason to believe that the chemical structure of C6 would directly induce DNA damage, but it was possible that C6 may have yet to be identified effects that indirectly result in accumulation of DNA damage. I hypothesized that the p53 induction I saw in sensitive cells (Figure 8-2) was not due to DNA damage induction. I used immunofluorescent staining and confocal microscopy to quantify the presence of γ-H2AX in treated MV4:11 cells as a marker of DNA damage. Upon DNA double-strand break induction the histone H2AX is rapidly phosphorylated to generate γ-H2AX (Sharma, Singh et al. 2012). γ-H2AX foci formation acts a signal to mark sites of DNA lesions and recruit proteins involved in DNA repair. Because γ-H2AX spreads rapidly over a megabase region of chromatin around a DNA lesion, nuclear γ-H2AX staining as a marker of DNA damage can easily be visualized and quantified by confocal microscopy.

To determine whether C6 treatment induces DNA damage, I first treated MV4:11 cells for 3 days with 4 μM C6 or C6nc, or DMSO. Cells were treated for three days at 2x the GI_{50} of C6 because at this concentration and time point robust proliferative inhibition and p53 induction were

observed. As a positive control for DNA damage induction, MV4:11 cells were treated with 2 μM of the DNA damaging drug camptothecin (CPT) for 1 hour. After treating the cells, I fixed and then stained the cells with a primary antibody specific for γ-H2AX and a secondary antibody conjugated to Alexa488. The samples were imaged using an SP5 Leica scanning confocal microscope, ensuring that the laser power and gain settings were the same for all samples. The DNA intercalating stain DRAQ5 was used as a nuclear counter stain. Representative confocal images for γ-H2AX and DRAQ5 stained cells are shown in Figure 8-5A. I also quantified nuclear γ-H2AX staining intensity for all cells in 5 representative fields using Fiji software. Box and whisker plots showing quantification of γ-H2AX staining intensity in arbitrary units (AU) can be found in Figure 8-5B. I found that as expected, the DNA damaging drug camptothecin robustly increased γ-H2AX staining intensity compared to DMSO. In contrast, γ-H2AX staining in DMSO, C6 and C6nc treated cells was very faint and there was no statistically significant difference in γ-H2AX staining intensity between these three treatments. Figure 8-5 indicates that C6 does not induce DNA damage detectable by this method.

Effect of WDR5 WIN site inhibition on nucleolar stress induction

The nucleolus functions as the site of ribosomal RNA (rRNA) transcription and processing, and the assembly of the ribosomal subunits (James, Wang et al. 2014). A failure in ribosome protein biogenesis or rRNA transcription that leads to impaired cellular homeostasis is termed “nucleolar stress”. In addition to being the site of ribosome biogenesis, the nucleolus also serves as a sensor for when this biological process is perturbed and activates signaling pathways that block cell growth and induce apoptosis. The most well-characterized nucleolar stress pathway involves translocation of specific ribosomal proteins from the nucleoli to the cytosol when ribosome biogenesis is inhibited or an imbalance of ribosomal proteins is produced (Russo and Russo 2017). In the cytosol, the ribosomal proteins bind to HDM2, the E3 ubiquitin ligase that negatively regulates p53, allowing p53 levels to rise and promote cell cycle arrest and apoptosis. Because we found that expression of roughly half of all RPGs is decreased, translational capacity is reduced, and p53 is induced after WDR5 WIN site inhibition in sensitive cells, I hypothesized that WDR5 WIN site inhibition induces nucleolar stress.

In order to test my hypothesis, I needed to identify an easily quantifiable marker of nucleolar stress. It is known that nucleolar stress stimulates dramatic changes in the protein composition of the nucleoli (Yang, Wang et al. 2016). For example, translocation of nucleophosmin (NPM1)

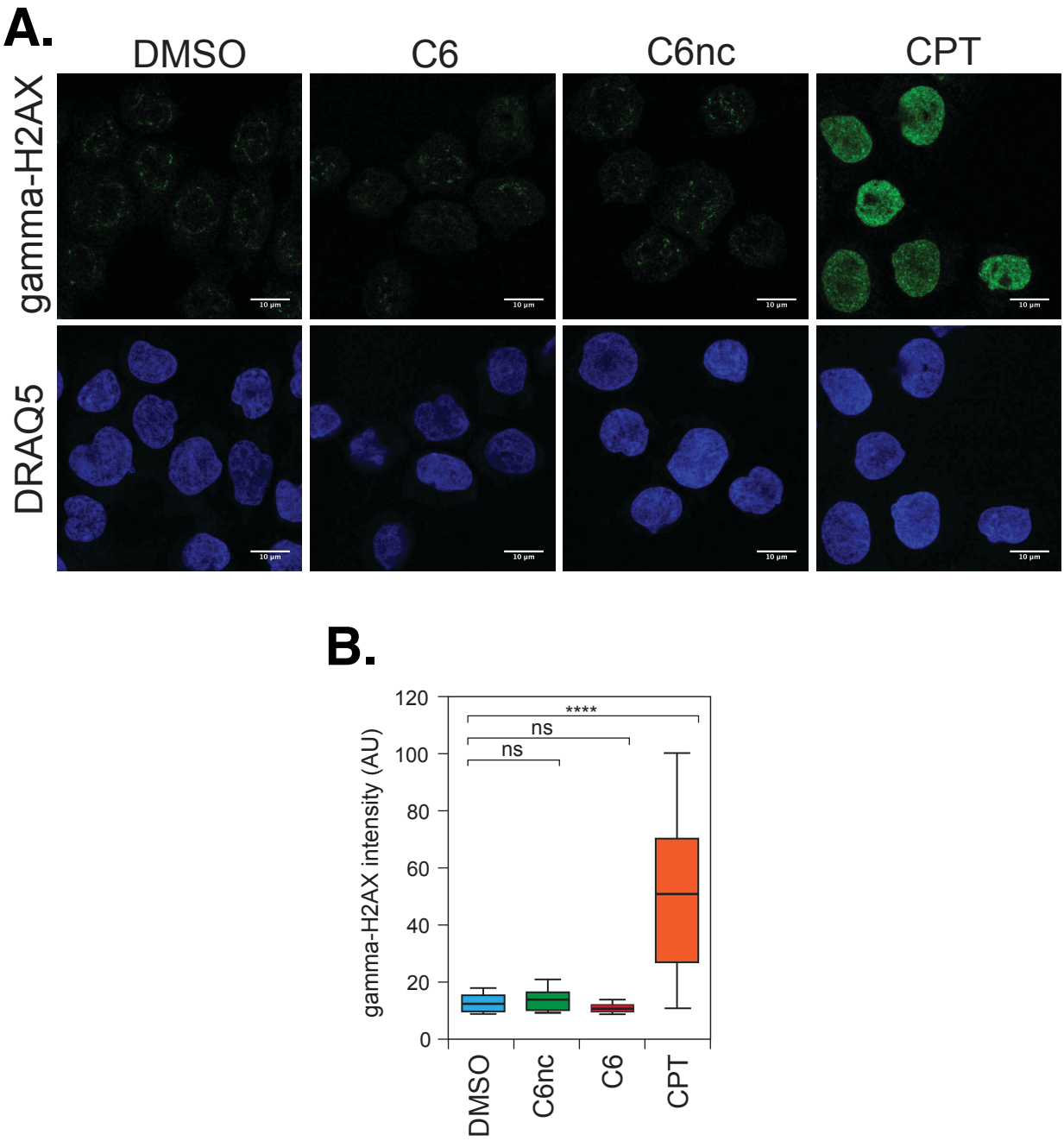

Figure 8-5. WDR5 WIN site inhibition does not induce DNA damage. (A) Representative immunofluorescent confocal images of MV4:11 cells treated for 3 days with 4 µM C6 or C6nc and stained for either gamma-H2AX (top panel) or nuclei (DRAQ5; lower panel). As a control for gamma-H2AX induction, cells were treated with 2 µM Camptothecin (CPT) for one hour. (D) Box and whisker plots showing quantification of gamma-H2AX staining intensity (arbitrary units: AU) in MV4:11 cells treated with DMSO, 4 µM C6 or C6nc for three days. 'ns' means no significant difference (DMSO vs. C6nc p = 0.95; DMSO vs. C6 p = 0.85). '****' means highly significant (p <0.0001). p values were determined by one-way ANOVA with a post-hoc Dunnett's test.

from the nucleolus to the nucleoplasm occurs in response to nucleolar stress. Although the function of NPM1 in nucleolar stress signaling has not been fully elucidated, its translocation appears to be a general event in the nucleolar stress response regardless of the stress stimulus. Therefore, redistribution of NPM1 from the nucleolus to the nucleoplasm can be used as a marker for nucleolar stress induction. I hypothesized that WDR5 WIN site inhibition would cause NPM1 redistribution from the nucleolus to the nucleoplasm in sensitive cell lines, indicating an induction of nucleolar stress.

Immunofluorescence and confocal microscopy was used to visualize NPM1 localization in cells after WDR5 WIN site inhibition. I first treated MV4:11 cells with 4 μM C6 or C6nc, or DMSO for 6 hours because at this short time point, WDR5 displacement and reduced expression of protein synthesis genes could already be observed, as shown in chapters VI and VII respectively. No change in NPM1 localization was observed after 6 hours for any treatment (data not shown). Therefore, I extended the treatment time to 3 days in order to see if NPM1 relocalization occurs after a more prolonged inhibition of WDR5. As for the 6 hour treated samples, three-day treated cells were affixed to slides using a cytospin. The cells were fixed using paraformaldehyde and then permeabilized using Triton X-100 to allow the antibody to better penetrate the cells. The slides were then stained using a primary antibody against NPM1 and a secondary antibody conjugated to the fluorophore Alexa488. The DNA-intercalating stain DRAQ5 was used as a nuclear counterstain. The slides were imaged using an SP5 Leica scanning confocal microscope, ensuring that the laser power and gain settings used were the same for each sample. As a positive control for nucleolar stress, I also treated MV4:11 cells with actinomycin D (ActD). Actinomycin D is a small molecule that preferentially intercalates into GC-rich DNA sequences like those found in genes encoding rRNA (Bensaude 2011). When bound to DNA, actinomycin D inhibits transcription by PolI, and thus blocks rRNA production. Actinomycin D has been shown to induce nucleolar stress and redistribution of NPM1 from the nucleoli to the nucleoplasm (Chan, Bloom et al. 1999, Brodska, Holoubek et al. 2016).

Representative confocal microscopy images for nucleophosmin and DRAQ5 stained MV4:11 cells after each treatment can be seen in Figure 8-6A. In the DMSO treated cells, nucleophosmin is located primarily within the nucleoli as evidenced by the bright green structures scattered within the nuclei and relatively little green staining within the nucleoplasm. In contrast, the positive control, actinomycin D, shows much more uniform bright green staining

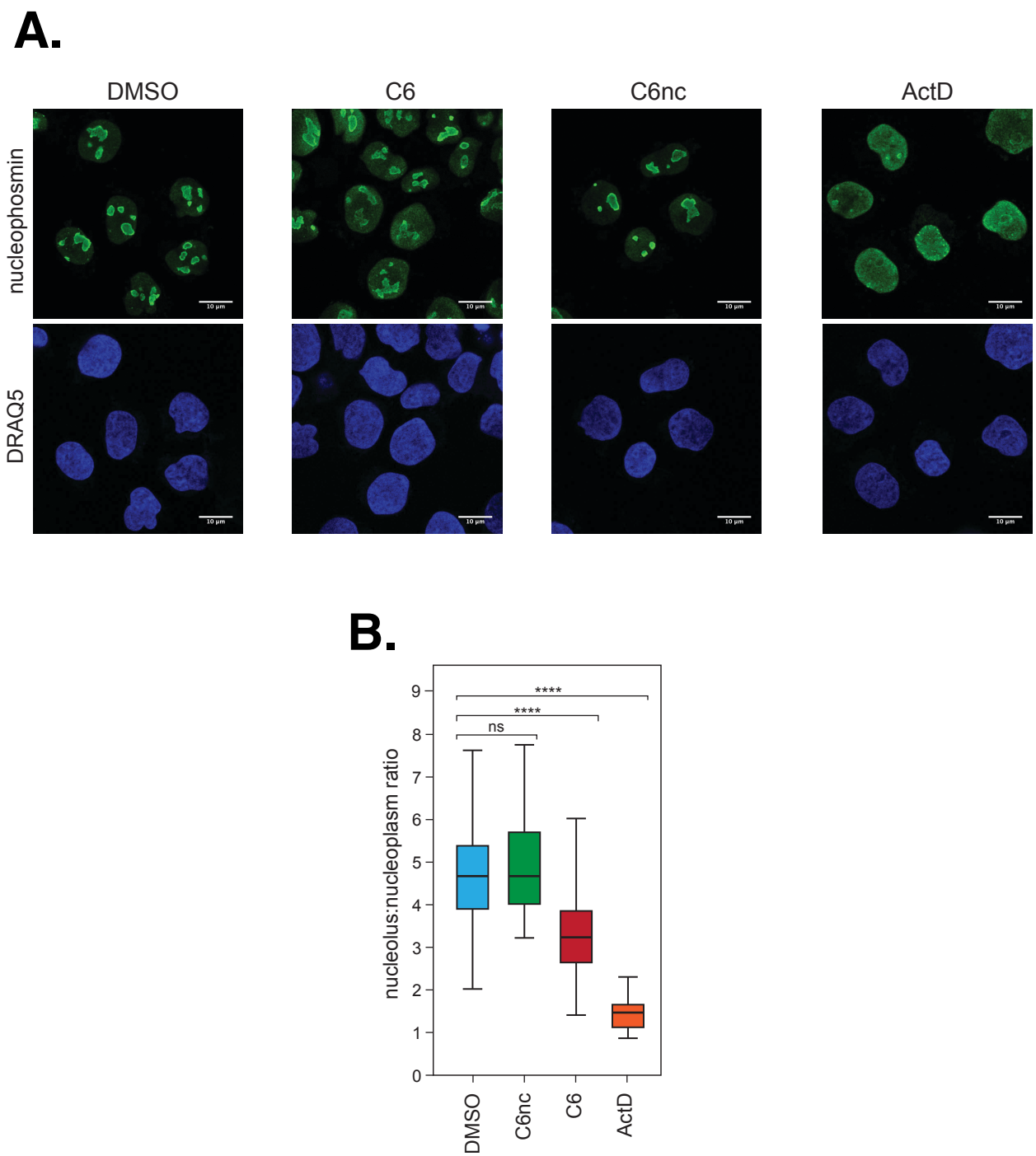

Figure 8-6. WDR5 WIN site inhibition induces nucleolar stress. (A) Representative immunofluorescent confocal images of MV4:11 cells treated for 3 days with 4 μM C6 or C6nc , or DMSO and stained for nucleophosmin or DRAQ5 (nuclear stain). Actinomycin D (ActD) treatment is a positive control for induction of nucleolar stress. (B) Quantification of the nucleolar : nucleoplasmic ratio of NPM1 in MV4:11 cells treated with 4 μM C6 or C6nc, DMSO or for three days. “ns” means no significant difference (p=0.1). '****' highly significant (p<0.0001). p-values were determined by one-way ANOVA with a post-hoc Dunnett’s test.

throughout the nucleus, indicating that nucleophosmin has redistributed from the nucleoli to the nucleoplasm and nucleolar stress has been induced. The negative control compound C6nc looked phenotypically very similar to DMSO treatment, while C6 treatment appeared to have more nucleoplasmic staining than DMSO but less than actinomycin D. In order to more quantitatively analyze these data, the ratio of nuclear to nucleoplasmic NPM1 staining in individual cells from two biological replicates was quantified using Fiji and plotted as box and whisker plots (Figure 8-6B). I found that no statically significant decrease in nucleolar to nucleoplasmic ratio of nucleophosmin was seen with C6nc treatment compared to DMSO. In contrast, both C6 and the positive control actinomycin D (ActD) showed reduced nucleolar to nucleoplasmic ratios. Thus, I determined that nucleolar stress induction after WDR5 WIN site inhibition can be seen after decreased expression in protein synthesis components, decreased translational capacity, and increased p53 protein levels are observed.

Effect of WDR5 WIN site inhibition on p53 stability

I showed in Figure 8-2 that p53 protein levels are induced upon WDR5 WIN site inhibition in sensitive cells, yet p53 mRNA expression was not induced in the RNA-seq data set (chapter VII). This finding indicates that p53 must be post-transcriptionally induced. In figure 8-6, I also demonstrate that WDR5 WIN site inhibition induces nucleolar stress. It is known that nucleolar stress can lead to post-transcriptional induction of p53 by inhibiting the interaction between p53 and HDM2, the E3 ubiquitin ligase that negatively regulates p53, thus, allowing p53 protein levels to rise (Russo and Russo 2017). I hypothesized that p53 is up-regulated at the protein level upon WDR5 WIN site inhibition by inhibition of the p53/HDM2 interaction and therefore the stability of p53 will be increased upon WDR5 WIN site inhibition.

To monitor the rate of p53 protein turnover after C6 treatment, I performed a cycloheximide (CHX) chase assay. Cycloheximide is a small molecule that binds to ribosomes and blocks protein translation. Adding cycloheximide to cells prevents production of new proteins and allows for tracking of the rate of p53 protein degradation over time by Western blot. As a positive control for inhibition of the p53/HDM2 interaction and increased p53 half life, I treated cells with 2 μM Nutlin-3, a small molecule inhibitor of the HDM2–p53 interaction (Vassilev, Vu et al. 2004). Prior to completion of the CHX chase assay, I performed a titration of Nutlin-3 in MV4:11 cells compared to C6 to identify the concentration of Nutlin-3 that induced p53 at levels comparable to 2 μM of C6 after 24 hours. 2 μM Nultlin-3 was determined to induce roughly equivalent levels

of p53 as 2 μM C6 (data not shown). To perform the CHX chase assay, I treated MV4:11 cells with 2 μM of C6, 2 μM Nutlin-3, or DMSO for 24 hours (Figure 8-7). As expected, Nutlin-3 increased the half life of p53 by an estimated ~4-fold in response to CHX treatment compared to DMSO. Compound C6, in contrast, had no detectable effects on p53 half life. The induction of p53 I observe in response to WIN site inhibition, therefore, is not due to an increase in the stability of the p53 protein.

Effect of WDR5 WIN site inhibition on p53 translation

The gene expression analyses presented in the previous chapter and the data presented in the previous subsection demonstrate that while p53 protein levels are induced upon WDR5 WIN site inhibition, p53 is not transcriptionally up-regulated, as determined by the RNA-seq presented in chapter VII, nor is the stability of the p53 protein increased. By process of elimination, we reasoned that p53 must be translationally induced. We were next interested in directly testing whether the translation of p53 is increased upon WDR5 WIN site inhibitor treatment in sensitive cells. To monitor induction of p53 translation, Dr. April Weissmiller in our laboratory performed a ribosome fractionation assay (Yang, Halaby et al. 2006) to quantify how C6 treatment alters the amount of TP53 mRNA associated with polysomes versus monosome. An increase in the amount of TP53 mRNA associated with polysomes would indicate an up-regulation of p53 translation.

To perform the ribosome fractionation, Dr. Weissmiller treated MV4:11 cells with 5 μM C6, or DMSO for 24 hours then lysed the cells for 10 minutes on ice. Debris was cleared by centrifugation and a portion of the supernatant was collected to represent the total RNA sample. Polysomes in the supernatant after the initial centrifugation step were recovered by a subsequent high speed centrifugation. Pelleted polysomes were collected and the supernatant served as the monosomal fraction. RNA from total, polysomal, and monosomal fractions were extracted, purified and DNAse treated. The extracted RNA was reverse transcribed into cDNA and the differences in cDNA levels between fractions were quantified by qPCR. cDNAs of interest were normalized to the house “keeping gene” GAPDH and then the percent of the total RNA for monosomal or polysomal fractions were calculated (Figure 8-8). Indeed, we found that C6 promoted an accumulation of polysome-associated mRNAs for TP53 relative to DMSO treated cells. As a negative control, Dr. Weissmiller also tested for polysome enrichment of RPL14 and RPS14 mRNAs, which are not induced in expression after WDR5 WIN site inhibition

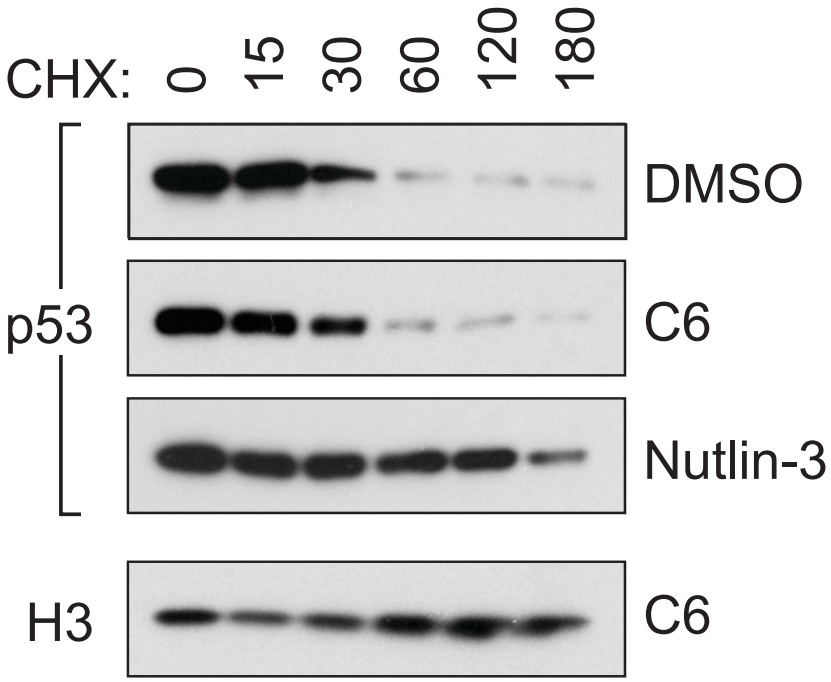

Figure 8-7. WDR5 WIN site inhibition does not increase p53 protein stability. MV4:11 cells were treated with DMSO, 2 μM C6, or 2 μM Nutlin-3 for 24 hours, after which cycloheximide was added and proteins sampled at the indicated time points (CHX; in minutes). p53 and histone H3 (loading control, shown here for the C6 treatment) were detected by Western blotting. The film exposures shown here were selected so that the band intensity of p53 at 0 min CHX is the same for all treatments so that the kinetics of p53 decay could be compared. When the same exposure time was used, p53 levels were higher at 0 min CHX for C6 and Nutlin-3 treatment compared to DMSO (not shown).

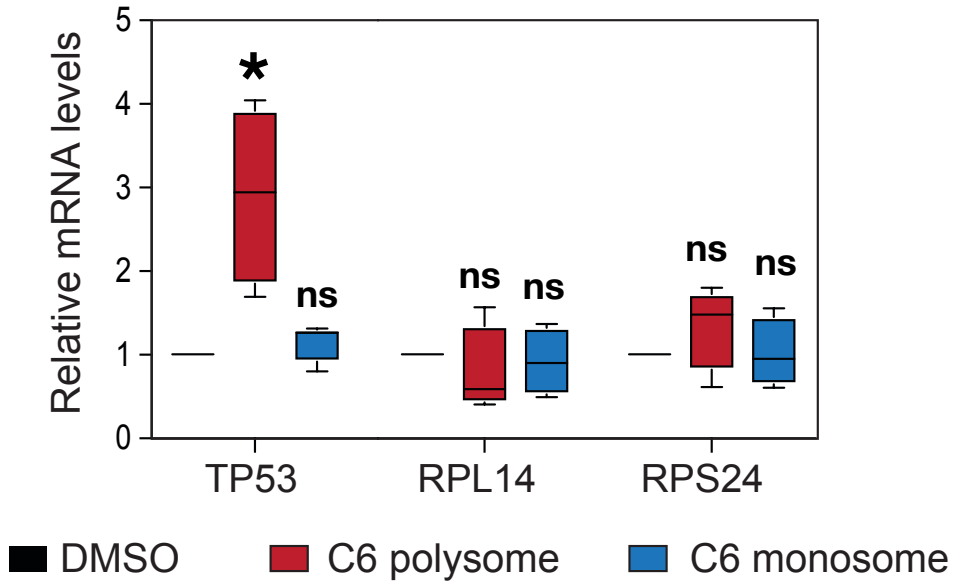

Figure 8-8. WDR5 WIN site inhibition increases p53 translation. p53 RT–qPCR analysis of the indicated mRNA levels in polysomal or monosomal fractions collected following treatment of MV4:11 cells with 5 μM C6, or DMSO, for 24 hours. Data are shown as a box-and-whisker plots of relative mRNA changes of indicated genes in each fraction, relative to DMSO. Boxes extend from the 25th to 75th percentile with the median marked by the middle line, whiskers extend from the minimum to the maximum point. n = 4. p-values for C6 polysome and C6 monosome compared to DMSO were determined by two-tailed Student's t-test. "ns" means not significant ($p > 0.05$), and "*" means $p < 0.05$.

in the RNA-seq. RPL14 and RPS14 mRNAs were not enriched in the polysome fraction after C6 treatment relative to DMSO-treated cells. The increase in TP53 mRNA in the polysome fraction, amidst a backdrop of decreased overall protein translational capacity, strongly implies that WIN site inhibition induces p53 via a selective induction of TP53 mRNA translation.

Effect of p53 knock-down on cellular sensitivity to WDR5 WIN site inhibition

The data presented in this thesis strongly suggest that p53 contributes to the biological response to WDR5 WIN site inhibition in sensitive cells. For example, WT p53 expression correlates with sensitivity of cells to C3 and C6 (chapter IV). In MV4:11 cells, C6 induces markers of apoptosis (chapter IV) and represses cell cycle genes (chapter VII). p53 is known to be a master regulator of both apoptosis and the cell cycle (Sullivan, Galbraith et al. 2018). Both p53 and the canonical p53 target gene p21 are induced after inhibitor treatment, and gene set enrichment analysis indicated that genes induced by C6 in the MV4:11 RNA-seq data are enriched in p53 targets genes. Based on these observations, I hypothesized that sensitivity of cell lines induced by WDR5 WIN site inhibition could be rescued by reducing the expression of p53.

Expression of an mRNA of interest can be depleted in cells by introduction of a plasmid that expresses a short hairpin RNA (shRNA). shRNAs consist of two complementary 19-22 bp RNA sequences linked by a short 4-11 nt loop (Moore, Guthrie et al. 2010). The 19-22 bp segment of the shRNA construct can be customized to target the mRNA of interested. After transcription of the shRNA sequence from a plasmid in cells, the shRNA is exported to the cytosol where it is recognized by the endogenous enzyme, Dicer. Dicer processes the shRNA into a short interfering RNA (siRNA). The siRNA then binds to the target mRNA via Watson-Crick base pairing and the siRNA/mRNA complex is incorporated into the RNA-Induced Silencing (RISC) Complex. The RISC complex catalyses cleavage and facilitates degradation of the targeted mRNA, thus decreasing expression of the gene of interest.

I used shRNA mediated knock-down to reduce the expression of p53 in MV4:11 cells. I purchased two different lentiviral shRNA plasmids from Addgene with shRNAs targeting p53 (sh_941 and sh_427) (Kim, Lee et al. 2007), as well was a negative control non-targeting “scramble” shRNA (scr). Lentiviral transduction of the shRNA plasmids in MV4:11 cells allowed for stable integration of the shRNA construct and sustained knock-down of p53. The plasmids

used also contained the GFP gene, which allowed me to use fluorescence activated cell sorting (FACS) to collect GFP+ cells and eliminate untransduced GFP- cells. Western blotting of whole cell lysates was used to confirm that the shRNAs caused knock-down of p53 protein levels in the GFP+ cells. Histone H3 was used as a loading control (Figure 8-9A). I treated the scramble (scr), sh_941 and sh_427 expressing cells with 2 μM C6 or C6nc for 24 hours as a control to determine if p53 can still be induced after C6 treatment (Figure 8-9A). As expected, p53 could still be robustly detected in the scramble cell line and p53 was increased in expression after C6 treatment indicating that the scramble shRNA did not effect the normal response to WDR5 inhibition. In contrast, both sh_427 and sh_941 reduced the expression of p53 compared to the scramble control, confirming that knock-down of p53 had occurred. Neither p53 shRNA construct was able to abolish p53 protein expression. The level of p53 knock-down was different between the two shRNAs, with sh_941 inducing a slightly stronger knock-down than sh_427. In both cases, the p53 shRNA cell lines could still induce a small increase in p53 levels after C6 treatment.

After confirming that both p53 targeting shRNAs reduced p53 protein expression but the scramble shRNA did not, I performed a three-day proliferation assay as described in chapter IV with C6 and C6nc treatment (Figure 8-9B). I found that the cells expressing the non-targeting scramble shRNA retained the same sensitivity to C6 as untransduced MV4:11 cells with a GI_{50} of 2 μM. In contrast, sh_427 increased the MV4:11 GI_{50} 4-fold to 8 μM and sh_941 increased the GI_{50} 7.5-fold to 15 μM. Notably, the difference in magnitude of p53 knock-down between sh_427 and sh_941 was advantageous because I observed that the degree of rescue correlated with the degree of p53 knock-down. sh_941 showed both a stronger p53 knock-down and stronger rescue than sh_427. Neither of the p53 shRNAs were able to completely rescue sensitivity to C6 in MV4:11 cells. I hypothesized that this may be due to the fact that the p53 expression was not completely abolished and therefore a full p53 knockout may be needed. The effects of p53 knockout on MV4:11 cell sensitivity to WDR5 WIN site inhibition will be the subject of the next subsection.

Finally, as a control I wanted to test if the primary effects of WDR5 WIN site inhibition, such as reduced WDR5-bound RPG mRNA expression, could still be detected in the MV4:11 p53 knock-down cell lines. I treated the MV4:11 p53 or scramble knock-down cell lines for 24 hours with 2 μM C6 or C6nc and then harvested total RNA using a Zymo Research RNA mini-prep kit. I then

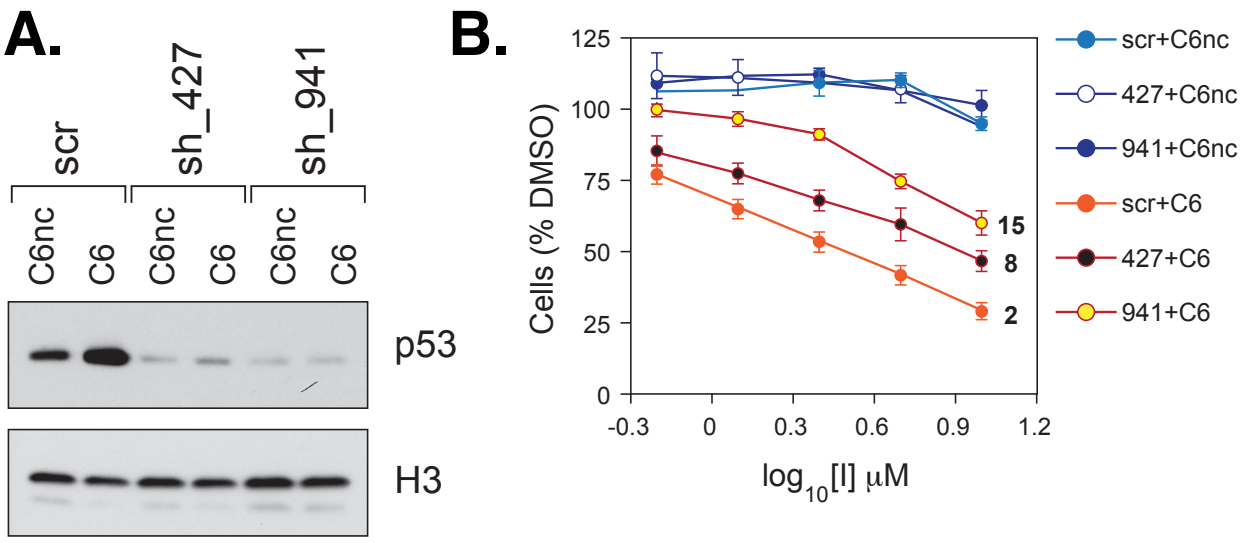

Figure 8-9. p53 knock-down rescues sensitivity of MV4:11 cells to WDR5 WIN site inhibition. (A) Western blot showing the expression of p53 and histone H3 loading control in MV4:11 cells expressing non-targeting scramble shRNA (scr) or shRNAs targeting p53 (sh_427 and sh_941) after 24 hour treatment with either 2 μM C6 or C6nc. (B) Three-day proliferation assay of MV4:11 cells expressing non-targeting scramble shRNA (scr) or p53 targeting shRNAs (427 and 941) treated with C6 or C6nc. The GI_{50}s in uM concentration for the scramble shRNA or targeting p53 shRNAs are shown to the right of the proliferation curves. n = 2 with error bars representing standard error of the mean.

reversed transcribed the total RNA to produce cDNA and quantified the relative expression of four ribosomal protein genes by qPCR (Figure 8-10). Relative mRNA expression was normalized to GAPDH expression for all ribosomal protein genes tested. I found that expression of the two RPGs bound by WDR5, *RPS24* and *RPL35*, was reduced by about 50% with C6 treatment compared to C6nc for all three shRNAs. In contrast, expression of *RPS11*, which is not bound by WDR5 did not decrease in expression after C6 treatment for all three shRNAs. A decrease in expression after C6 treatment did reached statistical significance for *RPL14,* but the magnitude of the decrease was less than 10% compared to C6nc treatment, indicating that it was probably not a biologically significant decrease in *RPL14* expression. Figure 8-10 indicates that MV4:11 cells can still respond to the primary mechanism of action of C6 treatment (i.e., WDR5 displacement/reduced WDR5-bound RPG repression) despite knock-down of p53. I concluded that p53 acts down-stream of the primary mode of action of WDR5 WIN site inhibition to mediate a large part of the cellular response to C6.

Effect of p53 knock-out on cellular sensitivity to WDR5 WIN site inhibition

The p53 knock-down experiment described above did not ablate p53 protein expression. As shown in Figure 8-9A, the knock-down cell lines were still able to slightly increase p53 expression in response to C6 compared to C6nc. I next wanted to more stringently test whether p53 is required for sensitivity to C6 by using CRISPR-Cas9 mediated genome editing to knockout p53 in MV4:11 cells. I hypothesized that the CRISPR-Cas9 mediated knockout of p53 would rescue sensitivity to C6 in MV4:11 cells.

Since its discovery as a primitive form of adaptive immunity in bacteria, the CRISPR-Cas9 genome editing system has been engineered to allow for editing of specific genomic DNA sequences in mammalian cells (Ran, Hsu et al. 2013). The CRISPR-Cas9 gene editing system is composed of two modules, the Cas9 endonuclease, which mediates double-strand DNA breakage, and the CRISPR RNA (crRNA), which targets the nuclease/RNA complex to the target genomic DNA sequence. The crRNA module can be customized to drive targeting of the Cas9 nuclease to a specific genomic locus by varying the sequence of a 20-bp segment of the crRNA called the guide sequence or gRNA. The 20-bp gRNA sequence directs the Cas9 nuclease to a specific genomic target by Watson-Crick base pairing with the DNA target. Upon cleavage of the targeted genomic DNA sequence by Cas9, the cell can use the Non-homologous End Joining (NHEJ) pathway to repair the double stranded DNA break. NHEJ is an

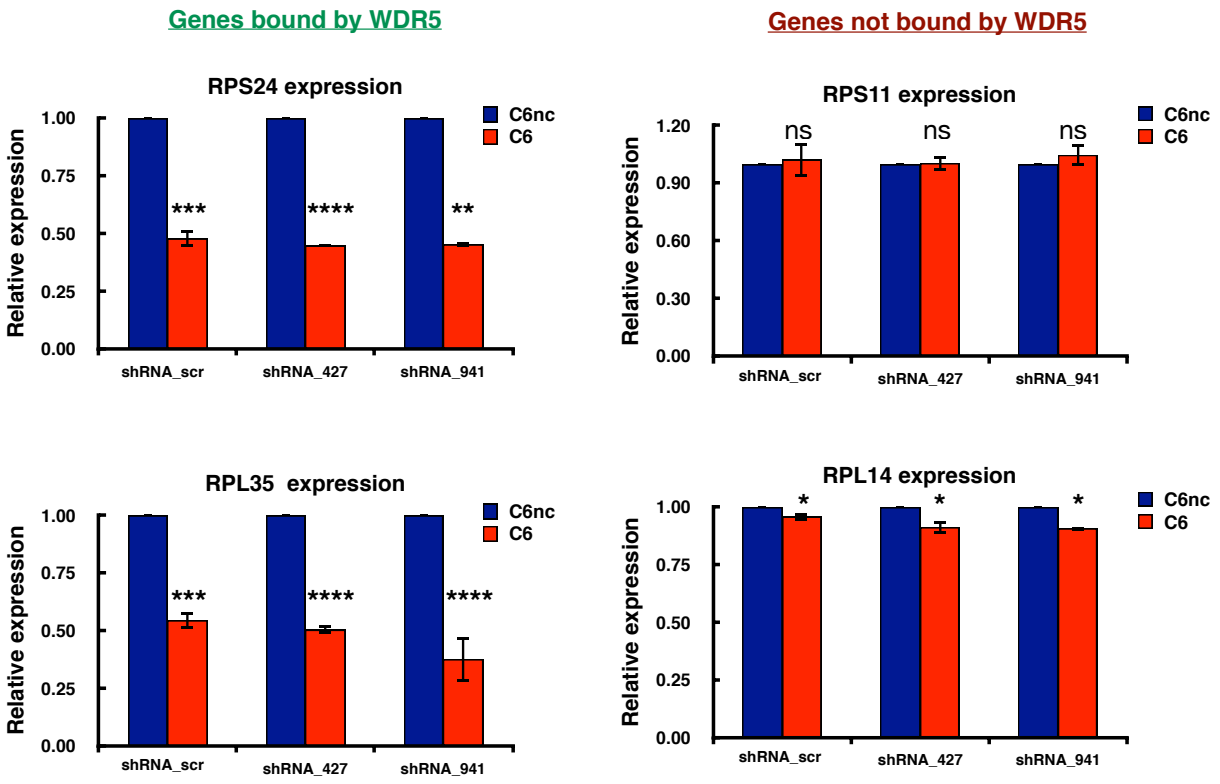

Figure 8-10. WDR5 WIN site inhibition reduces WDR5-bound RPG expression in p53 knock-down cells. Reverse-transcription/quantitative PCR (RT-qPCR) of mRNA levels from two WDR5-bound ribosomal protein genes (*RPS24* and *RPL35*) and two ribosomal protein genes not bound by WDR5 (*RPS11* and *RPL14*) in MV4:11 cells expressing the indicated shRNAs and treated with 2 μM C6 or C6nc for three days. Relative expression of the ribosomal protein genes is normalized to GAPDH mRNA expression. C6 treatment is normalized to C6nc treatment. n = 3 and error bars represent the standard error of the mean. "ns" no significant difference ($p > 0.05$), "****" means $p < 0.0001$), "***" means $p < 0.001$, "**" means $p < 0.01$, "*" means $p < 0.05$. p-values were determined for C6 treatment compared to C6nc treatment for each knock-down by two-tailed Student's t-test.

error-prone process that commonly results in small insertions or deletions (indels). Indels can cause frame shifts which ultimately ablate expression of the edited gene.

In order to use CRISPR-Cas9 genome editing to knock-out p53, I purchased the pLentiCRISPR v2 plasmid from Genscript containing a gRNA sequence targeting human *TP53*. All of the pLentiCRISPR v2 plasmids sold by Genscript use gRNA sequences designed and validated by the laboratory of Feng Zhang at the Broad institute. The pLentiCRISPR v2 plasmid contains genes for the Cas9 nuclease, all required RNA sequences and puromycin resistance. Lentiviral transduction was used to introduce the pLentiCRISPR v2/*TP53* gRNA plasmid into MV4:11 cells. As a negative control, I also transduced cells with the same plasmid containing a gRNA sequence of my own design that targets EGFP. After lentiviral transduction of MV4:11 cells, I selected for transduced cells by treating the culture with 2 μg/ml puromycin for 8 days. This concentration and duration of puromycin treatment was determined to be sufficient to kill all untransduced MV4:11. Once puromycin selection was complete, the population of cells was single cell sorted using a flow cytometer into the wells of a 96-well plate to isolate clones. Once the clones had grown out, I screened for p53 knockout by western blot and confirmed indel generation in both p53 alleles by Tracking of Indels by Deconvolution (TIDE), a web tool that compares Sanger sequencing traces from WT cells and a CRISPR-edited clone to find the mutations present in the edited clone (Brinkman, Chen et al. 2014).

The TIDE analysis indicated that for the representative MV4:11 p53 knock-out clones 1 and 8 (1p and 8) two mutations were present with a frequency of ~ 50% each, indicating that two p53 alleles are present in MV4:11 cells, both alleles were mutated and no WT p53 sequence remains (Figure 8-11). TIDE determined that for clone 1, a 14 base pair deletion was formed in one allele and a 4 base pair deletion was formed on the other allele upstream of the Cas9 cut site. Both deletions resulted in formation of premature STOP codons causing truncations and loss of roughly 50% of the C-terminal end of p53. TIDE determined that for clone 8, a 34 base pair deletion was formed in one allele and a 5 base pair deletion was formed on the other allele upstream of the Cas9 cut site. As for clone 1, these deletions resulted in premature STOP codon formation and truncation of the p53 protein. Clones 1p and 8p do not have detectable levels of p53 expression (Figure 8-12A). TIDE also determined that p53 is not mutated in either of two representative EGPF gRNA clones, 4e and 5e (data not shown). The Western blot in Figure 8-12A demonstrates that clones 4e and 5e express p53. A difference in the basal levels

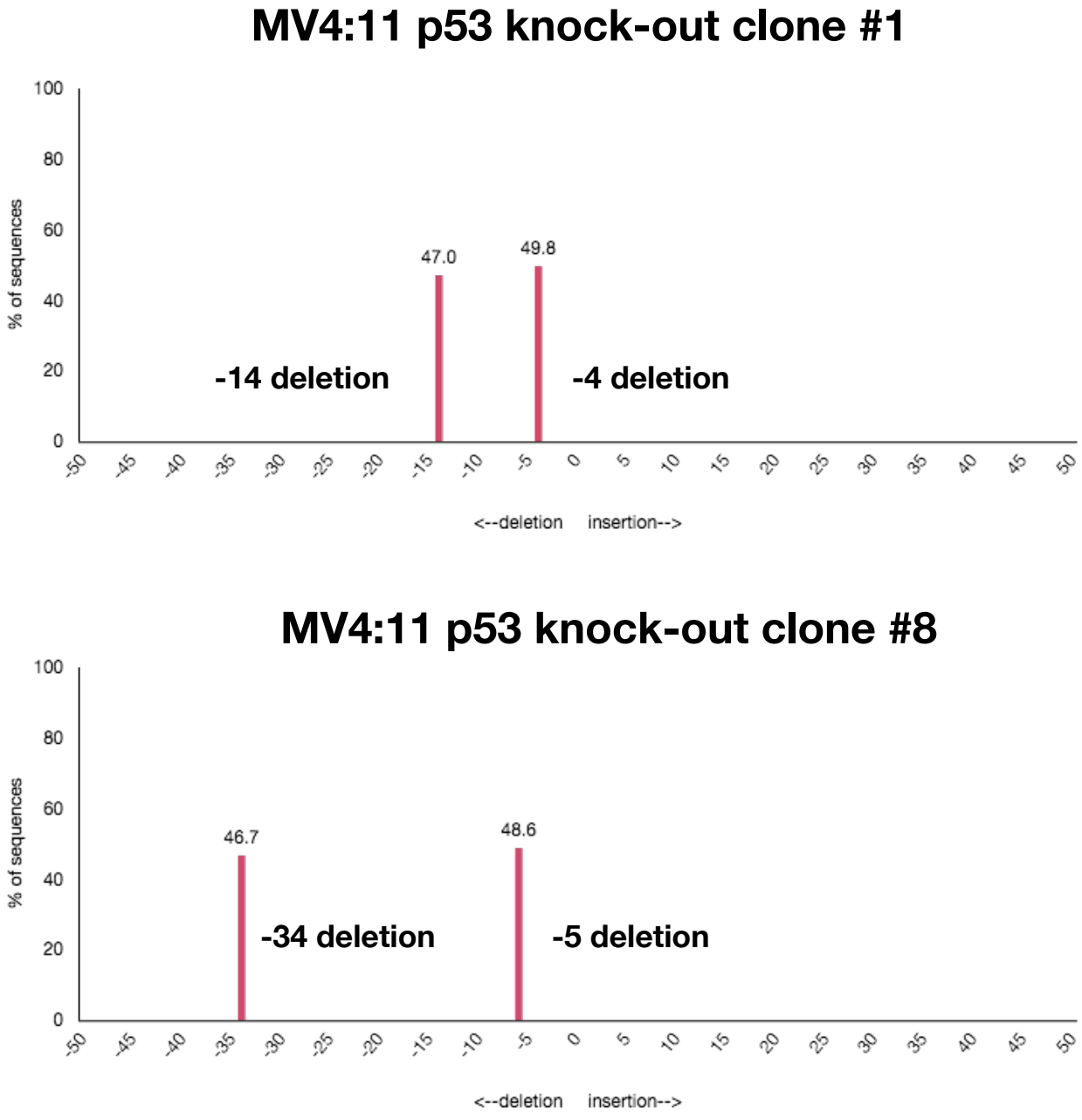

Figure 8-11. TIDE analysis of MV4:11 p53 knock-out clones. The p53 indels produced by CRISPR gene editing and their frequencies in MV4:11 p53 knock-out clones #1 and #8, as determined by TIDE are shown.

of p53 expression between the 4e and 5e clones was noted, although both clones increased p53 expression upon 24 hour C6 treatment. The biological reason for the difference in basal p53 expression in 4e and 5e is not known.

To test if the MV4:11 p53 knockout clones have reduced sensitivity to WDR5 WIN site inhibition, I performed a three-day proliferation assay with two EGFP CRISPR clones (4e and 5e) and two p53 knock out clones (1p and 8p) after C6 treatment as described in chapter IV (Figure 8-12B). I found that as expected, p53 knock-out reduced sensitivity of MV4:11 cells to C6. C6 increased the GI_{50} of p53 knockout clone 8p to 15 μM and 1p to 18 μM, compared to the GI_{50} of ~3 μM in WT MV4:11 cells. The EGFP CRISPR clones 4e and 5e retained sensitivity very close to WT MV4:11 cells with GI_{50}'s of 4 μM and 5 μM, respectively. The p53 knockout clones indicate that p53 is required for robust sensitivity to WDR5 WIN site inhibition in MV4:11 cells.

To corroborate my findings, I repeated the p53 CRISPR knockout in a second sensitive MLL-leukemia cell line, Molm13. I used the same methods as for MV4:11 cells described above to generate and validate Molm13 p53 knockout and control EGFP gRNA clones. The results of the TIDE analysis used to detect the indels formed in Molm13 p53 knock-out clones 2 and 4 are shown in Figure 8-13. For both clone 2 and 4, only one p53 allele was detected, as determined by the 100% frequency of a single indel detected and no WT p53 allele detected. From this finding, I concluded that Molm13 cells have only one p53 allele. TIDE determined that for clone 2, a 2 base pair deletion was formed and for clone 4, an 11 base pair deletion was formed upstream of the Cas9 cut site. As for the MV4:11 p53 CRISPR clones, the deletions generated in the Molm13 clones resulted in generation of premature STOP codons and truncation of roughly 50% of the C-terminal end of p53. The p53 knockout clones did not have detectable levels of p53 by Western blot (Figure 8-14A). A Western blot showing the p53 and H3 loading control expression in two representative Molm13 EGFP gRNA clones (2e and 3e) confirmed that the EGFP control clones both induce p53 after 3 μM C6 treatment for 24 hours, but not after C6nc treatment. As for the MV4:11 clones, I performed a three-day proliferation assay with C6 treatment for the Molm13 clones. Consistent with my MV4:11 CRISPR clone data, I found that p53 knockout decreased the sensitivity of Molm13 cells to C6. C6 increased the GI_{50} of both p53 knockout clones to 18 μM, compared to the 7 μM GI_{50}s for the EGFP CRISPR clones 4e and 5e. Together, the use of CRISPR-mediated p53 knockout in two sensitive leukemia cell lines

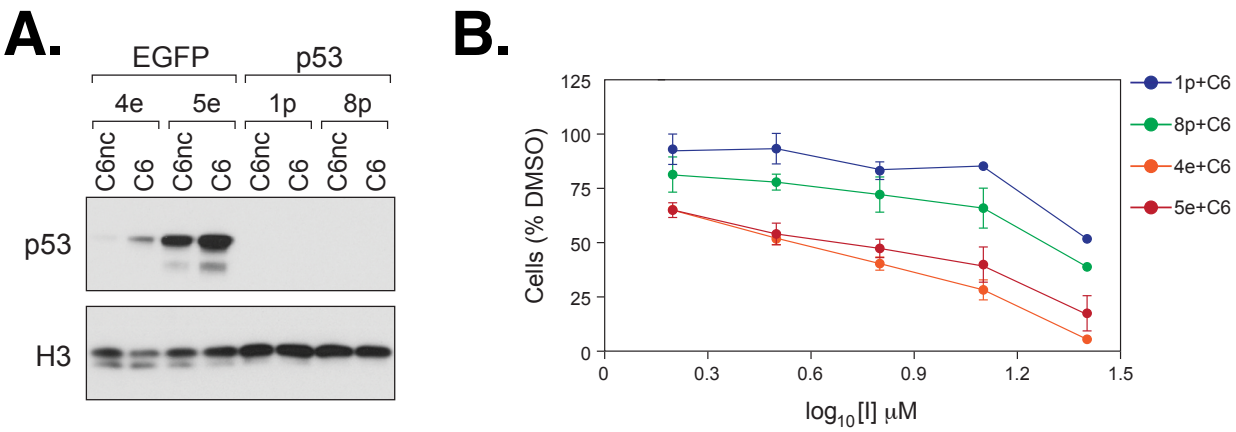

Figure 8-12. p53 knock-out rescues sensitivity of MV4:11 cells to WDR5 WIN site inhibition. (A) Western blot showing p53 levels in clones of MV4:11 cells CRISPR-targeted with either an EGFP (clones 4e and 5e) or a p53 (clones 1p and 8p) gRNA. Cells were treated with C6 or C6nc at 2 µM for 24 hours prior to analysis. (B)Three-day proliferation assay curves for MV4:11 EGFP or p53 knock-out clones after C6 treatment. n = 2, error bars represent the standard error of the mean.

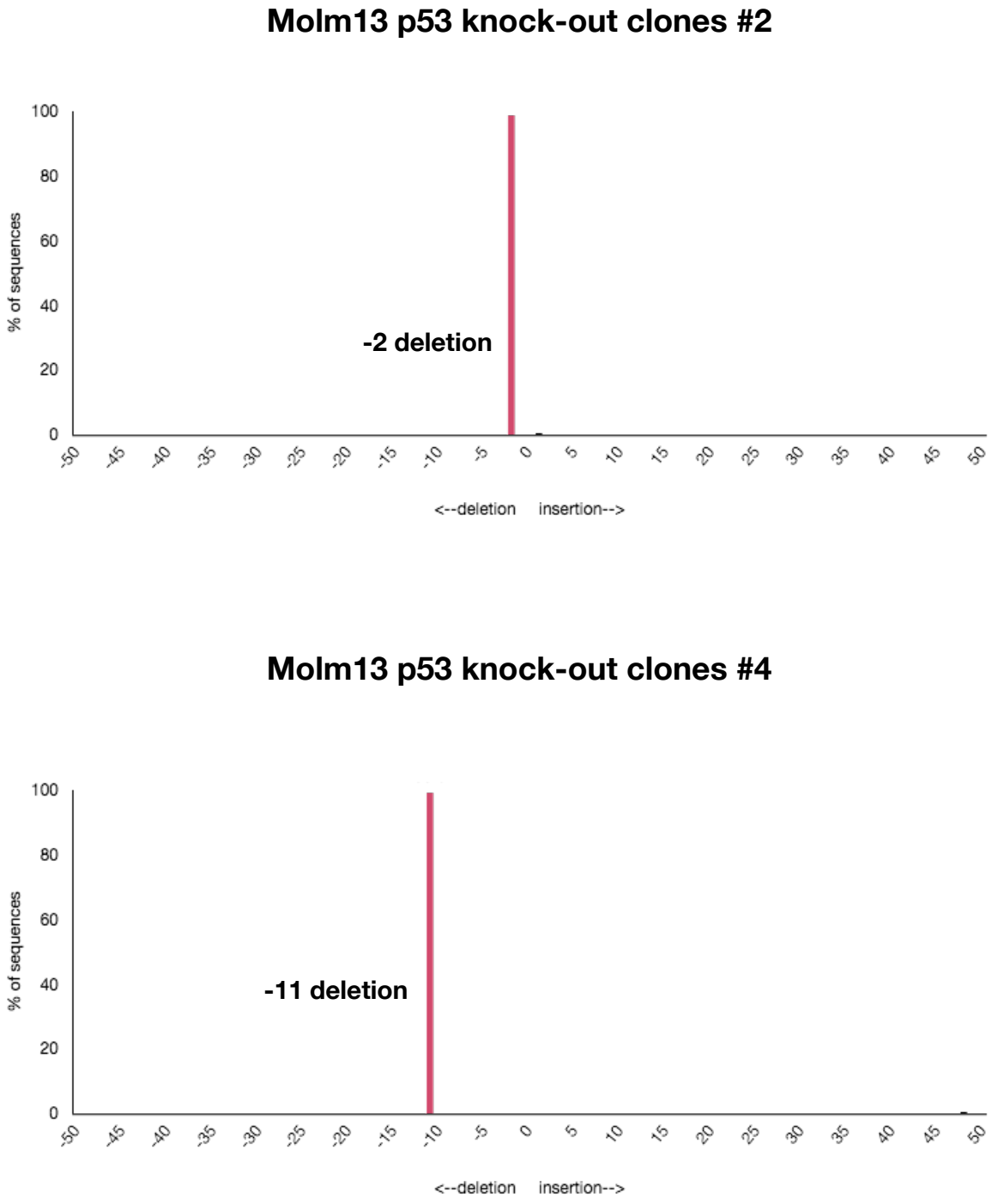

Figure 8-13. TIDE analysis of Molm13 p53 knock-out clones. The p53 indels produced by CRISPR gene editing and their frequencies in Molm13 p53 knock-out clones #2 and #4, as determined by TIDE are shown.

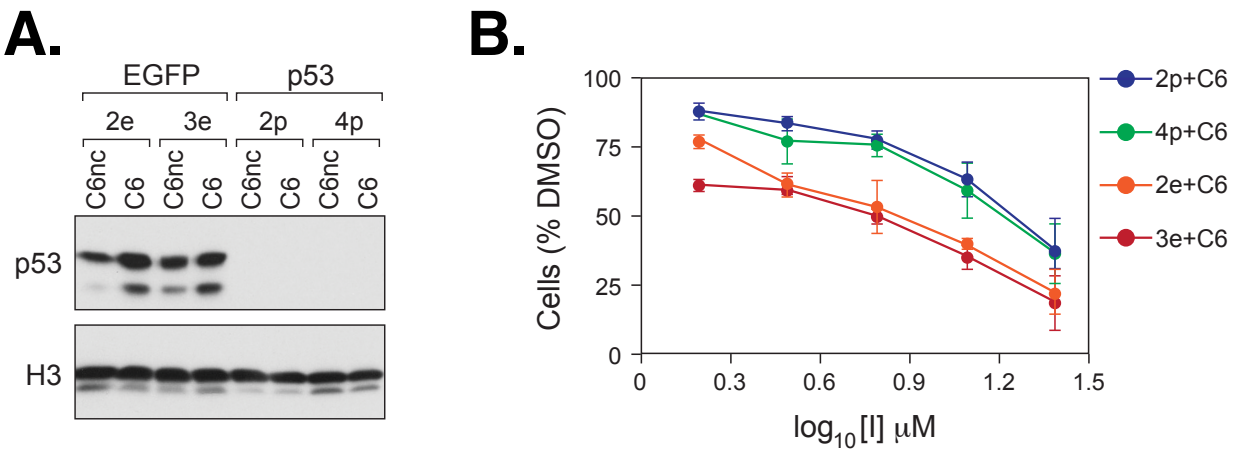

Figure 8-14. p53 knock-out rescues sensitivity of Molm13 cells to WDR5 WIN site inhibition. (A) Western blot showing p53 levels in clones of Molm13 cells CRISPR-targeted with either an EGFP (clones 2e and 3e) or a p53 (clones 2p and 4p) gRNA. Cells were treated with C6 or C6nc at 3 μM for 24 hours prior to analysis. (B) Three-day proliferation assay curves for Molm13 EGFP or p53 knock-out clones after C6 treatment. n = 2, error bars represent the standard error of the mean.

demonstrate that while p53 knockout did not completely rescue sensitively to C6, a significant portion of the mechanism of cellular inhibition in response to C6 is p53-dependent.

I found that both p53 knock-down and p53 knockout significantly reduced the sensitivity of MV4:11 and Molm13 cells to C6 treatment, yet sensitivity was not completely rescued for high compound doses. There are both p53-dependent and p53-independent nucleolar stress pathways (James, Wang et al. 2014). It is possible that the portion of the cell killing not rescued by p53 knockout involves a nucleolar stress pathway that is p53-independent. Alternatively, the portion of the cell killing not reduced by p53 knockout could be due to pathways unrelated to nucleolar stress. Further testing of whether that the portion of the cell killing not rescued by p53 knockout is due to a p53-independent nucleolar stress response is hindered by a lack of detailed understanding of the many pathways activated by disrupted ribosome biogenesis (James, Wang et al. 2014). A more detailed understanding of these pathways is needed before a robust and meaningful experimental approach can be formulated to test for activation of p53-independent nucleolar stress.

Discussion

In previous chapters of this thesis I define the primary mode of action of WDR5 WIN site inhibitors and the changes in cell fate that occur upon inhibitor treatment, yet experimental findings that could mechanistically link the primary and secondary effects of WDR5 WIN site inhibition were lacking. Here we identified that displacement of WDR5 from chromatin at genes connected to protein synthesis leads to induction of translational inhibition, p53 translation and nucleolar stress. In doing so, we have provided a viable explanation for how WIN site inhibitors function in sensitive cells.

I determined that p53 is modestly induced in response to WDR5 WIN site inhibition and that p53 functions down-stream of the primary effects of WDR5 WIN site inhibition as evidenced by the fact that C6 still reduces WDR5-bound RPG expression in p53 knock-down cells. Several mechanism have been described for how dysregulation of ribosome protein biogenesis can lead to p53 protein induction. The best-characterized mechanism involves the ribosomal proteins RPL5 and RPL11, which upon ribosomal protein imbalance, leave the nucleolus and enter the cytoplasm (Russo and Russo 2017). In the cytoplasm, RPL5 and RPL11 directly bind to HDM2

preventing HDM2-p53 interaction. Preventing the HDM2-p53 interaction reduces p53 ubiquitination and leads to stabilization of the p53 protein. While initially this pathway appeared to be a possible explanation for what occurs in MV4:11 cells after WDR5 WIN site inhibition, several key pieces of data now suggest that this is unlikely to be the case. For example, RPL5 and RPL11 are both bound by WDR5 and repressed in the PRO-seq and RNA-seq, making it difficult to explain how a decrease in their expression could cause an increase in free RPL5 and RPL11 in the cytoplasm. Additionally, from the cycloheximide chase experiment and the polysome fractionation experiment, it was evident that p53 is induced translationally not by increased protein stability.

An alternative nucleolar stress pathway has been shown to increase *TP53* mRNA translation (Russo and Russo 2017). As for RPL5 and RPL11, when ribosomal protein levels are unbalanced, ribosome-free RPL26 can translocate to the cytoplasm and bind to the 5'-untranslated region of *TP53* mRNA to induce p53 translation. Yet again, the *RPL26* gene is bound by WDR5 and repressed in the RNA-seq and RPO-seq, making it uncertain whether this mechanism is feasible after WDR5 WIN site inhibition. Alternatively, there are indications that p53 protein synthesis can be induced when cap-dependent protein translation is perturbed (Harris, Wang et al. 2018). mRNA transcripts in eukaryotic cells typically contain a 5' m_7GpppN cap structure. Under normal conditions, translation is typically cap-dependent and the rate limiting step of translation is the binding of the 5' cap by translational initiation factors. However, during stressful conditions, transcripts containing internal ribosomal entry site (IRES) sequences can be preferentially translated in a cap-independent manner. The *TP53* mRNA transcript is known to contain an IRES in the 5′-untranslated region that is capable of driving cap-independent translation under stress conditions. The presence of an IRES sequences in the *TP53* transcript and the observation that five translational initiation factors (EIF3B, EIF3D, EIF4G1, EIF4G3, and EIF4A2) are bound by WDR5 provides a possible explanation of how p53 may be up-regulated in response to WDR5 WIN site inhibition. The mechanism underlying the the translational induction of p53 in sensitive cells is still unclear, but Dr. Caleb Howard is actively working on determining how the repertoire of transcripts associated with ribosomes may change after WDR5 WIN site inhibition to identify if a switch to cap-independent translation is occurring. Regardless of the mechanism by which p53 is translationally induced, the ability of WDR5 WIN site inhibitors to induce p53 independently of changes in protein stability may offer

unique therapeutic benefits since this is different from the effects of inhibitors of the HDM2/p53 interaction that have had mixed success in the clinic (Stegh 2012).

Because p53 is induced in MV4:11 cells after inhibitor treatment, the GSEA was subsequently performed (Figure 8-3), and indicated that the differentially expressed genes in MV4:11 cells were enriched in a previously defined list of p53 and p63 targets genes, providing support for the fact that the p53 induction is functional (Perez, Ott et al. 2007). K562 cells are p53 null, and therefore the assessment of p53 induction and subsequent GSEA was not completed for K562 cells. It should be noted that the set of genes used for the MV4:11 GSEA included both p53 and p63 target genes. p63, along with p73 and p53, make up the p53 family of transcription factors that regulate expression of genes that control apoptosis and cell cycle progression. K562 cells do express p63 and p73 (Marques-Garcia, Ferrandiz et al. 2009, Feng, Cao et al. 2011). Investigation of p63 or p73 induction in K562 and MV4:11 cells was not completed. Specific assessment of the contribution of p63 and p73 to the cellular response in MV4:11 and K562 cells could be completed in the future.

In this chapter, I determined that WDR5 WIN site inhibitor treatment induces nucleolar stress. The concept of targeting ribosome biosynthesis to induce nucleolar stress has gained momentum in recent years as a viable strategy to treat cancer (Pelletier, Thomas et al. 2018). Inducing nucleolar stress may have promise in other diseases of ribosome dysfunction, such as myelodysplastic syndrome as well (Rinker, Dueber et al. 2016). Most of the successes in this area to date have centered on inhibition of ribosomal RNA transcription, typically by agents like actinomycnin D and BMH-21, that upon low dose treatment intercalate into the GC-rich DNA sequences at genes encoding rRNA (Bensaude 2011, Colis, Peltonen et al. 2014). However, upon high dose treatment the DNA intercalation is less specific and so there are concerns that these drugs could cause unwanted DNA damage. In the experiments described above, I found that nucleolar stress induction occurs after three-day C6 treatment but not 6 hour treatment as evidenced by NPM1 localization. In the future, further investigation of the timing of nucleolar stress induction would help us to determine whether nucleolar stress is an early or late response to WDR5 WIN site inhibition and better temporally place nucleolar stress induction in the timeline of events that occur after WIN site inhibition.

The induction of nucleolar stress by WIN site blockade could have tremendous value over rRNA transcription targeting agents. As presented in this chapter, WDR5 WIN site inhibitor treatment does not induce DNA damage and it is possible that the specific pattern of RPG imbalance caused by WIN site inhibitors has advantages over rRNA inhibition. Instead of general inhibition of ribosome biogenesis, WIN site inhibitors will only directly impact the expression of RPGs to which WDR5 is bound. Thus far, WDR5-bound RPGs appear to be conserved, and if this conservation withstands further challenge it will be possible to predict which RPGs are inhibited by WDR5 WIN site inhibition in different cancer types. In fact, different cancer types have been shown to have consistent and distinguishable patterns of RPG expression that differ between tumor types and normal tissues, but retain sufficient remnants of normal tissue patterning to allow for the tissue of origin to be easily discerned (Dolezal, Dash et al. 2018). The consistent signatures of RPG expression within cancer types suggests that ribosome dysgenesis in cancer cells is not random, and it may be possible to match WIN site inhibitor therapy with specific patterns of ribosome protein gene alterations in cancer patients in order to best take advantage of the nucleolar stress response. Together, the studies presented in this chapter provide more details as to how WDR5 WIN site inhibitors function in sensitive cells and help to better forecast their potential therapeutic uses.

CHAPTER IX

DISCUSSION

A novel discovery of a WDR5 WIN site function

It is well-established that WDR5 contains two protein-protein interaction domains and that all mapped protein interactions with WDR5 occur at one of these two sites (Guarnaccia and Tansey 2018). However, it was unclear how either of these two protein-protein interaction domains contribute to localizing WDR5 to chromatin. Experiments detailed in chapter VI of this thesis that utilize both genetic and chemical perturbation of the WDR5 WIN site have identified that the WIN site is required to tether WDR5 to chromatin. The WIN site had not previously been demonstrated to be required for chromatin engagement. Furthermore, we found that WDR5 WIN site-dependent enrichment occurs at genes that account for ~ 40% of the small and ~ 70% of the large ribosomal subunit proteins as well as the five translational initiation factors, EIF3B, EIF3D, EIF4G1, EIF4G3, and EIF4A2. Upon WIN site inhibition, expression of WDR5-bound genes is repressed, indicating that the WIN site is critical for proper regulation of specific components of the protein synthesis machinery. A link between WDR5 and RPGs has not previously been reported. Our findings led to the model that WIN site-mediated binding to chromatin at the RPGs is required for robust expression of these genes and that robust expression of these RPGs is needed to maintain homeostatic protein translation which allows cells to proliferate normally (Figure 9-1 left panel).

The WDR5-bound RPGs were found to be conserved across cell types, strongly suggesting that the preferential binding of WDR5 to some, but not all, RPGs serves an important biological function. Perhaps it is important that the conserved set of RPGs is regulated in unison, and thus, binding of a common regulatory factor, such as WDR5, ensures that expression of these RPGs is coordinated. Alternatively, maybe the presence of WDR5 at some but not all RPGs serves a protective role by purposely inducing an imbalance in ribosomal proteins, nucleolar stress, p53 induction, cell cycle arrest and apoptosis in response to stimuli, such as oncogene

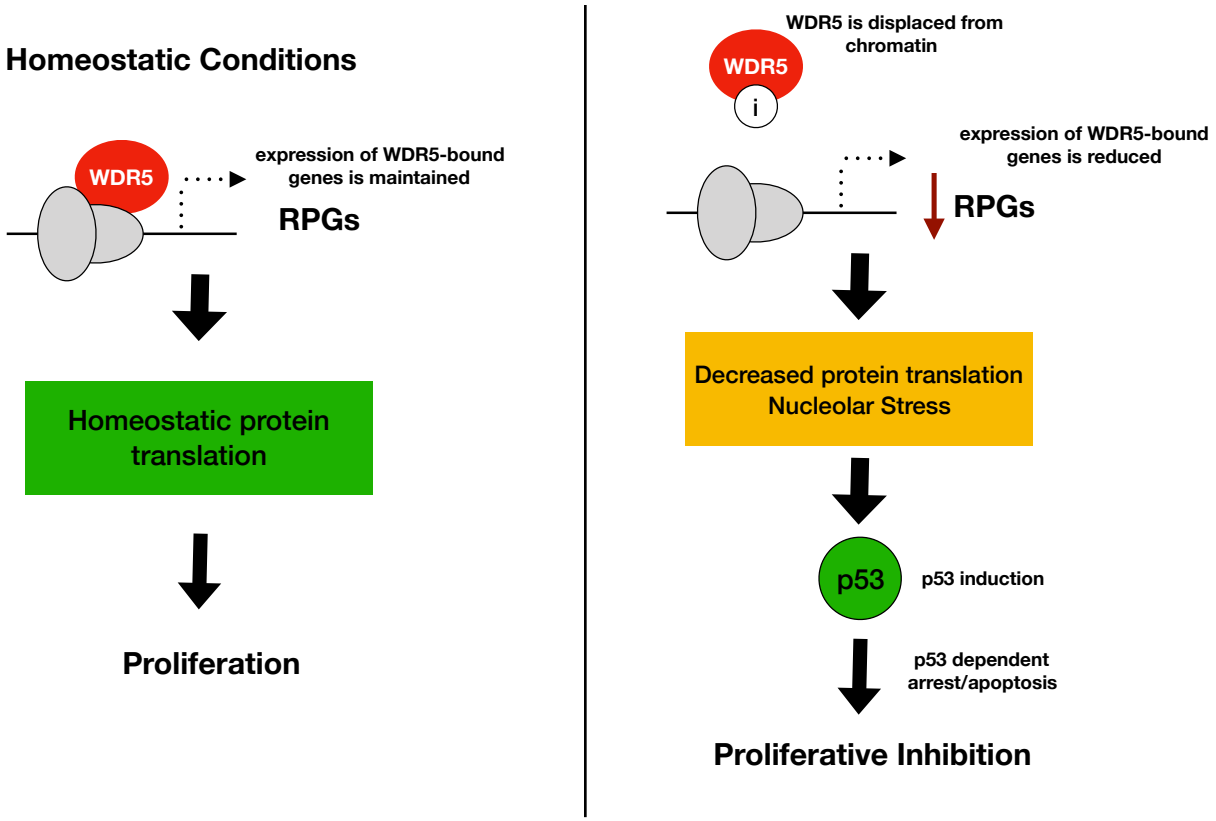

Figure 9-1. Model of WDR5 WIN site function and the mechanism of WDR5 WIN site inhibition. (Left) Under homeostatic conditions, WDR5 is bound to a select set of ribosomal protein genes (RPGs). WDR5 engagement with chromatin at these genes is required for robust RPG expression, homeostatic protein translation and cellular proliferation. (Right) Upon WDR5 inhibitor treatment, the inhibitor binds to the WIN site of WDR5 causing WDR5 to be displaced from chromatin. Displacement of WDR5 leads to decreased expression of WDR5-bound RPGs, decreased protein translation, p53 induction, proliferative arrest and apoptosis.

expression, that promote an aberrant increase in protein synthesis and cellular transformation. Overall, the biological reasoning behind why WDR5 is critical for robust expression of ~ 50% of all RPGs is still unknown.

It is also still unknown what the WIN site of WDR5 is binding to at RPGs to allow for chromatin engagement. WDR5 contains no known DNA binding domain so it is highly unlikely that WDR5 binds to DNA directly. Instead, WDR5 probably binds to some chromatin associated factor that contains a WIN motif. This could be one of the many WIN motif containing WDR5 binders that are already known (see chapter I), or one that is yet to be identified. Audra Foshage in our lab has been sought to identify a common DNA sequence motif within WDR5-bound genes, which might help to implicate a known chromatin associated protein that contains a WIN motif and binds the DNA motif. Our lab has identified that WDR5-bound RPGs are enriched in E-box sequences (CACGTG), a motif that MYC binds. Dr. Lance Thomas has also determined that MYC does not recruit WDR5 to chromatin, as a mutation in MYC that blocks interaction with WDR5 prevents MYC binding to chromatin but not WDR5 binding to chromatin (Thomas, Wang et al. 2015). Another E-box binding protein might recruit WDR5 to RPGs. Further investigation of proteins that containing WIN motifs and may be responsible for recruiting WDR5 to RPGs is needed. A proteomic investigation in our lab that may help to uncover binders of WDR5 responsible for recruiting WDR5 to chromatin is discussed below in the Future Directions.

It has also been proposed that WDR5 is recruited to chromatin through its WIN site-mediated epigenetic reader function (Figure 1-1C). For example, since WDR5 preferentially binds to H3K4me2 (Migliori, Muller et al. 2012) and the promoters of genes that are enriched in WDR5 were also shown to be enriched in H3K4me2 (Xu, Li et al. 2016), it has been suggested that WDR5 reads H3K4me2 at WDR5 bound genes and then facilitates H3K4me3 (Han, Guo et al. 2006). However, there are some conceptual problems with this hypothesis, and thus, I think WDR5 is unlikely to be functioning in this manner. When looking more closely at the distribution of WDR5 and H3K4me2 at WDR5-bound genes, Dr. Lance Thomas in our lab has found that H3K4me2 and WDR5 do not overlap, as H3K4me2 is enriched upstream and downstream of WDR5 but is low where WDR5 is bound. This observation makes it unlikely that WDR5 engages H3K4me2 on chromatin. Additionally, binding at the WDR5 WIN site is mutually exclusive, so WDR5 can not be bound to H3K4me2 and a functional HMT complex at the same time. The same issue exists for WDR5 binding to H3R2me2 at poised genes to facilitate gene activation by though SET/MLL-mediated H3K4me2 and me3. Furthermore, even if WDR5 is functioning as

an epigenetic reader at the RPGs, the question would still remain for how WDR5 can be specifically recruited to particular RPGs, as the thousands of poised or active genes enriched in H3R2me2 and H3K4me3, respectively, vastly outnumber the relatively few genes bound by WDR5. Thus, I believe that another factor such as a protein complex or a more complex RPG-specific epigenetic signature that is yet to be identified would be needed for WDR5 recruitment to RPGs.

Finally, how WDR5 functions at RPGs still remains to be determined. As reported in chapters VI and VII, H3K4me3 was not found to be reduced after C6 treatment despite WDR5 displacement and reduced expression of WDR5-bound genes. This suggests that WDR5 promotes expression of RPGs in a manner that is independent of HMT complexes. Instead, WDR5 could be functioning as part of the NSL complex that mediates H4K16ac to promote transcriptional activation. WDR5 has also been shown to be a member of nucleosome remodeling complexes (Suganuma, Gutierrez et al. 2008, Thompson, Tremblay et al. 2008, Wang, Du et al. 2014, Ee, McCannell et al. 2017). Therefore, WDR5 may function to establish chromatin architecture that is permissive for transcription. The interaction of WDR5 with MYC (Thomas, Wang et al. 2015) may also facilitate RPG expression. We know that WDR5 and MYC co-localize to RPGs (Thomas, Wang et al. 2015, and unpublished data), though the full identify and function of the MYC/WDR5 complex has not been characterized. While there are many possibilities for how WDR5 may function at RPGs, due to the fact that MYC is bound to WDR5 by the WBM and that binding of the WBM on WDR5 is mutually exclusive, I believe that WDR5 is unlikely to be present in a canonical previously described complex at RPGs. Thus, I believe that it is likely that a yet to be characterized WDR5 and MYC containing multi-protein complex exists at RPGs and contributes to robust expression. How WDR5 and MYC could promote the expression of RPGs and the other proteins or maybe epigenetic marks that interact with WDR5 at RPGs remains unknown and requires further investigation.

The mechanism of action of WDR5 WIN site inhibitors

Based on my studies, I have formed a novel model for how WDR5 WIN site inhibitors function in MLL-leukemia cells (Figure 9-1 right panel). Through the use of ChIP and ChIP-seq we determined that ~ 90% of WDR5 is displaced from chromatin within the first several hours of WDR5 WIN site inhibition. Loss of WDR5 binding to chromatin results in a rapid reduction in

transcription of WDR5-bound genes, as evidenced by PRO-seq. These studies were the first to determine that WDR5-bound RPGs represent the primary and direct transcriptional targets of WDR5 WIN site inhibition. We found that in sensitive cells, the secondary effects of WDR5 WIN site inhibition include a decrease in protein translational capacity, and induction of nucleolar stress and p53 protein levels, which lead to p53-dependent apoptosis. This model is supported by the data obtained using our inhibitors C3 and C6 as well as the structurally distinct small molecule WDR5 inhibitor OICR-9429 (Grebien, Vedadi et al. 2015), indicating that this is common mode of action of WDR5 WIN site inhibitors.

The contribution of p53 to the cellular response to WIN site inhibition had not previously been identified. Perhaps since only WT p53 MLL-fusion cell lines were tested in previous WDR5 inhibitors studies (Cao, Townsend et al. 2014, Gupta, Xu et al. 2018), a correlation between sensitivity and WT p53 could not be found. Although the level of p53 induction I observed in MV4:11 and Molm13 cells was modest in magnitude, it was reproducible and shown to be functional through the use of gene set enrichment analysis and p53 knockout. We concluded that p53 induction is a significant event in the response to WDR5 WIN site inhibition. This argument is further strengthened by the finding that the three-day proliferation assay GI_{50} of nutlin-3 in MV4:11 cells is ~1 μM (Figure 9-2A) and when MV4:11 cells are treated with the GI_{50} of C6 (2 μM) and the GI_{50} of nutlin-3 (1 μM), the levels of p53 and p21 are roughly equivalent (Figure 9-2B). Importantly, these data indicate that nutlin-3 and C6 can still cause significant p53-mediated cell killing even though the magnitude of p53 induction is fairly low. An important distinction to be made between nutlin-3 and WIN site inhibition is that while nultin-3 induces p53 by increasing protein stability (Vassilev, Vu et al. 2004), C6 induces p53 through increased *TP53* mRNA translation. Clinical trials for HDM2 inhibitors that increase p53 stability have demonstrated efficacy in several cancer types, but considerable hematological and gastrointestinal toxicities were also noted (Tisato, Voltan et al. 2017). Perhaps the induction of p53 through an alternative pathway, such as the increased translation of p53 mRNA caused by C6, could mitigate these negative effects.

There are gaps in our knowledge that remain regarding the mechanism of action of C3 and C6. For example, since we do not know what complex or WDR5 function is needed for robust RPG expression, we also do not know what complex or function is inhibited at RPGs when the WIN site of WDR5 is blocked. Also, the mode by which p53 translation is increased is unclear. A

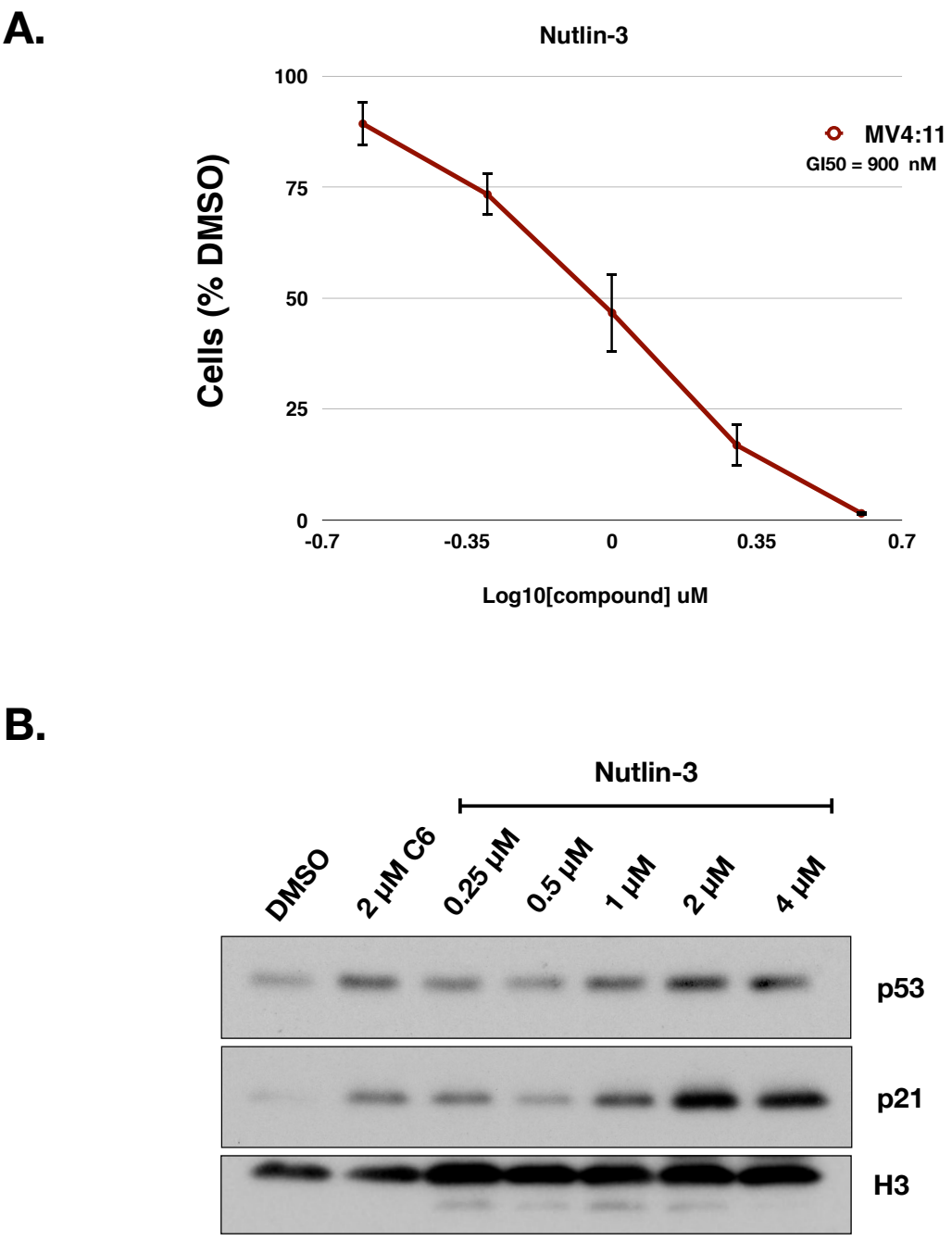

Figure 9-2. The GI_{50} of nutlin-3 induces p53 levels comparable to the GI_{50} of C6.
(A) Three day proliferation assay curve for MV4:11 cells treated with nutlin-3. n = 2. Error bars represent the standard error or the mean. (B) Western blot probing for p53, p21 and H3 (loading control) in MV4:11 cell whole cell lysates after three-day treatment with the indicated compounds.

nucleolar stress response pathway has been described that promotes p53 translation by direct binding of RPL26 to the *TP53* mRNA transcript when ribosome biogenesis is impaired (Russo and Russo 2017). However, RPL26 is a WDR5-bound gene and is repressed upon inhibitor treatment, making it uncertain if RLP26 can exert this function after WIN site inhibition. Another possibility is that reduced expression of the translational initiation factors EIF3B, EIF3D, EIF4G1, EIF4G3, and EIF4A2 blocks cap-dependent protein translation, which requires initiation factor binding to mRNA transcripts. p53 protein translation has been shown to be induced through the use of an IRES sequence in the 5' UTR when cap-dependent protein translation is perturbed (Harris, Wang et al. 2018). Further mechanistic investigation is needed to determine what function of WDR5 is blocked at WDR5-bound genes, if cap-dependent translation is inhibited, and how decreased WDR5-bound gene expression leads to increased p53 translation.

Although we do not understand why only a defined subset of RPGs are controlled by WDR5, it is possible that biased distribution of WDR5 at some, but not all, RPGs contributes to the efficacy of cellular inhibition. In this way, WIN-site inhibition would cause not just a decrease in ribosome production, but also an imbalance in the stoichiometry of ribosome subunits that more potently triggers a nucleolar stress response. Other anti-cancer inhibitors that target the ribosome biogenesis pathway including actinomycin D, BMH-21, and CX-546 have been described, although these compounds inhibit rRNA production by blocking PolI transcription at rRNA genes (Bywater, Poortinga et al. 2012, Colis, Peltonen et al. 2014, Brodska, Holoubek et al. 2016). Thus, the mechanism of induction of nucleolar stress by broadly inhibiting RPGs expression by WIN site inhibition is a novel approach. This approach may possess benefits over rRNA transcription inhibitors, as these compounds cause DNA damage at high concentrations since they function by intercalating into DNA. WIN site inhibitors and PolI inhibitors may even be able to be used together to exert an even stronger synergistic induction of nucleolar stress while decreasing the concentrations of each drugs needed, thus potentially decreasing toxicity.

A possible drawback to inhibiting the WIN site of WDR5 is that the WIN site is utilized for interaction with many different proteins involved in diverse cellular processes (Guarnaccia and Tansey 2018). Since all of the known WDR5 WIN site binders and our inhibitors all engage WDR5 by making a critical pi-stacking interaction with Phe133A and Phe263, C3 and C6 can not selectively inhibit some WIN site binders but not others. Inhibiting all WIN site binders simultaneously may have unforeseen toxic effects on normal cellular processes in a whole organism since the full gamut of WDR5 WIN site functions is still being uncovered. Thus, it will

be important to rigorously validate the vulnerabilities that make cancer cells highly sensitive to WIN site inhibition and can provide a large therapeutic window to limit possible toxicity in normal tissues.

Vulnerabilities of WDR5 WIN site inhibition and therapeutic implications

The primary mechanism of WDR5 WIN site inhibition was determined to be displacement of WDR5 from chromatin at some but not all RPGs. As opposed to a general inhibition of ribosome biogenesis, WIN site inhibitors will only directly impact the expression of those RPGs to which WDR5 is bound, which appears to be a conserved set of genes across cell types. If WDR5-bound RPGs are in fact found to be the same regardless of cell type upon further testing, we will be able to predict which RPGs consistently respond to WIN site blockade. It has been shown that the that specific patterns of RPG expression can distinguish between between cell types, and furthermore, can differentiate between normal and malignant cells from the that same tissue of origin(Dolezal, Dash et al. 2018). By systematic analysis of the relationship between altered RPG expression and cellular sensitivity to WIN site inhibition, it may be possible to matched WDR5 WIN site inhibitor therapy to specific patterns of ribosome protein gene alterations in cancer patients.

We also discovered that the primary mechanism of action of WDR5 WIN site inhibition is the same in both sensitive and insensitive cells (chapter VI), indicating that something downstream of the primary effects must determine if a cell will be sensitivity to WDR5 WIN site inhibition or not. I empirically determined that in the context of the leukemia cell lines tested, sensitivity to WDR5 WIN site inhibition correlates with expression of an MLL-fusion protein and WT p53. This finding implies that WT p53 cells will be more sensitive to WDR5 WIN site inhibition than p53 null cells. Fortunately, WT p53 is commonly retained in MLL-fusion leukemias (Wiederschain, Kawai et al. 2005) and about 50% of cancers in general (Sigal and Rotter 2000). While I found that a significant portion of cell killing is p53-dependent in MV4:11 and Molm13 cells, I have not directly tested for whether expression of an MLL-fusion is needed to confer sensitivity to WIN site inhibition. Even if an MLL-fusion is found to be a genetic vulnerability to WDR5 WIN site inhibition, mechanistically it is unclear how the fusion protein is connected to WDR5. The connection could be direct or a synthetic lethal interaction. It has recently been discovered that the MLL-ENL fusion binds to a small set of genes that are functionally connected to protein

synthesis. While the set of genes bound by MLL-ENL and WDR5 have little overlap (Garcia-Cuellar, Buttner et al. 2016), they are functionally connected. Perhaps MLL-ENL regulation at protein synthesis genes causes a shift in the protein synthesis homeostasis that then causes increased sensitivity to repression of WDR5-bound RPGs. None of the cell lines that I tested express an ENL fusion, and it is unclear if a similar set of genes is regulated by the MLL-AF9 and MLL-AF4 fusions which are expressed in the Molm13 and MV4:11 cells used in my studies. Thus, identification of the MLL-AF9 and MLL-AF4 regulated genes would be needed to understand of the fusion proteins and WDR5 are directly connected. Further experimentation is needed to better elucidate if expression of an MLL-fusion contributes to sensitivity to WIN site inhibition, and if so, what the mechanism is that underlies the sensitivity.

Due to the current lack of clarity in whether an MLL-fusion protein is a genetic vulnerability to WDR5 WIN site inhibition, we still do not understand why K562 cells are so resistant to such a broad assault on production of the protein synthesis machinery. We have not yet tested if protein synthesis is decreased after WDR5 WIN site inhibition in these cells. Perhaps K562 cells evade the anti-proliferative effects of C6 by somehow compensating for reduced RPG expression to maintain the normal translational capacity. An experimental approach that may shed light on genes or pathways needed for K562 cells resistance is presented in the Future Directions section below.

We concluded that WDR5 inhibitors likely kill the MV4:11 and Molm13 cells in an MLL1 independent fashion, which is consistent with the recent finding that MLL1 is dispensable in for MLL-fusion cells (Mishra, Zaffuto et al. 2014). Yet the *in vitro* HMT assay data shown in chapter III indicates that C6 selectively inhibits the HMT activity of MLL1 but not other SET/MLL family HMTs. This finding suggests that inhibiting the MLL1 activity via WDR5 WIN site inhibition may bring about cell death in cancer cells that are driven by MLL1. Thus, the mode by which WDR5 WIN site inhibitors kill different types of cancer cells may be context dependent. For example, p53 gain-of-function cancer cells have been predicted to be reliant on MLL1 due to the observations that the p53 gain-of-function mutants over-express MLL1, have elevated levels of H3K4me3 and are sensitive to OICR-9429 (Zhu, Sammons et al. 2015). Aberrant MLL1 activity has also been implicated in leukemia cells expressing mutant C/EPBα (Grebien, Vedadi et al. 2015). Therefore in these cancers, as well as others that are MLL1-dependent (Vedadi, Blazer et al. 2017), the ability of our inhibitors to selectively target the HMT activity of MLL1 complexes may be exploited for therapeutic gain.

WDR5 WIN site inhibition may also be used for therapeutic gain in cancers that over-express WDR5. WDR5 over-expression has been reported in several cancer types including colon cancer (Neilsen, Chakraborty et al. 2018), gastric cancer (Sun, Guo et al. 2018), AML and ALL (Ge, Song et al. 2016), bladder cancer (Chen, Xie et al. 2015) and squamous cell carcinoma (Wu, Diao et al. 2018). Displacement of WDR5 from chromatin via WDR5 WIN site inhibition may prevent WDR5 from performing its functions that promote tumorigenesis in cells with WDR5 over-expression. Due to the multitude of interactions occurring at the WIN site of WDR5 and the plethora of biological functions that WDR5 possesses, it is quite possible that other genetic vulnerabilities to WDR5 WIN site inhibition in cancer cells have yet to be identified.

Future Directions

While the experiments presented in this thesis yielded significant new knowledge about how the WDR5 WIN site and inhibitors of this site function, several topics would benefit from further investigation. For example, more information could be gleaned regarding the genetic vulnerabilities that confer sensitivity to C3 and C6. The proliferation assays presented in chapter IV empirically identified a correlation between sensitivity to WIN site inhibition and expression of both an MLL-fusion and wild type p53 in leukemia cell lines. In chapter VIII, I directly assessed the role of wild type p53 in conferring sensitivity to compound treatment by using shRNA-mediated knock-down and knock-out of p53. I found that a significant proportion of cell killing is p53-dependent. However, I have not yet directly assessed whether expression of an MLL-fusion in a wild type p53 background confers sensitivity to WDR5 WIN site inhibition.

In order to test the hypothesis that expression of an MLL-fusion is needed for MLL-leukemia cell line sensitivity, leukemia cell lines that are isogenic except for the presence of an MLL-fusion would be needed to minimize possible confounding effects produced by different genetic backgrounds. MLL-leukemia cell lines can be produced by transducing primary mouse bone marrow cells with lentivirus to stably introduce a gene encoding MLL-AF9 or MLL-ENL fusion proteins. Experimental procedures to produce mouse MLL-AF9 and MLL-ENL leukemia cells in this manner are established (Stubbs and Krivtsov 2017). I would also need to produce a leukemia cell line that has an MLL-leukemia phenotype, but dose not express an MLL-fusion. In MLL-leukemia cells, the MLL-fusion drives over-expression of HOXA9 and MIES1, two transcription factors that promote a proliferative and stem-like state. Over-expression of HOXA9

and MIES1 has been shown to induce transformation of primary mouse bone marrow cells to generate leukemia cells that are phenotypically very similar to cells transformed with an MLL-fusion (Kroon, Krosl et al. 1998). Therefore, by over expressing HOXA9 and MIES1, which are downstream of the MLL-fusion, I could produce a leukemia cell line that has a MLL-leukemia phenotype but does not express an MLL-fusion. After transduction of the mouse bone marrow cells with the MLL-fusions or HOXA9/MIES1, the cells could be subjected to three serial passages in methylcellulose media to isolate transformed cells (Stubbs and Krivtsov 2017). The colonies of transformed leukemia cells can then be pooled to produce a non-clonal population to mitigate the subtle differences that may exist between clones. The populations of leukemia cells can then be subjected to a three-day proliferation assay with C6 and C6nc treatment. If an MLL-fusion does in fact contribute to sensitivity to WDR5 WIN site inhibition, I would expect to find that the MLL-AF9 and MLL-ENL expressing cells would be sensitive to C6 but the HOXA9/MIES1 expressing cells would not be sensitive to C6.

If the MLL-fusion cells were found to be more sensitive to 6 treatment than the HOXA9/MEIS1 expressing cells, further experimentation could be done to determine if there is a direct connection between genes regulated by WDR5 and the MLL-fusion or if it is a synthetic lethal interaction. Recently, it was found that the MLL-ENL fusion protein binds to a small cohort of genes functionally connected to protein synthesis (Garcia-Cuellar, Buttner et al. 2016), but none of the cell lines tested so far express an MLL-ENL fusion. The ChIP-seq analysis could be extended to MLL-AF9 using the transformed mouse bone marrow cells described above to determine the overlap of MLL-AF9 and WDR5-bound genes. This analysis may help to determine if MLL-fusion proteins and WDR5 regulate genes that are functionally connected.

It is possible that upon completion of the proliferation experiment stated above, that there is no difference in sensitivity to C6 of MLL-fusion and HOXA9/MIES1 transformed mouse cells, indicating that the MLL-fusion protein itself does not confer sensitivity. Additionally, even if the the MLL-fusion cells are more sensitive than the HOXA9/MIES1 transformed mouse cells, it is possible that MLL-fusion proteins don't bind to WDR5-bound genes, indicating that the interaction between the fusion protein and inhibitors is synthetic and not direct. These findings would leave us with little new information for what confers sensitivity to WDR5 WIN site inhibitors. Fully understanding how sensitivity to WIN site inhibition is conferred is imperative in order to predict which patients may benefit from a targeted WDR5 therapy. Therefore, Dr. Caleb

Howard in our lab is currently employing an unbiased approach to identify genes and/or pathways that are required for sensitivity to C6 in MV4:11 cells. Dr. Howard transduced MV4:11 cells with lentivirus to introduce plasmids that allow for stable expression the Cas9 nuclease and the genome-scale CRISPR-Cas9 knockout (GeCKO) gRNA library (Shalem, Sanjana et al. 2014). The GeCKO guide RNA library allows for CRISPR-mediated knock-out of 18,080 genes with 64,751 unique guide sequences (about 3 guides per gene). The cells were transduced at a low multiplicity of infection to ensure expression of only one gRNA per cells. The CRISPRed cells were then cultured in the presence of C6 or DMSO to deplete sensitive cells from the population. The guide RNAs present in the population after DMSO or C6 treatment can be identified by next generation sequencing. gRNAs that are overrepresented at the end of the experiment represent genes that are needed for sensitivity to WDR5 WIN site inhibition in MV4:11 cells. The GeCKO library screen was also performed in K562 cells to identify genes that are needed for resistance to C6, and are therefore the corresponding gRNAs are depleted from the population after C6 treatment. Dr. Howard is currently awaiting the sequencing results of these experiments and we are optimistic that the results will greatly aid in understanding what genes or pathways contribute to conferring sensitivity to WDR5 WIN site inhibition.

In addition to the GeCKO library screening, we are interested in obtaining more information about possible genetic vulnerabilities to WDR5 WIN site inhibition by performing high-throughput screening of many different cancer cell lines. For this purpose, Horizon Discovery Group will perform their OncoSignature high throughput screening service for a select set of WDR5 WIN site inhibitors discovered by the Fesik lab. The OncoSignature screen involves screening 300 diverse and clinically relevant cancer cell lines with our WDR5 WIN site inhibitors in proliferation assay, either as a single agent or in combination with up to 350 standard of care anti-caner drugs. The cell lines used also have annotated genetic information available. OncoSignature screening will help to identify sensitive and resistant cell types, aid in future patient stratification, and identify efficacious drug combinations. The data from this screen will be available within the next few months.

When considering other possible vulnerabilities to WDR5 WIN site inhibitors besides MLL-fusion proteins, two proteins come to mind. First, WT MLL1 has been proposed to contribute to MLL-leukemogenesis (Ballabio and Milne 2014), yet Patricia Ernst has recently shown that MLL1 is dispensable for MLL1 leukemogenesis (Mishra, Zaffuto et al. 2014). Her finding supports my

argument that WDR5 dose not reduce H3K4me3 at WDR5-displaced genes and therefore work by blocking some non-MLL1 associated function of WDR5. If this is true, I would expect there to be no difference in sensitivity of MLL1 WT and MLL1-null MLL-leukemia cells. We were gifted MLL1-null and non-targeted control Molm14 clones from Patricia Ernst in order to test my hypothesis in the future.

Second, we reasoned that MYC driven tumors would be sensitive to WDR5 WIN site inhibition. MYC is dysregulated in the majority of cancers and drives expression of genes that promote oncogenic changes in proliferation, metabolism, protein synthesis and genomic stability. MYC has traditionally been considered “undruggable” because it is highly unstructured in solution and only adopts a more defined conformation when bound to other proteins, making structure-activity relationship (SAR) drug design difficult (Thomas, Foshage et al. 2015). Our lab has found that MYC interacts with the WBM site of WDR5, and this interaction is required for MYC to associate with chromatin and drive tumorigenesis (Thomas, Wang et al. 2015). Since the WIN site is needed for WDR5 chromatin association (as reported in this thesis) and MYC requires interaction with the WBM of WDR5 to be recruited to chromatin, it may be possible to indirectly displace MYC from chromatin by WDR5 WIN site inhibition. Dr. Lance Thomas in our lab is actively investigating the effects of WDR5 WIN site inhibition on MYC/chromatin association and the cellular effects of WIN site blockade in a Burkitt’s lymphoma model, a cancer in which MYC is over-expressed (Kanda, Hu et al. 2000). Dr. April Weissmiller in our lab is also investigating the effects of WDR5 WIN site inhibition on neuroblastoma cell lines, a type of cancer in which N-MYC is amplified in 25% of cases and is associated with poor prognosis (Huang and Weiss 2013).

Questions also still remain about the precise molecular response that occurs after WDR5 displacement but that leads to proliferative arrest and apoptosis. As described in chapters VI, we found that WDR5 is displaced from five translational initiation factors and the expression of the genes decreased in the RNA-seq data described in chapter VII. As reported in chapter VIII, we found that protein translation is inhibited in C6 treated cells. These findings coupled with the observation that p53 is translationally induced upon C6 treatment, as detailed in chapter VIII, suggests a shift in the translatome may be occurring in response to WDR5 WIN site inhibition, perhaps through perturbation of cap-dependent translation which requires translational initiation factors (Yang, Halaby et al. 2006). The full repertoire of translated mRNA transcripts can be

assessed by monitoring the association of mRNA transcripts with polysomes after WDR5 inhibitor or vehicle control treatment. The polysome associated mRNAs can then be collected, purified and identified by next generation sequencing (Brar and Weissman 2015). Inhibition of cap-dependent translation would be supported by an observed increase in polysome association of mRNA transcripts containing IRES sequences, a phenomenon known to occur when cap-dependent translation is inhibited (Yang, Halaby et al. 2006). This experiment is currently underway and could shed more light on the events that occur after WDR5 displacement to bring about cell death.

Additionally, further investigation of the how the nucleolar stress pathway is induced in response to WIN site inhibition could be completed. As stated in chapter VIII, no redistribution of nucleophosmin was seen after only a 6 our treatment, but was observed after 3 days of treatment with the inhibitors. A time course analysis could be completed to obtain higher temporal resolution of when nucleolar stress is induced. In chapter VIII I also noted that while p53 knock-out partially rescued sensitivity to WDR5 WIN site inhibition it was not a complete rescue. Perhaps the p53-independent cell killing is due to nucleolar stress signaling that does not require p53. p53 independent nucleolar stress response pathways have been identified, although the they are currently poorly understood (James, Wang et al. 2014). In the future, as the p53-dependent and independent nucleolar stress response pathways become more clearly delineated the contribution of these pathways to the cellular response to WDR5 WIN site inhibition can be directly tested.

After completion of the studies presented in this thesis, it is also still unknown how the set of proteins bound to WDR5 changes after C3 or C6 treatment. By identifying the protein binders of WDR5 that are altered after compound treatment, it could help us to determine which WDR5-containing complexes are disrupted by WIN site inhibition and to narrow in on how WDR5 functions at WDR5 RPGs to promote expression. Affinity-based protein purification combined with mass spectrometry–based proteomics would allow for the identification and quantification of the proteins bound to WDR5 with and without compound treatment. Alissa Guarnaccia, a graduate student in our lab, is currently analyzing and validating data obtained using SILAC to identify changes in WDR5 associated proteins upon C6 treatment. To perform her SILAC experiment, Alissa grew cells in the presence of either media that contained normal, or “light”, amino acids or media that contained “heavy” amino acid isotopes (Mann 2006). She then made

whole cell extracts from heavy and light treated cells. C6 was added to the “heavy” lysate to disrupt the WIN site. A WDR5 IP was then performed for both heavy and light lysates and the precipitated WDR5 complexes were analyzed by mass-spectrometry. Incorporation of the heavy amino acids into proteins leads to a known mass shift compared with the proteins that contains the light amino acids. Thus, SILAC allows for the quantification of the ratio of peptides identified in the light (no C6) and heavy (C6 treated) lysates, and can determine proteins that are less associated, more associated and equally associated with WDR5 when the WIN site is inhibited.

Finally, as stated in chapter III, neither C3 nor C6 are amenable to *in vivo* assessment of WDR5 WIN site inhibition efficacy in mouse cancer models. Our first-generation compound C3 lacks superb cellular potency, and while C6 is more potent, C6 is cleared too rapidly from the blood circulation to maintain exposure at or above the proliferation assay GI_{50}s. In order to progress WDR5 WIN site inhibition as a cancer therapeutic strategy, it is imperative to demonstrate efficacy in an animal model. More potent compounds with more balanced pharmacokinetic properties than C3 and C6 are needed before *in vivo* studies can be done. An iterative process of structure activity relationship (SAR) drug design has been continued by the Fesik laboratory since the discovery of C6 to optimize our WDR5 WIN site inhibitors. To date, they have been able to produce compounds with nearly a 1,000-fold increase in WDR5 binding affinity. Our collaborators at the National Cancer Institute (NCI) and University of New Mexico are actively pursuing pilot studies to assess the maximum tolerable dose and efficacy of these more potent WDR5 WIN site inhibitors in a MV4:11 mouse xenograph model.

In summary, several exciting further investigations are underway in the Tansey lab. Together the future directions described above will help to fill in the gaps of our knowledge surrounding the source of vulnerability to WDR5 WIN site inhibition, the molecular events that occur after WDR5 displacement from chromatin that lead to cell death, and the protein complexes that are perturbed by WDR5 WIN site inhibition. The continued development of optimized compounds will also allow for *in vivo* efficacy studies that will hopefully lead to selection of a clinical candidate compound and WDR5 inhibitor clinical trials.

REFERENCES

Adelman, K. and J. T. Lis (2012). "Promoter-proximal pausing of RNA polymerase II: emerging roles in metazoans." Nat Rev Genet **13**(10): 720-731.

Aho, E. R., J. Wang, R. D. Gogliotti, G. C. Howard, J. Phan, P. Acharya, J. D. Macdonald, K. Cheng, S. L. Lorey, B. Lu, S. Wenzel, A. M. Foshage, J. Alvarado, F. Wang, J. G. Shaw, B. Zhao, A. M. Weissmiller, L. R. Thomas, C. R. Vakoc, M. D. Hall, S. W. Hiebert, Q. Liu, S. R. Stauffer, S. W. Fesik and W. P. Tansey (2019). "Displacement of WDR5 from Chromatin by a WIN Site Inhibitor with Picomolar Affinity." Cell Rep **26**(11): 2916-2928 e2913.

Alicea-Velazquez, N. L., S. A. Shinsky, D. M. Loh, J. H. Lee, D. G. Skalnik and M. S. Cosgrove (2016). "Targeted Disruption of the Interaction between WD-40 Repeat Protein 5 (WDR5) and Mixed Lineage Leukemia (MLL)/SET1 Family Proteins Specifically Inhibits MLL1 and SETd1A Methyltransferase Complexes." J Biol Chem **291**(43): 22357-22372.

Ang, Y. S., S. Y. Tsai, D. F. Lee, J. Monk, J. Su, K. Ratnakumar, J. Ding, Y. Ge, H. Darr, B. Chang, J. Wang, M. Rendl, E. Bernstein, C. Schaniel and I. R. Lemischka (2011). "Wdr5 mediates self-renewal and reprogramming via the embryonic stem cell core transcriptional network." Cell **145**(2): 183-197.

Aranda, S., G. Mas and L. Di Croce (2015). "Regulation of gene transcription by Polycomb proteins." Sci Adv **1**(11): e1500737.

Ballabio, E. and T. A. Milne (2012). "Molecular and Epigenetic Mechanisms of MLL in Human Leukemogenesis." Cancers (Basel) **4**(3): 904-944.

Ballabio, E. and T. A. Milne (2014). "Epigenetic control of gene expression in leukemogenesis: Cooperation between wild type MLL and MLL fusion proteins." Mol Cell Oncol **1**(2): e955330.
Barski, A., S. Cuddapah, K. Cui, T. Y. Roh, D. E. Schones, Z. Wang, G. Wei, I. Chepelev and K. Zhao (2007). "High-resolution profiling of histone methylations in the human genome." Cell **129**(4): 823-837.

Bennett, R. L. and J. D. Licht (2018). "Targeting Epigenetics in Cancer." Annu Rev Pharmacol Toxicol **58**: 187-207.

Bensaude, O. (2011). "Inhibiting eukaryotic transcription: Which compound to choose? How to evaluate its activity?" Transcription **2**(3): 103-108.

Bernt, K. M., N. Zhu, A. U. Sinha, S. Vempati, J. Faber, A. V. Krivtsov, Z. Feng, N. Punt, A. Daigle, L. Bullinger, R. M. Pollock, V. M. Richon, A. L. Kung and S. A. Armstrong (2011). "MLL-rearranged leukemia is dependent on aberrant H3K79 methylation by DOT1L." Cancer Cell **20**(1): 66-78.

Biswas, D., T. A. Milne, V. Basrur, J. Kim, K. S. Elenitoba-Johnson, C. D. Allis and R. G. Roeder (2011). "Function of leukemogenic mixed lineage leukemia 1 (MLL) fusion proteins through distinct partner protein complexes." Proc Natl Acad Sci U S A **108**(38): 15751-15756.

Bolger, A. M., M. Lohse and B. Usadel (2014). "Trimmomatic: a flexible trimmer for Illumina sequence data." Bioinformatics **30**(15): 2114-2120.

Bolshan, Y., M. Getlik, E. Kuznetsova, G. A. Wasney, T. Hajian, G. Poda, K. T. Nguyen, H. Wu, L. Dombrovski, A. Dong, G. Senisterra, M. Schapira, C. H. Arrowsmith, P. J. Brown, R. Al-Awar, M. Vedadi and D. Smil (2013). "Synthesis, Optimization, and Evaluation of Novel Small Molecules as Antagonists of WDR5-MLL Interaction." ACS Med Chem Lett **4**(3): 353-357.

Borkin, D., S. He, H. Miao, K. Kempinska, J. Pollock, J. Chase, T. Purohit, B. Malik, T. Zhao, J. Wang, B. Wen, H. Zong, M. Jones, G. Danet-Desnoyers, M. L. Guzman, M. Talpaz, D. L. Bixby, D. Sun, J. L. Hess, A. G. Muntean, I. Maillard, T. Cierpicki and J. Grembecka (2015). "Pharmacologic inhibition of the Menin-MLL interaction blocks progression of MLL leukemia in vivo." Cancer Cell **27**(4): 589-602.

Brady, C. A. and L. D. Attardi (2010). "p53 at a glance." J Cell Sci **123**(Pt 15): 2527-2532.
Brar, G. A. and J. S. Weissman (2015). "Ribosome profiling reveals the what, when, where and how of protein synthesis." Nat Rev Mol Cell Biol **16**(11): 651-664.

Brennan, T. J., D. G. Edmondson and E. N. Olson (1990). "Aberrant regulation of MyoD1 contributes to the partially defective myogenic phenotype of BC3H1 cells." J Cell Biol **110**(4): 929-937.

Brinkman, E. K., T. Chen, M. Amendola and B. van Steensel (2014). "Easy quantitative assessment of genome editing by sequence trace decomposition." Nucleic Acids Res **42**(22): e168.

Brodska, B., A. Holoubek, P. Otevrelova and K. Kuzelova (2016). "Low-Dose Actinomycin-D Induces Redistribution of Wild-Type and Mutated Nucleophosmin Followed by Cell Death in Leukemic Cells." J Cell Biochem **117**(6): 1319-1329.

Bywater, M. J., G. Poortinga, E. Sanij, N. Hein, A. Peck, C. Cullinane, M. Wall, L. Cluse, D. Drygin, K. Anderes, N. Huser, C. Proffitt, J. Bliesath, M. Haddach, M. K. Schwaebe, D. M. Ryckman, W. G. Rice, C. Schmitt, S. W. Lowe, R. W. Johnstone, R. B. Pearson, G. A. McArthur and R. D. Hannan (2012). "Inhibition of RNA polymerase I as a therapeutic strategy to promote cancer-specific activation of p53." Cancer Cell **22**(1): 51-65.

Cao, F., E. C. Townsend, H. Karatas, J. Xu, L. Li, S. Lee, L. Liu, Y. Chen, P. Ouillette, J. Zhu, J. L. Hess, P. Atadja, M. Lei, Z. S. Qin, S. Malek, S. Wang and Y. Dou (2014). "Targeting MLL1 H3K4 methyltransferase activity in mixed-lineage leukemia." Mol Cell **53**(2): 247-261.
Carey, M. F., C. L. Peterson and S. T. Smale (2009). "Chromatin immunoprecipitation (ChIP)." Cold Spring Harb Protoc **2009**(9): pdb prot5279.

Carugo, A., G. Genovese, S. Seth, L. Nezi, J. L. Rose, D. Bossi, A. Cicalese, P. K. Shah, A. Viale, P. F. Pettazzoni, K. C. Akdemir, C. A. Bristow, F. S. Robinson, J. Tepper, N. Sanchez, S. Gupta, M. R. Estecio, V. Giuliani, G. I. Dellino, L. Riva, W. Yao, M. E. Di Francesco, T. Green, C. D'Alesio, D. Corti, Y. Kang, P. Jones, H. Wang, J. B. Fleming, A. Maitra, P. G. Pelicci, L. Chin, R. A. DePinho, L. Lanfrancone, T. P. Heffernan and G. F. Draetta (2016). "In Vivo Functional Platform Targeting Patient-Derived Xenografts Identifies WDR5-Myc Association as a Critical Determinant of Pancreatic Cancer." Cell Rep **16**(1): 133-147.

Chan, P. K., D. A. Bloom and T. T. Hoang (1999). "The N-terminal half of NPM dissociates from nucleoli of HeLa cells after anticancer drug treatments." Biochem Biophys Res Commun **264**(1): 305-309.

Chen, H., B. Lorton, V. Gupta and D. Shechter (2017). "A TGFbeta-PRMT5-MEP50 axis regulates cancer cell invasion through histone H3 and H4 arginine methylation coupled transcriptional activation and repression." Oncogene **36**(3): 373-386.

Chen, X., W. Xie, P. Gu, Q. Cai, B. Wang, Y. Xie, W. Dong, W. He, G. Zhong, T. Lin and J. Huang (2015). "Upregulated WDR5 promotes proliferation, self-renewal and chemoresistance in bladder cancer via mediating H3K4 trimethylation." Sci Rep **5**: 8293.

Chung, C. Y., Z. Sun, G. Mullokandov, A. Bosch, Z. A. Qadeer, E. Cihan, Z. Rapp, R. Parsons, J. A. Aguirre-Ghiso, E. F. Farias, B. D. Brown, A. Gaspar-Maia and E. Bernstein (2016). "Cbx8 Acts Non-canonically with Wdr5 to Promote Mammary Tumorigenesis." Cell Rep **16**(2): 472-486.

Colis, L., K. Peltonen, P. Sirajuddin, H. Liu, S. Sanders, G. Ernst, J. C. Barrow and M. Laiho (2014). "DNA intercalator BMH-21 inhibits RNA polymerase I independent of DNA damage response." Oncotarget **5**(12): 4361-4369.

Core, L. J., J. J. Waterfall and J. T. Lis (2008). "Nascent RNA sequencing reveals widespread pausing and divergent initiation at human promoters." Science **322**(5909): 1845-1848.

Cui, Z., H. Li, F. Liang, C. Mu, Y. Mu, X. Zhang and J. Liu (2018). "Effect of high WDR5 expression on the hepatocellular carcinoma prognosis." Oncol Lett **15**(5): 7864-7870.

Daigle, S. R., E. J. Olhava, C. A. Therkelsen, A. Basavapathruni, L. Jin, P. A. Boriack-Sjodin, C. J. Allain, C. R. Klaus, A. Raimondi, M. P. Scott, N. J. Waters, R. Chesworth, M. P. Moyer, R. A. Copeland, V. M. Richon and R. M. Pollock (2013). "Potent inhibition of DOT1L as treatment of MLL-fusion leukemia." Blood **122**(6): 1017-1025.

Darzynkiewicz, Z., E. Bedner and P. Smolewski (2001). "Flow cytometry in analysis of cell cycle and apoptosis." Semin Hematol **38**(2): 179-193.

Dessimoz, C. and N. Škunca (2017). The gene ontology handbook. New York, Humana Press ; Springer Open.

Dharmarajan, V., J. H. Lee, A. Patel, D. G. Skalnik and M. S. Cosgrove (2012). "Structural basis for WDR5 interaction (Win) motif recognition in human SET1 family histone methyltransferases." J Biol Chem **287**(33): 27275-27289.

Dias, J., N. Van Nguyen, P. Georgiev, A. Gaub, J. Brettschneider, S. Cusack, J. Kadlec and A. Akhtar (2014). "Structural analysis of the KANSL1/WDR5/KANSL2 complex reveals that WDR5 is required for efficient assembly and chromatin targeting of the NSL complex." Genes Dev **28**(9): 929-942.

Dobin, A., C. A. Davis, F. Schlesinger, J. Drenkow, C. Zaleski, S. Jha, P. Batut, M. Chaisson and T. R. Gingeras (2013). "STAR: ultrafast universal RNA-seq aligner." Bioinformatics **29**(1): 15-21.
Dolezal, J. M., A. P. Dash and E. V. Prochownik (2018). "Diagnostic and prognostic implications of ribosomal protein transcript expression patterns in human cancers." BMC Cancer **18**(1): 275.

Dong, Y. Z., X. M. Meng and G. S. Li (2018). "Long non-coding RNA SNHG15 indicates poor prognosis of non-small cell lung cancer and promotes cell proliferation and invasion." Eur Rev Med Pharmacol Sci **22**(9): 2671-2679.

Dunning, K. and A. O. Safo (2011). "The ultimate Wright-Giemsa stain: 60 years in the making." Biotech Histochem **86**(2): 69-75.

Ee, L. S., K. N. McCannell, Y. Tang, N. Fernandes, W. R. Hardy, M. R. Green, F. Chu and T. G. Fazzio (2017). "An Embryonic Stem Cell-Specific NuRD Complex Functions through Interaction with WDR5." Stem Cell Reports **8**(6): 1488-1496.

Feng, J., T. Liu, B. Qin, Y. Zhang and X. S. Liu (2012). "Identifying ChIP-seq enrichment using MACS." Nat Protoc **7**(9): 1728-1740.

Feng, Q., H. L. Cao, W. Xu, X. R. Li, Y. Q. Ren and L. F. Du (2011). "Apoptosis induced by genipin in human leukemia K562 cells: involvement of c-Jun N-terminal kinase in G(2)/M arrest." Acta Pharmacol Sin **32**(4): 519-527.

Garcia-Cuellar, M. P., C. Buttner, C. Bartenhagen, M. Dugas and R. K. Slany (2016). "Leukemogenic MLL-ENL Fusions Induce Alternative Chromatin States to Drive a Functionally Dichotomous Group of Target Genes." Cell Rep **15**(2): 310-322.

Ge, Z., E. J. Song, Y. I. Kawasawa, J. Li, S. Dovat and C. Song (2016). "WDR5 high expression and its effect on tumorigenesis in leukemia." Oncotarget **7**(25): 37740-37754.

Golomb, L., S. Volarevic and M. Oren (2014). "p53 and ribosome biogenesis stress: the essentials." FEBS Lett **588**(16): 2571-2579.

Gomez, J. A., O. L. Wapinski, Y. W. Yang, J. F. Bureau, S. Gopinath, D. M. Monack, H. Y. Chang, M. Brahic and K. Kirkegaard (2013). "The NeST long ncRNA controls microbial susceptibility and epigenetic activation of the interferon-gamma locus." Cell **152**(4): 743-754.

Grebien, F., M. Vedadi, M. Getlik, R. Giambruno, A. Grover, R. Avellino, A. Skucha, S. Vittori, E. Kuznetsova, D. Smil, D. Barsyte-Lovejoy, F. Li, G. Poda, M. Schapira, H. Wu, A. Dong, G. Senisterra, A. Stukalov, K. V. M. Huber, A. Schonegger, R. Marcellus, M. Bilban, C. Bock, P. J. Brown, J. Zuber, K. L. Bennett, R. Al-Awar, R. Delwel, C. Nerlov, C. H. Arrowsmith and G. Superti-Furga (2015). "Pharmacological targeting of the Wdr5-MLL interaction in C/EBPalpha N-terminal leukemia." Nat Chem Biol **11**(8): 571-578.

Gu, P., X. Chen, R. Xie, J. Han, W. Xie, B. Wang, W. Dong, C. Chen, M. Yang, J. Jiang, Z. Chen, J. Huang and T. Lin (2017). "lncRNA HOXD-AS1 Regulates Proliferation and Chemo-Resistance of Castration-Resistant Prostate Cancer via Recruiting WDR5." Mol Ther **25**(8): 1959-1973.

Guarnaccia, A. D. and W. P. Tansey (2018). "Moonlighting with WDR5: A Cellular Multitasker." J Clin Med **7**(2).

Guccione, E., C. Bassi, F. Casadio, F. Martinato, M. Cesaroni, H. Schuchlautz, B. Luscher and B. Amati (2007). "Methylation of histone H3R2 by PRMT6 and H3K4 by an MLL complex are mutually exclusive." Nature **449**(7164): 933-937.

Guenther, M. G., L. N. Lawton, T. Rozovskaia, G. M. Frampton, S. S. Levine, T. L. Volkert, C. M. Croce, T. Nakamura, E. Canaani and R. A. Young (2008). "Aberrant chromatin at genes encoding stem cell regulators in human mixed-lineage leukemia." Genes Dev **22**(24): 3403-3408.

Gupta, A., J. Xu, S. Lee, S. T. Tsai, B. Zhou, K. Kurosawa, M. S. Werner, A. Koide, A. J. Ruthenburg, Y. Dou and S. Koide (2018). "Facile target validation in an animal model with intracellularly expressed monobodies." Nat Chem Biol **14**(9): 895-900.

Hah, N., C. G. Danko, L. Core, J. J. Waterfall, A. Siepel, J. T. Lis and W. L. Kraus (2011). "A rapid, extensive, and transient transcriptional response to estrogen signaling in breast cancer cells." Cell **145**(4): 622-634.

Hah, N., S. Murakami, A. Nagari, C. G. Danko and W. L. Kraus (2013). "Enhancer transcripts mark active estrogen receptor binding sites." Genome Res **23**(8): 1210-1223.

Han, Z., L. Guo, H. Wang, Y. Shen, X. W. Deng and J. Chai (2006). "Structural basis for the specific recognition of methylated histone H3 lysine 4 by the WD-40 protein WDR5." Mol Cell **22**(1): 137-144.

Harris, B. R. E., D. Wang, Y. Zhang, M. Ferrari, A. Okon, M. P. Cleary, C. R. Wagner and D. Q. Yang (2018). "Induction of the p53 Tumor Suppressor in Cancer Cells through Inhibition of Cap-Dependent Translation." Mol Cell Biol **38**(10).

Hayashida, N. (2015). "Set1/MLL complex is indispensable for the transcriptional ability of heat shock transcription factor 2." Biochem Biophys Res Commun **467**(4): 805-812.

Hekmatshoar, Y., T. Ozkan, B. Altinok Gunes, S. Bozkurt, A. Karadag, A. Z. Karabay and A. Sunguroglu (2018). "Characterization of imatinib-resistant K562 cell line displaying resistance mechanisms." Cell Mol Biol (Noisy-le-grand) **64**(6): 23-30.

Huang, M. and W. A. Weiss (2013). "Neuroblastoma and MYCN." Cold Spring Harb Perspect Med **3**(10): a014415.

Jafari, R., H. Almqvist, H. Axelsson, M. Ignatushchenko, T. Lundback, P. Nordlund and D. Martinez Molina (2014). "The cellular thermal shift assay for evaluating drug target interactions in cells." Nat Protoc **9**(9): 2100-2122.

James, A., Y. Wang, H. Raje, R. Rosby and P. DiMario (2014). "Nucleolar stress with and without p53." Nucleus **5**(5): 402-426.

Jorgensen, H. G., E. K. Allan, N. E. Jordanides, J. C. Mountford and T. L. Holyoake (2007). "Nilotinib exerts equipotent antiproliferative effects to imatinib and does not induce apoptosis in CD34+ CML cells." Blood **109**(9): 4016-4019.

Kalluri, R. and R. A. Weinberg (2009). "The basics of epithelial-mesenchymal transition." J Clin Invest **119**(6): 1420-1428.

Kanda, K., H. M. Hu, L. Zhang, J. Grandchamps and L. M. Boxer (2000). "NF-kappa B activity is required for the deregulation of c-myc expression by the immunoglobulin heavy chain enhancer." J Biol Chem **275**(41): 32338-32346.

Karatas, H., Y. Li, L. Liu, J. Ji, S. Lee, Y. Chen, J. Yang, L. Huang, D. Bernard, J. Xu, E. C. Townsend, F. Cao, X. Ran, X. Li, B. Wen, D. Sun, J. A. Stuckey, M. Lei, Y. Dou and S. Wang (2017). "Discovery of a Highly Potent, Cell-Permeable Macrocyclic Peptidomimetic (MM-589)

Targeting the WD Repeat Domain 5 Protein (WDR5)-Mixed Lineage Leukemia (MLL) Protein-Protein Interaction." J Med Chem **60**(12): 4818-4839.
Karatas, H., E. C. Townsend, D. Bernard, Y. Dou and S. Wang (2010). "Analysis of the binding of mixed lineage leukemia 1 (MLL1) and histone 3 peptides to WD repeat domain 5 (WDR5) for the design of inhibitors of the MLL1-WDR5 interaction." J Med Chem **53**(14): 5179-5185.

Karatas, H., E. C. Townsend, F. Cao, Y. Chen, D. Bernard, L. Liu, M. Lei, Y. Dou and S. Wang (2013). "High-affinity, small-molecule peptidomimetic inhibitors of MLL1/WDR5 protein-protein interaction." J Am Chem Soc **135**(2): 669-682.

Kim, J. S., C. Lee, C. L. Bonifant, H. Ressom and T. Waldman (2007). "Activation of p53-dependent growth suppression in human cells by mutations in PTEN or PIK3CA." Mol Cell Biol **27**(2): 662-677.

Kim, J. Y., T. Banerjee, A. Vinckevicius, Q. Luo, J. B. Parker, M. R. Baker, I. Radhakrishnan, J. J. Wei, G. D. Barish and D. Chakravarti (2014). "A role for WDR5 in integrating threonine 11 phosphorylation to lysine 4 methylation on histone H3 during androgen signaling and in prostate cancer." Mol Cell **54**(4): 613-625.

Kim, K. H. and J. M. Sederstrom (2015). "Assaying Cell Cycle Status Using Flow Cytometry." Curr Protoc Mol Biol **111**: 28 26 21-11.

Knutson, S. K., T. J. Wigle, N. M. Warholic, C. J. Sneeringer, C. J. Allain, C. R. Klaus, J. D. Sacks, A. Raimondi, C. R. Majer, J. Song, M. P. Scott, L. Jin, J. J. Smith, E. J. Olhava, R. Chesworth, M. P. Moyer, V. M. Richon, R. A. Copeland, H. Keilhack, R. M. Pollock and K. W. Kuntz (2012). "A selective inhibitor of EZH2 blocks H3K27 methylation and kills mutant lymphoma cells." Nat Chem Biol **8**(11): 890-896.

Kroon, E., J. Krosl, U. Thorsteinsdottir, S. Baban, A. M. Buchberg and G. Sauvageau (1998). "Hoxa9 transforms primary bone marrow cells through specific collaboration with Meis1a but not Pbx1b." EMBO J **17**(13): 3714-3725.

Kwak, H., N. J. Fuda, L. J. Core and J. T. Lis (2013). "Precise maps of RNA polymerase reveal how promoters direct initiation and pausing." Science **339**(6122): 950-953.
Lakin, N. D. and S. P. Jackson (1999). "Regulation of p53 in response to DNA damage." Oncogene **18**(53): 7644-7655.

Lampronti, I., N. Bianchi, M. Borgatti, E. Fibach, E. Prus and R. Gambari (2003). "Accumulation of gamma-globin mRNA in human erythroid cells treated with angelicin." Eur J Haematol **71**(3): 189-195.

Langmead, B. and S. L. Salzberg (2012). "Fast gapped-read alignment with Bowtie 2." Nat Methods **9**(4): 357-359.

Langmead, B., C. Trapnell, M. Pop and S. L. Salzberg (2009). "Ultrafast and memory-efficient alignment of short DNA sequences to the human genome." Genome Biol **10**(3): R25.

Li, Y., J. Han, Y. Zhang, F. Cao, Z. Liu, S. Li, J. Wu, C. Hu, Y. Wang, J. Shuai, J. Chen, L. Cao, D. Li, P. Shi, C. Tian, J. Zhang, Y. Dou, G. Li, Y. Chen and M. Lei (2016). "Structural basis for activity regulation of MLL family methyltransferases." Nature **530**(7591): 447-452.

Liao, J., S. E. Humphrey, S. Poston and E. J. Taparowsky (2011). "Batf promotes growth arrest and terminal differentiation of mouse myeloid leukemia cells." Mol Cancer Res **9**(3): 350-363.
Liao, Y., G. K. Smyth and W. Shi (2014). "featureCounts: an efficient general purpose program for assigning sequence reads to genomic features." Bioinformatics **30**(7): 923-930.

Linden, M., J. M. Ward and S. Cherian (2012). Comparative Anatomy and Histology. P. M. Treuting and S. M. Dintzis. San Diego, Academic Press**:** 309-338.

Lizio, M., J. Harshbarger, H. Shimoji, J. Severin, T. Kasukawa, S. Sahin, I. Abugessaisa, S. Fukuda, F. Hori, S. Ishikawa-Kato, C. J. Mungall, E. Arner, J. K. Baillie, N. Bertin, H. Bono, M. de Hoon, A. D. Diehl, E. Dimont, T. C. Freeman, K. Fujieda, W. Hide, R. Kaliyaperumal, T. Katayama, T. Lassmann, T. F. Meehan, K. Nishikata, H. Ono, M. Rehli, A. Sandelin, E. A. Schultes, P. A. t Hoen, Z. Tatum, M. Thompson, T. Toyoda, D. W. Wright, C. O. Daub, M. Itoh, P. Carninci, Y. Hayashizaki, A. R. Forrest, H. Kawaji and F. consortium (2015). "Gateways to the FANTOM5 promoter level mammalian expression atlas." Genome Biol **16**: 22.

Love, M. I., W. Huber and S. Anders (2014). "Moderated estimation of fold change and dispersion for RNA-seq data with DESeq2." Genome Biol **15**(12): 550.

Lu, K., H. Tao, X. Si and Q. Chen (2018). "The Histone H3 Lysine 4 Presenter WDR5 as an Oncogenic Protein and Novel Epigenetic Target in Cancer." Front Oncol **8**: 502.

Mahat, D. B., H. Kwak, G. T. Booth, I. H. Jonkers, C. G. Danko, R. K. Patel, C. T. Waters, K. Munson, L. J. Core and J. T. Lis (2016). "Base-pair-resolution genome-wide mapping of active RNA polymerases using precision nuclear run-on (PRO-seq)." Nat Protoc **11**(8): 1455-1476.

Malek, R., R. P. Gajula, R. D. Williams, B. Nghiem, B. W. Simons, K. Nugent, H. Wang, K. Taparra, G. Lemtiri-Chlieh, A. R. Yoon, L. True, S. S. An, T. L. DeWeese, A. E. Ross, E. M.

Schaeffer, K. J. Pienta, P. J. Hurley, C. Morrissey and P. T. Tran (2017). "TWIST1-WDR5-Hottip Regulates Hoxa9 Chromatin to Facilitate Prostate Cancer Metastasis." Cancer Res **77**(12): 3181-3193.

Mann, M. (2006). "Functional and quantitative proteomics using SILAC." Nat Rev Mol Cell Biol **7**(12): 952-958.

Marques-Garcia, F., N. Ferrandiz, R. Fernandez-Alonso, L. Gonzalez-Cano, M. Herreros-Villanueva, M. Rosa-Garrido, B. Fernandez-Garcia, J. P. Vaque, M. M. Marques, M. E. Alonso, J. C. Segovia, J. Leon and M. C. Marin (2009). "p73 plays a role in erythroid differentiation through GATA1 induction." J Biol Chem **284**(32): 21139-21156.

Marschalek, R. (2011). "Mechanisms of leukemogenesis by MLL fusion proteins." Br J Haematol **152**(2): 141-154.

Mazurek, A., Y. Park, C. Miething, J. E. Wilkinson, J. Gillis, S. W. Lowe, C. R. Vakoc and B. Stillman (2014). "Acquired dependence of acute myeloid leukemia on the DEAD-box RNA helicase DDX5." Cell Rep **7**(6): 1887-1899.

Mendez, J. and B. Stillman (2000). "Chromatin association of human origin recognition complex, cdc6, and minichromosome maintenance proteins during the cell cycle: assembly of prereplication complexes in late mitosis." Mol Cell Biol **20**(22): 8602-8612.

Migliori, V., J. Muller, S. Phalke, D. Low, M. Bezzi, W. C. Mok, S. K. Sahu, J. Gunaratne, P. Capasso, C. Bassi, V. Cecatiello, A. De Marco, W. Blackstock, V. Kuznetsov, B. Amati, M. Mapelli and E. Guccione (2012). "Symmetric dimethylation of H3R2 is a newly identified histone mark that supports euchromatin maintenance." Nat Struct Mol Biol **19**(2): 136-144.

Milne, T. A., J. Kim, G. G. Wang, S. C. Stadler, V. Basrur, S. J. Whitcomb, Z. Wang, A. J. Ruthenburg, K. S. Elenitoba-Johnson, R. G. Roeder and C. D. Allis (2010). "Multiple interactions recruit MLL1 and MLL1 fusion proteins to the HOXA9 locus in leukemogenesis." Mol Cell **38**(6): 853-863.

Mishra, B. P., K. M. Zaffuto, E. L. Artinger, T. Org, H. K. Mikkola, C. Cheng, M. Djabali and P. Ernst (2014). "The histone methyltransferase activity of MLL1 is dispensable for hematopoiesis and leukemogenesis." Cell Rep **7**(4): 1239-1247.

Moore, C. B., E. H. Guthrie, M. T. Huang and D. J. Taxman (2010). "Short hairpin RNA (shRNA): design, delivery, and assessment of gene knockdown." Methods Mol Biol **629**: 141-158.
Neilsen, B. K., B. Chakraborty, J. L. McCall, D. E. Frodyma, R. L. Sleightholm, K. W. Fisher and R. E. Lewis (2018). "WDR5 supports colon cancer cells by promoting methylation of H3K4 and suppressing DNA damage." BMC Cancer **18**(1): 673.

Nicolae, C. M., E. R. Aho, A. H. Vlahos, K. N. Choe, S. De, G. I. Karras and G. L. Moldovan (2014). "The ADP-ribosyltransferase PARP10/ARTD10 interacts with proliferating cell nuclear antigen (PCNA) and is required for DNA damage tolerance." J Biol Chem **289**(19): 13627-13637.

Odho, Z., S. M. Southall and J. R. Wilson (2010). "Characterization of a novel WDR5-binding site that recruits RbBP5 through a conserved motif to enhance methylation of histone H3 lysine 4 by mixed lineage leukemia protein-1." J Biol Chem **285**(43): 32967-32976.

Oliver, F. J., G. de la Rubia, V. Rolli, M. C. Ruiz-Ruiz, G. de Murcia and J. M. Murcia (1998). "Importance of poly(ADP-ribose) polymerase and its cleavage in apoptosis. Lesson from an uncleavable mutant." J Biol Chem **273**(50): 33533-33539.

Patel, A., V. E. Vought, V. Dharmarajan and M. S. Cosgrove (2008). "A conserved arginine-containing motif crucial for the assembly and enzymatic activity of the mixed lineage leukemia protein-1 core complex." J Biol Chem **283**(47): 32162-32175.

Pelletier, J., G. Thomas and S. Volarevic (2018). "Ribosome biogenesis in cancer: new players and therapeutic avenues." Nat Rev Cancer **18**(1): 51-63.

Perez, C. A., J. Ott, D. J. Mays and J. A. Pietenpol (2007). "p63 consensus DNA-binding site: identification, analysis and application into a p63MH algorithm." Oncogene **26**(52): 7363-7370.

Qvit, N., S. J. S. Rubin, T. J. Urban, D. Mochly-Rosen and E. R. Gross (2017). "Peptidomimetic therapeutics: scientific approaches and opportunities." Drug Discov Today **22**(2): 454-462.
Ran, F. A., P. D. Hsu, J. Wright, V. Agarwala, D. A. Scott and F. Zhang (2013). "Genome engineering using the CRISPR-Cas9 system." Nat Protoc **8**(11): 2281-2308.

Rinker, E. B., J. C. Dueber, J. Qualtieri, J. Tedesco, B. Erdogan, A. Bosompem and A. S. Kim (2016). "Differential expression of ribosomal proteins in myelodysplastic syndromes." J Clin Pathol **69**(2): 176-180.

Riss, T. L., R. A. Moravec, A. L. Niles, S. Duellman, H. A. Benink, T. J. Worzella and L. Minor (2004). Cell Viability Assays. Assay Guidance Manual. G. S. Sittampalam, N. P. Coussens, K. Brimacombe et al. Bethesda (MD).

Russo, A. and G. Russo (2017). "Ribosomal Proteins Control or Bypass p53 during Nucleolar Stress." Int J Mol Sci **18**(1).

Sarbassov, D. D., D. A. Guertin, S. M. Ali and D. M. Sabatini (2005). "Phosphorylation and regulation of Akt/PKB by the rictor-mTOR complex." Science **307**(5712): 1098-1101.
Schafer, K. A. (1998). "The cell cycle: a review." Vet Pathol **35**(6): 461-478.

Schindelin, J., I. Arganda-Carreras, E. Frise, V. Kaynig, M. Longair, T. Pietzsch, S. Preibisch, C. Rueden, S. Saalfeld, B. Schmid, J. Y. Tinevez, D. J. White, V. Hartenstein, K. Eliceiri, P. Tomancak and A. Cardona (2012). "Fiji: an open-source platform for biological-image analysis." Nat Methods **9**(7): 676-682.

Schmittgen, T. D. and K. J. Livak (2008). "Analyzing real-time PCR data by the comparative C(T) method." Nat Protoc **3**(6): 1101-1108.

Schuetz, A., A. Allali-Hassani, F. Martin, P. Loppnau, M. Vedadi, A. Bochkarev, A. N. Plotnikov, C. H. Arrowsmith and J. Min (2006). "Structural basis for molecular recognition and presentation of histone H3 by WDR5." EMBO J **25**(18): 4245-4252.

Seila, A. C., J. M. Calabrese, S. S. Levine, G. W. Yeo, P. B. Rahl, R. A. Flynn, R. A. Young and P. A. Sharp (2008). "Divergent transcription from active promoters." Science **322**(5909): 1849-1851.

Senisterra, G., H. Wu, A. Allali-Hassani, G. A. Wasney, D. Barsyte-Lovejoy, L. Dombrovski, A. Dong, K. T. Nguyen, D. Smil, Y. Bolshan, T. Hajian, H. He, A. Seitova, I. Chau, F. Li, G. Poda, J. F. Couture, P. J. Brown, R. Al-Awar, M. Schapira, C. H. Arrowsmith and M. Vedadi (2013). "Small-molecule inhibition of MLL activity by disruption of its interaction with WDR5." Biochem J **449**(1): 151-159.

Shalem, O., N. E. Sanjana, E. Hartenian, X. Shi, D. A. Scott, T. Mikkelson, D. Heckl, B. L. Ebert, D. E. Root, J. G. Doench and F. Zhang (2014). "Genome-scale CRISPR-Cas9 knockout screening in human cells." Science **343**(6166): 84-87.

Sharma, A., K. Singh and A. Almasan (2012). "Histone H2AX phosphorylation: a marker for DNA damage." Methods Mol Biol **920**: 613-626.

Sigal, A. and V. Rotter (2000). "Oncogenic mutations of the p53 tumor suppressor: the demons of the guardian of the genome." Cancer Res **60**(24): 6788-6793.

Signer, R. A., J. A. Magee, A. Salic and S. J. Morrison (2014). "Haematopoietic stem cells require a highly regulated protein synthesis rate." Nature **509**(7498): 49-54.

Stegh, A. H. (2012). "Targeting the p53 signaling pathway in cancer therapy - the promises, challenges and perils." Expert Opin Ther Targets **16**(1): 67-83.

Stewart, H. J., G. A. Horne, S. Bastow and T. J. Chevassut (2013). "BRD4 associates with p53 in DNMT3A-mutated leukemia cells and is implicated in apoptosis by the bromodomain inhibitor JQ1." Cancer Med **2**(6): 826-835.

Strober, W. (2001). "Trypan blue exclusion test of cell viability." Curr Protoc Immunol **Appendix 3**: Appendix 3B.

Stubbs, M. C. and A. V. Krivtsov (2017). "Murine Retrovirally-Transduced Bone Marrow Engraftment Models of MLL-Fusion-Driven Acute Myelogenous Leukemias (AML)." Curr Protoc Pharmacol **78**: 14 42 11-14 42 19.

Suganuma, T., J. L. Gutierrez, B. Li, L. Florens, S. K. Swanson, M. P. Washburn, S. M. Abmayr and J. L. Workman (2008). "ATAC is a double histone acetyltransferase complex that stimulates nucleosome sliding." Nat Struct Mol Biol **15**(4): 364-372.

Sugawara, I., T. Iwahashi, K. Okamoto, Y. Sugimoto, H. Ekimoto, T. Tsuruo, T. Ikeuchi and S. Mori (1991). "Characterization of an etoposide-resistant human K562 cell line, K/eto." Jpn J Cancer Res **82**(9): 1035-1043.

Sullivan, K. D., M. D. Galbraith, Z. Andrysik and J. M. Espinosa (2018). "Mechanisms of transcriptional regulation by p53." Cell Death Differ **25**(1): 133-143.

Sun, T. T., J. He, Q. Liang, L. L. Ren, T. T. Yan, T. C. Yu, J. Y. Tang, Y. J. Bao, Y. Hu, Y. Lin, D. Sun, Y. X. Chen, J. Hong, H. Chen, W. Zou and J. Y. Fang (2016). "LncRNA GClnc1 Promotes Gastric Carcinogenesis and May Act as a Modular Scaffold of WDR5 and KAT2A Complexes to Specify the Histone Modification Pattern." Cancer Discov **6**(7): 784-801.

Sun, W., F. Guo and M. Liu (2018). "Up-regulated WDR5 promotes gastric cancer formation by induced cyclin D1 expression." J Cell Biochem **119**(4): 3304-3316.

Sun, Y., J. L. Bell, D. Carter, S. Gherardi, R. C. Poulos, G. Milazzo, J. W. Wong, R. Al-Awar, A. E. Tee, P. Y. Liu, B. Liu, B. Atmadibrata, M. Wong, T. Trahair, Q. Zhao, J. M. Shohet, Y. Haupt, J. H. Schulte, P. J. Brown, C. H. Arrowsmith, M. Vedadi, K. L. MacKenzie, S. Huttelmaier, G. Perini, G. M. Marshall, A. Braithwaite and T. Liu (2015). "WDR5 Supports an N-Myc Transcriptional Complex That Drives a Protumorigenic Gene Expression Signature in Neuroblastoma." Cancer Res **75**(23): 5143-5154.

Testa, U., W. Vainchenker, Y. Beuzard, P. Rouyer-Fessard, A. Guerrasio, M. Titeux, P. Lapotre, J. Bouguet, J. Breton-Gorius and J. Rosa (1982). "Hemoglobin expression in clones of K562 cell line." Eur J Biochem **121**(3): 649-655.

Thomas, L. R., A. M. Foshage, A. M. Weissmiller and W. P. Tansey (2015). "The MYC-WDR5 Nexus and Cancer." Cancer Res **75**(19): 4012-4015.

Thomas, L. R., Q. Wang, B. C. Grieb, J. Phan, A. M. Foshage, Q. Sun, E. T. Olejniczak, T. Clark, S. Dey, S. Lorey, B. Alicie, G. C. Howard, B. Cawthon, K. C. Ess, C. M. Eischen, Z. Zhao, S. W. Fesik and W. P. Tansey (2015). "Interaction with WDR5 promotes target gene recognition and tumorigenesis by MYC." Mol Cell **58**(3): 440-452.

Thompson, B. A., V. Tremblay, G. Lin and D. A. Bochar (2008). "CHD8 is an ATP-dependent chromatin remodeling factor that regulates beta-catenin target genes." Mol Cell Biol **28**(12): 3894-3904.

Thorsteinsdottir, U., E. Kroon, L. Jerome, F. Blasi and G. Sauvageau (2001). "Defining roles for HOX and MEIS1 genes in induction of acute myeloid leukemia." Mol Cell Biol **21**(1): 224-234.

Tisato, V., R. Voltan, A. Gonelli, P. Secchiero and G. Zauli (2017). "MDM2/X inhibitors under clinical evaluation: perspectives for the management of hematological malignancies and pediatric cancer." J Hematol Oncol **10**(1): 133.

Trievel, R. C. and A. Shilatifard (2009). "WDR5, a complexed protein." Nat Struct Mol Biol **16**(7): 678-680.

Tsherniak, A., F. Vazquez, P. G. Montgomery, B. A. Weir, G. Kryukov, G. S. Cowley, S. Gill, W. F. Harrington, S. Pantel, J. M. Krill-Burger, R. M. Meyers, L. Ali, A. Goodale, Y. Lee, G. Jiang, J. Hsiao, W. F. J. Gerath, S. Howell, E. Merkel, M. Ghandi, L. A. Garraway, D. E. Root, T. R. Golub, J. S. Boehm and W. C. Hahn (2017). "Defining a Cancer Dependency Map." Cell **170**(3): 564-576 e516.

van Nuland, R., A. H. Smits, P. Pallaki, P. W. Jansen, M. Vermeulen and H. T. Timmers (2013). "Quantitative dissection and stoichiometry determination of the human SET1/MLL histone methyltransferase complexes." Mol Cell Biol **33**(10): 2067-2077.

Vassilev, L. T., B. T. Vu, B. Graves, D. Carvajal, F. Podlaski, Z. Filipovic, N. Kong, U. Kammlott, C. Lukacs, C. Klein, N. Fotouhi and E. A. Liu (2004). "In vivo activation of the p53 pathway by small-molecule antagonists of MDM2." Science **303**(5659): 844-848.

Vedadi, M., L. Blazer, M. S. Eram, D. Barsyte-Lovejoy, C. H. Arrowsmith and T. Hajian (2017). "Targeting human SET1/MLL family of proteins." Protein Sci **26**(4): 662-676.

Vilhais-Neto, G. C., M. Fournier, J. L. Plassat, M. E. Sardiu, A. Saraf, J. M. Garnier, M. Maruhashi, L. Florens, M. P. Washburn and O. Pourquie (2017). "The WHHERE coactivator complex is required for retinoic acid-dependent regulation of embryonic symmetry." Nat Commun **8**(1): 728.

Waldman, S. A. (2002). "Does potency predict clinical efficacy? Illustration through an antihistamine model." Ann Allergy Asthma Immunol **89**(1): 7-11; quiz 11-12, 77.

Wang, F., K. O. Jeon, J. M. Salovich, J. D. Macdonald, J. Alvarado, R. D. Gogliotti, J. Phan, E. T. Olejniczak, Q. Sun, S. Wang, D. Camper, J. P. Yuh, J. G. Shaw, J. Sai, O. W. Rossanese, W. P. Tansey, S. R. Stauffer and S. W. Fesik (2018). "Discovery of Potent 2-Aryl-6,7-dihydro-5 H-pyrrolo[1,2- a]imidazoles as WDR5-WIN-Site Inhibitors Using Fragment-Based Methods and Structure-Based Design." J Med Chem **61**(13): 5623-5642.

Wang, L., Y. Du, J. M. Ward, T. Shimbo, B. Lackford, X. Zheng, Y. L. Miao, B. Zhou, L. Han, D. C. Fargo, R. Jothi, C. J. Williams, P. A. Wade and G. Hu (2014). "INO80 facilitates pluripotency gene activation in embryonic stem cell self-renewal, reprogramming, and blastocyst development." Cell Stem Cell **14**(5): 575-591.

Wang, Y. L., F. Faiola, M. Xu, S. Pan and E. Martinez (2008). "Human ATAC Is a GCN5/PCAF-containing acetylase complex with a novel NC2-like histone fold module that interacts with the TATA-binding protein." J Biol Chem **283**(49): 33808-33815.

Wei, J., M. Wunderlich, C. Fox, S. Alvarez, J. C. Cigudosa, J. S. Wilhelm, Y. Zheng, J. A. Cancelas, Y. Gu, M. Jansen, J. F. Dimartino and J. C. Mulloy (2008). "Microenvironment determines lineage fate in a human model of MLL-AF9 leukemia." Cancer Cell **13**(6): 483-495.

Wiederschain, D., H. Kawai, A. Shilatifard and Z. M. Yuan (2005). "Multiple mixed lineage leukemia (MLL) fusion proteins suppress p53-mediated response to DNA damage." J Biol Chem **280**(26): 24315-24321.

Wu, M. and H. B. Shu (2011). "MLL1/WDR5 complex in leukemogenesis and epigenetic regulation." Chin J Cancer **30**(4): 240-246.

Wu, M. Z., Y. P. Tsai, M. H. Yang, C. H. Huang, S. Y. Chang, C. C. Chang, S. C. Teng and K. J. Wu (2011). "Interplay between HDAC3 and WDR5 is essential for hypoxia-induced epithelial-mesenchymal transition." Mol Cell **43**(5): 811-822.

Wu, Y., P. Diao, Z. Li, W. Zhang, D. Wang, Y. Wang and J. Cheng (2018). "Overexpression of WD repeat domain 5 associates with aggressive clinicopathological features and unfavorable prognosis in head neck squamous cell carcinoma." J Oral Pathol Med **47**(5): 502-510.

Wysocka, J., T. Swigut, T. A. Milne, Y. Dou, X. Zhang, A. L. Burlingame, R. G. Roeder, A. H. Brivanlou and C. D. Allis (2005). "WDR5 associates with histone H3 methylated at K4 and is essential for H3 K4 methylation and vertebrate development." Cell **121**(6): 859-872.

Xu, J., L. Li, J. Xiong, A. denDekker, A. Ye, H. Karatas, L. Liu, H. Wang, Z. S. Qin, S. Wang and Y. Dou (2016). "MLL1 and MLL1 fusion proteins have distinct functions in regulating leukemic transcription program." Cell Discov **2**: 16008.

Yang, D. Q., M. J. Halaby and Y. Zhang (2006). "The identification of an internal ribosomal entry site in the 5'-untranslated region of p53 mRNA provides a novel mechanism for the regulation of its translation following DNA damage." Oncogene **25**(33): 4613-4619.

Yang, K., M. Wang, Y. Zhao, X. Sun, Y. Yang, X. Li, A. Zhou, H. Chu, H. Zhou, J. Xu, M. Wu, J. Yang and J. Yi (2016). "A redox mechanism underlying nucleolar stress sensing by nucleophosmin." Nat Commun **7**: 13599.

Yang, Y. W., R. A. Flynn, Y. Chen, K. Qu, B. Wan, K. C. Wang, M. Lei and H. Y. Chang (2014). "Essential role of lncRNA binding for WDR5 maintenance of active chromatin and embryonic stem cell pluripotency." Elife **3**: e02046.

Yanovich, S., R. E. Hall and D. A. Gewirtz (1989). "Characterization of a K562 multidrug-resistant cell line." Cancer Res **49**(16): 4499-4503.

Yates, J. A., T. Menon, B. A. Thompson and D. A. Bochar (2010). "Regulation of HOXA2 gene expression by the ATP-dependent chromatin remodeling enzyme CHD8." FEBS Lett **584**(4): 689-693.

Zhang, X., X. Zheng, H. Yang, J. Yan, X. Fu, R. Wei, X. Xu, Z. Zhang, A. Yu, K. Zhou, J. Ding, M. Geng and X. Huang (2018). "Piribedil disrupts the MLL1-WDR5 interaction and sensitizes MLL-rearranged acute myeloid leukemia (AML) to doxorubicin-induced apoptosis." Cancer Lett **431**: 150-160.

Zhou, H., L. Liu, J. Huang, D. Bernard, H. Karatas, A. Navarro, M. Lei and S. Wang (2013). "Structure-based design of high-affinity macrocyclic peptidomimetics to block the menin-mixed lineage leukemia 1 (MLL1) protein-protein interaction." J Med Chem **56**(3): 1113-1123.

Zhu, J., M. A. Sammons, G. Donahue, Z. Dou, M. Vedadi, M. Getlik, D. Barsyte-Lovejoy, R. Al-awar, B. W. Katona, A. Shilatifard, J. Huang, X. Hua, C. H. Arrowsmith and S. L. Berger (2015). "Gain-of-function p53 mutants co-opt chromatin pathways to drive cancer growth." Nature **525**(7568): 206-211.

Zuber, J., J. Shi, E. Wang, A. R. Rappaport, H. Herrmann, E. A. Sison, D. Magoon, J. Qi, K. Blatt, M. Wunderlich, M. J. Taylor, C. Johns, A. Chicas, J. C. Mulloy, S. C. Kogan, P. Brown, P. Valent, J. E. Bradner, S. W. Lowe and C. R. Vakoc (2011). "RNAi screen identifies Brd4 as a therapeutic target in acute myeloid leukaemia." Nature **478**(7370): 524-528.